

UNIVERSITY OF OKLAHOMA

GRADUATE COLLEGE

SMALL MOLECULE DESIGN STRATEGIES FOR PROBING STRUCTURE-ACTIVITY  
RELATIONSHIPS: BACTERIAL VIRULENCE MODULATION VIA CPXRA  
ACTIVATION, THE TOTAL SYNTHESIS OF PICRASMA ALKALOIDS, AND  
CORONAVIRUS MAIN PROTEASE INHIBITORS

A DISSERTATION

SUBMITTED TO THE GRADUATE FACULTY

In partial fulfillment of the requirements for the

Degree of

DOCTOR OF PHILOSOPHY

By

JESSICA JEANORA HAYES GARDNER

Norman, Oklahoma

2022

SMALL MOLECULE DESIGN STRATEGIES FOR PROBING STRUCTURE-ACTIVITY  
RELATIONSHIPS: BACTERIAL VIRULENCE MODULATION VIA CPXRA  
ACTIVATION, THE TOTAL SYNTHESIS OF PICRAMMA ALKALOIDS, AND  
CORONAVIRUS MAIN PROTEASE INHIBITORS

A DISSERTATION APPROVED FOR THE  
DEPARTMENT OF CHEMISTRY AND BIOCHEMISTRY

BY THE COMMITTEE CONSISTING OF

Dr. Shanteri Singh, Co-Chair

Dr. Adam Duerfeldt, Co-Chair

Dr. Edgar A. O'Rear

Dr. Daniel T. Glatzhofer

Dr. Robert Cichewicz

© Copyright by JESSICA JEANORA HAYES GARDNER

All Rights Reserved.

## **Dedication**

*This dissertation is dedicated to Madeline C. Panis and Catalina D. Carbonell,*

*for I have never met women as strong and intelligent as they,*

*and I can only wish to live up to their legacy.*

## Abstract

The overall aim of my work is to contribute to molecular design strategies for early lead development while probing structure-activity relationships via the design and synthesis of small molecules. This dissertation will tell three distinct stories:

**1. Exploitation of CpxRA as a target for virulence modulation in Gram-negative bacteria.** An initial structure-activity relationship study of the 2,3,4,9-tetrahydro-1*H*-carbazol-1-amine scaffold for activation of the CpxRA two-component signal transduction system (2CSTS) identified compound 2.26, which activates CpxRA with ~30-fold improvement in CpxA phosphatase inhibition over the initial hit. In murine models, 2.26 was found to reduce bacterial recovery in the urine, kidneys, and bladder, with efficacy similar to ciprofloxacin. The proteomes of uropathogenic *E. coli* strain CFT073 *cpxA* deletion mutant versus 2.26-treated CFT073 were compared, providing insights into the mechanism behind CpxRA pharmacologic activation. Compound 2.26 provides a novel antibacterial mechanism as it does not exhibit bactericidal activity, but it reduces the expression of virulence factors, as demonstrated by cellular assays, animal studies, and proteomic analysis.

**2. Work towards the total synthesis of Picrasidine natural product family members.** The unique bis- $\beta$ -carboline scaffold within the *Picrasma quassioides* alkaloids exhibit a diverse range of biological activities. Picrasidine C is particularly interesting for its demonstrated efficacy in subtype-selective PPAR $\alpha$  agonism as a promising treatment for diabetic retinopathy. Two approaches were considered for synthesizing picrasidine C and other *Picrasma* alkaloid family members: (1) iterative  $\beta$ -carboline ring construction, and (2) functionalization of the  $\beta$ -carboline ring. While the total synthesis of picrasidine C was unsuccessful, six new *Picrasma* alkaloid analogs were synthesized. The two mono- and four bis- $\beta$ -carboline compounds have the capacity to serve as building blocks for the *Picrasma* family of alkaloids because of their reactive functional groups. An acid-catalyzed Pictet-Spengler enamine cyclization cascade was discovered, providing efficient access to indoloquinolizine heterocycles.

**3. The rational design and synthesis of SARS-CoV-2 M<sup>pro</sup> inhibitors.** Severe acute respiratory syndrome coronavirus 2 (SARS-CoV-2) is the virus responsible for the COVID-19 global pandemic. In an effort to join the fight against this public health catastrophe, 25 compounds from our existing small molecule library were submitted for evaluation in a phenotypic viral replication inhibition assay. While the compounds shared remarkable structural similarities to coronavirus-active drugs, the results found them all inactive. Utilizing in silico modelling and fragment-based design, three structural scaffolds (urea, piperazinone, and peptidomimetic) were proposed for small molecule inhibitors of the SARS-CoV-2 main protease (M<sup>pro</sup>). 18 peptidomimetic compounds were rapidly synthesized from 4-component Ugi coupling reactions and evaluated in-house for M<sup>pro</sup> inhibition activity. When compared to the control, 3 of my peptidomimetic compounds were found to moderately inhibit protease activity. M<sup>pro</sup> will be highlighted as a promising target for anti-coronavirus therapeutics.

## Acknowledgements

Finishing this dissertation was the single most difficult task I have ever attempted, and it would be physically impossible for me to have done it by myself. The community I built for myself in Oklahoma was surprising yet tremendous. It truly takes a village.

Eric Gardner, Quentin Avila, Bre Schlitzer, Steve Schlitzer, Dustin Dimas, Rob Fogle, and Dan Sheffield. There is literally nothing that we couldn't do once we set our minds to it. We are absolutely unstoppable, and I am not exaggerating. I just want to thank you all for existing.

Susan Nimmo. My teacher, my mentor, and my friend. First you helped me through some tough problems in the NMR lab, and then you just helped me through life. You opened my eyes to ideas that I couldn't even fathom the magnitude of. I always learn something when I talk to you, and you're just generally fun to be around. I should thank you for existing also.

The Duerfeldt lab and the people I've met through it. Cat Bishop, you are an inspiration and I love you. Dinesh Nath, I could always count on you for some philosophical ranting. Katelyn Stevens, I wish I could give you a hug but you're too far away. Quentin Avila, when are we starting our campaign for Emperors of the world?

The Society of Chemical and Biochemical Researchers, a blessing and a curse. Marcee Olvera, I was proud to hand my title down to you. You were the last President to understand the vision that our generation had for the Department. A glorious leader and a kind friend, I am happy we got to work together. Ally Fairman, you're always there when we need you. You are a loyal friend, and I appreciate you. Quentin Avila, where are those plans for our world takeover? Okay, seriously though, you were the rock to my insane, babbling brook. There's a reason you made it onto my acknowledgements page three times.

Bre Schlitzer, because you need your own blurb. Do you remember my first general exam? Because I do, vividly. You made me a birthday cake during our very first semester in Oklahoma, and it's those kinds of little things that mean the world to me. You were the only one who could seriously keep my sanity in check, so I guess I owe my intact brain to you.

Lisa, Julie, and David Gardner. You happily and thoroughly absorbed me into your family, and I cannot express the joy that you all have brought me. Not to mention that you let me steal Eric away to Colorado. Eric Gardner, you are what I look forward to every day. If I got anything worth keeping from the state of Oklahoma, it's you. You didn't just keep me sane, you kept me alive. Again, I'm not exaggerating.

Michelle, William, and William Hayes. Home is when we are together.

## Table of Contents

<b>Chapter 1: Introduction .....</b>	<b>1</b>
1.1 Two-component signal transduction systems and virulence modulation in Gram-negative bacteria.....	1
1.1.1 An overview of resistance and Gram-negative bacteria.....	1
1.1.2 CpxRA phosphatase inhibition and 2CSTS as antibacterial targets.....	4
1.1.3 Summary of accomplishments.....	5
1.2 Natural product total synthesis and <i>Picrasma</i> alkaloids.....	6
1.2.1 Natural products and the utility of total synthesis.....	6
1.2.2 The synthesis of $\beta$ -carbolines and related alkaloids.....	10
1.2.3 Interests in picrasidine C as a subtype selective PPAR $\alpha$ agonist and its implications in diabetic retinopathy.....	15
1.2.4 Overview of <i>Picrasma</i> alkaloids and picrasidine family members.....	20
1.2.5 Summary of accomplishments.....	22
1.3 Overview of SARS-CoV-2 protease inhibitors.....	23
1.3.1 Significance: COVID-19 global pandemic.....	23
1.3.2 Introduction to SARS-CoV-2 protease inhibitors.....	25
1.3.3 Summary of what was accomplished.....	29
1.4 References for Chapter 1 .....	30

<b>Chapter 2. Virulence modulation in Gram-negative bacteria via small molecule activation of CpxRA.....</b>	<b>52</b>
2.1 Introduction.....	54
2.2 Results and discussion .....	57
2.2.1 A-ring substitution. ....	57
2.2.2 C-ring deconstruction.....	60
2.2.3 Significance of the primary amine.....	63
2.2.4 Probing the mechanisms of CpxRA modulation. ....	65
2.3 Conclusions and future directions.....	73
2.4 Experimental.....	75
2.4.1 General Chemistry Methods .....	75
2.4.2 Synthetic Procedures.....	76
2.4.3 Biological evaluation .....	83
2.4.5 Proteomic analysis .....	86
2.5 References for Chapter 2 .....	88
<b>Appendix I. Spectra Relevant to Chapter 2.....</b>	<b>94</b>
<b>Chapter 3: <math>\beta</math>-carboline synthesis and functionalization for studies toward the total synthesis of picrasidine alkaloids.....</b>	<b>109</b>
3.1 Introduction to <i>Picrasma</i> alkaloids.....	110
3.1.1 <i>Picrasma</i> alkaloids in traditional medicine.....	110



3.1.2 Overview of $\beta$ -carbolines and existing synthetic methods. ....	112
3.2 Retrosynthetic analysis .....	117
3.2.1 Iterative $\beta$ -carboline ring construction (Approach 1). ....	117
3.2.2 $\beta$ -carboline functionalization (Approach 2).....	119
3.3 Results and discussion for Approach 1 .....	121
3.3.1 Step 1: Pictet-Spengler cyclization with cyclopentene-1-aldehyde for the formation of THBC 3.34 (PSR1). ....	122
3.3.2 Step 2: Oxidative aromatization of THBC 3.34.....	126
3.3.3 Step 3: Oxidative cleavage to construct the linker region .....	131
3.3.4 Step 4: Generating the second $\beta$ -carboline system from key aldehyde intermediate 3.38 via Pictet-Spengler cyclization (PSR2).....	134
3.3.5 Exploring the enamine reactivity of compound 3.41.....	137
3.3.6 Discovery and structural characterization of compound 3.44. ....	144
3.4 Results and discussion for Approach 2.....	150
3.4.1 A preliminary study on $\beta$ -carboline functionalization, with inspiration from pyridine chemistry.....	150
3.4.2 Discussion on the products of $\beta$ -carboline substitution reactions.....	153
3.5 Conclusions and future directions.....	155
3.5.1 Six new <i>Picrasma</i> alkaloid analogues were synthesized. ....	155
3.5.2 A novel cascade reaction for access to indoloquinolizines was discovered. ....	156

3.5.3	Complex pentacyclic ring system was synthesized from enamine 3.41 and DDQ. ..	157
3.5.4	Approach 2 provides preliminary studies for developing methodology for the direct functionalization of $\beta$ -carbolines. ....	158
3.6	Experimental .....	160
3.6.1	General chemistry methods.....	160
3.6.2	Synthetic procedures for Approach 1. ....	161
3.6.3	Synthetic procedures for Approach 2. ....	167
3.7	References for Chapter 3 .....	169
<b>Appendix II. Spectra Relevant to Chapter 3 .....</b>		<b>185</b>
<b>Chapter 4: SARS-CoV-2 protease inhibitors .....</b>		<b>200</b>
4.1	Introduction.....	201
4.1.1	SARS-CoV-2 and the COVID-19 global pandemic. ....	201
4.1.2	Learning from older coronaviruses: potential antiviral targets.....	203
4.2	Results and discussion .....	208
4.2.1	Structural comparisons inspire viral replication inhibition screen of existing compounds in the Duerfeldt lab library.....	208
4.2.2	Structure and function of M <sup>Pro</sup> provides insights for the rational design of M <sup>Pro</sup> inhibitors. ....	212
4.2.3	Synthesis of peptidomimetic analogs.....	218
4.2.4	Preliminary biological evaluation for M <sup>Pro</sup> inhibition.....	222

4.3 Conclusions.....	225
4.4 Perspective .....	227
4.5 Experimental.....	229
4.5.1 General chemistry methods.....	229
4.5.2 Synthetic procedures.....	229
4.5.3 Computational methods. ....	235
4.5.4 Viral replication cellular assay.....	235
4.5.5 Enzymatic inhibition assays.....	236
4.6 References for Chapter 4 .....	237
<b>Appendix II. Spectra Relevant to Chapter 4 .....</b>	<b>253</b>

## Table of Figures:

Figure 1.1. General antibiotic resistance mechanisms in Gram-negative bacteria. ....	2
Figure 1.2. New antibiotic drug applications approved by FDA by year interval up to 2019.....	3
Figure 1.3. 2CSTS signaling overview. ....	4
Figure 1.4. Structural evolution towards lead compound. ....	6
Figure 1.5. The general $\beta$ -carboline and tetrahydro- $\beta$ -carboline structure. ....	7
Figure 1.6. $\beta$ -carboline-containing natural products and biologically active compounds.....	8
Figure 1.7. Depiction of isolation process of bis- $\beta$ -carbolines conducted by Yao et al. ....	9
Figure 1.8. Stages of Diabetic Retinopathy through retinal images. ....	15
Figure 1.9. Structures of PPAR active compounds referenced in this section. ....	18
Figure 1.10. Structures of $\beta$ -carboline alkaloids from <i>Picrasma quassioides</i> extracts.....	21
Figure 1.11. Cumulative COVID-19 cases in ten countries by date.....	24
Figure 1.12. (A – C) Compounds with reported antiviral activity, and (D) Existing compounds in the Duerfeldt lab small molecule library. ....	27
Figure 1.13. Structural evolution from ML188 to JG58.....	29
Figure 2.1. CpxRA signaling overview. ....	55
Figure 2.2. Initial SAR reported on the 2,3,4,9-tetrahydro-1 <i>H</i> -carbazol-1-amine chemotype.....	56
Figure 2.3. SAR strategy and rationale for the targeted analogs. ....	57
Figure 2.4. $\beta$ -galactosidase activity of A-ring substituted analogs.....	59
Figure 2.5. Results of “substituent-walk” around the A-ring. ....	60
Figure 2.6. Effects of C-ring deconstruction. ....	61
Figure 2.7. Assessment of amine substitution and stereochemical requirements.....	62
Figure 2.8. Structure of seco-amide analogs synthesized and assessed for CpxRA modulation..	63

Figure 2.9. Intracellular uptake of compounds 2.6 and 2.33 into isogenic <i>E. coli</i> strains that exhibit different efflux efficiencies and controlled permeability of the outer membrane. ....	64
Figure 2.10. Compounds 2.23 and 2.26 induce phospho-CpxR accumulation.....	67
Figure 2.11. Recovery of bacteria from mice urine, bladder, and kidney samples. ....	69
Figure 2.12. Principal component analysis (PCA) of total protein abundance of WT-C26, VC, and Cpx samples.....	71
Figure 2.13. Venn diagram showing the number of proteins differentially expressed in the compound treated versus wild-type and <i>cpxA</i> mutant versus wild-type.....	72
Figure 3.1. Structures of $\beta$ -carboline alkaloids from <i>Picrasma quassioides</i> extracts.....	110
Figure 3.2. The general $\beta$ -carboline structure and IUPAC numbering system.....	113
Figure 3.3. Representative structures of picrasidine C (3.1) and G (3.8) to show differentiation between the two structurally distinct $\beta$ -carboline ring systems.....	115
Figure 3.4 Structure of mono- $\beta$ -carboline alkaloids. ....	116
Figure 3.5. Structure of proposed di-substituted methoxy tryptamine J.....	121
Figure 3.6. Generalized reaction for Step 2. ....	126
Figure 3.7. Criegee mechanism of Ozonolysis. ....	131
Figure 3.8. Structure of mCPBA oxidation product 3.37. ....	133
Figure 3.9. Structure of compound 3.42 showing the (A) atom numbering system and (B) key HMBC correlations to C1' (blue arrows) and C10 (green arrows). ....	141
Figure 3.10. Structure of epoxide product 3.43. ....	142
Figure 3.11. Structure of compound 3.44 showing the (A) atom numbering system and (B) the key HMBC (green arrows), TOCSY (red arrows), and COSY (blue bold bonds) correlations. ....	147
Figure 3.12. Structures and 3D models for three diastereomers of compound 3.44.....	149

Figure 3.13. Pyridine functionalization reactions by (A and B) Knochel and (C) Caubère. ....	151
Figure 3.14. Predicted pKa values of C-H in unsubstituted pyridine (left) and $\beta$ -carboline (right). .....	153
Figure 3.15. Structures of products 3.47 and 3.48 from $\beta$ -carboline substitution reactions. ....	153
Figure 3.16. Structures of novel <i>Picrasma</i> alkaloid analogues. ....	156
Figure 3.17. Representative examples of indoloquinolizine natural products. ....	157
Figure 3.18. Structures of iboga-type alkaloids <i>ervaoffines</i> A and C. ....	158
Figure 4.1. Daily COVID-19 cases in the United States from April 2020 – April 2022. ....	202
Figure 4.2. Atomic model of the external structure of the SARS-CoV-2 virus. ....	204
Figure 4.3. Structures of antiviral compounds referred to in Table 4.15. ....	207
Figure 4.4. Compounds with reported antiviral activity in coronaviruses. ....	209
Figure 4.5. Structurally diverse molecules from the existing Duerfeldt Lab library. ....	210
Figure 4.6. Structure of SARS-CoV-2 M <sup>Pro</sup> dimer. ....	213
Figure 4.7. The active site of SARS-CoV-2 with bound substrates. ....	214
Figure 4.8. SARS-CoV M <sup>Pro</sup> inhibition of ML188 and its enantiomers. ....	215
Figure 4.9. Representation of the rationale design for three M <sup>Pro</sup> inhibitor scaffolds: (A) urea, (B) piperazine, and (C) peptidomimetic. ....	217
Figure 4.10. Structures of peptidomimetic compounds. ....	221
Figure 4.11. Illustration of the principle behind FRET-based protease assay kit. ....	222
Figure 4.12. Boxplot of percent inhibition values for each compound. ....	224
Figure 4.13. Structural evolution from ML188 to JG58. ....	225
Figure 4.14. Structure of Pfizer's orally active M <sup>Pro</sup> inhibitors. ....	226

## **Chapter 1: Introduction**

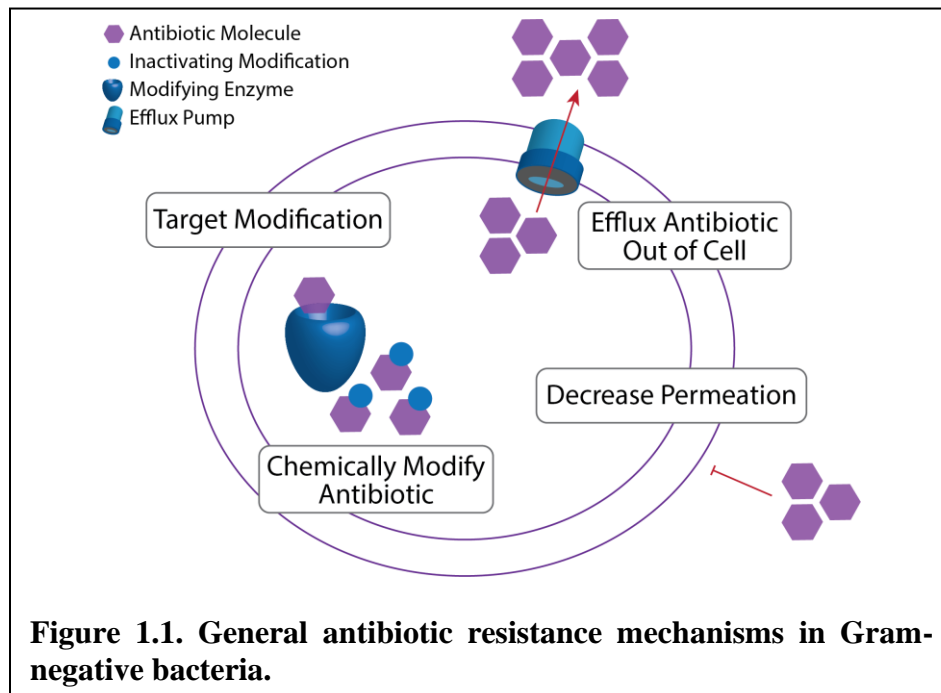
The overall aim of my work is to contribute to molecular design strategies for early lead development while probing structure-activity relationships via the design and synthesis of small molecules. This dissertation will tell three distinct stories: (1) exploitation of CpxRA as a target for virulence modulation in Gram-negative bacteria, (2) the total synthesis of Picrasidine natural product family members, and (3) the rational design and synthesis of SARS-CoV-2 M<sup>pro</sup> inhibitors.

### **1.1 Two-component signal transduction systems and virulence modulation in Gram-negative bacteria.**

#### **1.1.1 An overview of resistance and Gram-negative bacteria.**

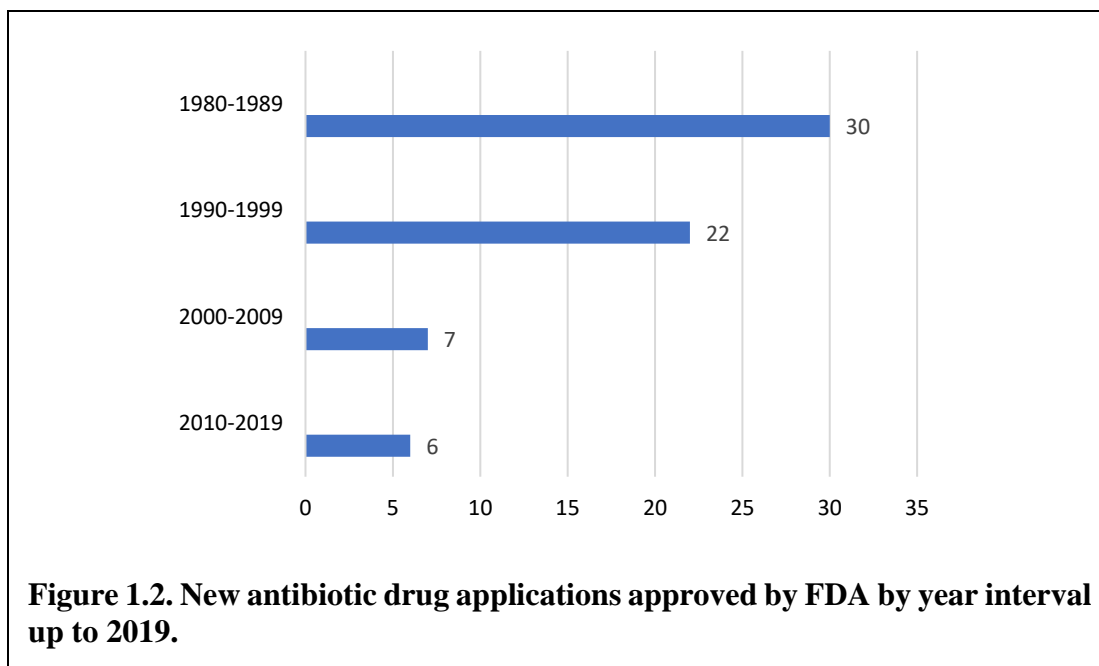
The need to develop novel therapeutics to treat drug-resistant infections is a global public health concern, especially for infections caused by multi-drug resistant (MDR) Gram-negative pathogens. MDR pathogens such as the Enterobacteriaceae family (*Escherichia coli*, *Klebsiella pneumoniae*, *Enterobacter* spp.) are commonly associated with nosocomial infections, which contribute to the deaths of 99,000 patients per year.<sup>1</sup> Gram-negative bacterial envelopes feature a uniquely protective outer membrane (OM), distinguishing them from Gram-positive bacteria.<sup>2</sup> The OM is one of the main reasons for resistance to a wide range of antibiotics,<sup>3</sup> because the OM is an extra barrier that antibiotics must traverse to access their targets. Gram-positive bacteria lack this important layer, which contributes to the importance of developing new therapeutics for MDR pathogens. Gram-negative pathogens exhibit resistance due to a range of mechanisms that prevent antimicrobial action. Common mechanisms of drug resistance leveraged by bacteria include expulsion of drugs by efflux pumps,<sup>4</sup> degradation of drugs by enzymes that irreversibly modify

and inactivate antibiotics,<sup>5</sup> alteration of the target binding site, and decreased membrane permeability (**Figure 1.1**).<sup>6</sup>



For example, *K. pneumoniae* is becoming an increasing threat as some strains carry the carbapenemase gene permitting resistance to colistin, a last-line antibiotic.<sup>7</sup> Many extraintestinal pathogenic *E. coli* strains cause high incidence of morbidity and mortality as a result of extended spectrum beta-lactamases.<sup>8</sup> Urinary tract infection (UTI) is the most common form of extraintestinal infection due to *E. coli*, and *E. coli* is one of the most common causative agents of all types of UTIs with approximately 80% of uncomplicated UTIs in the United States caused by uropathogenic *Escherichia coli* (UPEC).<sup>9</sup> Several common strains of UPEC express extended-spectrum  $\beta$ -lactamase and quinolone resistance, rendering first-line defense antibiotics ineffective. With the growing number of MDR pathogens, common infections typically considered manageable—such as urinary tract, surgical wound, and respiratory infections—could soon become untreatable.<sup>10</sup>





Despite the undeniable need for antibiotics with novel mechanisms of action, only two new classes of antibiotics have reached the market since 1962,<sup>11</sup> and the number of new antibiotics developed and approved has steadily decreased over the past three decades (**Figure 1.2**).<sup>12</sup> The current arsenal of antibacterials target a limited number of essential enzymes and processes, and resistance evolution now outpaces our ability to derivatize known chemotypes and advance the new entities through clinical evaluation. Modern approaches for developing new antibiotics include identifying new targets, but, despite great effort, very few new targets have been identified for Gram-negative bacteria in the last 50 years. In contrast to the dogma that only compounds that completely inhibit cell growth will find clinical utility, one strategy gaining significant traction is to render organisms vulnerable to host immune clearance by targeting virulence determinants or processes that control the expression of pathogenicity. In this context, bacterial two-component signal transduction systems (2CSTS) represent promising targets.

### 1.1.2 CpxRA phosphatase inhibition and 2CSTS as antibacterial targets.

Bacterial 2CSTS are an attractive target for antibacterial studies because there are no mammalian homologs and involve the phosphorylation of amino acids that differ from the targets of mammalian phosphatases and kinases.<sup>13</sup> Bacteria have evolved 2CSTS, which are generally composed of a histidine kinase (HK) and a response regulator (RR), to respond to environmental changes.<sup>14</sup> Bacterial 2CSTS are conserved across many drug-resistant Gram-negative pathogens and are known to regulate gene transcription involved in cell growth, envelope integrity, quorum sensing, and expression of virulence factors.<sup>15</sup> As such, modulation of these systems represents a promising antibacterial strategy and is expected to exhibit complementarity to existing approaches. 2CSTS activators do not cause cell death but have the potential to downregulate the expression of virulence factors, allowing the host's immune system to clear the infection.

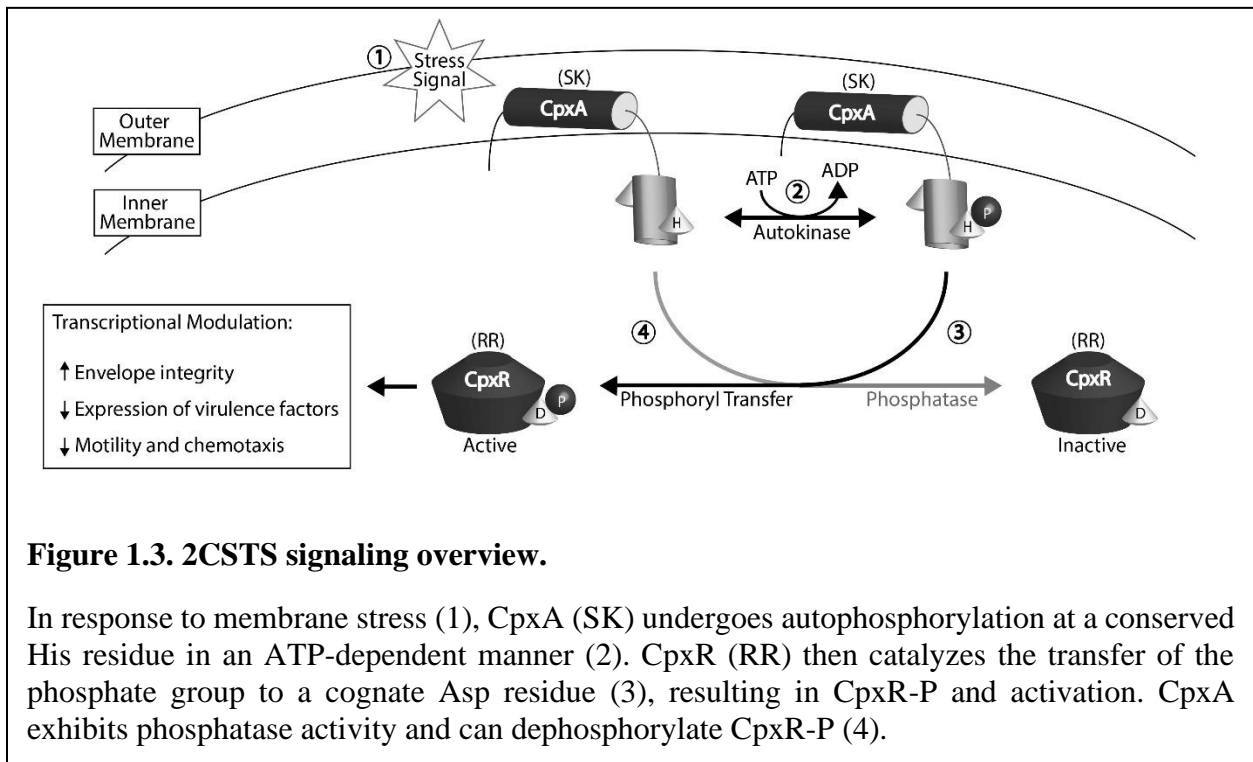


**Figure 1.3. 2CSTS signaling overview.**

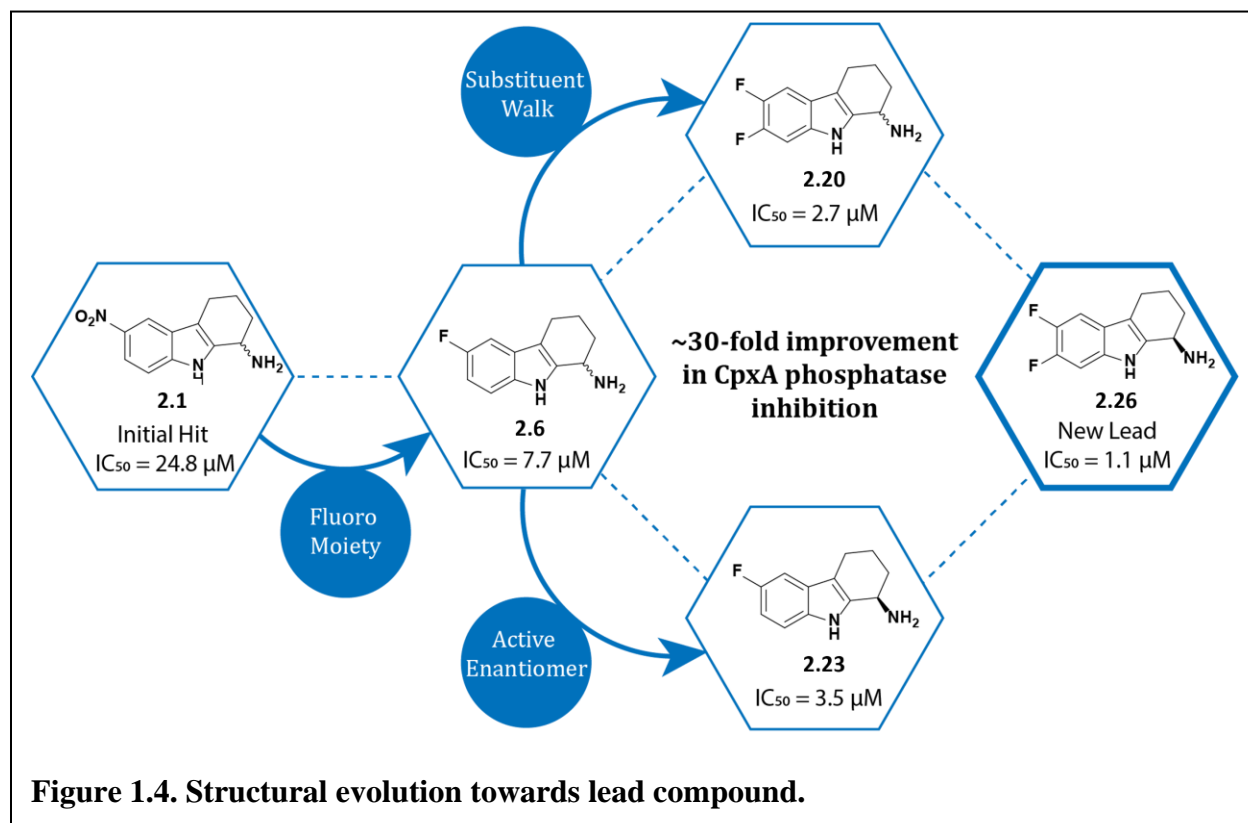
In response to membrane stress (1), CpxA (SK) undergoes autophosphorylation at a conserved His residue in an ATP-dependent manner (2). CpxR (RR) then catalyzes the transfer of the phosphate group to a cognate Asp residue (3), resulting in CpxR-P and activation. CpxA exhibits phosphatase activity and can dephosphorylate CpxR-P (4).

CpxRA is a 2CSTS found in many drug-resistant Gram-negative pathogens and genetic activation of CpxRA abolishes the virulence of a number of pathogens in murine models. CpxRA, composed of signal kinase CpxA and its corresponding response regulator CpxR, is a 2CSTS found in many drug-resistant Gram-negative bacteria. The CpxRA system regulates the transcription of approximately 100 genes where its activation results in the upregulation of envelope integrity maintenance factors and the downregulation of secreted virulence factors. An overview of the CpxRA signaling pathway is provided in **Figure 1.3**. Briefly, in response to envelope stress, CpxA autophosphorylates on a histidine residue and donates a phosphoryl group to an aspartic acid residue on CpxR. CpxA also has phosphatase activity for phosphorylated CpxR (CpxR-P), and in the absence of envelope stress, CpxA acts as a phosphatase and CpxR remains inactive (**Figure 1.3**). Thus, accumulation of CpxR-P is indicative of activation of the CpxRA system.

### **1.1.3 Summary of accomplishments.**

Recently, 2,3,4,9-tetrahydro-1*H*-carbazol-1-amines were shown to activate the CpxRA system by inhibiting the phosphatase activity of CpxA. **Chapter 1** will report collaborative efforts on the initial structure-activity relationships of this scaffold by focusing on three approaches: 1) A-ring substitution, 2) B-ring deconstruction to provide N-arylated amino acid derivatives and 3) C-ring elimination to give 2-ethylamino substituted indoles. This molecular deconstruction approach, outlined in **Figure 1.4**, helped to identify a new lead compound **2.26**, which manifests a ~30-fold improvement in CpxA phosphatase inhibition over the initial hit, compound **2.1**. The activity of **2.26** was assessed in mouse UTI models for its ability to alter UPEC cell fitness in the urine, bladder, and kidneys. Genetic- versus chemo-modulation of the CpxRA 2CSTS was assessed with bacterial cell assays, human urine samples, and proteomics analysis. This work provides useful structure-activity relationships and a foundation for which to advance the

carbazolamine tools towards uncovering new biology and further understanding the biological significance and therapeutic potential of CpxRA and 2CSTS in general.



## 1.2 Natural product total synthesis and *Picrasma* alkaloids

### 1.2.1 Natural products and the utility of total synthesis.

Natural products and their synthetic analogs have been a consistent source of new therapeutics to treat a number of ailments and diseases. Historically, natural products have played a key role in drug discovery,<sup>16</sup> especially for cancer and infectious diseases,<sup>17</sup> but also in other therapeutic areas, such as cardiovascular and metabolic disorders.<sup>18</sup> The original written records on medicinal applications of natural sources date back thousands of years. For example, in 2600 BC the sophisticated medical system of Mesopotamia listed ~1,000 plant-derived medicines, the

most preserved record of Egyptian medicine is the “Ebers Papyrus” from about 1550 BC, and traditional Chinese medicine has been extensively documented over thousands of years.<sup>19</sup>

Medicinal plants used in those ancient times were only applied on an empirical basis, since knowledge of pharmacological activities and mechanisms of their active constituents were nonexistent. Fortunately, isolation techniques, chemical synthesis methodology, and mechanistic studies have since evolved tremendously to allow for significant drug discovery advancements. For instance, a German apothecary assistant, Friedrich Sertürner, succeeded in isolating morphine from opium as early as 1817. Sertürner published a comprehensive paper on morphine’s isolation, crystallization, crystal structure, and pharmacological properties (first studied in stray dogs and then self-experiments).<sup>20</sup> Since then, many bioactive natural products, primarily alkaloids<sup>21</sup> (e.g., quinine,<sup>22</sup> caffeine,<sup>23</sup> nicotine,<sup>24</sup> cocaine<sup>25</sup>), have been isolated from their natural sources.<sup>19</sup> For example, early transformations of traditional medicine into modern drugs include the antimalarial alkaloid quinine isolated from *Cinchona* bark in 1820.<sup>26</sup>

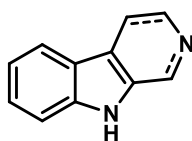
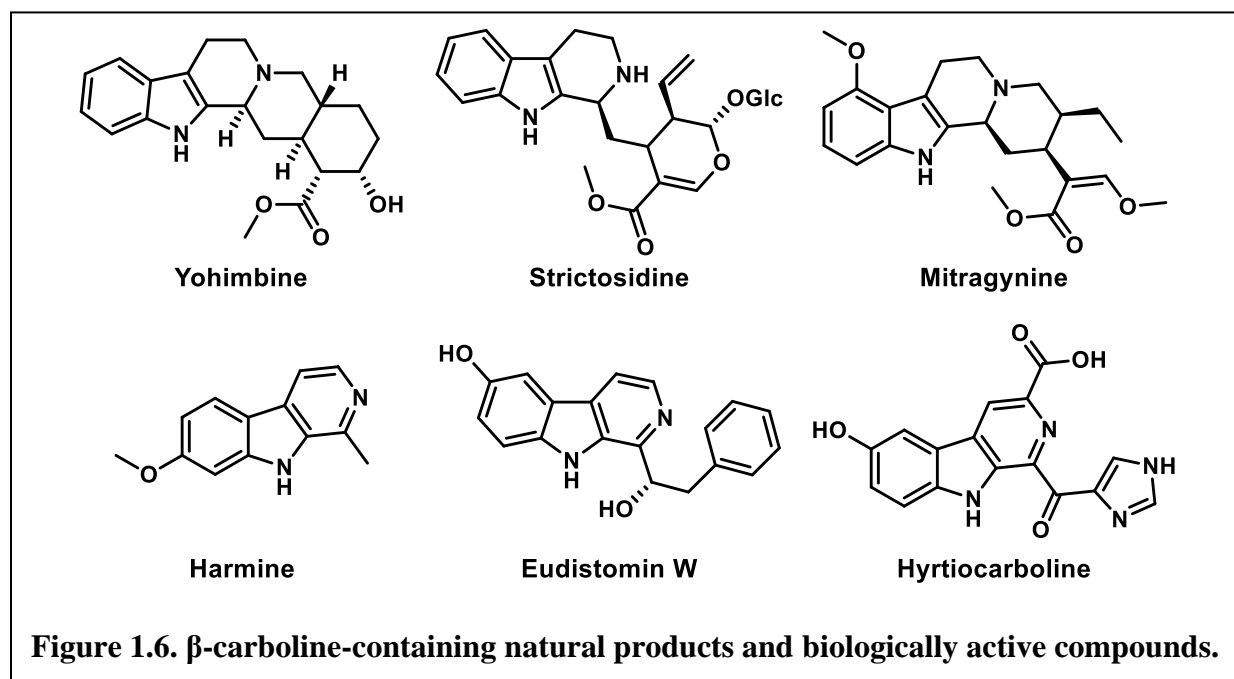


**Figure 1.5. The general  $\beta$ -carboline and tetrahydro- $\beta$ -carboline structure.**

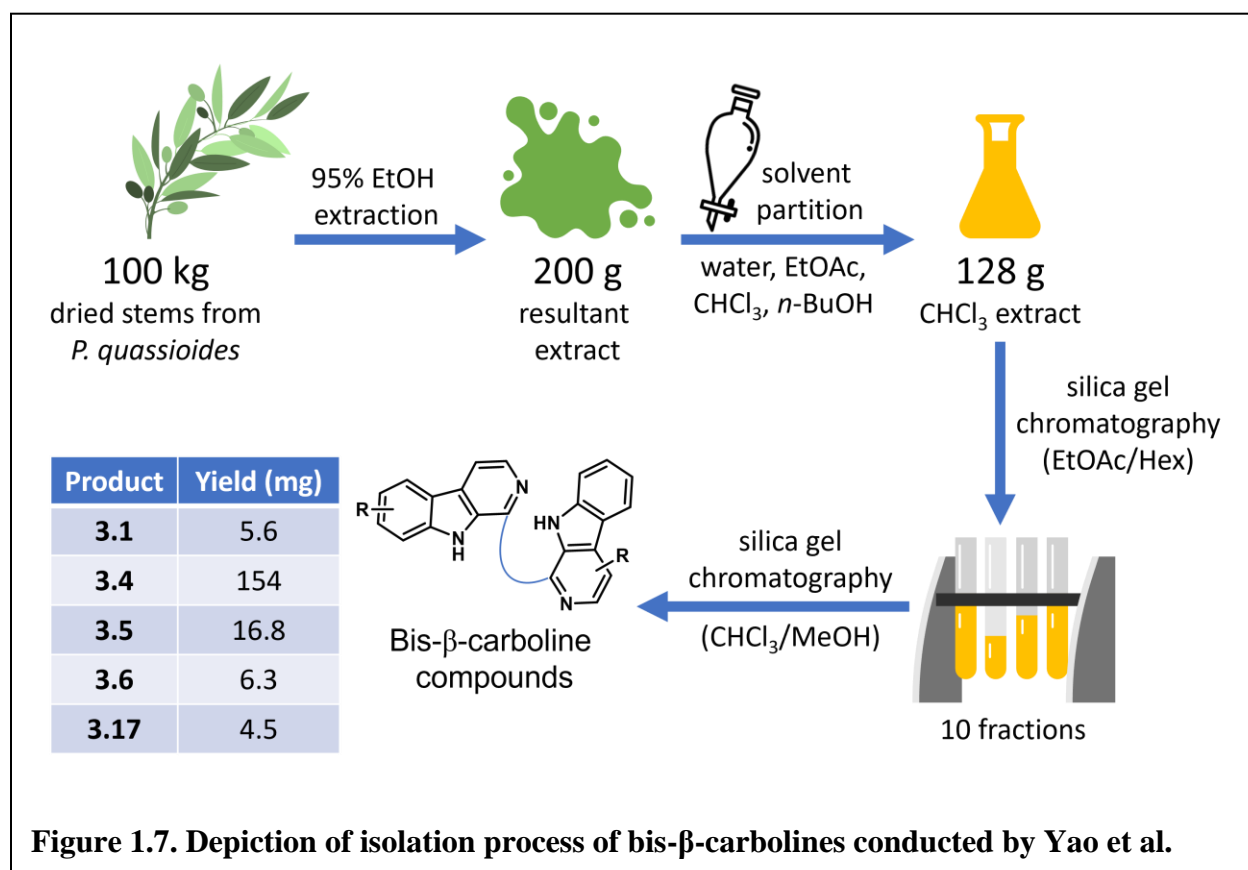
Generally defined as naturally occurring organic compounds containing one or more basic nitrogen atoms, alkaloids are a large and structurally diverse group of natural products provided by a vast range of organisms, and they exhibit a broad spectrum of biological activities.<sup>27</sup> Within the alkaloid class of natural products, the  $\beta$ -carboline and its saturated relative, tetrahydro- $\beta$ -carboline (THBC), are widely present. Classified by a tricyclic 9H-pyrido[3,4-b]indole framework

(**Figure 1.5**), the  $\beta$ -carboline scaffold can be observed in diverse natural sources encompassing a variety of biological activities. Examples of this chemical family include yohimbine ( $\alpha_2$ -adrenergic receptor antagonist),<sup>28</sup> strictosidine (common biosynthetic intermediate),<sup>29</sup> mitragynine (partial  $\mu$ -opioid agonist),<sup>30</sup> harmine (monoamine oxidase inhibitor),<sup>31</sup> eudistomins (cytotoxic, antitumor, and antiviral properties),<sup>32</sup> hyrtiocarboline (antiproliferative activity against lung and lymphoma cancer cell lines)<sup>33</sup> (**Figure 1.6**).



One challenge in plant-derived natural product drug discovery involves accessibility of starting materials. The lab-intensive and time-consuming extraction and isolation process serves as a bottle neck in drug development, because the amounts of active ingredients in natural medicines are usually fairly low.<sup>34</sup> One example of a low-yielding yet pharmaceutically important natural product family is the *Picrasma* alkaloids. The isolation process of the bis- $\beta$ -carboline quassidine compounds from *Picrasma quassioides* stems by Yao et al.<sup>35</sup> exemplifies the tedious isolation work of natural product drug discovery and is depicted in **Figure 1.7**. Briefly, the

resultant ethanol extract from 100 kg of plant material is dried, diluted with water, then partitioned between ethyl acetate, chloroform, and *n*-butanol. Dried chloroform-soluble material (128 g) was then purified via silica gel chromatography to afford ten fractions, which were further purified to obtain 5.6 mg of picrasidine C (**3.1**), 154 mg of quassidine B (**3.4**), 16.8 mg of quassidine C (**3.5**), 6.3 mg of quassidine D (**3.6**), and 4.5 mg of quassidine A (**3.17**).<sup>35</sup> These compounds and their structures will be further discussed in **Section 1.2.4** of this chapter (**Figure 1.10**), but the complex process of converting 100 kg of plant material into mere milligrams of pharmacologically relevant compounds exemplifies an important challenge when developing natural product-derived medicines.



When natural product isolation is not sustainable or scalable, opportunity arises for the development of routes to provide synthetic access to natural products. The prototypical example

of this is paclitaxel (Taxol), a transformational anticancer drug. Extraction from natural sources required material from thousands of trees to obtain sufficient quantities for clinical use. This consumption of the Yew tree is largely responsible for the ~30% decline in Pacific Yew populations over the last three generations, ultimately leading to the addition of the Pacific Yew tree to the “Near Threatened” species list.<sup>36</sup> This ecological impact and the general scarcity of Taxol prompted a formidable challenge to synthetic chemists. The first total synthesis of Taxol was completed in 1994,<sup>37</sup> but several other synthetic strategies have followed.<sup>38–40</sup> Complex total syntheses, not only provides an alternative source of important molecules, but it also opens diversification opportunities not often accessible through semi-synthesis efforts and gives rise to new synthetic methodologies that can impact the broader scientific community. Thus, total synthesis is a valuable tool capable of providing scientific impact well beyond the boundaries of the initial goal of obtaining the target molecule.

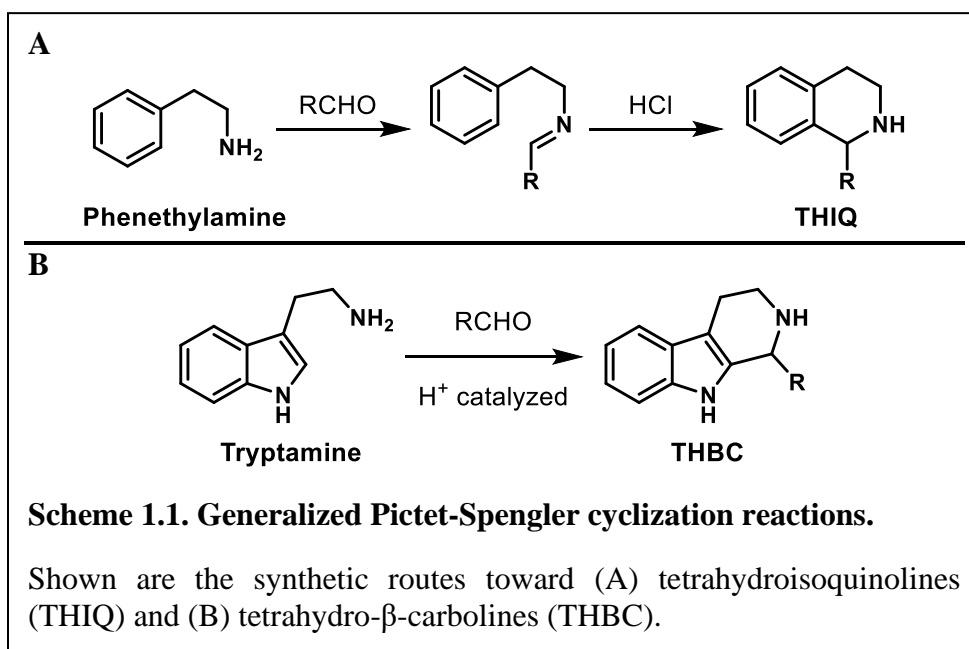
### **1.2.2 The synthesis of $\beta$ -carbolines and related alkaloids.**

As mentioned in the previous section,  $\beta$ -carboline-containing alkaloids exhibit a widespread range of pharmacological activities. The  $\beta$ -carboline heterocycle is also a very important synthetic intermediate for a variety of pharmaceutically relevant natural products and drug molecules.<sup>41</sup> The structure of  $\beta$ -carboline consists of an indole skeleton fused to a pyridine ring. While the synthesis of  $\beta$ -carboline can be completed via metal-catalyzed<sup>42</sup> or biosynthetic<sup>43</sup> methods, the most straightforward and widely applicable reaction for the synthesis of  $\beta$ -carbolines is the Pictet-Spengler cyclization reaction.

Discovered in 1911 by Ame Pictet and Theodor Spengler, the Pictet-Spengler reaction (PSR) is a condensation reaction between a  $\beta$ -arylethylamine and a carbonyl compound (aldehyde or ketone) followed by ring closure.<sup>44</sup> The PSR was originally used to transform phenethylamine

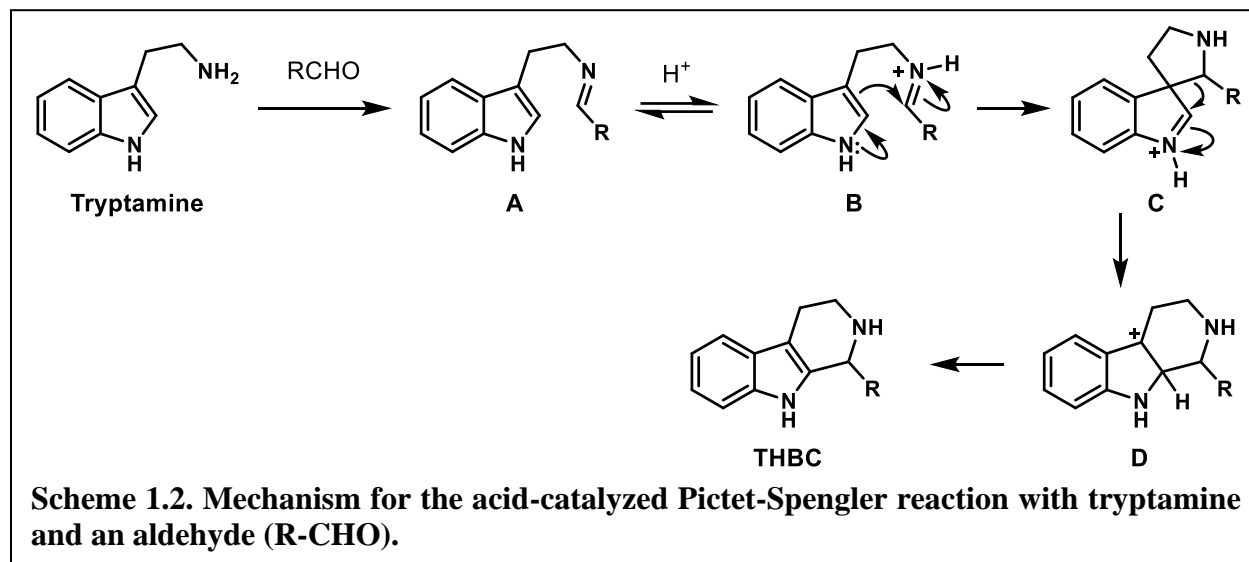


to tetrahydroisoquinolines (**Scheme 1.1A**), but it is more well-known and widely used today for the formation of tetrahydro- $\beta$ -carbolines (THBC) from tryptamine starting materials (**Scheme 1.1B**).<sup>45</sup> Tetrahydroisoquinolines (THIQ) and THBCs represent key elements of an immense range of structurally complex synthetic products, including thousands of naturally occurring indole and isoquinoline alkaloids. The multifunctional PSR has significant synthetic value, since the amine and aldehyde components can vary widely, allowing for the construction of structurally diverse THIQ and THBC ring systems.



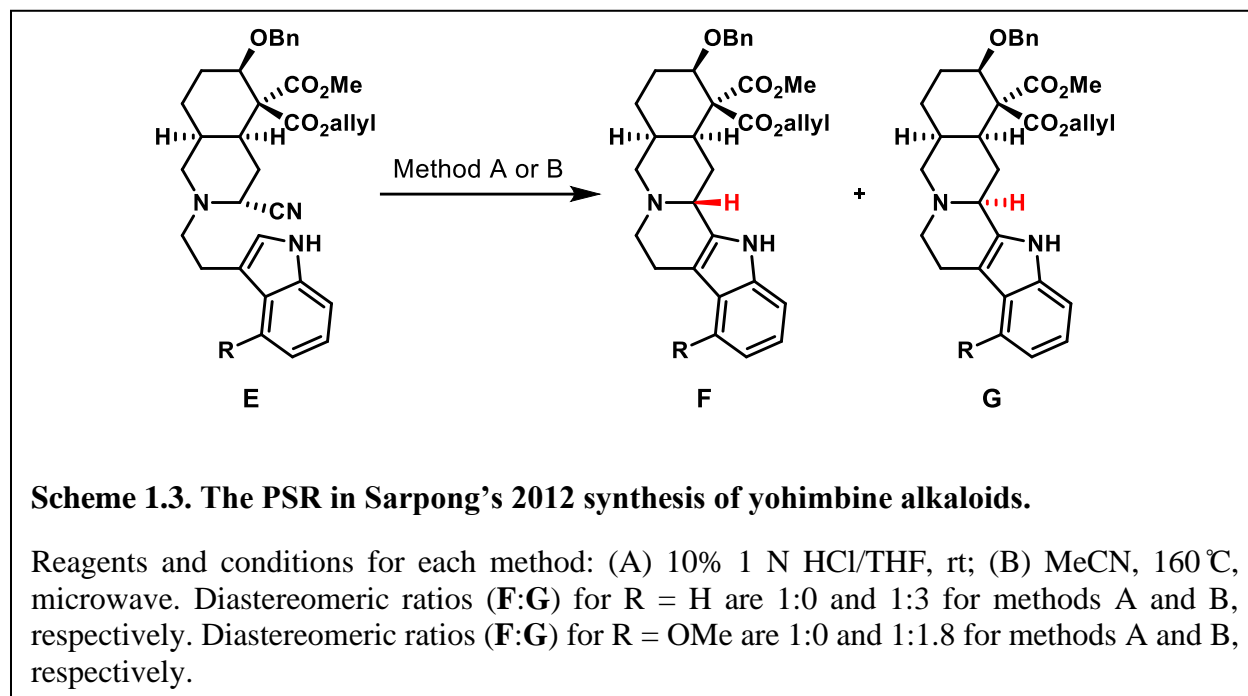
The general mechanism for the formation of THBC from tryptamine and a generic aldehyde (R-CHO) is shown in **Scheme 1.2**. The mechanism begins with the formation of imine **A**, following a condensation reaction. Protonation by the acid catalyst then provides iminium intermediate **B**, which exhibits stronger electrophilicity than its non-protonated counterpart. Cyclization follows where nucleophilic attack from the indole 3-position onto the iminium carbon atom results in spirocyclic intermediate **C**, which readily undergoes ring expansion to form the

piperidine fused tricyclic system (**D**). Re-aromatization of the indole ring provides the energetic “sink” to produce the final THBC product.



This mechanism has been extensively studied, especially in the context of condensations with highly reactive indoles such as tryptamine.<sup>46</sup> Cook et al. reviewed the PSR of benzaldehyde and tryptamine and found the yields for THBC formation to be higher in aprotic media as opposed to aqueous media.<sup>47</sup> The electrophilicity of the imine double bond was the limiting factor, which determined whether cyclization would proceed. Shudo et al. identified a linear relationship between the rate of cyclization and the acidity of the reaction media by carrying out kinetic studies of the PSR with phenethylamines and various benzaldehydes in the presence of trifluoroacetic acid (TFA), trifluoromethanesulfonic acid (TFSA), or a mixture of the two.<sup>48</sup> It was found that the imine is not electrophilic enough for ring closure, but the iminium ion is capable of undergoing the cyclization reaction. Combined, the results of these two studies suggest that prototypical PSR conditions involve a strong acid such as trifluoroacetic acid (TFA) in aprotic media. However, the PSR can occur under a wide variety of reaction conditions, including but not limited to 1) Lewis

acid-mediated enantioselective PSRs,<sup>49</sup> 2) base-mediated PSRs,<sup>50</sup> 3) substitution of tryptophan for tryptamine,<sup>51</sup> 4) PSRs of ketimines derived from alkyl ketones,<sup>52</sup> and 5) enzyme-catalyzed biosynthetic PSRs.<sup>53</sup>



The multifaceted PSR has been relied upon for the synthesis of numerous  $\beta$ -carboline-containing natural products and biologically relevant molecules, and its adaptability allows for its utilization in future total synthesis projects, as well. The total synthesis of yohimbine alkaloids by Sarpong et al. is an exemplary application of PSR versatility. In their synthetic studies,<sup>54</sup> indole-containing aminonitrile **E** was subjected to PSR conditions, with special attention paid to the role that arene nucleophilicity plays in the stereoselectivity of pentacycle formation (**Scheme 1.3**). Treatment of **E** (R = H) with hydrochloric acid (10% 1 N HCl in tetrahydrofuran at 23 °C, method A) resulted in the exclusive formation of  $\beta$ -diastereomer **F**, while the thermal PSR (heating **E** to 160 °C in acetonitrile, method B) afforded a mixture of diastereomers (**Scheme 1.3**). Notably, method A consistently selected for a single diastereomer (**F**), even when employing 4- or 6-

methoxyindole analogs of **E**. Method B, on the other hand, gave disparate diastereoselectivities influenced greatly by the nature of the indole fragment. This specific study is interesting because it demonstrates the versatility of the PSR from two different approaches: (1) variability in indole constituents alters arene nucleophilicity and (2) aminonitrile moieties provide an alternate imine precursor. It was previously reported by Stork et al. that the iminium intermediate forms when the cyanide from the aminonitrile moiety undergoes elimination upon refluxing in acetonitrile.<sup>55</sup>

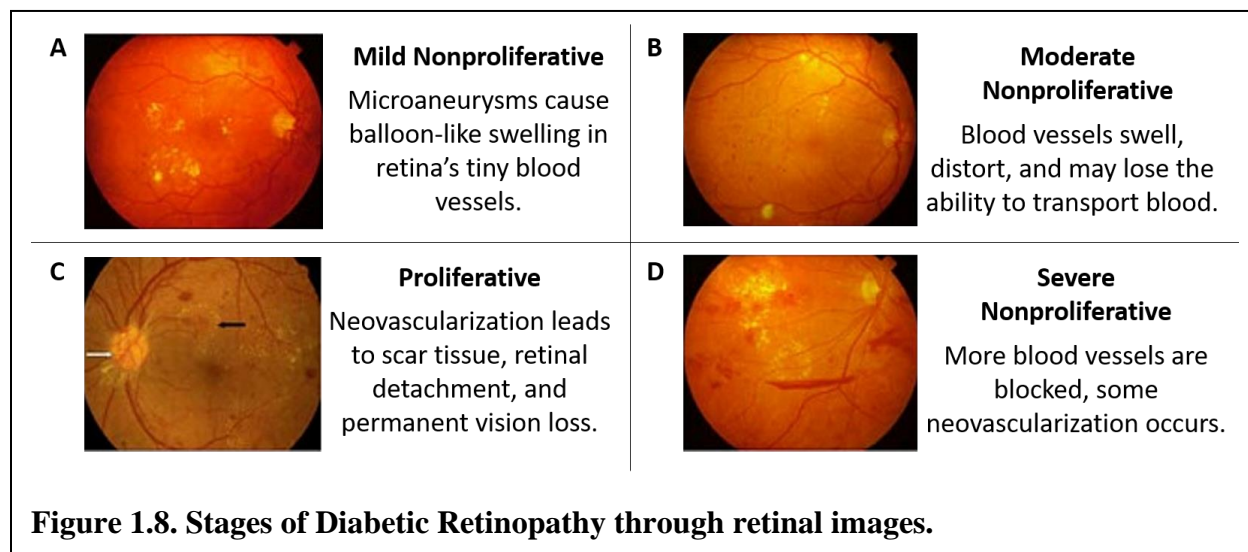
Among the many advantages of PSRs, this acid-catalyzed reaction also has green chemistry implications because of its efficient atom economy and a byproduct of only one water molecule. The PSR is one of the most direct and efficient synthetic methods for the construction of important privileged pharmacophores such as THIQs, THBCs, and poly-heterocycles embodying them.<sup>56</sup> This reaction is also highly variable, however. The abundant versatility of the PSR makes it both an invaluable tool and a challenging puzzle for synthetic chemistry, as reaction conditions must be tuned and optimized to specific substrates. Highlighted examples of parameters and constituents that are amenable to modification are as follows:<sup>57</sup>

1. Increased nucleophilicity of the amine-containing reagent, or increased electrophilicity of the carbonyl component can affect PSR reaction rates.<sup>58</sup>
2. Solvent choice, temperature, amount of acid, and reaction time influence the final results of the PSR.<sup>59</sup>
3. Stereoselectivity can be influenced by chiral carbonyl derivatives<sup>60</sup> or chiral auxiliaries.<sup>61,62</sup>

The PSR might be extremely adaptable and useful, but elegance and efficiency must still be fine-tuned, especially for complex structural architectures.

### 1.2.3 Interests in picrasidine C as a subtype selective PPAR $\alpha$ agonist and its implications in diabetic retinopathy.

Diabetic retinopathy (DR), a common complication of diabetes, is a leading cause of blindness in developed countries.<sup>63</sup> It is projected that nearly all type 1 diabetes patients and 60% of type 2 diabetes patients will be diagnosed with some form of DR after 20 years of disease, as the prevalence of DR grows proportionally to the duration of diabetes.<sup>64</sup> DR is classified into two categories, namely nonproliferative diabetic retinopathy (NPDR) and proliferative diabetic retinopathy (PDR), characterized by absence or presence retinal neovascularization, respectively.<sup>65</sup> NPDR is further divided into mild, moderate and severe stages, representative images of the retina at each stage are in **Figure 1.8**.<sup>66</sup>

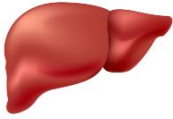




With severe, sight-threatening DR, there are few commonly used intervention treatments currently available. The first is laser photocoagulation, which applies light energy to the retina with the aim of stopping the growth and development of new blood vessels.<sup>67</sup> The second is vitrectomy, a surgical procedure to remove some or all of the vitreous humor, the eye's clear

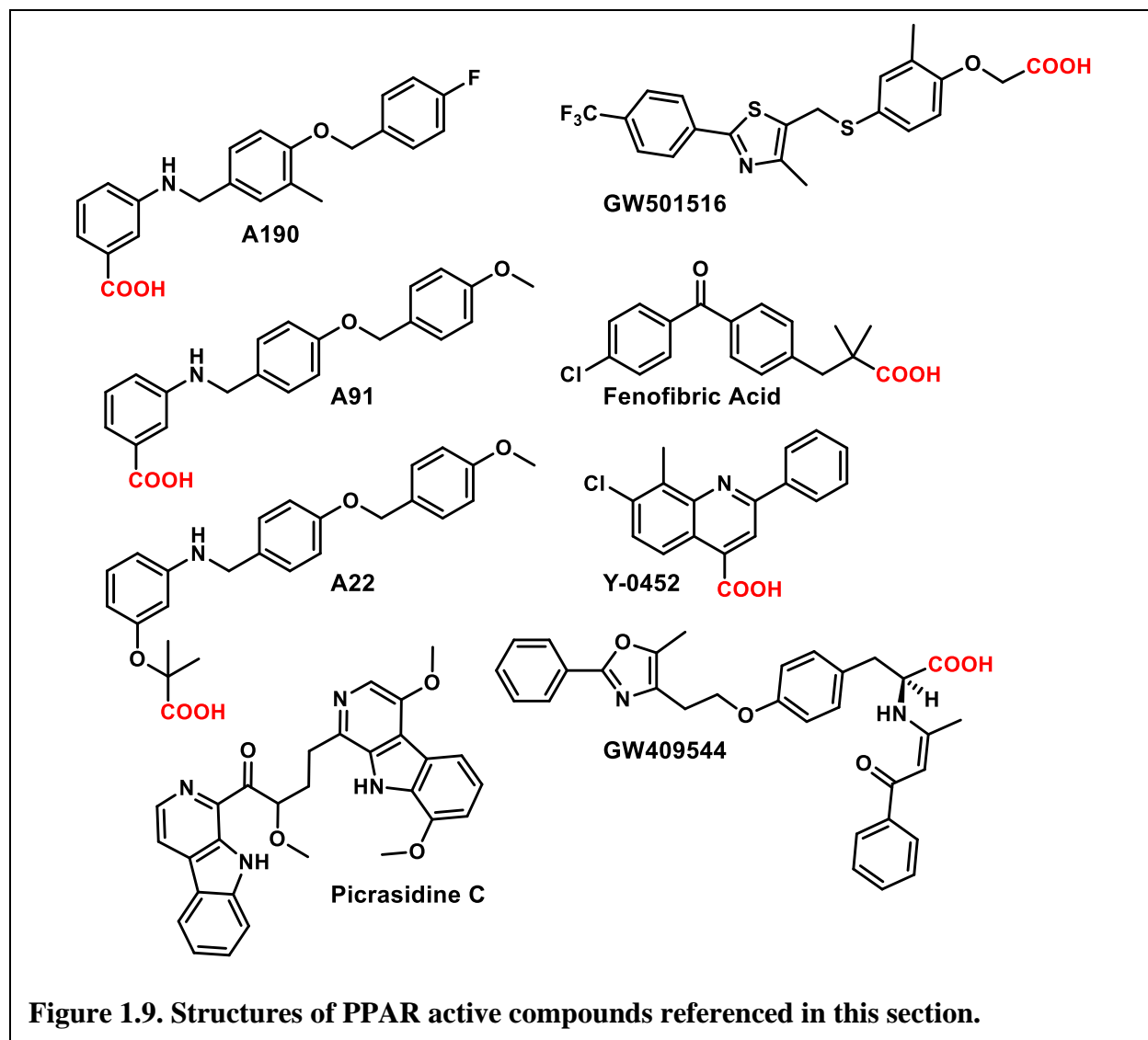
internal jelly.<sup>68</sup> Finally, intravitreal injections of anti-vascular endothelial growth factor (VEGF) drugs inhibit angiogenesis and vascular permeability, sometimes resulting in reduced pressure build up in the eye from fluid retention to help improve vision.<sup>69</sup> These treatments are effective in reducing vision loss, but they only address signs and symptoms rather than providing a cure for DR.<sup>70</sup> The long-term efficacy of anti-VEGF therapy has also been thoroughly questioned and evidence of a therapeutic “ceiling” for such treatments limit improvement of visual acuity.<sup>71</sup> As such, with uncomfortable recovery times and possible surgical complications, there is an obvious and undeniable need for non-invasive DR treatments.

One target gaining significant traction for the development of diabetes and DR chemotherapeutics is PPAR $\alpha$ . The peroxisome proliferator-activated receptors (PPARs) are transcription factors that play essential roles in the regulation of glucose, lipid, and cholesterol metabolism.<sup>72</sup> Notably, they were originally named PPARs because of their ability to induce peroxisome proliferation in rodents, but this function is not believed to occur in humans.<sup>73</sup> In humans, the PPAR superfamily comprises three subtypes (PPAR $\alpha$ , PPAR $\gamma$ , and PPAR $\delta$ ), a group of nuclear receptor proteins that bind to fatty acids and regulate energy production, lipid metabolism, and inflammation in a ligand-dependent manner.<sup>74</sup> While the PPARs share functional similarities and significant sequence homologies, isoform distribution varies depending on tissue location (**Table 1.1**), allowing for selectively targeting individual isoforms.<sup>75</sup>

**Table 1.1. Main metabolic functions regulated by PPARs.<sup>75</sup>**

		Liver 	Muscle 	Adipose Tissue 
Lipid utilization	PPAR $\alpha$	<ul style="list-style-type: none"> <li>- Fatty acid oxidation</li> <li>- Response to fasting</li> </ul>	<ul style="list-style-type: none"> <li>- Fatty acid oxidation</li> <li>- Energy uncoupling</li> </ul>	
	PPAR $\delta$		<ul style="list-style-type: none"> <li>- Fatty acid oxidation</li> <li>- Energy uncoupling</li> </ul>	<ul style="list-style-type: none"> <li>- Fatty acid oxidation</li> <li>- Energy uncoupling</li> </ul>
Lipid storage and insulin sensitivity	PPAR $\gamma$	<ul style="list-style-type: none"> <li>- Lipogenesis</li> <li>- Insulin sensitivity</li> </ul>	<ul style="list-style-type: none"> <li>- Insulin sensitivity</li> </ul>	<ul style="list-style-type: none"> <li>- Adipocyte differentiation</li> <li>- Adipocyte survival</li> <li>- Lipogenesis</li> <li>- Adipokine secretion</li> <li>- Insulin sensitivity</li> </ul>

The isoform that our lab is interested in is PPAR $\alpha$ , because its agonists have shown therapeutic effects towards the treatment of DR by influencing the regulation of inflammatory factors (TNF- $\alpha$ , intercellular adhesion molecule-1 (ICAM-1), and VEGF),<sup>76</sup> mitochondrial function, apoptosis, and neovascularization in the diabetic retina.<sup>77</sup> The therapeutic effects of PPAR $\alpha$  agonists have also been confirmed in the Fenofibrate Intervention and Event Lowering in Diabetes FIELD<sup>78</sup> clinical study in which fenofibrate, an orally administered fibric acid derivative, reduced the progression rates of DR in patients with type 2 diabetes. Since fenofibrate is weakly potent,<sup>79</sup> only shows modest selectivity for PPAR $\alpha$  over other PPAR subtypes,<sup>80</sup> and has dose-limiting adverse effects such as hepatotoxicity and renal failure,<sup>81</sup> novel PPAR $\alpha$  agonists are desired to allow the continued development and clinical exploitation of PPAR $\alpha$  agonism for the treatment of DR.



Several compounds are currently in the pipeline for PPAR-targeting drugs (representative structures in **Figure 1.9**). The major challenge presented by the search for PPAR $\alpha$  agonists is subtype selectivity. Fortunately, the PPAR isoforms crystallize well and the existence of several apo and ligand bound structures provides tools for structure-based design. Several groups have since demonstrated the capability of selectively targeting specific PPAR isoforms, and select examples are featured in **Table 1.2**. GW409544 is a good example of a non-selective PPAR $\alpha$  agonist ( $EC_{50} = 2.3$  nM) because of its shared affinity for PPAR $\gamma$  ( $EC_{50} = 0.28$  nM) as well.<sup>82</sup> In contrast, GW501516 exhibits exclusive subtype selectivity for PPAR $\delta$  agonism ( $EC_{50} = 24$  nM).<sup>83</sup>



Recently, our lab published the structure-guided evolution of PPAR $\alpha$  selective agonists arising from a novel 2-phenyl-4-carboxyquinoline chemotype.<sup>84</sup> Leveraging *in silico* methods to provide structural guidance for PPAR $\alpha$  selectivity, the quinoline core was deconstructed to develop less rigid and more elongated compounds such as A22,<sup>84</sup> A91,<sup>85</sup> and A190,<sup>86</sup> while demonstrating how minor structural modifications can affect isoform selectivity. In this chemotype, A22 incorporates the fibrate head-group and is a pan-PPAR agonist, while A190 and A91 are highly selective for PPAR $\alpha$ . Interestingly, the methyl group in A190 dramatically improves binding affinity to PPAR $\alpha$  isoform (~38-fold),<sup>85</sup> demonstrating the “magic methyl” effect, a phenomena in medicinal chemistry where dramatic change in affinity can be seen with the addition of a single methyl group in a very specific position.<sup>87</sup> See **Figure 1.9** and **Table 1.2** for structures and EC<sub>50</sub> values, respectively.

**Table 1.2. PPAR agonism of select compounds to demonstrate isoform selectivity.**

Compound	Experiment	EC <sub>50</sub>		
		PPAR $\alpha$	PPAR $\delta$	PPAR $\gamma$
GW501516 <sup>83</sup>	a	ND	24 nM <sup>a</sup>	ND
GW409544 <sup>82</sup>	b	2.3 nM	>10 $\mu$ M	0.28 nM
A91 <sup>85</sup>	c	4.43 $\mu$ M	>100 $\mu$ M	>100 $\mu$ M
A190 <sup>85</sup>	c	0.037 $\mu$ M	>100 $\mu$ M	>100 $\mu$ M
A22 <sup>84</sup>	c	25.3 $\mu$ M	38.6 $\mu$ M	18.3 $\mu$ M
Y-0452 <sup>84</sup>	c	52.4 $\mu$ M	ND	ND
Picrasidine C <sup>88</sup>	c	10 $\mu$ M	ND	ND
Rosiglitazone <sup>82</sup>	b	>10 $\mu$ M	>10 $\mu$ M	0.018 $\mu$ M

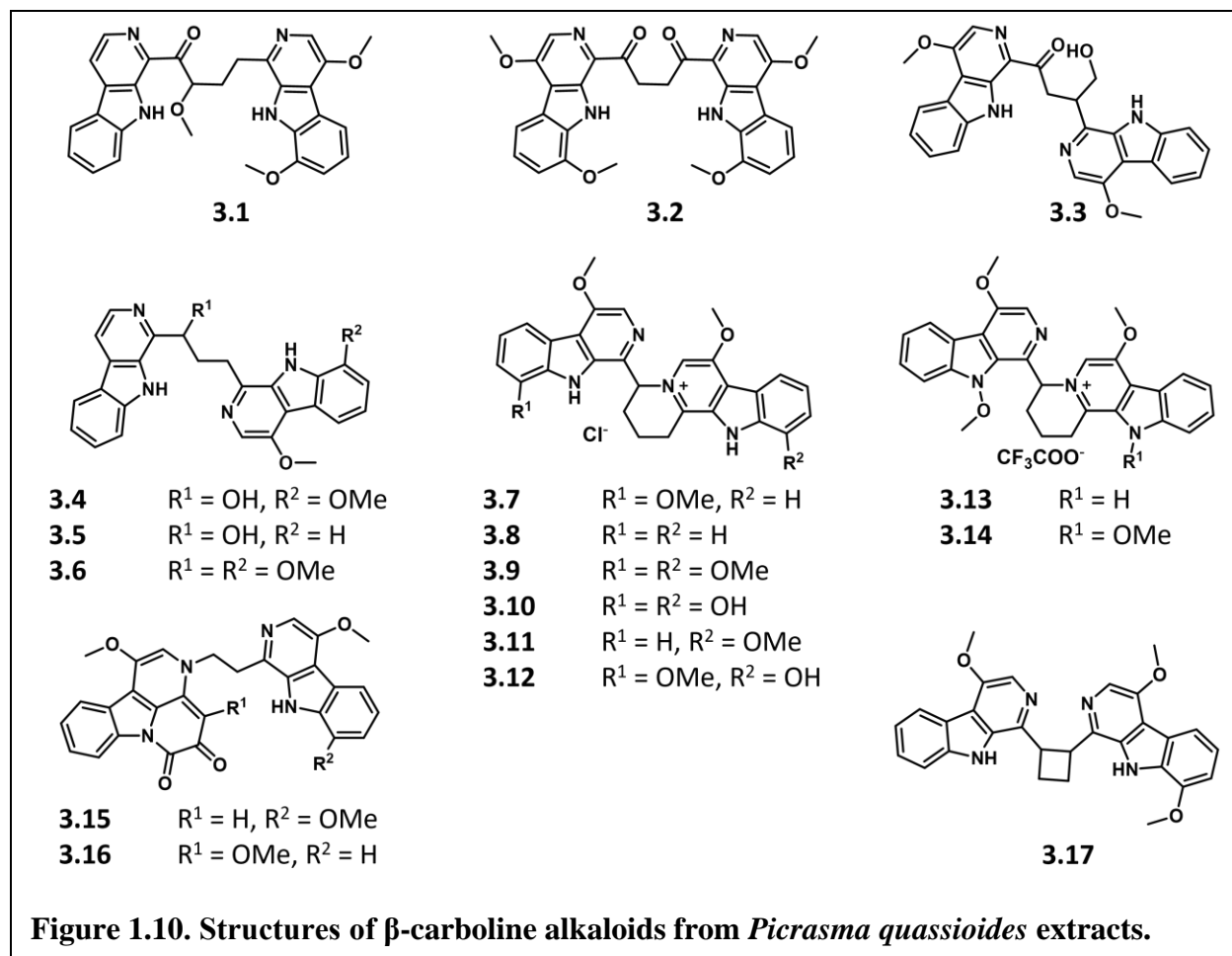
Data are represented as the EC<sub>50</sub> of the corresponding (a) activation of mouse PPAR-GAL4 chimeric receptor, (b) activation of human PPAR-GAL4 chimeric receptor, or (c) human PPAR agonism in luciferase reporter cell lines. ND = No Data.

With our interest in developing selective PPAR $\alpha$  agonists, we became interested in the natural product picrasidine C (**3.1**), which was recently reported to selectively induce mRNA expression of PPAR $\alpha$ -regulated genes in a concentration-dependent manner.<sup>88</sup> Compound **1** is a

pseudo dimeric  $\beta$ -carboline alkaloid first isolated from the root wood of *Picrasma quassioides* (Simaroubaceae, Japanese name “Nigaki”) in 1983.<sup>89</sup> Interestingly, picrasidine C is structurally different from traditional PPAR $\alpha$  agonists, as it does not include the seemingly integral carboxylic acid pharmacophore (atoms labeled in red in **Figure 1.9**). Because of the stark structural difference of **3.1** compared to prototypical PPAR $\alpha$  agonists, this natural product opens new chemical space for the development of PPAR $\alpha$  agonists. This, along with the poor isolation yields (see **Figure 1.7** and section **1.2.1**) of **3.1** provide for an attractive total synthesis project. The successful completion of the total synthesis of this compound would not only help to elucidate its absolute stereochemistry (active enantiomer is unknown), but also enable structure-activity relationship studies expected to lead to more optimal leads.

#### **1.2.4 Overview of *Picrasma* alkaloids and picrasidine family members.**

Picrasidine C is only one member of the large family of *Picrasma* alkaloids. The various pharmacological benefits exhibited by *P. quassioides* extracts are attributed to approximately 94 distinct phytochemicals<sup>90</sup> that are structurally categorized as quassinoids,<sup>91</sup>  $\beta$ -carbolines,<sup>92,93</sup> canthinones,<sup>94</sup> and neolignans,<sup>95</sup> among others. **Chapter 3** will specifically focus on the bis- $\beta$ -carboline-containing alkaloids (**3.1** – **3.17**). Representative structures and biological relevance of such compounds are shown in **Figure 1.10** and **Table 1.3**, respectively. It is important to note that while compounds **3.15** and **3.16** contain a bis- $\beta$ -carboline-type system, they are structurally categorized as canthinones because of their distinct diketo ring fused to the  $\beta$ -carboline skeleton.



Interestingly, both picrasidine C (**3.1**) and N (**3.16**) were found to modulate lipid and glucose homeostasis via peroxisome proliferator-activated receptor (PPAR) agonism. They differ in subtype-selectivity, however, as **3.1** promotes PPAR $\alpha$  transcriptional activity<sup>88</sup> while **3.16** is a selective PPAR $\beta/\delta$  agonist.<sup>96</sup> Structure-activity relationship (SAR) studies within the *Picrasma* alkaloid class are integral to identify key structural motifs that dictate biological activity and target specificity. Effective SAR studies require synthetic derivatives of bioactive molecules. The work towards the total synthesis of **3.1** and other *Picrasma* family members will be discussed in **Chapter 3**.

**Table 1.3. Source and biological relevance of bis- $\beta$ -carboline alkaloids from *Picrasma quassioides* plant extracts.**

Compound No.	Compound Name	Extract Source	Significance or Activity
3.1	Picrasidine C	Stem or bark	Glucose and lipid homeostasis <sup>88</sup>
3.2	Picrasidine R	Root bark	Unknown <sup>97</sup>
3.3	Picrasidine H	Root bark	Unknown <sup>97</sup>
3.4	Quassidine B	Stem	Anti-inflammatory <sup>35</sup>
3.5	Quassidine C	Stem	Anti-inflammatory <sup>35</sup>
3.6	Quassidine D	Stem	Anti-inflammatory <sup>35</sup>
3.7	Picrasidine F	Stem or bark	Antibacterial <sup>92</sup>
3.8	Picrasidine G	Stem or bark	Antibacterial <sup>92</sup> , Cytotoxic <sup>98</sup>
3.9	Picrasidine S	Stem or bark	Antibacterial <sup>92</sup>
3.10	Picrasidine T	Bark	Synthetically relevant <sup>99</sup>
3.11	Quassidine I	Stem	Cytotoxic <sup>100</sup>
3.12	Quassidine J	Stem	Cytotoxic <sup>100</sup>
3.13	NMCA 1	Stem	Neuroprotection <sup>101</sup>
3.14	NMCA 2	Stem	Neuroprotection <sup>101</sup>
3.15	Picrasidine M	Root bark	Unknown <sup>102</sup>
3.16	Picrasidine N	Root bark	Glucose and lipid homeostasis <sup>96</sup>
3.17	Quassidine A	Stem	Anti-inflammatory <sup>35</sup>

NMCA = N-methoxy- $\beta$ -carboline alkaloids

### 1.2.5 Summary of accomplishments.

**Chapter 3** focuses on progress towards the total synthesis of picrasidine C (**3.1**). Two approaches were considered for this total synthesis: (1) construction of the heterocycle from structural fragments and (2) functionalization of an existing  $\beta$ -carboline ring. While the total synthesis of picrasidine C remains to be completed, **Approach 1** resulted in the synthesis of six new and structurally diverse *Picrasma*-like alkaloid analogs (two mono- $\beta$ -carbolines and four bis- $\beta$ -carboline compounds), laying the foundation for future picrasidine and quassidine synthetic advancement. The new analogs feature reactive functional groups (enamine, carbonyls, and epoxides), providing synthetic handles to enable further diversification. Notably, in the midst of exploring **Approach 1**, a novel cascade reaction for the formation of indoloquinolizine heterocycles was discovered. Concurrently,  $\beta$ -carboline C-H functionalization for **Approach 2**

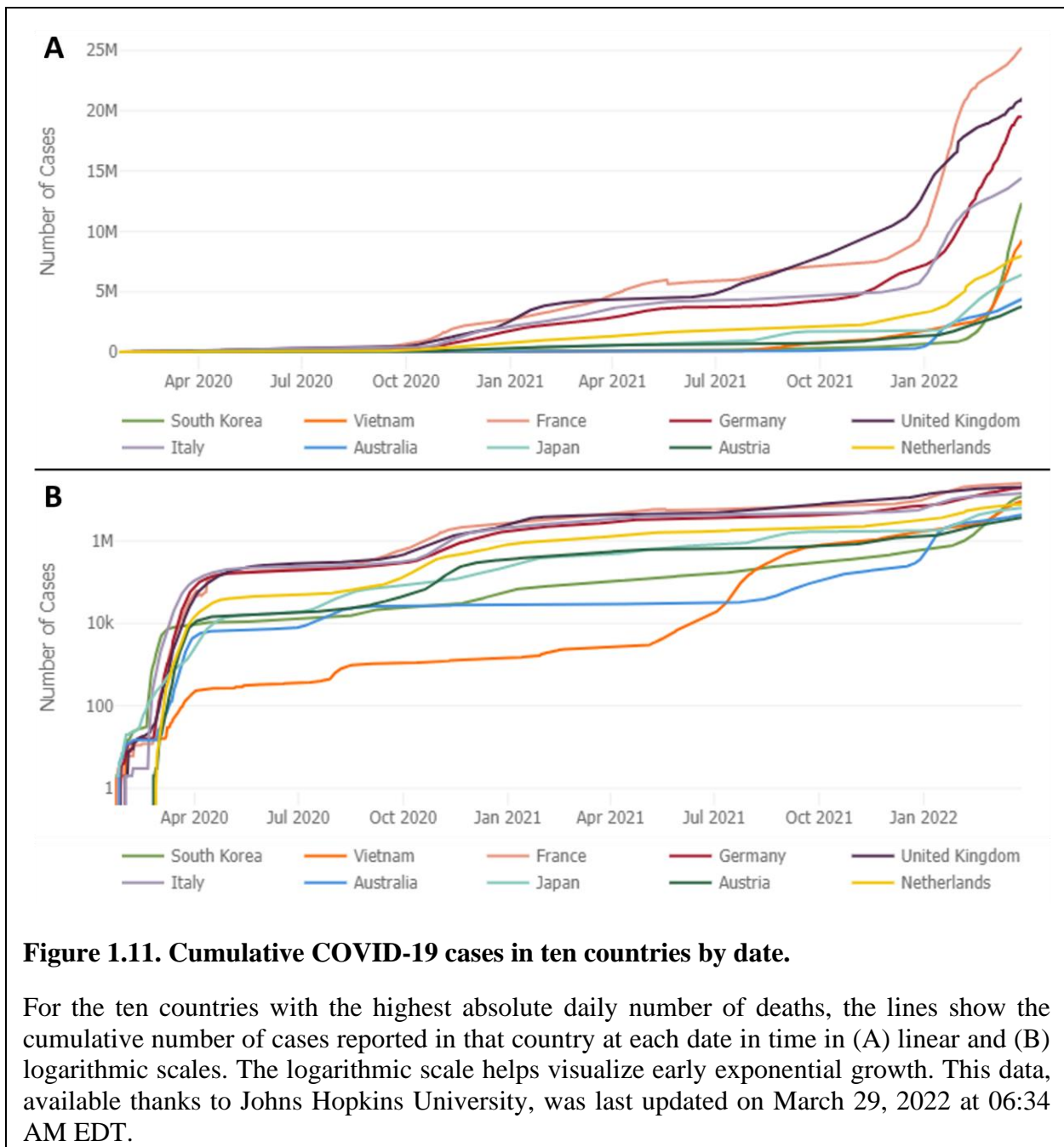
was explored via lithiation reactions. Some minor successes in direct  $\beta$ -carboline substitution demonstrates advancement in  $\beta$ -carboline functionalization methodology. The experimental details and results of both approaches will be discussed in **Chapter 3**.

### **1.3 Overview of SARS-CoV-2 protease inhibitors**

#### **1.3.1 Significance: COVID-19 global pandemic.**

The novel severe acute respiratory syndrome coronavirus 2 (SARS-CoV-2), initially detected in Wuhan City, Hubei province, China and announced to the World Health Organization (WHO) on December 31, 2019,<sup>103</sup> quickly took the world by storm. The outbreak rapidly spread at alarming rates, reaching over 50 countries at the start of March 2020,<sup>104</sup> then over 100 countries the following week,<sup>105</sup> which led to the monumental announcement on March 11, 2020 where the WHO declared the coronavirus disease 2019 (COVID-19) outbreak a global pandemic.

The global death toll from COVID-19 surpassed 200,000 by April 2020, estimating an approximately 5.9% case fatality rate.<sup>106</sup> As the numbers continued to rise steadily, governments all around the world turned to drastic measures to slow disease spread, implementing a range of stringent policies including stay-at-home lockdowns, school and workplace closures, cancellation of events and public gatherings, and restrictions on public transport.<sup>107</sup> Economies were left devastated<sup>108</sup> and healthcare systems were vastly overwhelmed.<sup>109</sup> As of March 2022, we have been living through this pandemic for over two years, and ~490 million infections have been reported, resulting in over six million deaths.<sup>110</sup> With the world in turmoil, scientists everywhere fully focused their research efforts to fight this global pandemic, because the need for effective treatment was obvious and immediate.



As several research labs including my own were forced to shut down while we cowered in fear and hid from the deadly, airborne virus, scientists everywhere were implored to rally together to fight off the novel coronavirus SARS-CoV-2 in attempts to bring an end to the global pandemic. For example, in response to this ongoing public health emergency, the Center for Systems Science

and Engineering (CSSE) at Johns Hopkins University in Baltimore, Maryland developed an online interactive dashboard to visualize and track reported COVID-19 cases in real time. First shared publicly on January 22, 2020, it helped to provide researchers, public health authorities, and the general public with a user-friendly tool to track the outbreak as it unfolds.<sup>110</sup> The exponential growth of cumulative COVID-19 cases in the ten countries with the highest absolute daily number of deaths is visualized in **Figure 1.11**, thanks to their database. As of March 2022, over two years into the pandemic, COVID-19 has infected over 480 million people resulting in over six million deaths.<sup>110</sup>

On a personal note, when the University of Oklahoma forced the closure of research labs starting on March 24, 2020, with no plans of reopening, it was the first time in my scientific career where I was incapable and unallowed to continue research. Working from home as a synthetic chemist proved to be rather difficult and, ultimately, unproductive, so when my university generously requested for research proposals to join in the fight against COVID-19, I jumped at the chance of returning to the lab. My colleague, Quentin Avila, and I worked together to submit a proposal where we aimed to translate our lab's small molecule research into creating a library of SARS-CoV-2 main protease ( $M^{pro}$ ) inhibitors. The following work funded by the COVID-19-Related Rapid Response Research Seed Grant will be discussed in **Chapter 4**.

### **1.3.2 Introduction to SARS-CoV-2 protease inhibitors.**

Despite the tragedy that comes with pandemic-lethal viruses, we are fortunate to utilize data gathered during previous coronavirus-related epidemics outbreaks in order to advance our knowledge and develop treatment options for the new SARS-CoV-2. SARS-CoV-2 shares 82% sequence homology with the 2003 severe acute respiratory syndrome coronavirus (SARS-CoV).<sup>111</sup> Another human coronavirus associated with the Middle East respiratory syndrome (MERS-CoV)

killed ~36% (584 of 1621) of patients infected globally, mainly in Saudi Arabia and South Korea.<sup>112</sup> Clinical presentation of COVID-19 also seem to resemble SARS-CoV infections.<sup>113</sup>

Since SARS-CoV-2 exhibits significant homology to previous variants, along with the availability of its genome sequence,<sup>114</sup> *in silico* modeling and computational drug screening proved to be a useful technique to accelerate drug discovery programs. To advance our efforts even more quickly, drugs either already approved by the Food and Drug Administration (FDA) or currently in the pipeline provided a suitable starting point. The current approach for discovering new coronavirus treatment options remains limited to drug repurposing.<sup>115</sup> Broadly acting antivirals, antiparasitics, and antibiotics are being employed to treat COVID-19 clinically, usually with emergency authorization, but no effective chemotherapeutic that specifically targets SARS-CoV-2 proteins has yet to be successfully brought to market.

Two proteins gaining significant traction for their essential role in virus-mediated RNA replication are the 3-chymotrypsin-like protease (3CL<sup>pro</sup>), also known as the main protease (M<sup>pro</sup>),<sup>116</sup> and the papain-like protease (PL<sup>pro</sup>).<sup>117</sup> A comparison of the MERS-CoV, SARS-CoV, and SARS-CoV-2 M<sup>pro</sup> sequence revealed that the SARS-CoV-2 M<sup>pro</sup> is 96% and 51% similar to SARS-CoV and MERS-CoV, respectively.<sup>118</sup>

Since our lab had previously designed protease<sup>119</sup> and phosphatase<sup>120</sup> inhibitors for bacterial targets and built a library of ~300 chemically diverse compounds, we were well-positioned to contribute to the search for active SARS-CoV-2 replication inhibitors. Several known coronavirus M<sup>pro</sup> and PL<sup>pro</sup> inhibitors contain structural similarities to existing compounds in the Duerfeldt lab small molecule library.



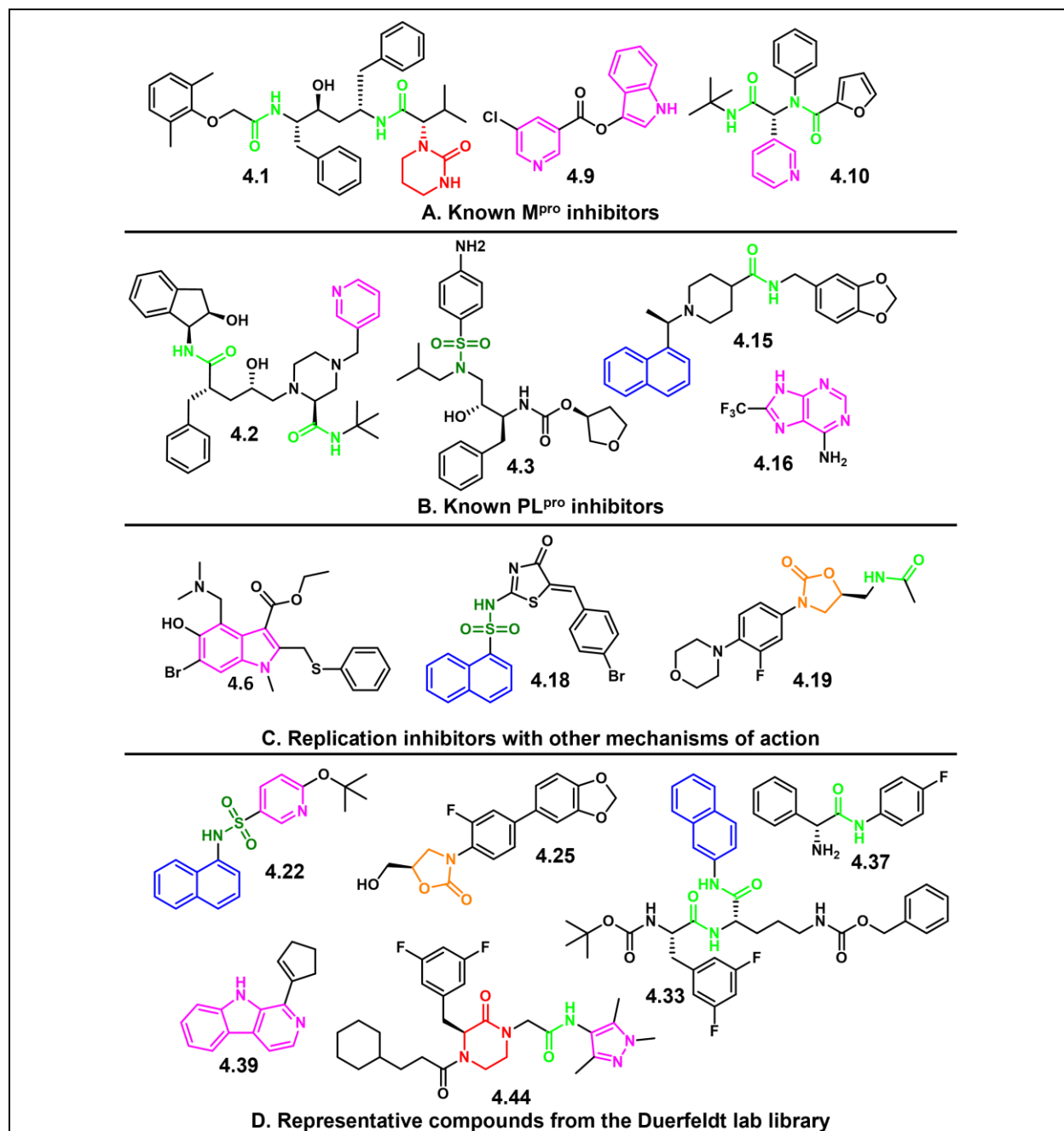


**Figure 1.12. (A – C) Compounds with reported antiviral activity, and (D) Existing compounds in the Duerfeldt lab small molecule library.**

Notable functional groups are highlighted in blue (naphthalene), light blue (aldehyde), light green (amide), dark green (sulfonamide), red (aza-lactam), orange (oxazolidinone), and magenta (nitrogen heterocycles).

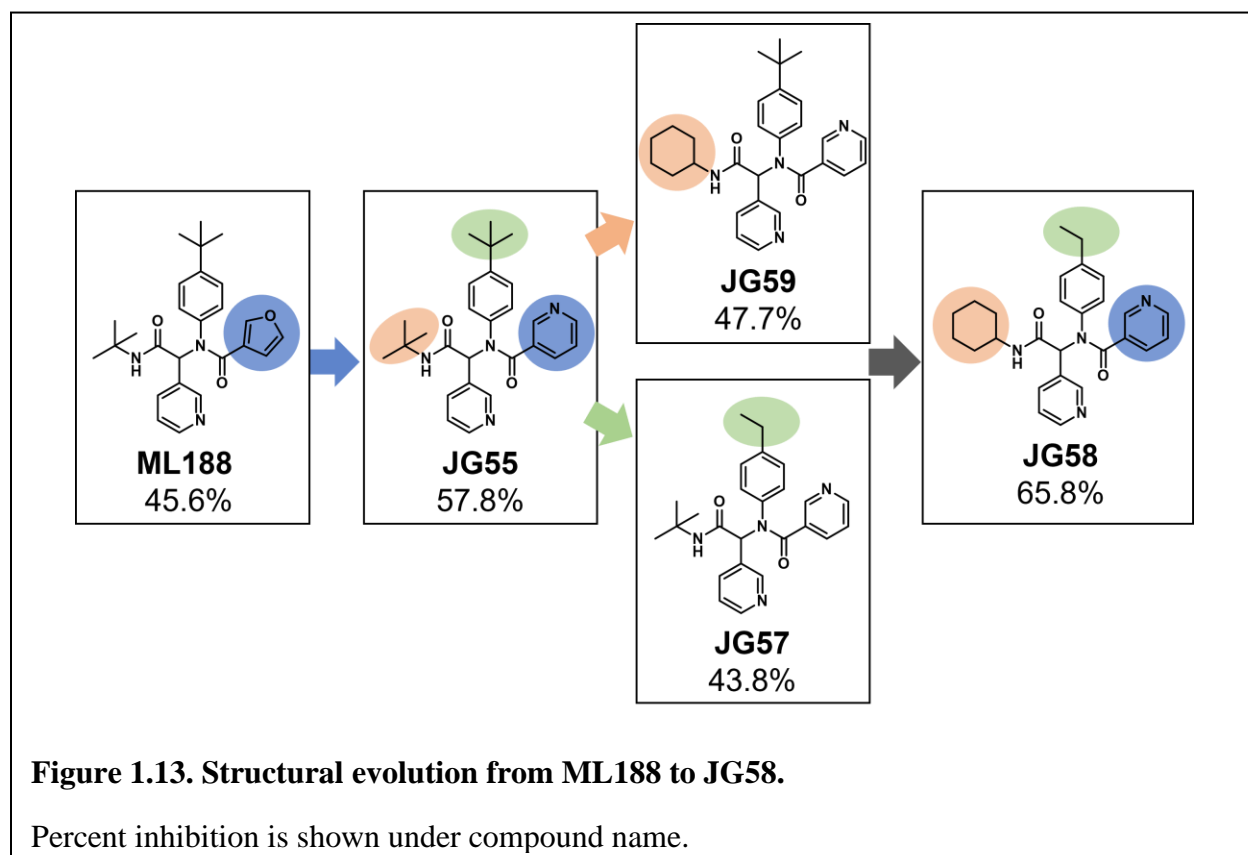
Various X-ray crystallography studies found several M<sup>pro</sup> and PL<sup>pro</sup> inhibitors (**Figure 1.12A** and **Figure 1.12B**, respectively) or viral replication inhibitors of under characterized mechanisms (**Figure 1.2C**) belonging to different chemical classes.<sup>115</sup> Notably, the naphthalene amide **4.15** displayed SARS-CoV antiviral activity with no associated cytotoxicity,<sup>121</sup> and naphthalene sulfonamide **4.18** was found to inhibit viral replication, although the exact mechanism is unknown.<sup>122</sup> We have several naphthalene-containing compounds in our library, as well as naphthalene sulfonamides such as **4.22** (**Figure 1.12D**). Also notable is lopinavir (**4.1**), a peptide-based compound featured in clinical trials for treating coronavirus patients,<sup>123</sup> which exhibits some structural similarity to our peptide-based protease inhibitors (**4.33**). Finally, linezolid (**4.19**), an oxazolidinone antimicrobial<sup>124</sup> that generally inhibits protein synthesis,<sup>125</sup> was recently found to effectively treat pneumonia symptoms in COVID-19 patients.<sup>126</sup> Our lab has recently developed a number of oxazolidinone analogs, such as **4.25**, thus motivating us to submit our compounds for viral replication inhibition evaluation. Other compounds from **Figure 1.12D** represent just a few of the chemical classes that our library has to offer:  $\beta$ -carbolenes (**4.39**), piperazinones (**4.44**), and peptidic compounds (**4.33** and **4.37**). Due to the relatedness of our existing compound collection to known coronavirus replication inhibitors, we hypothesized that assessment of our library featuring structurally diverse scaffolds will expand the chemical space being explored during the search of SARS-CoV-2 inhibitors.

Since the coronavirus PL<sup>pro</sup> is involved in regulation of host interferon and nuclear factor  $\kappa$ B (NF- $\kappa$ B) pathways,<sup>127</sup> and dysregulation of NF- $\kappa$ B can lead to inflammatory diseases and tumorigenesis,<sup>128</sup> it is possible that PL<sup>pro</sup> inhibitors might lead to more off-target downstream (and potentially detrimental) effects. Especially with recent reports on the safety profiles of M<sup>pro</sup>

inhibitors,<sup>129,130</sup> we decided to focus our efforts on exploring the chemical space and structure-activity relationships (SAR) of M<sup>Pro</sup> inhibitors.

### 1.3.3 Summary of what was accomplished.

25 compounds from the Duerfeldt lab small molecule library were sent to Dr. John Teijaro at the Scripps Research Institute (TSRI) for evaluation in an established phenotypic cellular assay.<sup>131</sup> In this assay, compounds (initial concentration of 1  $\mu$ M) were added to the wells concomitantly with SARS-CoV-2, and morphological changes in cells were monitored over 3 days to determine viral cytopathic effect (CPE). Unfortunately, all of our submitted compounds were found to be inactive, and further studies on existing compounds in our library were halted.



In continuation of our goal to expand the chemical space and structural diversity of M<sup>pro</sup> inhibitors, we gained inspiration from a remarkable database provided by Diamond Light Source.<sup>132</sup> With their database and our own preliminary *in silico* modelling, novel chemotypes of inhibitors were identified, inspiring three scaffolds for us to explore and evaluate for M<sup>pro</sup> inhibition (urea, piperazine, and peptidomimetic). I was personally tasked with synthesizing peptidomimetic compounds. Using the multi-component Ugi coupling reaction,<sup>133</sup> I was able to rapidly generate 18 bis-amide compounds which were evaluated for protease activity with a commercial FRET-based assay kit. ML188 (**4.10**) was used as the positive control because it is a known non-covalent M<sup>pro</sup> inhibitor.<sup>134,135</sup> From this small SAR project, **JG58** was found to exhibit ~20% higher inhibition activity compared to ML188 (**Figure 1.13**). Our preliminary work towards expanding the chemical space of coronavirus protease inhibitors will be discussed in **Chapter 4**.

#### 1.4 References for Chapter 1

- (1) Santajit, S.; Indrawattana, N. Mechanisms of Antimicrobial Resistance in ESKAPE Pathogens. *Biomed Res Int* **2016**, *2016*, 2475067. <https://doi.org/10.1155/2016/2475067>.
- (2) Oliveira, J.; Reygaert, W. C. Gram Negative Bacteria. In *StatPearls*; StatPearls Publishing: Treasure Island (FL), 2021.
- (3) Breijyeh, Z.; Jubeh, B.; Karaman, R. Resistance of Gram-Negative Bacteria to Current Antibacterial Agents and Approaches to Resolve It. *Molecules* **2020**, *25* (6), 1340. <https://doi.org/10.3390/molecules25061340>.
- (4) Li, X.-Z.; Plésiat, P.; Nikaido, H. The Challenge of Efflux-Mediated Antibiotic Resistance in Gram-Negative Bacteria. *Clin Microbiol Rev* **2015**, *28* (2), 337–418. <https://doi.org/10.1128/CMR.00117-14>.

- (5) Ruppé, É.; Woerther, P.-L.; Barbier, F. Mechanisms of Antimicrobial Resistance in Gram-Negative Bacilli. *Ann Intensive Care* **2015**, *5*, 21. <https://doi.org/10.1186/s13613-015-0061-0>.
- (6) Naas, T.; Dortet, L.; Iorga, B. I. Structural and Functional Aspects of Class A Carbapenemases. *Curr Drug Targets* **2016**, *17* (9), 1006–1028. <https://doi.org/10.2174/1389450117666160310144501>.
- (7) Kidd, T. J.; Mills, G.; Sá-Pessoa, J.; Dumigan, A.; Frank, C. G.; Insua, J. L.; Ingram, R.; Hobley, L.; Bengoechea, J. A. A *Klebsiella Pneumoniae* Antibiotic Resistance Mechanism That Subdues Host Defences and Promotes Virulence. *EMBO Mol Med* **2017**, *9* (4), 430–447. <https://doi.org/10.15252/emmm.201607336>.
- (8) Russo, T. A.; Johnson, J. R. Medical and Economic Impact of Extraintestinal Infections Due to *Escherichia Coli*: Focus on an Increasingly Important Endemic Problem. *Microbes Infect* **2003**, *5* (5), 449–456. [https://doi.org/10.1016/s1286-4579\(03\)00049-2](https://doi.org/10.1016/s1286-4579(03)00049-2).
- (9) Johnson, J. R. Virulence Factors in *Escherichia Coli* Urinary Tract Infection. *Clin Microbiol Rev* **1991**, *4* (1), 80–128. <https://doi.org/10.1128/CMR.4.1.80>.
- (10) Boucher, H. W.; Talbot, G. H.; Bradley, J. S.; Edwards, J. E.; Gilbert, D.; Rice, L. B.; Scheld, M.; Spellberg, B.; Bartlett, J. Bad Bugs, No Drugs: No ESKAPE! An Update from the Infectious Diseases Society of America. *Clin Infect Dis* **2009**, *48* (1), 1–12. <https://doi.org/10.1086/595011>.
- (11) Coates, A. R.; Halls, G.; Hu, Y. Novel Classes of Antibiotics or More of the Same? *British Journal of Pharmacology* **2011**, *163* (1), 184–194. <https://doi.org/10.1111/j.1476-5381.2011.01250.x>.

- (12) CDC. What Exactly is Antibiotic Resistance?  
<https://www.cdc.gov/drugresistance/about.html> (accessed 2021 -10 -27).
- (13) van Rensburg, J. J.; Fortney, K. R.; Chen, L.; Krieger, A. J.; Lima, B. P.; Wolfe, A. J.; Katz, B. P.; Zhang, Z.; Spinola, S. M. Development and Validation of a High-Throughput Cell-Based Screen To Identify Activators of a Bacterial Two-Component Signal Transduction System. *Antimicrob. Agents Chemother.* **2015**, *59* (7), 3789–3799.  
<https://doi.org/10.1128/AAC.00236-15>.
- (14) Tiwari, S.; Jamal, S. B.; Hassan, S. S.; Carvalho, P. V. S. D.; Almeida, S.; Barh, D.; Ghosh, P.; Silva, A.; Castro, T. L. P.; Azevedo, V. Two-Component Signal Transduction Systems of Pathogenic Bacteria As Targets for Antimicrobial Therapy: An Overview. *Frontiers in Microbiology* **2017**, *8*, 1878. <https://doi.org/10.3389/fmicb.2017.01878>.
- (15) Stock, A. M.; Robinson, V. L.; Goudreau, P. N. Two-Component Signal Transduction. *Annu. Rev. Biochem.* **2000**, *69* (1), 183–215. <https://doi.org/10.1146/annurev.biochem.69.1.183>.
- (16) Atanasov, A. G.; Zotchev, S. B.; Dirsch, V. M.; Supuran, C. T. Natural Products in Drug Discovery: Advances and Opportunities. *Nat Rev Drug Discov* **2021**, *20* (3), 200–216.  
<https://doi.org/10.1038/s41573-020-00114-z>.
- (17) Newman, D. J.; Cragg, G. M. Natural Products as Sources of New Drugs from 1981 to 2014. *J Nat Prod* **2016**, *79* (3), 629–661. <https://doi.org/10.1021/acs.jnatprod.5b01055>.
- (18) Waltenberger, B.; Mocan, A.; Šmejkal, K.; Heiss, E. H.; Atanasov, A. G. Natural Products to Counteract the Epidemic of Cardiovascular and Metabolic Disorders. *Molecules* **2016**, *21* (6), 807. <https://doi.org/10.3390/molecules21060807>.
- (19) Atanasov, A. G.; Waltenberger, B.; Pferschy-Wenzig, E.-M.; Linder, T.; Wawrosch, C.; Uhrin, P.; Temml, V.; Wang, L.; Schwaiger, S.; Heiss, E. H.; Rollinger, J. M.; Schuster, D.;

- Breuss, J. M.; Bochkov, V.; Mihovilovic, M. D.; Kopp, B.; Bauer, R.; Dirsch, V. M.; Stuppner, H. Discovery and Resupply of Pharmacologically Active Plant-Derived Natural Products: A Review. *Biotechnol Adv* **2015**, *33* (8), 1582–1614. <https://doi.org/10.1016/j.biotechadv.2015.08.001>.
- (20) Sertuerner. Ueber Das Morphinum, Eine Neue Salzfähige Grundlage, Und Die Mekonsäure, Als Hauptbestandtheile Des Opiums. *Annalen der Physik* **1817**, *55* (1), 56–89. <https://doi.org/10.1002/andp.18170550104>.
- (21) Hosztafi, S. The Discovery of Alkaloids. *Pharmazie* **1997**, *52* (7), 546–550.
- (22) Achan, J.; Talisuna, A. O.; Erhart, A.; Yeka, A.; Tibenderana, J. K.; Baliraine, F. N.; Rosenthal, P. J.; D’Alessandro, U. Quinine, an Old Anti-Malarial Drug in a Modern World: Role in the Treatment of Malaria. *Malar J* **2011**, *10*, 144. <https://doi.org/10.1186/1475-2875-10-144>.
- (23) Runge, F. F. Neueste phytochemische Entdeckungen zur Begründung einer wissenschaftlichen Phytochemie; G. Reimer: Verlin, 1820; pp 144–159.
- (24) Henningfield, J. E.; Zeller, M. Nicotine Psychopharmacology Research Contributions to United States and Global Tobacco Regulation: A Look Back and a Look Forward. *Psychopharmacology* **2006**, *184* (3), 286–291. <https://doi.org/10.1007/s00213-006-0308-4>.
- (25) Pomara, C.; Cassano, T.; D’Errico, S.; Bello, S.; Romano, A. D.; Riezzo, I.; Serviddio, G. Data Available on the Extent of Cocaine Use and Dependence: Biochemistry, Pharmacologic Effects and Global Burden of Disease of Cocaine Abusers. *CMC* **2012**, *19* (33), 5647–5657. <https://doi.org/10.2174/092986712803988811>.

- (26) Corson, T. W.; Crews, C. M. Molecular Understanding and Modern Application of Traditional Medicines: Triumphs and Trials. *Cell* **2007**, *130* (5), 769–774. <https://doi.org/10.1016/j.cell.2007.08.021>.
- (27) Cushnie, T. P. T.; Cushnie, B.; Lamb, A. J. Alkaloids: An Overview of Their Antibacterial, Antibiotic-Enhancing and Antivirulence Activities. *International Journal of Antimicrobial Agents* **2014**, *44* (5), 377–386. <https://doi.org/10.1016/j.ijantimicag.2014.06.001>.
- (28) Millan, M. J.; Newman-Tancredi, A.; Audinot, V.; Cussac, D.; Lejeune, F.; Nicolas, J.-P.; Cogé, F.; Galizzi, J.-P.; Boutin, J. A.; Rivet, J.-M.; Dekeyne, A.; Gobert, A. Agonist and Antagonist Actions of Yohimbine as Compared to Fluparoxan at A2-Adrenergic Receptors (AR)s, Serotonin (5-HT)1A, 5-HT1B, 5-HT1D and Dopamine D2 and D3 Receptors. Significance for the Modulation of Frontocortical Monoaminergic Transmission and Depressive States. *Synapse* **2000**, *35* (2), 79–95. [https://doi.org/10.1002/\(SICI\)1098-2396\(200002\)35:2<79::AID-SYN1>3.0.CO;2-X](https://doi.org/10.1002/(SICI)1098-2396(200002)35:2<79::AID-SYN1>3.0.CO;2-X).
- (29) Mizukami, H.; Nordlov, H.; Lee, S.-L.; Scott, A. I. Purification and Properties of Strictosidine Synthetase (an Enzyme Condensing Tryptamine and Secologanin) from *Catharanthus Roseus* Cultured Cells. *Biochemistry* **1979**, *18* (17), 3760–3763. <https://doi.org/10.1021/bi00584a018>.
- (30) Hassan, Z.; Muzaimi, M.; Navaratnam, V.; Yusoff, N. H. M.; Suhaimi, F. W.; Vadivelu, R.; Vicknasingam, B. K.; Amato, D.; von Hörsten, S.; Ismail, N. I. W.; Jayabalan, N.; Hazim, A. I.; Mansor, S. M.; Müller, C. P. From Kratom to Mitragynine and Its Derivatives: Physiological and Behavioural Effects Related to Use, Abuse, and Addiction. *Neuroscience & Biobehavioral Reviews* **2013**, *37* (2), 138–151. <https://doi.org/10.1016/j.neubiorev.2012.11.012>.



- (31) Marwat, S. K.; Rehman, F. ur. Chapter 70 - Medicinal and Pharmacological Potential of Harmala (*Peganum Harmala* L.) Seeds. In *Nuts and Seeds in Health and Disease Prevention*; Preedy, V. R., Watson, R. R., Patel, V. B., Eds.; Academic Press: San Diego, 2011; pp 585–599. <https://doi.org/10.1016/B978-0-12-375688-6.10070-2>.
- (32) Schupp, P.; Poehner, T.; Edrada, R.; Ebel, R.; Berg, A.; Wray, V.; Proksch, P. Eudistomins W and X, Two New  $\beta$ -Carbolines from the Micronesian Tunicate Eudistoma Sp. *J. Nat. Prod.* **2003**, *66* (2), 272–275. <https://doi.org/10.1021/np020315n>.
- (33) Inman, W. D.; Bray, W. M.; Gassner, N. C.; Lokey, R. S.; Tenney, K.; Shen, Y. Y.; TenDyke, K.; Suh, T.; Crews, P. A  $\beta$ -Carboline Alkaloid from the Papua New Guinea Marine Sponge *Hirtios Reticulatus*. *J Nat Prod* **2010**, *73* (2), 255–257. <https://doi.org/10.1021/np9005426>.
- (34) Zhang, Q.-W.; Lin, L.-G.; Ye, W.-C. Techniques for Extraction and Isolation of Natural Products: A Comprehensive Review. *Chinese Medicine* **2018**, *13* (1), 20. <https://doi.org/10.1186/s13020-018-0177-x>.
- (35) Jiao, W.-H.; Gao, H.; Li, C.-Y.; Zhao, F.; Jiang, R.-W.; Wang, Y.; Zhou, G.-X.; Yao, X.-S. Quassidines A–D, Bis- $\beta$ -Carboline Alkaloids from the Stems of *Picrasma Quassioides*. *J. Nat. Prod.* **2010**, *73* (2), 167–171. <https://doi.org/10.1021/np900538r>.
- (36) Howes, M.-J. R.; Quave, C. L.; Collemare, J.; Tatsis, E. C.; Twilley, D.; Lulekal, E.; Farlow, A.; Li, L.; Cazar, M.-E.; Leaman, D. J.; Prescott, T. A. K.; Milliken, W.; Martin, C.; De Canha, M. N.; Lall, N.; Qin, H.; Walker, B. E.; Vásquez-Londoño, C.; Allkin, B.; Rivers, M.; Simmonds, M. S. J.; Bell, E.; Battison, A.; Felix, J.; Forest, F.; Leon, C.; Williams, C.; Nic Lughadha, E. Molecules from Nature: Reconciling Biodiversity Conservation and Global Healthcare Imperatives for Sustainable Use of Medicinal Plants and Fungi. *PLANTS, PEOPLE, PLANET* **2020**, *2* (5), 463–481. <https://doi.org/10.1002/ppp3.10138>.

- (37) Nicolaou, K. C.; Yang, Z.; Liu, J. J.; Ueno, H.; Nantermet, P. G.; Guy, R. K.; Claiborne, C. F.; Renaud, J.; Couladouros, E. A.; Paulvannan, K.; Sorensen, E. J. Total Synthesis of Taxol. *Nature* **1994**, *367* (6464), 630–634. <https://doi.org/10.1038/367630a0>.
- (38) Danishefsky, S. J.; Masters, J. J.; Young, W. B.; Link, J. T.; Snyder, L. B.; Magee, T. V.; Jung, D. K.; Isaacs, R. C. A.; Bornmann, W. G.; Alaimo, C. A.; Coburn, C. A.; Di Grandi, M. J. Total Synthesis of Baccatin III and Taxol. *J. Am. Chem. Soc.* **1996**, *118* (12), 2843–2859. <https://doi.org/10.1021/ja952692a>.
- (39) Kanda, Y.; Nakamura, H.; Umemiya, S.; Puthukanoori, R. K.; Murthy Appala, V. R.; Gaddamanugu, G. K.; Paraselli, B. R.; Baran, P. S. Two-Phase Synthesis of Taxol. *J. Am. Chem. Soc.* **2020**, *142* (23), 10526–10533. <https://doi.org/10.1021/jacs.0c03592>.
- (40) Hall, N. Creating Complexity – the Beauty and Logic of Synthesis. *Chem. Commun.* **2003**, No. 6, 661–664. <https://doi.org/10.1039/B212248K>.
- (41) Domínguez, G.; Pérez-Castells, J. Chemistry of B-Carbolines as Synthetic Intermediates. *Eur. J. Org. Chem.* **2011**, *2011* (36), 7243–7253. <https://doi.org/10.1002/ejoc.201100931>.
- (42) Milen, M.; Ábrányi-Balogh, P. Synthesis of  $\beta$ -Carbolines (Microreview). *Chem Heterocycl Comp* **2016**, *52* (12), 996–998. <https://doi.org/10.1007/s10593-017-1997-9>.
- (43) Stöckigt, J.; Antonchick, A. P.; Wu, F.; Waldmann, H. The Pictet-Spengler Reaction in Nature and in Organic Chemistry. *Angew. Chem. Int. Ed.* **2011**, *50* (37), 8538–8564. <https://doi.org/10.1002/anie.201008071>.
- (44) Pictet, A.; Spengler, Theod. Über Die Bildung von Isochinolin-Derivaten Durch Einwirkung von Methylal Auf Phenyl-Äthylamin, Phenyl-Alanin Und Tyrosin. *Berichte der deutschen chemischen Gesellschaft* **1911**, *44* (3), 2030–2036. <https://doi.org/10.1002/cber.19110440309>.

- (45) Zheng, C.; Xia, Z.-L.; You, S.-L. Unified Mechanistic Understandings of Pictet-Spengler Reactions. *Chem* **2018**, *4* (8), 1952–1966. <https://doi.org/10.1016/j.chempr.2018.06.006>.
- (46) Whaley, W. M.; Govindachari, T. R. The Pictet-Spengler Synthesis of Tetrahydroisoquinolines and Related Compounds. In *Organic Reactions*; John Wiley & Sons, Ltd, 2011; pp 151–190. <https://doi.org/10.1002/0471264180.or006.03>.
- (47) Cox, E. D.; Cook, J. M. The Pictet-Spengler Condensation: A New Direction for an Old Reaction. *Chem. Rev.* **1995**, *95* (6), 1797–1842. <https://doi.org/10.1021/cr00038a004>.
- (48) Yokoyama, A.; Ohwada, T.; Shudo, K. Prototype Pictet–Spengler Reactions Catalyzed by Superacids. Involvement of Dicationic Superelectrophiles. *J. Org. Chem.* **1999**, *64* (2), 611–617. <https://doi.org/10.1021/jo982019e>.
- (49) Yamada, H.; Kawate, T.; Matsumizu, M.; Nishida, A.; Yamaguchi, K.; Nakagawa, M. Chiral Lewis Acid-Mediated Enantioselective Pictet–Spengler Reaction of Nb-Hydroxytryptamine with Aldehydes. *J. Org. Chem.* **1998**, *63* (18), 6348–6354. <https://doi.org/10.1021/jo980810h>.
- (50) Sharma, S. D.; Bhaduri, S.; Kaur, G. Diastereoselective Synthesis of 1,3-Disubstituted 1,2,3,4-Tetrahydro- $\beta$ -Carbolines Using Pictet-Spengler Reaction in Non-Acidic Aprotic Media. *Indian. J. Org. Chem.* **2007**, *38* (14), 2710–2715. <https://doi.org/10.1002/chin.200714162>.
- (51) Nören-Müller, A.; Wilk, W.; Saxena, K.; Schwalbe, H.; Kaiser, M.; Waldmann, H. Discovery of a New Class of Inhibitors of Mycobacterium Tuberculosis Protein Tyrosine Phosphatase B by Biology-Oriented Synthesis. *Angew Chem Int Ed Engl* **2008**, *47* (32), 5973–5977. <https://doi.org/10.1002/anie.200801566>.

- (52) Bou-Hamdan, F. R.; Leighton, J. L. Highly Enantioselective Pictet–Spengler Reactions with  $\alpha$ -Ketoamide-Derived Ketimines: Access to an Unusual Class of Quaternary  $\alpha$ -Amino Amides. *Angewandte Chemie* **2009**, *121* (13), 2439–2442. <https://doi.org/10.1002/ange.200806110>.
- (53) Rueffer, M.; Nagakura, N.; Zenk, M. H. Strictosidine, the Common Precursor for Monoterpenoid Indole Alkaloids with 3  $\alpha$  and 3  $\beta$  Configuration. *Tetrahedron Letters* **1978**, *19* (18), 1593–1596. [https://doi.org/10.1016/S0040-4039\(01\)94613-1](https://doi.org/10.1016/S0040-4039(01)94613-1).
- (54) Lebold, T. P.; Wood, J. L.; Deitch, J.; Lodewyk, M. W.; Tantillo, D. J.; Sarpong, R. A Divergent Approach to the Synthesis of the Yohimbine Alkaloids Venenatine and Alstovenine. *Nature Chem* **2013**, *5* (2), 126–131. <https://doi.org/10.1038/nchem.1528>.
- (55) Stork, G.; Tang, P. C.; Casey, M.; Goodman, B.; Toyota, M. Regiospecific and Stereoselective Syntheses of ( $\pm$ )-Reserpine and (–)-Reserpine. *J. Am. Chem. Soc.* **2005**, *127* (46), 16255–16262. <https://doi.org/10.1021/ja055744x>.
- (56) Ingallina, C.; D’Acquarica, I.; Delle Monache, G.; Ghirga, F.; Quaglio, D.; Ghirga, P.; Berardozi, S.; Markovic, V.; Botta, B. The Pictet-Spengler Reaction Still on Stage. *Curr Pharm Des* **2016**, *22* (12), 1808–1850. <https://doi.org/10.2174/1381612822666151231100247>.
- (57) Calcaterra, A.; Mangiardi, L.; Delle Monache, G.; Quaglio, D.; Balducci, S.; Berardozi, S.; Iazzetti, A.; Franzini, R.; Botta, B.; Ghirga, F. The Pictet-Spengler Reaction Updates Its Habits. *Molecules* **2020**, *25* (2), 414. <https://doi.org/10.3390/molecules25020414>.
- (58) Maryanoff, B. E.; Zhang, H.-C.; Cohen, J. H.; Turchi, I. J.; Maryanoff, C. A. Cyclizations of N-Acyliminium Ions. *Chem Rev* **2004**, *104* (3), 1431–1628. <https://doi.org/10.1021/cr0306182>.

- (59) Pulka, K.; Misicka, A. Influence of Reaction Conditions on Products of the Pictet–Spengler Condensation. *Tetrahedron* **2011**, *67* (10), 1955–1959. <https://doi.org/10.1016/j.tet.2011.01.018>.
- (60) Larghi, E. L.; Amongero, M.; Bracca, A. B. J.; Kaufman, T. S. The Intermolecular Pictet–Spengler Condensation with Chiral Carbonyl Derivatives in the Stereoselective Syntheses of Optically-Active Isoquinoline and Indole Alkaloids. *Arkivoc* **2005**, *2005* (12), 98–153. <https://doi.org/10.3998/ark.5550190.0006.c09>.
- (61) Waldmann, H.; Schmidt, G.; Henke, H.; Burkard, M. Asymmetric Pictet–Spengler Reactions Employing N,N-Phthaloyl Amino Acids as Chiral Auxiliary Groups. *Angewandte Chemie International Edition in English* **1995**, *34* (21), 2402–2403. <https://doi.org/10.1002/anie.199524021>.
- (62) Schmidt, G.; Waldmann, H.; Henke, H.; Burkard, M. Asymmetric Control in the Pictet–Spengler Reaction by Means of N-Protected Amino Acids as Chiral Auxiliary Groups. *Chemistry – A European Journal* **1996**, *2* (12), 1566–1571. <https://doi.org/10.1002/chem.19960021215>.
- (63) Engelgau, M. M.; Geiss, L. S.; Saaddine, J. B.; Boyle, J. P.; Benjamin, S. M.; Gregg, E. W.; Tierney, E. F.; Rios-Burrows, N.; Mokdad, A. H.; Ford, E. S.; Imperatore, G.; Venkat Narayan, K. M. The Evolving Diabetes Burden in the United States. *Ann Intern Med* **2004**, *140* (11), 945–950. <https://doi.org/10.7326/0003-4819-140-11-200406010-00035>.
- (64) Amos, A. F.; McCarty, D. J.; Zimmet, P. The Rising Global Burden of Diabetes and Its Complications: Estimates and Projections to the Year 2010. *Diabet Med* **1997**, *14 Suppl 5*, S1-85.

- (65) Tarr, J. M.; Kaul, K.; Chopra, M.; Kohner, E. M.; Chibber, R. Pathophysiology of Diabetic Retinopathy. *ISRN Ophthalmology* **2013**, *2013*, e343560. <https://doi.org/10.1155/2013/343560>.
- (66) Fong, D. S.; Aiello, L.; Gardner, T. W.; King, G. L.; Blankenship, G.; Cavallerano, J. D.; Ferris, F. L.; Klein, R. Retinopathy in Diabetes. *Diabetes Care* **2004**, *27* (suppl 1), s84–s87. <https://doi.org/10.2337/diacare.27.2007.S84>.
- (67) Evans, J. R.; Michelessi, M.; Virgili, G. Laser Photocoagulation for Proliferative Diabetic Retinopathy. *Cochrane Database Syst Rev* **2014**, No. 11, CD011234. <https://doi.org/10.1002/14651858.CD011234.pub2>.
- (68) Constantin, B. D.; Andrei, B.; Andreea, M. Vitrectomy Surgery of Diabetic Retinopathy Complications. *Rom J Ophthalmol* **2016**, *60* (1), 31–36.
- (69) Virgili, G.; Parravano, M.; Evans, J. R.; Gordon, I.; Lucenteforte, E. Anti-vascular Endothelial Growth Factor for Diabetic Macular Oedema: A Network Meta-analysis. *Cochrane Database of Systematic Reviews* **2018**, No. 10. <https://doi.org/10.1002/14651858.CD007419.pub6>.
- (70) Mitchell, P.; Wong, T. Y. Management Paradigms for Diabetic Macular Edema. *American Journal of Ophthalmology* **2014**, *157* (3), 505-513.e8. <https://doi.org/10.1016/j.ajo.2013.11.012>.
- (71) Ciulla, T. A.; Pollack, J. S.; Williams, D. F. Visual Acuity Outcomes and Anti-VEGF Therapy Intensity in Diabetic Macular Oedema: A Real-World Analysis of 28 658 Patient Eyes. *British Journal of Ophthalmology* **2021**, *105* (2), 216–221. <https://doi.org/10.1136/bjophthalmol-2020-315933>.

- (72) Dunning, K. R.; Anastasi, M. R.; Zhang, V. J.; Russell, D. L.; Robker, R. L. Regulation of Fatty Acid Oxidation in Mouse Cumulus-Oocyte Complexes during Maturation and Modulation by PPAR Agonists. *PLOS ONE* **2014**, *9* (2), e87327. <https://doi.org/10.1371/journal.pone.0087327>.
- (73) Corton, J. C.; Peters, J. M.; Klaunig, J. E. The PPAR $\alpha$ -Dependent Rodent Liver Tumor Response Is Not Relevant to Humans: Addressing Misconceptions. *Arch Toxicol* **2018**, *92* (1), 83–119. <https://doi.org/10.1007/s00204-017-2094-7>.
- (74) Decara, J.; Rivera, P.; López-Gambero, A. J.; Serrano, A.; Pavón, F. J.; Baixeras, E.; Rodríguez de Fonseca, F.; Suárez, J. Peroxisome Proliferator-Activated Receptors: Experimental Targeting for the Treatment of Inflammatory Bowel Diseases. *Frontiers in Pharmacology* **2020**, *11*.
- (75) Feige, J. N.; Gelman, L.; Michalik, L.; Desvergne, B.; Wahli, W. From Molecular Action to Physiological Outputs: Peroxisome Proliferator-Activated Receptors Are Nuclear Receptors at the Crossroads of Key Cellular Functions. *Progress in Lipid Research* **2006**, *45* (2), 120–159. <https://doi.org/10.1016/j.plipres.2005.12.002>.
- (76) Deng, G.; Moran, E. P.; Cheng, R.; Matlock, G.; Zhou, K.; Moran, D.; Chen, D.; Yu, Q.; Ma, J.-X. Therapeutic Effects of a Novel Agonist of Peroxisome Proliferator-Activated Receptor Alpha for the Treatment of Diabetic Retinopathy. *Invest. Ophthalmol. Vis. Sci.* **2017**, *58* (12), 5030. <https://doi.org/10.1167/iovs.16-21402>.
- (77) Chen, Y.; Hu, Y.; Lin, M.; Jenkins, A. J.; Keech, A. C.; Mott, R.; Lyons, T. J.; Ma, J. Therapeutic Effects of PPAR $\alpha$  Agonists on Diabetic Retinopathy in Type 1 Diabetes Models. *Diabetes* **2013**, *62* (1), 261–272. <https://doi.org/10.2337/db11-0413>.

- (78) Keech, A. C.; Mitchell, P.; Summanen, P. A.; O'Day, J.; Davis, T. M. E.; Moffitt, M. S.; Taskinen, M.-R.; Simes, R. J.; Tse, D.; Williamson, E.; Merrifield, A.; Laatikainen, L. T.; d'Emden, M. C.; Crimet, D. C.; O'Connell, R. L.; Colman, P. G.; FIELD study investigators. Effect of Fenofibrate on the Need for Laser Treatment for Diabetic Retinopathy (FIELD Study): A Randomised Controlled Trial. *Lancet* **2007**, *370* (9600), 1687–1697. [https://doi.org/10.1016/S0140-6736\(07\)61607-9](https://doi.org/10.1016/S0140-6736(07)61607-9).
- (79) Noonan, J. E.; Jenkins, A. J.; Ma, J.-X.; Keech, A. C.; Wang, J. J.; Lamoureux, E. L. An Update on the Molecular Actions of Fenofibrate and Its Clinical Effects on Diabetic Retinopathy and Other Microvascular End Points in Patients With Diabetes. *Diabetes* **2013**, *62* (12), 3968–3975. <https://doi.org/10.2337/db13-0800>.
- (80) Fruchart, J.-C. Selective Peroxisome Proliferator-Activated Receptor $\alpha$  Modulators (SPPARM $\alpha$ ): The next Generation of Peroxisome Proliferator-Activated Receptor  $\alpha$ -Agonists. *Cardiovasc Diabetol* **2013**, *12*, 82. <https://doi.org/10.1186/1475-2840-12-82>.
- (81) Knickelbein, J. E.; Abbott, A. B.; Chew, E. Y. Fenofibrate and Diabetic Retinopathy. *Curr Diab Rep* **2016**, *16* (10), 90. <https://doi.org/10.1007/s11892-016-0786-7>.
- (82) Xu, H. E.; Lambert, M. H.; Montana, V. G.; Plunket, K. D.; Moore, L. B.; Collins, J. L.; Oplinger, J. A.; Kliewer, S. A.; Gampe, R. T.; McKee, D. D.; Moore, J. T.; Willson, T. M. Structural Determinants of Ligand Binding Selectivity between the Peroxisome Proliferator-Activated Receptors. *Proceedings of the National Academy of Sciences* **2001**, *98* (24), 13919–13924. <https://doi.org/10.1073/pnas.241410198>.
- (83) Oliver, W. R.; Shenk, J. L.; Snaith, M. R.; Russell, C. S.; Plunket, K. D.; Bodkin, N. L.; Lewis, M. C.; Winegar, D. A.; Sznajdman, M. L.; Lambert, M. H.; Xu, H. E.; Sternbach, D. D.; Kliewer, S. A.; Hansen, B. C.; Willson, T. M. A Selective Peroxisome Proliferator-



- Activated Receptor  $\delta$  Agonist Promotes Reverse Cholesterol Transport. *Proc. Natl. Acad. Sci. U.S.A.* **2001**, 98 (9), 5306–5311. <https://doi.org/10.1073/pnas.091021198>.
- (84) Dou, X.-Z.; Nath, D.; Shin, Y.; Ma, J.-X.; Duerfeldt, A. S. Structure-Guided Evolution of a 2-Phenyl-4-Carboxyquinoline Chemotype into PPAR $\alpha$  Selective Agonists: New Leads for Oculovascular Conditions. *Bioorganic & Medicinal Chemistry Letters* **2018**, 28 (16), 2717–2722. <https://doi.org/10.1016/j.bmcl.2018.03.010>.
- (85) Dou, X.; Nath, D.; Shin, H.; Nurmemmedov, E.; Bourne, P. C.; Ma, J.-X.; Duerfeldt, A. S. Evolution of a 4-Benzyloxy-Benzylamino Chemotype to Provide Efficacious, Potent, and Isoform Selective PPAR $\alpha$  Agonists as Leads for Retinal Disorders. *J Med Chem* **2020**, 63 (6), 2854–2876. <https://doi.org/10.1021/acs.jmedchem.9b01189>.
- (86) Dou, X.; Duerfeldt, A. S. Small-Molecule Modulation of PPARs for the Treatment of Prevalent Vascular Retinal Diseases. *International Journal of Molecular Sciences* **2020**, 21 (23), 9251. <https://doi.org/10.3390/ijms21239251>.
- (87) Schönherr, H.; Cernak, T. Profound Methyl Effects in Drug Discovery and a Call for New C–H Methylation Reactions. *Angewandte Chemie International Edition* **2013**, 52 (47), 12256–12267. <https://doi.org/10.1002/anie.201303207>.
- (88) Zhao, S.; Kanno, Y.; Li, W.; Sasaki, T.; Zhang, X.; Wang, J.; Cheng, M.; Koike, K.; Nemoto, K.; Li, H. Identification of Picrasidine C as a Subtype-Selective PPAR $\alpha$  Agonist. *J. Nat. Prod.* **2016**, 79 (12), 3127–3133. <https://doi.org/10.1021/acs.jnatprod.6b00883>.
- (89) Ohmoto, T.; Koike, K. Studies on the Constituents of *Picrasma Quassioides* BENNET. II. On the Alkaloidal Constituents. *Chem. Pharm. Bull.* **1983**, 31 (9), 3198–3204. <https://doi.org/10.1248/cpb.31.3198>.

- (90) Mohd Jamil, M. D. H.; Taher, M.; Susanti, D.; Rahman, M. A.; Zakaria, Z. A. Phytochemistry, Traditional Use and Pharmacological Activity of *Picrasma Quassioides*: A Critical Reviews. *Nutrients* **2020**, *12* (9), 2584. <https://doi.org/10.3390/nu12092584>.
- (91) Zhao, W.-Y.; Song, X.-Y.; Zhao, L.; Zou, C.-X.; Zhou, W.-Y.; Lin, B.; Yao, G.-D.; Huang, X.-X.; Song, S.-J. Quassinoids from *Picrasma Quassioides* and Their Neuroprotective Effects. *J. Nat. Prod.* **2019**, *82* (4), 714–723. <https://doi.org/10.1021/acs.jnatprod.8b00470>.
- (92) Guo-hua, S.; Wei-hua, J.; Fan, Y.; Hou-wen, L. Three Bis- $\beta$ -Carboline Alkaloids from *Picrasma Quassioides* and Their Bioactivities. *Chinese Traditional and Herbal Drugs* **2015**, *46* (6), 803–807. <https://doi.org/10.7501/j.issn.0253-2670.2015.06.004>.
- (93) Ohmoto, T.; Koike, K. Studies on the Constituents of *Picrasma Quassioides* BENNET. I. On the Alkaloidal Constituents. *Chemical & Pharmaceutical Bulletin* **1982**, *30* (4), 1204–1209. <https://doi.org/10.1248/cpb.30.1204>.
- (94) Jiang, M.-X.; Zhou, Y.-J. Canthin-6-One Alkaloids from *Picrasma Quassioides* and Their Cytotoxic Activity. *J Asian Nat Prod Res* **2008**, *10* (11–12), 1009–1012. <https://doi.org/10.1080/10286020802277956>.
- (95) Sung, Y.; Koike, K.; Nikaido, T.; Ohmoto, T.; Sankawa, U. Inhibitors of Cyclic AMP Phosphodiesterase in *Picrasma Quassioides* Bennet, and Inhibitory Activities of Related Beta-Carboline Alkaloids. *Chem Pharm Bull (Tokyo)* **1984**, *32* (5), 1872–1877. <https://doi.org/10.1248/cpb.32.1872>.
- (96) Zhao, S.; Kanno, Y.; Li, W.; Wakatabi, H.; Sasaki, T.; Koike, K.; Nemoto, K.; Li, H. Picrasidine N Is a Subtype-Selective PPAR $\beta/\delta$  Agonist. *J. Nat. Prod.* **2016**, *79* (4), 879–885. <https://doi.org/10.1021/acs.jnatprod.5b00909>.

- (97) Koike, K.; Ohmoto, T. Studies on the Alkaloids from *Picrasma Quassioides* BENNET. VII. : Structures of  $\beta$ -Carboline Dimer Alkaloids, Picrasidines-H and -R. *Chemical & Pharmaceutical Bulletin* **1986**, *34* (5), 2090–2093. <https://doi.org/10.1248/cpb.34.2090>.
- (98) Yamashita, N.; Kondo, M.; Zhao, S.; Li, W.; Koike, K.; Nemoto, K.; Kanno, Y. Picrasidine G Decreases Viability of MDA-MB 468 EGFR-Overexpressing Triple-Negative Breast Cancer Cells through Inhibition of EGFR/STAT3 Signaling Pathway. *Bioorganic & Medicinal Chemistry Letters* **2017**, *27* (11), 2608–2612. <https://doi.org/10.1016/j.bmcl.2017.03.061>.
- (99) Higuchi, T.; Ohmoto, T.; Koike, K. Picrasidine-T, a Dimeric  $\beta$ -Carboline Alkaloid from *Picrasma Quassioides*. *Phytochemistry* **1987**, *26*, 3375–3377.
- (100) Jiao, W.-H.; Chen, G.-D.; Gao, H.; Li, J.; Gu, B.-B.; Xu, T.-T.; Yu, H.-B.; Shi, G.-H.; Yang, F.; Yao, X.-S.; Lin, H.-W. ( $\pm$ )-Quassidines I and J, Two Pairs of Cytotoxic Bis- $\beta$ -Carboline Alkaloid Enantiomers from *Picrasma Quassioides*. *J. Nat. Prod.* **2015**, *78* (1), 125–130. <https://doi.org/10.1021/np500801s>.
- (101) Zhang, J.; Zhao, S.-S.; Xie, J.; Yang, J.; Chen, G.-D.; Hu, D.; Zhang, W.-G.; Wang, C.-X.; Yao, X.-S.; Gao, H. N-Methoxy- $\beta$ -Carboline Alkaloids with Inhibitory Activities against A $\beta$ 42 Aggregation and Acetylcholinesterase from the Stems of *Picrasma Quassioides*. *Bioorganic Chemistry* **2020**, *101*, 104043. <https://doi.org/10.1016/j.bioorg.2020.104043>.
- (102) Ohmoto, T.; Koike, K. Studies on the Alkaloids from *Picrasma Quassioides* BENNET. V. Structures of Picrasidines L, M, and P. *Chem. Pharm. Bull.* **1985**, *33* (9), 3847–3851. <https://doi.org/10.1248/cpb.33.3847>.
- (103) Zhou, P.; Yang, X.-L.; Wang, X.-G.; Hu, B.; Zhang, L.; Zhang, W.; Si, H.-R.; Zhu, Y.; Li, B.; Huang, C.-L.; Chen, H.-D.; Chen, J.; Luo, Y.; Guo, H.; Jiang, R.-D.; Liu, M.-Q.; Chen,

Y.; Shen, X.-R.; Wang, X.; Zheng, X.-S.; Zhao, K.; Chen, Q.-J.; Deng, F.; Liu, L.-L.; Yan, B.; Zhan, F.-X.; Wang, Y.-Y.; Xiao, G.; Shi, Z.-L. Discovery of a Novel Coronavirus Associated with the Recent Pneumonia Outbreak in Humans and Its Potential Bat Origin. *bioRxiv* January 23, 2020, p 2020.01.22.914952. <https://doi.org/10.1101/2020.01.22.914952>.

(104) Coronavirus Disease (COVID-19) Situation Reports <https://www.who.int/emergencies/diseases/novel-coronavirus-2019/situation-reports>.

(105) Ravelo, J. L.; Jerving, S. COVID-19 in 2020 — a timeline of the coronavirus outbreak <https://www.devex.com/news/sponsored/covid-19-in-2020-a-timeline-of-the-coronavirus-outbreak-99634>.

(106) Zhang, L.; Lin, D.; Sun, X.; Curth, U.; Drosten, C.; Sauerhering, L.; Becker, S.; Rox, K.; Hilgenfeld, R. Crystal Structure of SARS-CoV-2 Main Protease Provides a Basis for Design of Improved  $\alpha$ -Ketoamide Inhibitors. *Science* **2020**, eabb3405. <https://doi.org/10.1126/science.abb3405>.

(107) Ritchie, H.; Mathieu, E.; Rodés-Guirao, L.; Appel, C.; Giattino, C.; Ortiz-Ospina, E.; Hasell, J.; Macdonald, B.; Beltekian, D.; Roser, M. Coronavirus Pandemic (COVID-19). *Our World in Data* **2020**.

(108) Oum, S.; Kates, J.; Wexler, A. Economic Impact of COVID-19 on PEPFAR Countries. *KFF*, 2022.

(109) How Covid is Straining the Healthcare System <https://health.clevelandclinic.org/how-the-pandemic-is-straining-the-healthcare-system-and-what-you-can-do-to-help/>.

- (110) Dong, E.; Du, H.; Gardner, L. An Interactive Web-Based Dashboard to Track COVID-19 in Real Time. *The Lancet Infectious Diseases* **2020**, *20* (5), 533–534. [https://doi.org/10.1016/S1473-3099\(20\)30120-1](https://doi.org/10.1016/S1473-3099(20)30120-1).
- (111) Morse, J. S.; Lalonde, T.; Xu, S.; Liu, W. R. Learning from the Past: Possible Urgent Prevention and Treatment Options for Severe Acute Respiratory Infections Caused by 2019-nCoV. *Chembiochem* **2020**, *21* (5), 730–738. <https://doi.org/10.1002/cbic.202000047>.
- (112) Kumar, V.; Tan, K.-P.; Wang, Y.-M.; Lin, S.-W.; Liang, P.-H. Identification, Synthesis and Evaluation of SARS-CoV and MERS-CoV 3C-like Protease Inhibitors. *Bioorganic & Medicinal Chemistry* **2016**, *24* (13), 3035–3042. <https://doi.org/10.1016/j.bmc.2016.05.013>.
- (113) Huang, C.; Wang, Y.; Li, X.; Ren, L.; Zhao, J.; Hu, Y.; Zhang, L.; Fan, G.; Xu, J.; Gu, X.; Cheng, Z.; Yu, T.; Xia, J.; Wei, Y.; Wu, W.; Xie, X.; Yin, W.; Li, H.; Liu, M.; Xiao, Y.; Gao, H.; Guo, L.; Xie, J.; Wang, G.; Jiang, R.; Gao, Z.; Jin, Q.; Wang, J.; Cao, B. Clinical Features of Patients Infected with 2019 Novel Coronavirus in Wuhan, China. *Lancet* **2020**, *395* (10223), 497–506. [https://doi.org/10.1016/S0140-6736\(20\)30183-5](https://doi.org/10.1016/S0140-6736(20)30183-5).
- (114) Wu, F.; Zhao, S.; Yu, B.; Chen, Y.-M.; Wang, W.; Song, Z.-G.; Hu, Y.; Tao, Z.-W.; Tian, J.-H.; Pei, Y.-Y.; Yuan, M.-L.; Zhang, Y.-L.; Dai, F.-H.; Liu, Y.; Wang, Q.-M.; Zheng, J.-J.; Xu, L.; Holmes, E. C.; Zhang, Y.-Z. A New Coronavirus Associated with Human Respiratory Disease in China. *Nature* **2020**, *579* (7798), 265–269. <https://doi.org/10.1038/s41586-020-2008-3>.
- (115) Pillaiyar, T.; Meenakshisundaram, S.; Manickam, M. Recent Discovery and Development of Inhibitors Targeting Coronaviruses. *Drug Discovery Today* **2020**, S1359644620300416. <https://doi.org/10.1016/j.drudis.2020.01.015>.

- (116) Ohnishi, K.; Hattori, Y.; Kobayashi, K.; Akaji, K. Evaluation of a Non-Prime Site Substituent and Warheads Combined with a Decahydroisoquinolin Scaffold as a SARS 3CL Protease Inhibitor. *Bioorganic & Medicinal Chemistry* **2019**, *27* (2), 425–435. <https://doi.org/10.1016/j.bmc.2018.12.019>.
- (117) Arya, R.; Das, A.; Prashar, V.; Kumar, M. Potential Inhibitors against Papain-like Protease of Novel Coronavirus (SARS-CoV-2) from FDA Approved Drugs. *8*.
- (118) Cho, E.; Rosa, M.; Anjum, R.; Mehmood, S.; Soban, M.; Mujtaba, M.; Bux, K.; Moin, S. T.; Tanweer, M.; Dantu, S.; Pandini, A.; Yin, J.; Ma, H.; Ramanathan, A.; Islam, B.; Mey, A. S. J. S.; Bhowmik, D.; Haider, S. Dynamic Profiling of  $\beta$ -Coronavirus 3CL Mpro Protease Ligand-Binding Sites. *J. Chem. Inf. Model.* **2021**, *61* (6), 3058–3073. <https://doi.org/10.1021/acs.jcim.1c00449>.
- (119) Lavey, N. P.; Shadid, T.; Ballard, J. D.; Duerfeldt, A. S. Clostridium Difficile ClpP Homologues Are Capable of Uncoupled Activity and Exhibit Different Levels of Susceptibility to Acyldepsipeptide Modulation. *ACS Infect. Dis.* **2019**, *5* (1), 79–89. <https://doi.org/10.1021/acsinfecdis.8b00199>.
- (120) Li, Y.; Gardner, J. J.; Fortney, K. R.; Leus, I. V.; Bonifay, V.; Zgurskaya, H. I.; Pletnev, A. A.; Zhang, S.; Zhang, Z.-Y.; Gribble, G. W.; Spinola, S. M.; Duerfeldt, A. S. First-Generation Structure-Activity Relationship Studies of 2,3,4,9-Tetrahydro-1H-Carbazol-1-Amines as CpxA Phosphatase Inhibitors. *Bioorganic & Medicinal Chemistry Letters* **2019**, *29* (14), 1836–1841. <https://doi.org/10.1016/j.bmcl.2019.05.003>.
- (121) Ghosh, A. K.; Takayama, J.; Rao, K. V.; Ratia, K.; Chaudhuri, R.; Mulhearn, D. C.; Lee, H.; Nichols, D. B.; Baliji, S.; Baker, S. C.; Johnson, M. E.; Mesecar, A. D. Severe Acute Respiratory Syndrome Coronavirus Papain-like Novel Protease Inhibitors: Design,

- Synthesis, Protein–Ligand X-Ray Structure and Biological Evaluation. *J. Med. Chem.* **2010**, *53* (13), 4968–4979. <https://doi.org/10.1021/jm1004489>.
- (122) Milewska, A.; Nowak, P.; Owczarek, K.; Szczepanski, A.; Zarebski, M.; Hoang, A.; Berniak, K.; Wojarski, J.; Zeglen, S.; Baster, Z.; Rajfur, Z.; Pyrc, K. Entry of Human Coronavirus NL63 into the Cell. *Journal of Virology* **2018**, *92* (3). <https://doi.org/10.1128/JVI.01933-17>.
- (123) Chu, C.; Cheng, V.; Hung, I.; Wong, M.; Chan, K.; Chan, K.; Kao, R.; Poon, L.; Wong, C.; Guan, Y.; Peiris, J.; Yuen, K. Role of Lopinavir/Ritonavir in the Treatment of SARS: Initial Virological and Clinical Findings. *Thorax* **2004**, *59* (3), 252–256. <https://doi.org/10.1136/thorax.2003.012658>.
- (124) Roger, C.; Roberts, J. A.; Muller, L. Clinical Pharmacokinetics and Pharmacodynamics of Oxazolidinones. *Clin Pharmacokinet* **2018**, *57* (5), 559–575. <https://doi.org/10.1007/s40262-017-0601-x>.
- (125) Swaney, S. M.; Aoki, H.; Ganoza, M. C.; Shinabarger, D. L. The Oxazolidinone Linezolid Inhibits Initiation of Protein Synthesis in Bacteria. *Antimicrob Agents Chemother* **1998**, *42* (12), 3251–3255. <https://doi.org/10.1128/AAC.42.12.3251>.
- (126) Moghadam, V. D.; Momenimovahed, Z.; Ghorbani, M.; Khodadadi, J. Linezolid a Potential Treatment for COVID-19 Coinfections. *Braz J Anesthesiol* **2021**, *71* (2), 198. <https://doi.org/10.1016/j.bjane.2020.12.019>.
- (127) Shin, D.; Mukherjee, R.; Grewe, D.; Bojkova, D.; Baek, K.; Bhattacharya, A.; Schulz, L.; Widera, M.; Mehdipour, A. R.; Tascher, G.; Geurink, P. P.; Wilhelm, A.; van der Heden van Noort, G. J.; Ovaa, H.; Müller, S.; Knobloch, K.-P.; Rajalingam, K.; Schulman, B. A.; Cinatl, J.; Hummer, G.; Ciesek, S.; Dikic, I. Papain-like Protease Regulates SARS-CoV-2

Viral Spread and Innate Immunity. *Nature* **2020**, 587 (7835), 657–662.  
<https://doi.org/10.1038/s41586-020-2601-5>.

(128) Pfeffer, L. M. The Role of Nuclear Factor KB in the Interferon Response. *J Interferon Cytokine Res* **2011**, 31 (7), 553–559. <https://doi.org/10.1089/jir.2011.0028>.

(129) Lin, Y.; Zang, R.; Ma, Y.; Wang, Z.; Li, L.; Ding, S.; Zhang, R.; Wei, Z.; Yang, J.; Wang, X. Xanthohumol Is a Potent Pan-Inhibitor of Coronaviruses Targeting Main Protease. *International Journal of Molecular Sciences* **2021**, 22 (22), 12134.  
<https://doi.org/10.3390/ijms222212134>.

(130) Owen, D. R.; Allerton, C. M. N.; Anderson, A. S.; Aschenbrenner, L.; Avery, M.; Berritt, S.; Boras, B.; Cardin, R. D.; Carlo, A.; Coffman, K. J.; Dantonio, A.; Di, L.; Eng, H.; Ferre, R.; Gajiwala, K. S.; Gibson, S. A.; Greasley, S. E.; Hurst, B. L.; Kadar, E. P.; Kalgutkar, A. S.; Lee, J. C.; Lee, J.; Liu, W.; Mason, S. W.; Noell, S.; Novak, J. J.; Obach, R. S.; Ogilvie, K.; Patel, N. C.; Pettersson, M.; Rai, D. K.; Reese, M. R.; Sammons, M. F.; Sathish, J. G.; Singh, R. S. P.; Stepan, C. M.; Stewart, A. E.; Tuttle, J. B.; Updyke, L.; Verhoest, P. R.; Wei, L.; Yang, Q.; Zhu, Y. An Oral SARS-CoV-2 Mpro Inhibitor Clinical Candidate for the Treatment of COVID-19. *Science* **2021**, 374 (6575), 1586–1593.  
<https://doi.org/10.1126/science.abl4784>.

(131) Bakowski, M. A.; Beutler, N.; Wolff, K. C.; Kirkpatrick, M. G.; Chen, E.; Nguyen, T.-T. H.; Riva, L.; Shaabani, N.; Parren, M.; Ricketts, J.; Gupta, A. K.; Pan, K.; Kuo, P.; Fuller, M.; Garcia, E.; Tejjaro, J. R.; Yang, L.; Sahoo, D.; Chi, V.; Huang, E.; Vargas, N.; Roberts, A. J.; Das, S.; Ghosh, P.; Woods, A. K.; Joseph, S. B.; Hull, M. V.; Schultz, P. G.; Burton, D. R.; Chatterjee, A. K.; McNamara, C. W.; Rogers, T. F. Drug Repurposing Screens Identify



- Chemical Entities for the Development of COVID-19 Interventions. *Nat Commun* **2021**, *12* (1), 1–14. <https://doi.org/10.1038/s41467-021-23328-0>.
- (132) O'Reilly, M.; Cleasby, A.; Davies, T. G.; Hall, R. J.; Ludlow, R. F.; Murray, C. W.; Tisi, D.; Jhoti, H. Crystallographic Screening Using Ultra-Low-Molecular-Weight Ligands to Guide Drug Design. *Drug Discovery Today* **2019**, *24* (5), 1081–1086. <https://doi.org/10.1016/j.drudis.2019.03.009>.
- (133) Ugi, I. The  $\alpha$ -Addition of Immonium Ions and Anions to Isonitriles Accompanied by Secondary Reactions. *Angewandte Chemie International Edition in English* **1962**, *1* (1), 8–21. <https://doi.org/10.1002/anie.196200081>.
- (134) Jacobs, J.; Grum-Tokars, V.; Zhou, Y.; Turlington, M.; Saldanha, S. A.; Chase, P.; Eggler, A.; Dawson, E. S.; Baez-Santos, Y. M.; Tomar, S.; Mielech, A. M.; Baker, S. C.; Lindsley, C. W.; Hodder, P.; Mesecar, A.; Stauffer, S. R. Discovery, Synthesis, And Structure-Based Optimization of a Series of *N*-(*Tert*-Butyl)-2-(*N*-Arylamido)-2-(Pyridin-3-Yl) Acetamides (ML188) as Potent Noncovalent Small Molecule Inhibitors of the Severe Acute Respiratory Syndrome Coronavirus (SARS-CoV) 3CL Protease. *J. Med. Chem.* **2013**, *56* (2), 534–546. <https://doi.org/10.1021/jm301580n>.
- (135) Turlington, M.; Chun, A.; Tomar, S.; Eggler, A.; Grum-Tokars, V.; Jacobs, J.; Daniels, J. S.; Dawson, E.; Saldanha, A.; Chase, P.; Baez-Santos, Y. M.; Lindsley, C. W.; Hodder, P.; Mesecar, A. D.; Stauffer, S. R. Discovery of *N*-(Benzo[1,2,3]Triazol-1-Yl)-*N*-(Benzyl)Acetamido)Phenyl) Carboxamides as Severe Acute Respiratory Syndrome Coronavirus (SARS-CoV) 3CLpro Inhibitors: Identification of ML300 and Noncovalent Nanomolar Inhibitors with an Induced-Fit Binding. *Bioorganic & Medicinal Chemistry Letters* **2013**, *23* (22), 6172–6177. <https://doi.org/10.1016/j.bmcl.2013.08.112>.

## Chapter 2. Virulence modulation in Gram-negative bacteria via small molecule activation of CpxRA

**Abstract.** Two-component signal transduction systems (2CSTS) provide the means for bacteria to sense and react to changes in the environment. Aberrant 2CSTS activity leads to faulty gene transcription and can alter bacterial cell-growth, quorum sensing, biofilm behavior, antibacterial resistance, and virulence. As such, modulation of these systems represents a promising antibacterial strategy that complements existing bacteriostatic and bactericidal approaches. CpxRA is a 2CSTS found in many drug-resistant Gram-negative pathogens. Genetic activation of CpxRA abolishes the virulence of a number of pathogens in human and murine infection models. Recently, 2,3,4,9-tetrahydro-1*H*-carbazol-1-amines were shown to activate the CpxRA system by inhibiting the phosphatase activity of CpxA. In this chapter, I report collaborative efforts towards the initial structure-activity relationships of this scaffold which identified compound **2.26** that manifests a ~30-fold improvement in CpxA phosphatase inhibition over the initial hit. Comparison of amino and *des*-amino derivatives of this chemotype in isogenic cell lines, differing in membrane permeability and efflux capabilities, demonstrates that the amine is required not only for target engagement but also for permeation and accumulation in *Escherichia coli*. Compound **2.26** was then evaluated for its efficacy to treat urinary tract infections (UTIs) in murine models. We found that **2.26** reduced bacterial recovery in the urine, bladder, and kidneys, with efficacy similar to ciprofloxacin. A proteomic comparison of the uropathogenic *E. coli* (UPEC) strain CFT073 *cpxA* deletion mutant versus **2.26**-treated CFT073 allowed us to analyze the differences between genetic and pharmacologic activation of CpxRA. Since treatment of CFT073 by **2.26** does not inhibit bacterial growth but still fosters accumulation of CpxR-P and downregulates virulence determinants, we have demonstrated that CpxA phosphatase inhibitors

may be useful in treating UTIs caused by UPEC. The initial SAR studies producing lead compound **2.26**, its evaluation in murine UTI models, and our proteomics analysis will be discussed in this chapter.

**Allocation of Contribution.** The following chapter is reproduced in part and with permission from “First-generation structure-activity relationship studies of 2,3,4,9-tetrahydro-1*H*-carbazol-1-amines as CpxA phosphatase inhibitors,” Yangxiong Li, **Jessi J. Gardner**, Katherine R. Fortney, Inga V. Leus, Vincent Bonifay, Helen I. Zgurskaya, Alexandre Pletnev, Sheng Zhang, Zhong-Yin Zhang, Gordon W. Gribble, Stanley M. Spinola, Adam S. Duerfeldt. *Bioorg and Med Chem Lett.* **2019**, 29, 1836-1841. DOI: j.bmcl.2019.05.003,<sup>1</sup> and “CpxA Phosphatase Inhibitor Activates CpxRA and Is a Potential Treatment for Uropathogenic Escherichia Coli in a Murine Model of Infection,” Fortney, K. R.; Smith, S. N.; van Rensburg, J. J.; Brothwell, J. A.; **Gardner, J. J.**; Katz, B. P.; Ahsan, N.; Duerfeldt, A. S.; Mobley, H. L. T.; Spinola, S. M. *Microbiol Spectr.* **2022**, e02430-21. DOI: 10.1128/spectrum.02430-21.<sup>2</sup> Further permissions related to the material excerpted in this chapter should be directed to Elsevier or the American Society for Microbiology.

I produced the results presented in this chapter with the following exceptions: My colleague, Dr. Yangxiong Li, and I contributed equally to the synthesis of fluorine-containing compounds **2.14** – **2.20** and **2.23** – **2.26**. A-ring substituted compounds **2.1** – **2.13** were synthesized by Dr. Li or provided by the Gribble group from Dartmouth College. Activity assays, modified *E. coli* strains ( $\Delta cpxA$ ), and evaluation of compounds in murine models were provided by the Spinola lab at the Indiana University School of Medicine and the Chemical Genomics Core facility in the Indiana CTSI. Intracellular accumulation assays were performed by Inga Leus and Vincent Bonifay within the Zgurskaya lab. Proteomic analysis was provided by Dr. Nagib Ahsan in the mass spectrometry core facility at the University of Oklahoma.

## 2.1 Introduction

The urgency to develop new modalities to treat drug-resistant infections is unquestionable, especially for those caused by multi- and extensively-drug resistant Gram-negative pathogens. Reports of infectious strains resistant to all known clinically approved antibiotics have surfaced and raise the possibility that common infections may soon become untreatable if new therapeutic advancements are not developed in a timely fashion.<sup>3</sup>

All currently available antibiotics inhibit a limited number of enzymes and processes that have essential functions for bacterial growth.<sup>4</sup> The dogma in the field is that only compounds that completely inhibit cell growth will prove to be clinically useful. Despite intensive efforts, few new targets or drug classes have been identified for Gram-negative bacteria in the past 50 years.<sup>5</sup> In fact, the ability to address resistance has resorted in large part to structural modification of known classes.<sup>6</sup> This approach typically provides only short-lived solutions, as new derivatives are susceptible to the rapid evolution of cross-resistance.<sup>7</sup> The reality is that bacterial resistance now outpaces our ability to derivatize known scaffolds and advance the new entities to the clinic. Thus, new targets, antibacterial chemotypes, and approaches are desperately required. In contrast to traditional approaches, one strategy that is gaining significant traction is to render organisms vulnerable to host immune clearance by targeting virulence determinants or processes that control the expression of virulence factors.<sup>8</sup>

In this context, bacterial two-component signal transduction systems (2CSTS) represent attractive targets for antibacterial drug discovery. In contrast to 2CSTS, that act usually at histidine and aspartate residues, mammalian signal transduction systems utilize kinases and phosphatases that act at tyrosine, serine, or threonine residues.<sup>9</sup> Because 2CSTS are ubiquitous in bacteria, are not found in mammals, and perform phosphorelay on different amino acids, they are excellent

antimicrobial targets. These systems consist of a sensory kinase (SK) and a response regulator (RR). In response to a stimulus (1, **Figure 2.1**), the SK autophosphorylates a conserved histidine (2, **Figure 2.1**), and a cognate RR catalyzes the transfer of this phosphate group to itself on an aspartic acid residue (3, **Figure 2.1**).<sup>10</sup> Phosphorylation of the RR leads to a biological response, usually resulting in changes to gene transcription. Some SKs also possess phospho-RR phosphatase activity (4, **Figure 2.1**) and are thus critical to signaling duration.<sup>9</sup> Loss of SK phosphatase activity leads to persistent RR phosphorylation and thus constitutive activation of the pathway.

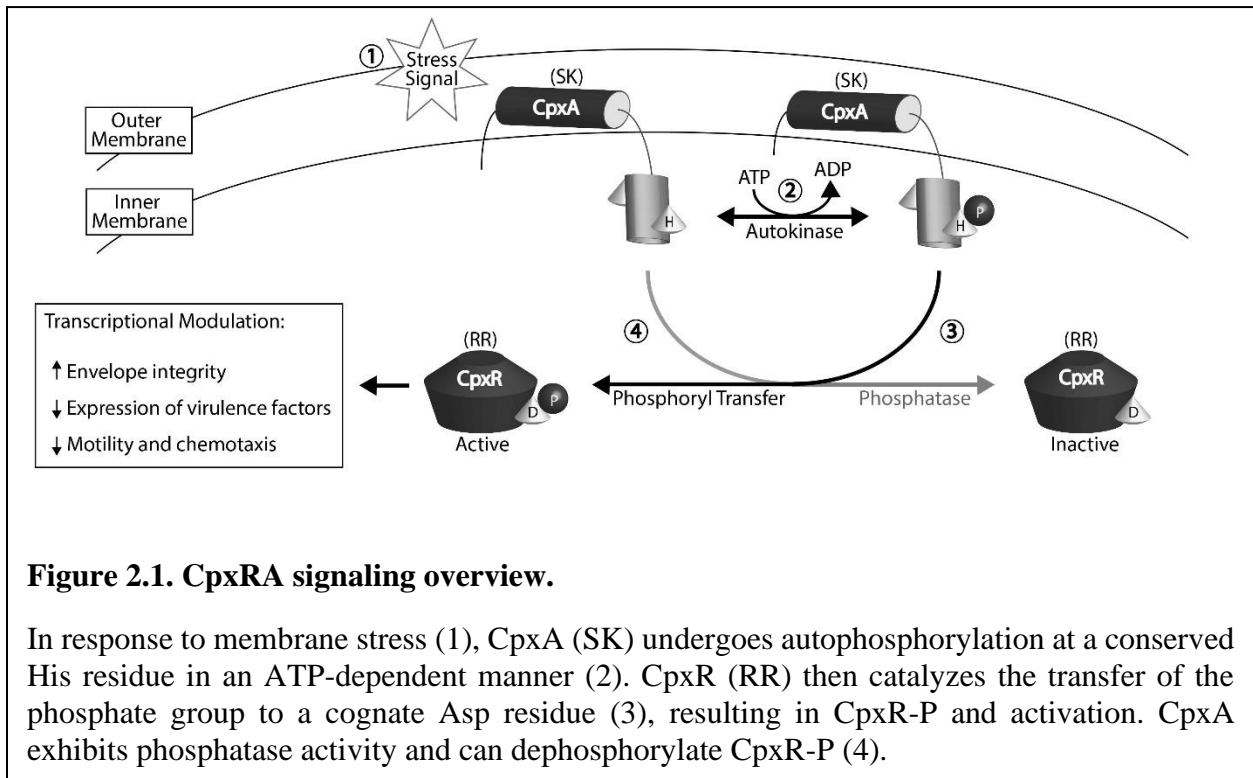


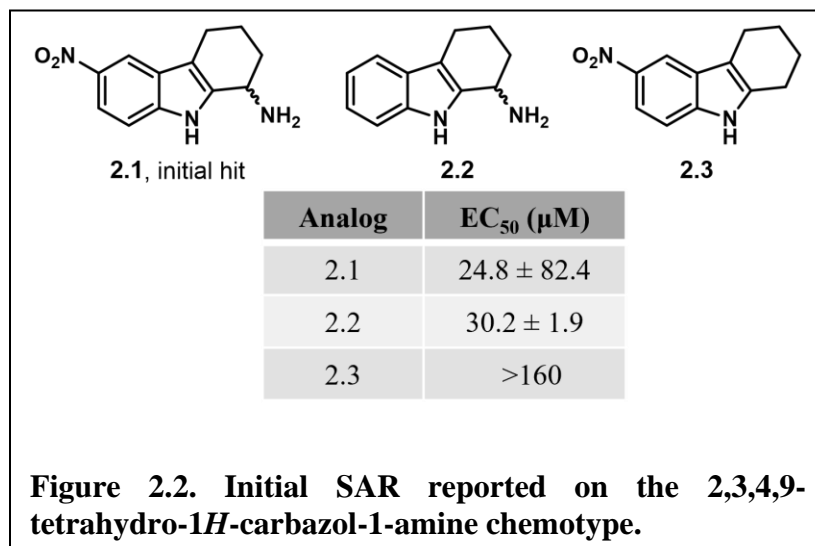
**Figure 2.1. CpxRA signaling overview.**

In response to membrane stress (1), CpxA (SK) undergoes autophosphorylation at a conserved His residue in an ATP-dependent manner (2). CpxR (RR) then catalyzes the transfer of the phosphate group to a cognate Asp residue (3), resulting in CpxR-P and activation. CpxA exhibits phosphatase activity and can dephosphorylate CpxR-P (4).

CpxRA, (SK = CpxA; RR = CpxR) is a 2CSTS found in many drug-resistant Gram-negative bacteria, including all members of the *Enterobacteriaceae*, *Neisseria gonorrhoeae*, and *Haemophilus ducreyi*. A major function of CpxRA is to alleviate membrane stress by reducing protein traffic through the cell membrane.<sup>10</sup> Activation of CpxRA reduces the expression of

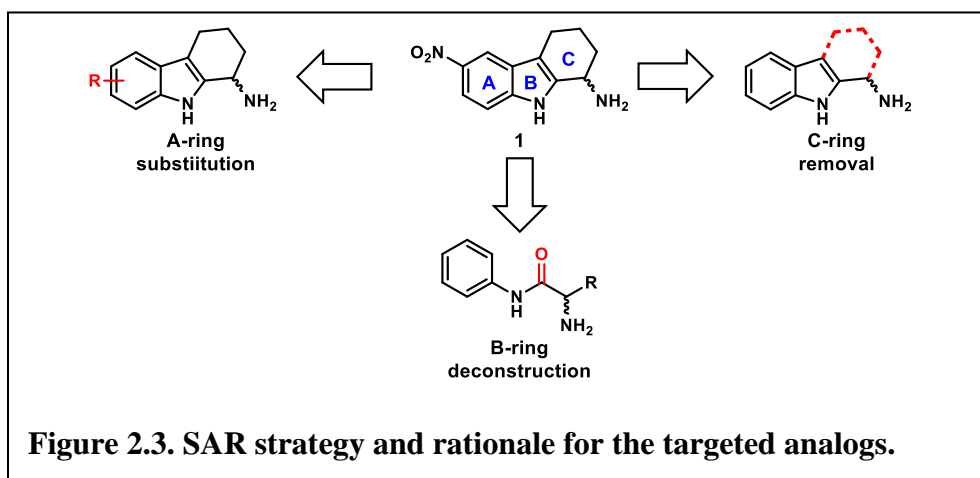
virulence factors, which must traverse the cytoplasmic membrane to reach the cell surface. Uncontrolled, genetic activation of CpxRA abolishes the virulence of *Salmonella enterica* serovar Typhimurium in mice.<sup>11</sup> Additionally, genetic activation of CpxRA abolishes the ability of *H. ducreyi* to cause disease in human volunteers,<sup>12</sup> of *N. gonorrhoeae* to infect mice,<sup>13</sup> and impairs the ability of uropathogenic *Escherichia coli* (UPEC) to cause pyelonephritis in mice.<sup>14</sup> Thus, activation of CpxRA impairs the ability of multiple extracellular and intracellular pathogens to infect their experimental or natural hosts.

Most of what is known about 2CSTS has been produced through genetic manipulation of the pathway constituents or by the development of a few small molecule inhibitors of these systems.<sup>15,16</sup> As such, the development of chemical probes to selectively modulate these systems is a valuable pursuit, as these tools could be used to advance the understanding of these pathways and provide a better picture of therapeutic utility. Recently, compound **2.1** (**Figure 2.2**) was shown to inhibit the phosphatase activity of CpxA, resulting in accumulation of CpxR-P and thus activation of the CpxRA system (**Figure 2.1**) as measured by a phospho-CpxR sensitive *lacZ* reporter in *E. coli* cells.<sup>17</sup> In this chapter, we report our initial progress in advancing the structure-activity relationships (SAR) for this 2,3,4,9-tetrahydro-1*H*-carbazol-1-amine scaffold.



## 2.2 Results and discussion

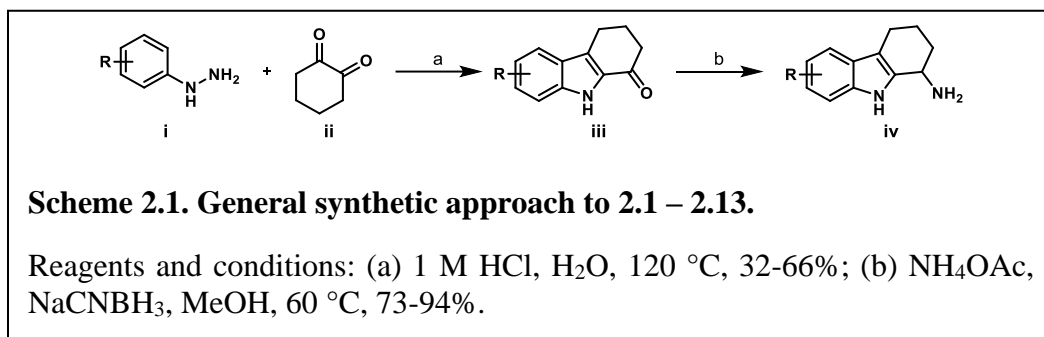
Results reported in the initial discovery paper indicate that the 6-nitro functionality is not required for CpxA phosphatase inhibition (**2.2, Figure 2.2**), but that removal of the primary amine abolishes activity (**2.3, Figure 2.2**). To advance the SAR on this chemotype, we focused on three major approaches to reveal structural motifs important for CpxA inhibition: 1) A-ring substitution, 2) B-ring deconstruction to provide N-arylated amino acid derivatives and 3) C-ring removal to give 2-alkylamino substituted indoles (**Figure 2.3**). Compounds were initially evaluated for their ability to activate a CpxR-responsive *lacZ* reporter in a modified *E. coli* strain.<sup>17</sup>



### 2.2.1 A-ring substitution.

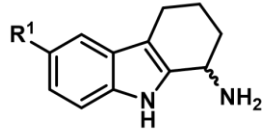
Due to previous observations that substitution is allowed on the 5-position of the indole and may provide a means to alter the potency of this class, we evaluated a number of substituents that ranged broadly in size, polarity, and hydrogen bonding capabilities. Analogs were prepared in straight forward fashion via a two-step process employing Fischer-indole methodology<sup>18</sup> followed by reductive amination (**Scheme 2.1**). As shown in **Figure 2.4**, the presence of a chlorine or fluorine at the 5-position (**2.5 – 2.6**) provided the best activity, favoring the smaller, fluorine (**2.6**).

While incorporation of bromine at this position was also evaluated, evidence of cytotoxicity and general activation of the stress response in the reporter strain was noted and thus the level of CpxRA activation could not be determined. Installation of a trifluoromethyl group at the 5-position (**2.7**) also provided equipotency to compound **2.1**. Incorporation of more electron rich substituents like a methoxy (**2.8**) or methyl (**2.9**) group was detrimental to activity. Inclusion of various other resonance mediated electron withdrawing groups such as a methyl ester (**2.10**), carboxylic acid (**2.11**), sulfonamide (**2.12**), or nitrile (**2.13**) failed to induce reporter activity beyond baseline, indicating no CpxA phosphatase inhibition for these analogs.



In hopes of revealing activity trends based on basic physicochemical Hansch parameters (e.g., lipophilicity ( $\pi$ ), size ( $E_s$ ), and electronics ( $\sigma_p$ )),  $-\log(EC_{50})$  values were plotted versus individual descriptors. Unfortunately, no obvious linear free energy relationship correlations are observed.





Analog	EC <sub>50</sub> (μM)	π	E <sub>s</sub>	σ <sub>p</sub>
2.1	24.8 ± 1.4	-0.28	-2.52	0.78
2.2	30.2 ± 1.1	0.0	0.0	0.0
2.4	ND <sup>a</sup>	0.86	-1.16	0.23
2.5	10.9 ± 3.4	0.71	-0.97	0.23
2.6	7.7 ± 0.2	0.14	-0.46	0.06
2.7	23.1 ± 7.7	0.88	-2.40	0.54
2.8	>100	-0.02	-0.55	-0.27
2.9	34.1 ± 1.8	0.56	-1.24	-0.17
2.10	>100	-0.01	-	0.45
2.11	>100	-0.28	-	0.45
2.12	>100	-1.82	-	0.57
2.13	>100	-0.57	-0.51	0.66

**2.1**, R<sup>1</sup> = NO<sub>2</sub>  
**2.2**, R<sup>1</sup> = H  
**2.4**, R<sup>1</sup> = Br  
**2.5**, R<sup>1</sup> = Cl  
**2.6**, R<sup>1</sup> = F  
**2.7**, R<sup>1</sup> = CF<sub>3</sub>  
**2.8**, R<sup>1</sup> = OMe  
**2.9**, R<sup>1</sup> = Me  
**2.10**, R<sup>1</sup> = COOMe  
**2.11**, R<sup>1</sup> = COOH  
**2.12**, R<sup>1</sup> = SO<sub>2</sub>NH<sub>2</sub>  
**2.13**, R<sup>1</sup> = CN

**Figure 2.4. β-galactosidase activity of A-ring substituted analogs.**

<sup>a</sup>Evidence of stress response activation due to cytotoxicity. Results are provided as the mean ± SEM of at least three separate experiments performed in triplicate. ND = not determined.

To further the interrogation of A-ring substitution, we performed a “substituent walk” to evaluate the optimal positioning for the fluoro and trifluoromethyl substituents. The observation that the 6-fluoro analog **2.16** exhibited near equipotency to **2.6** led us to synthesize and evaluate the 5,6-difluoro analog **2.20** (Figure 2.5). Gratifyingly, this substituent combination proved to be additive and improved activity ~3-fold from compound **2.6** and ~5-fold from compound **2.16** (Figure 2.5). Overall, in comparison to the initial hit **2.1** and the unsubstituted derivative **2.2**, compound **2.20** exhibits ~9-fold and ~11-fold improvements in cellular potency, respectively.

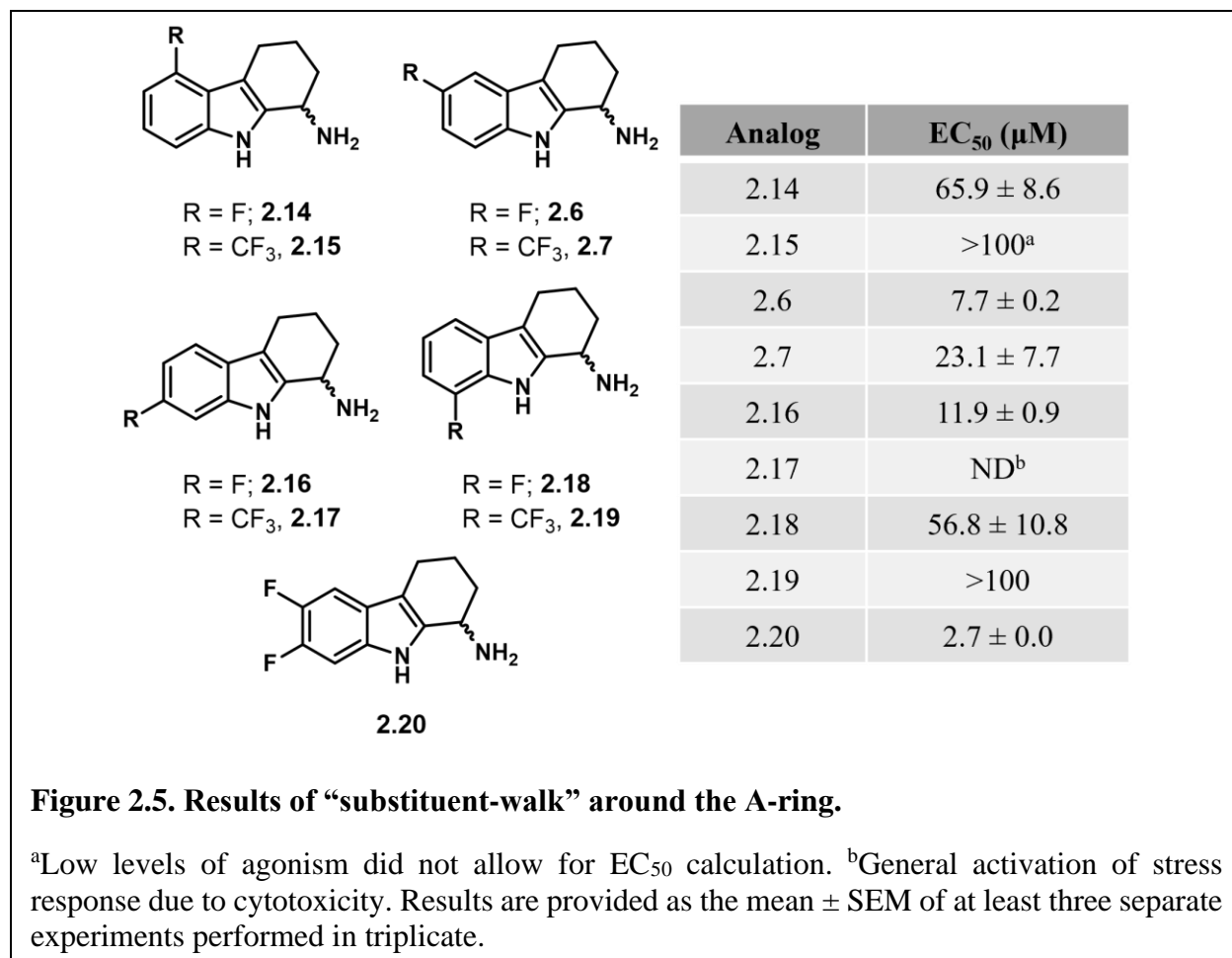
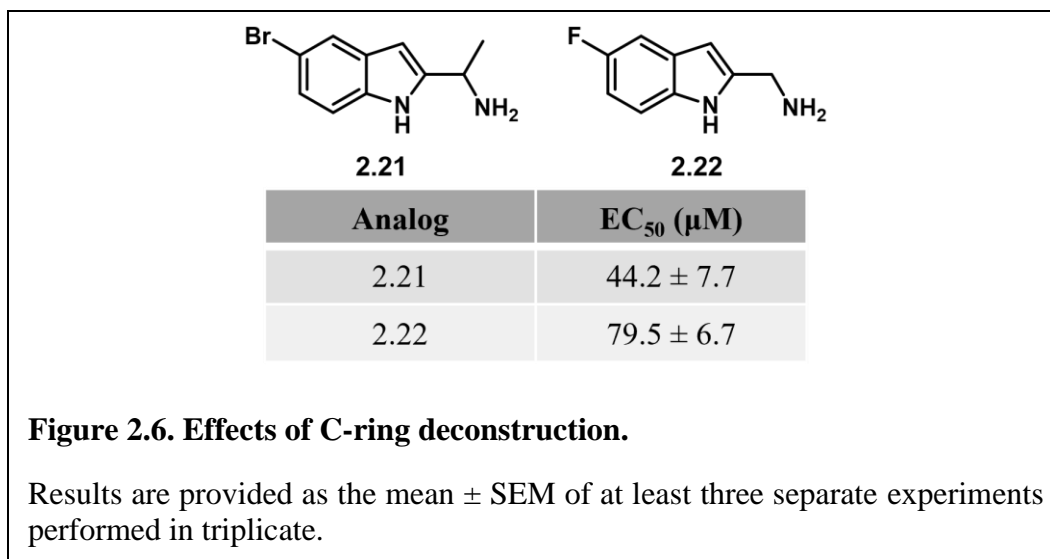


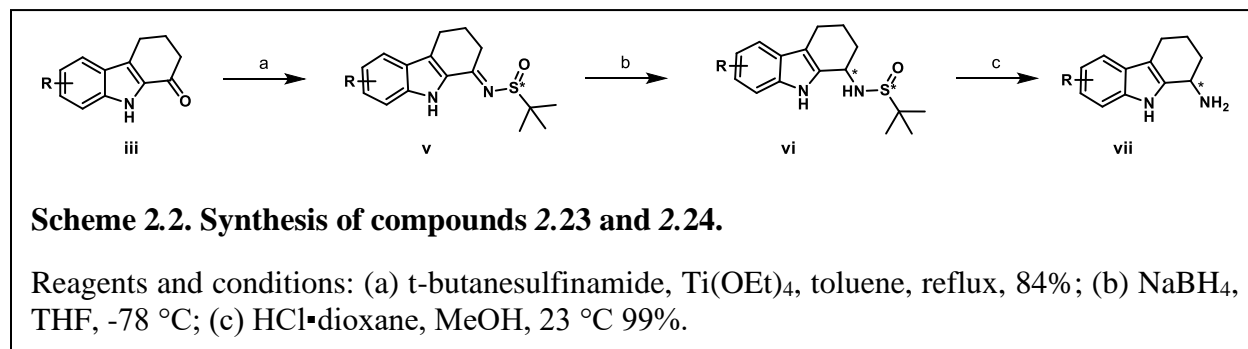
**Figure 2.5. Results of “substituent-walk” around the A-ring.**

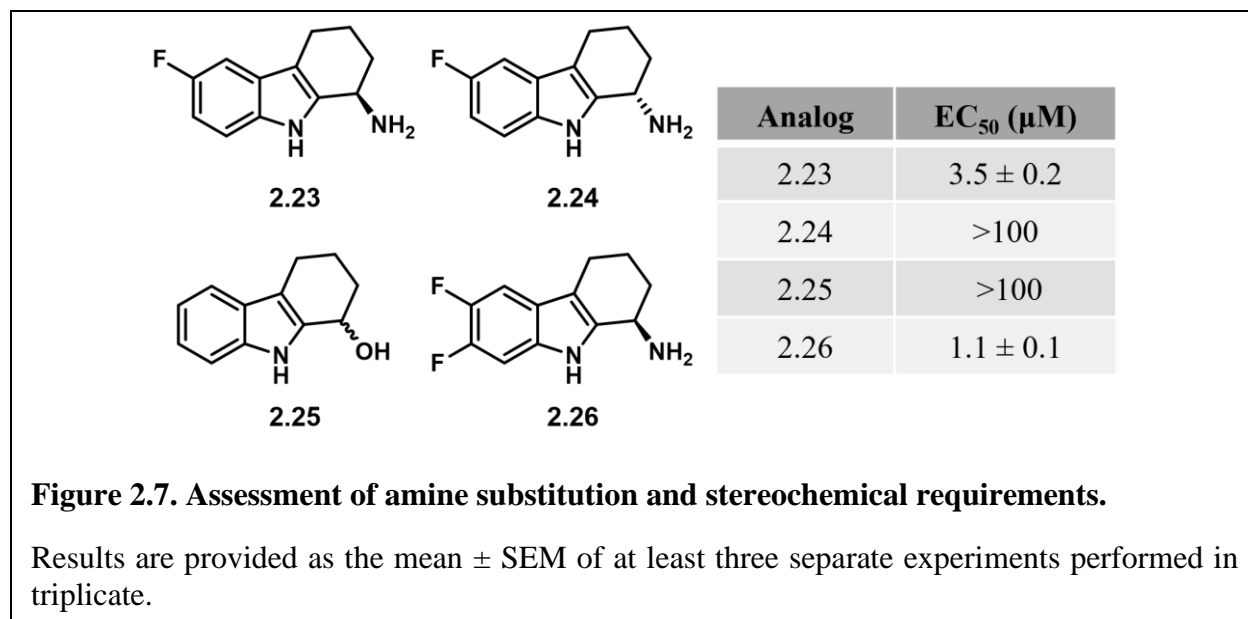
### 2.2.2 C-ring deconstruction.

In parallel to the A-ring studies, two derivatives lacking the intact C-ring were assessed for CpxRA agonism and thus provide insight into the importance of this feature. As shown in **Figure 2.6**, simplification of the 2,3,4,9-tetrahydro-1H-carbazol-1-amine scaffold to provide compound **2.21** resulted in a ~6-fold loss in activity when compared to **2.6**. Further simplification to compound **2.22**, however, resulted in an additional ~2-fold reduction in activity, even with the more active 5-fluoro A-ring. These initial results suggest that the C-ring is not necessary for target engagement, but likely provides beneficial conformational bias that improves ligand-target engagement. It is also worth noting that **2.21** showed no signs of general activation of the stress response, a complication observed for the related compound, **2.4**.



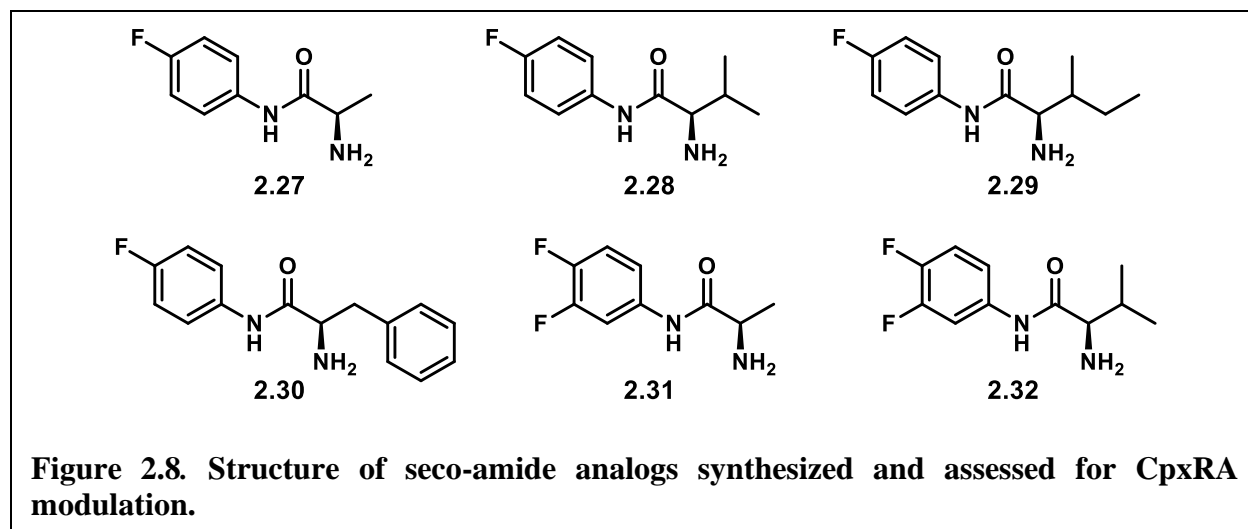
In addition to C-ring deconstruction, we were interested in probing the requirements associated with the primary amine. As mentioned previously, initial studies revealed the amine to be essential for activity (**Figure 2.2**). It was not known, however, if stereochemical preference exists at this position and/or if the amino group was simply providing hydrogen bond interactions that could be replenished with different functionalities. To probe these questions, we synthesized **2.23 – 2.25** (**Figure 2.7**). Access to enantiopure amines was achieved through the use of Ellman's sulfonamides as chiral auxiliaries to induce stereoselective reductive amination (**Scheme 2.2**). As shown in **Figure 2.7**, only one of the two enantiomers is active, with the (R)-enantiomer **2.23** being eutomer and the (S)-enantiomer **2.24** the distomer.





Additionally, replacement of the primary amine with a primary alcohol abolishes activity (compare **2.25** and **2.2**, **Figure 2.2**). As demonstrated by **2.26**, incorporation of the 5,6-difluoroindole with the (R) stereocenter produces the same enhancement in activity as noted with the racemic series and provides the most active compound identified in this series to date.

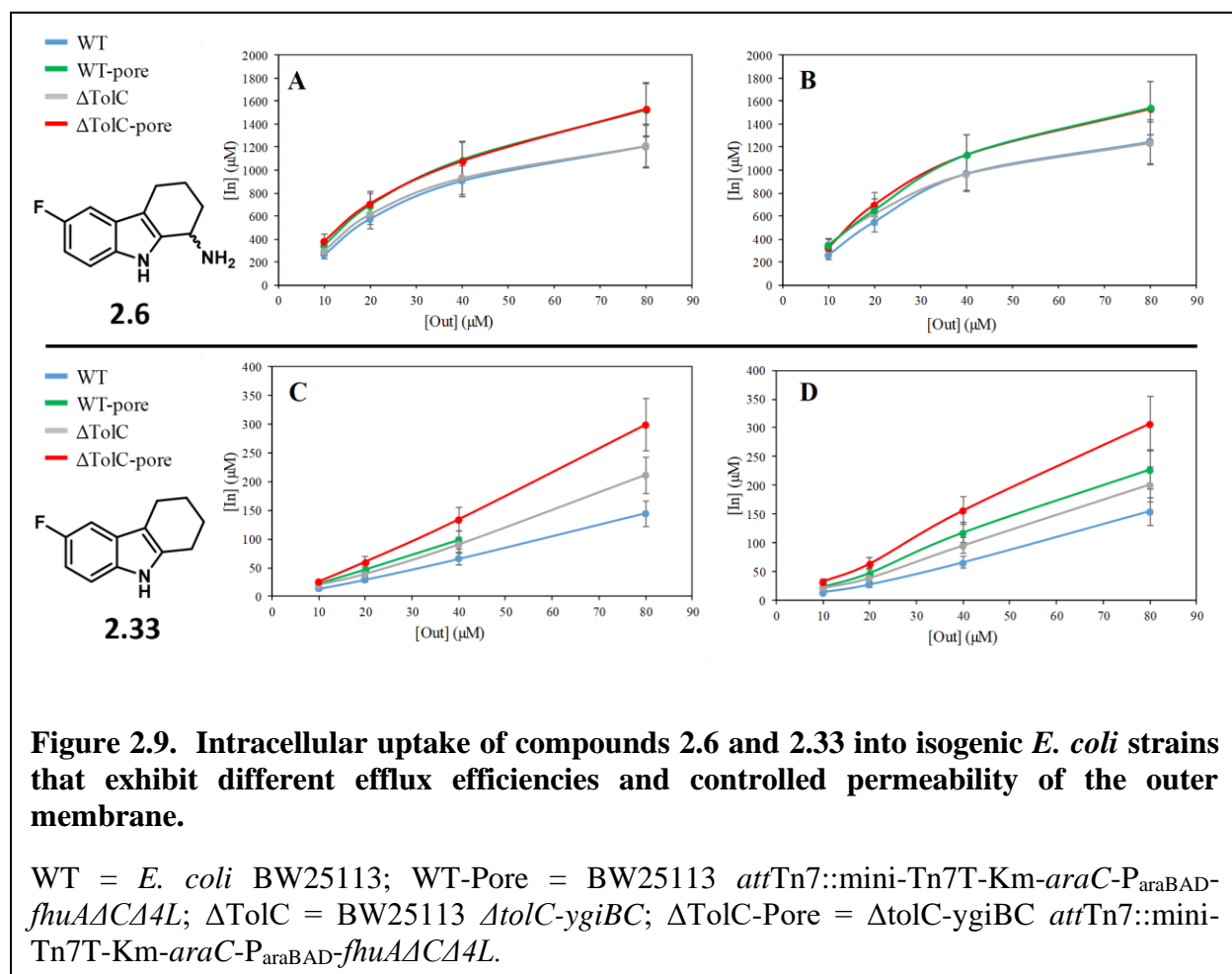
Considering the seemingly dispensable C-ring, the requirement for a primary amine, and necessity of (R) stereochemistry, we were intrigued by the possibility of simplifying this scaffold even further through the deconstruction of the B-ring to arrive at more synthetically tractable N-arylated amino acids. As shown in **Figure 2.3** this chemotype retains the requisite A-ring and the  $sp^2$  hybridization of the carbon alpha to the “indole” nitrogen. The resulting amide is expected to adopt the more energetically favored trans geometry,<sup>19</sup> thus providing a reasonable isostere for the parent indole, while alleviating the rigidity of the parent heterocycle. Unfortunately, all analogs synthesized in this series (**Figure 2.8**) were inactive at concentrations up to 80  $\mu\text{M}$ .



### 2.2.3 Significance of the primary amine.

The dependence of compound activity on the stereochemistry of the primary amine is indicative of interaction with a 3-dimensional binding pocket within CpxA. Additionally, our SAR indicates that the amine is essential for activity. In light of the recent work by the Hergenrother lab<sup>20</sup> that highlights the importance of primary amines in porin mediated transport, we were curious if the primary amine was also involved in permeation and/or accumulation of the 2,3,4,9-tetrahydro-1*H*-carbazol-1-amine chemotype in Gram-negative bacteria. To evaluate this, we utilized an established mass spectrometry method to determine the accumulation of compounds **2.6** and **2.33** in isogenic strains of *E. coli* with different efflux efficiencies and controlled permeability of the outer membrane. WT-Pore cells contain the wild-type repertoire of efflux pumps and the arabinose-controlled large pore that when expressed, permeabilizes the outer membrane to antibiotics as large as vancomycin.<sup>21</sup> The  $\Delta$ TolC cells are efflux-deficient derivatives lacking the outer membrane channel TolC required for the activity of various efflux pumps of *E. coli*. Cells with intact and hyperporinated (induced) outer membranes were incubated with increasing concentrations of compounds **2.6** and **2.33** and the intracellular accumulation was

analyzed after 1 and 40 minutes of incubation with compounds. As seen in **Figure 2.10**, compound **2.33**, which lacks the primary amine, is susceptible to efflux and suffers from poor permeability across the outer membrane. Compound **2.6** on the other hand contains the primary amine, accumulates at much higher intracellular levels overall, is still sensitive to efflux, albeit to a lesser extent, and accumulates less in wild-type than in efflux deficient *E. coli*. Additionally, **2.6** accumulates equally well in the cells with intact and hyperporinated outer membrane. These results clearly demonstrate that the primary amine is not only involved in target engagement but is also imperative to the permeation and accumulation in a Gram-negative organism.



#### **2.2.4 Probing the mechanisms of CpxRA modulation.**

**Compound 2.23 causes CpxR-P accumulation in CFT073.** As mentioned previously, **2.1** is believed to indirectly activate the CpxRA 2CSTS through the inhibition of CpxA phosphatase activity, thus rendering CpxR phosphorylated for an indefinite period of time. To confirm whether the results of the lacZ reporter assay observed for the more potent derivatives of compound **2.1** were consistent with mechanisms reported for **2.1**, we evaluated the ability of **2.23** to inhibit CpxA phosphatase activity through Phos-Tag methodology, gel visualization, and densitometry quantification of CpxR phosphorylation levels, exactly as described.<sup>17</sup> As is seen **Figure 2.10A** and as reported previously,<sup>17</sup> both the  $\Delta$ cpxA mutant and the compound-treated wild type (WT) expressed more CpxR than the untreated wild type, likely because CpxR-P positively autoregulates its transcription. Similar to compound **2.1**, treatment with compound **2.23** (10  $\mu$ M) caused a statistically significant increase in the ratio of CpxR-P to CpxR relative to the untreated wild type and the  $\Delta$ cpxA mutant. In contrast, activation in the  $\Delta$ cpxA mutant increased the accumulation of CpxR-P but did not cause a statistically significant increase in the ratio of CpxR-P to CpxR compared to the wild type. Taken together, the data suggest that pharmacological activation of CpxRA by inhibition of CpxA phosphatase activity yields different results than activation via deletion of cpxA, perhaps because CpxA kinase activity is retained in the pharmacological approach.

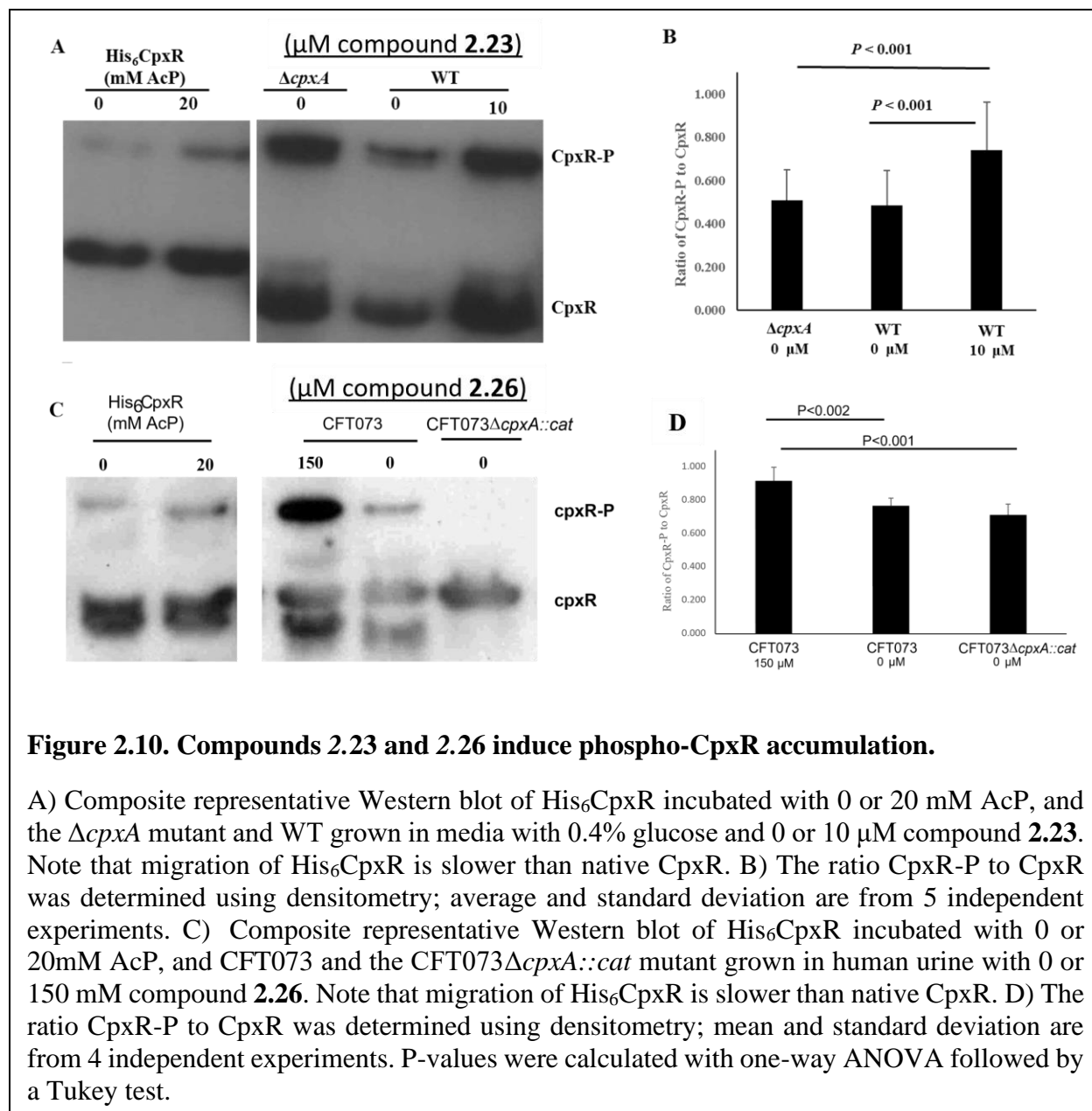
#### **Compound 2.26 causes CpxR-P accumulation in CFT073 cultured in human urine.**

After confirming the ability of compound **2.23** to modulate CpxR-P accumulation in the UPEC cell models, we extended the evaluation to its difluoro analog **2.26**, which had a mean EC<sub>50</sub> value (1.1  $\mu$ M) that was ~3-fold lower than **2.23**. Similar to the Phos-Tag methodology described above, we evaluated the ability of **2.26** to inhibit CpxA phosphatase activity in human urine samples,

which are absent of glucose. We chose 150  $\mu$ M as this was the approximate trough concentration of compound **2.6** detected in murine urine after 3 days of treatment. Compound **2.26**-treated WT (CFT073) induced accumulation of CpxR-P that was higher than that of the untreated WT and  $\Delta$ *cpxA* mutant (CFT073 $\Delta$ *cpxA::cat*) controls (**Figure 2.10C**). Consistent with the fact that CpxR-P positively increases *cpxR* transcription, total CpxR levels were higher in compound **2.26**-treated WT than in the WT and  $\Delta$ *cpxA* mutant controls. As expected, CFT073 $\Delta$ *cpxA::cat* failed to increase expression of CpxR or CpxR-P because urine lacks glucose, which is needed for the formation of acetyl phosphate.

Compound **2.26** increased the ratio of CpxR-P to CpxR in CFT073 by 1.3- ( $P < 0.002$ ) and 1.4- ( $P < 0.001$ ) fold, respectively, compared to the CFT073 and CFT073 $\Delta$ *cpxA::cat* controls (**Figure 2.10D**). These data suggest that treatment of CFT073 by **2.26** does not inhibit bacterial growth and fosters production of CpxR and accumulation of CpxR-P, and that CpxA acts as a net kinase during growth in human urine.

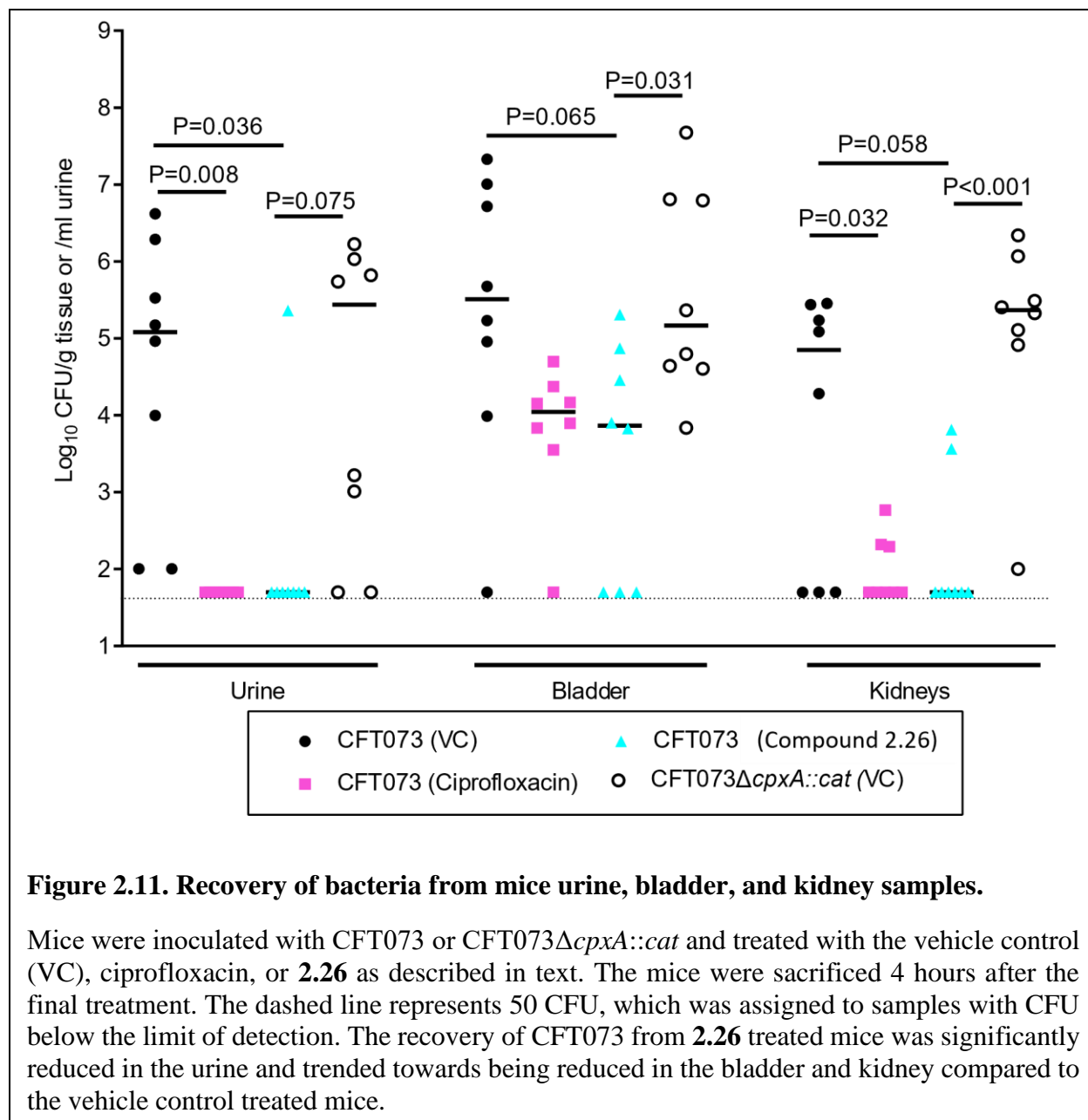




**Compound 2.26 is effective for treatment of UTIs in the murine model.** In the interest of investigating the ability of pharmacologically activated CpxR to mimic the *cpxA* deletion phenotype, we evaluated the efficacy of **2.26** for treatment of UTIs in the murine model.<sup>2</sup> The 4-arm trial included a group inoculated with CFT073 and treated with the vehicle control, a group inoculated with the CpxA deletion mutant (CFT073*ΔcpxA::cat*) and treated with the vehicle

control, a group inoculated with the parent UPEC strain (CFT073) and treated with compound **2.26**, and a group inoculated with CFT073 and treated with ciprofloxacin.

While the *cpxA* mutant was recovered at levels generally similar to those of the parent transformed with an empty vector, mice treated with ciprofloxacin or **2.26** retained a median of 1,000-fold less bacteria cells in urine and kidney samples and 10-fold less in bladder samples. Mice inoculated with CFT073 and treated with ciprofloxacin had significantly lower recoverable CFU in the urine ( $P = 0.008$ ) and kidneys ( $P = 0.032$ ) but not the bladder ( $P = 0.174$ ) compared to the CFT073 inoculated and vehicle treated controls (**Figure 2.11**). Treatment of mice inoculated with CFT073 with 100 mg/kg of **2.26** significantly lowered the recoverable CFU in the urine ( $P = 0.036$ ) and trended towards lowering the CFU in the bladder ( $P = 0.065$ ) and the kidneys ( $P = 0.067$ ) compared to the CFT073 inoculated and vehicle treated controls (**Figure 2.11**). In comparing the groups inoculated with CFT073 and treated with **2.26** or ciprofloxacin, there were no significant differences in the recoverable CFU in the urine, bladder, and kidneys (all  $P > 0.9$ ). Thus, our lead compound **2.26** was found to be as active as ciprofloxacin in mouse urine, bladder, and kidney samples, which is significant considering ciprofloxacin is believed the standard treatment for patients with complicated UTIs.<sup>22-24</sup>



**The proteome of 2.26-treated CFT073 grown in human urine is distinct from that of untreated CFT073.** To further probe mechanisms of the CpxRA 2CSTS and pharmacological versus genetic modulation, the proteome profiles of *E. coli* CFT073-UPEC samples were sequenced and analyzed in three groups: wild-type cells treated with compound **2.26**, *cpxA* deletion mutant, and wild-type cells treated with empty vector. A total of 22677 unique peptides corresponding to 2241 unique proteins were identified and quantified. Each protein was identified

with very high confidence level (1% FDR) for the sequence assignments after LC-MS/MS analysis. A label-free quantitative analysis among the three groups (WT-C26 = compound treated, Cpx = *cpxA* mutant, VC = control group) successfully quantified a total of 2241 proteins. The reproducibility among biological replicates and the differences between three groups were assessed using a principal component analysis (PCA) (**Figure 2.12**). The PCA showed high reproducibility among replicates based on the close clustering of the replicates for each group, with significant difference observed among the groups. Protein abundance ratios were calculated to give Cpx/VC, WT-C26/VC, and WT-C36/Cpx where differential protein regulation was defined as upregulated when the abundance ratio  $\geq 2.0$  or downregulated when the abundance ratio  $\leq 0.5$  at an adjusted p-value of  $<0.05$ .

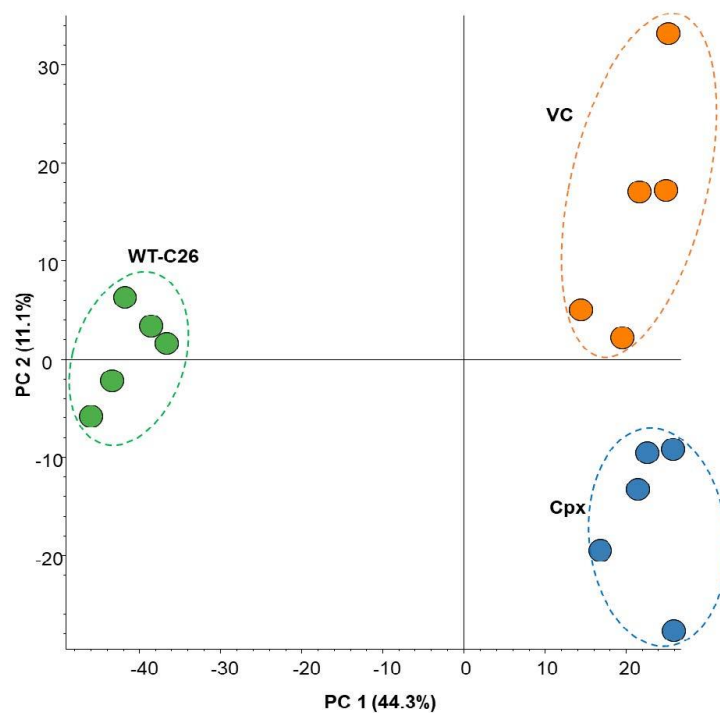
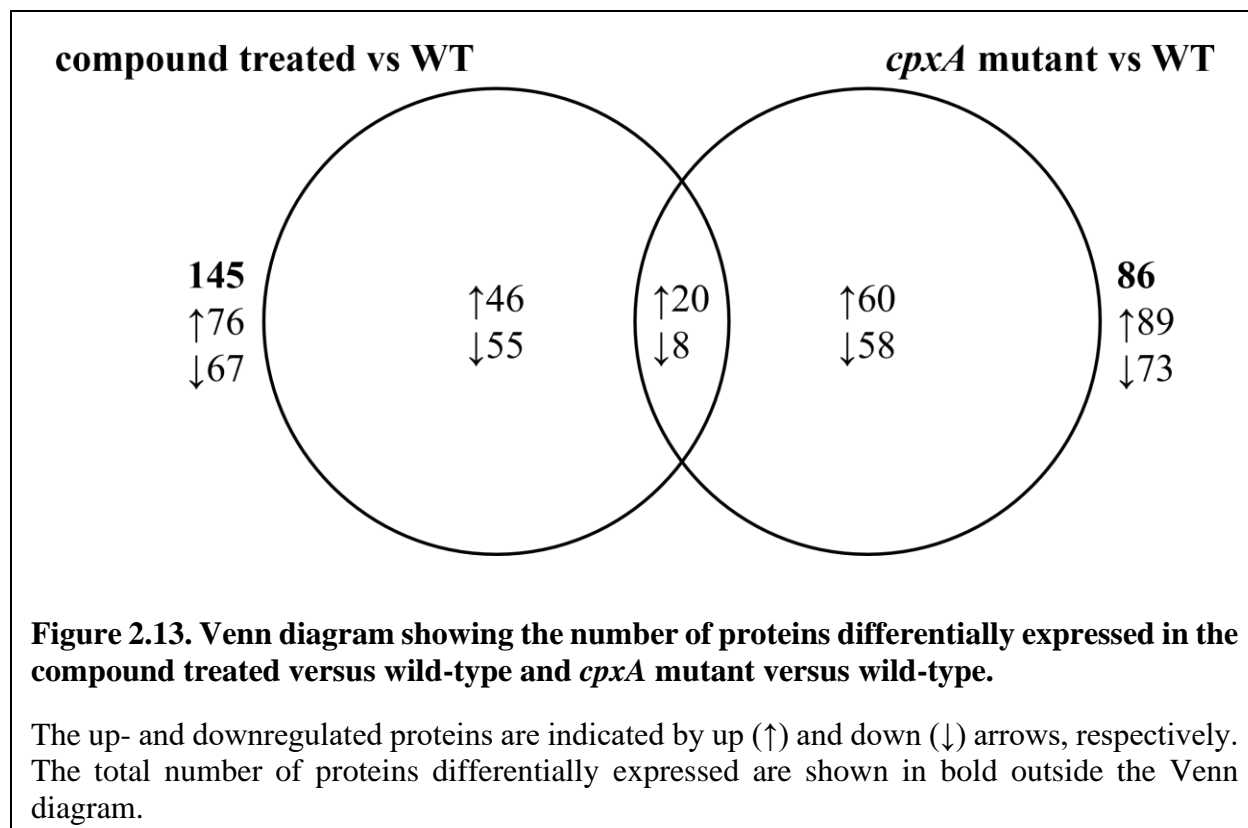


**Figure 2.12. Principal component analysis (PCA) of total protein abundance of WT-C26, VC, and Cpx samples.**

Total proteome identified from five biological replicates were subjected to quantitative analysis. PCA shows close clustering of the total normalized protein abundance (peak area) of the replicates of WT-C26, VC, and Cpx samples.

A comparison between compound treated cells and the wild-type untreated revealed 76 upregulated proteins and 67 downregulated proteins, whereas a comparison between the  $\Delta cpxA$  mutant and wild-type revealed 89 upregulated proteins and 73 downregulated proteins. Among these proteins, 20 were upregulated and 8 were downregulated in both the compound treated cells and the  $\Delta cpxA$  mutant (**Figure 2.13**). Interestingly, 4 of the downregulated proteins within these two groups are involved in metal ion transport and maintenance (**Table 2.1**) including those affiliated with iron (c5174, YcdO), zinc (ZntB, YgeY), and cobalt (YgeY) biology.



Iron is an essential nutrient for growth of *E. coli*, and since the availability of this element within the host is limited due to sequestration by human heme proteins, pathogenic *E. coli* have evolved a variety of mechanisms to acquire iron from host sources.<sup>25</sup> For instance, siderophores are small molecular ion chelators whose primary function are to scavenge iron.<sup>26</sup> Transport of iron associated with siderophores requires specific outer membrane receptors such as TonB and its accessory proteins, ExbB and ExbD.<sup>27</sup> Gene ID c5174 is putatively associated with the iron-regulated outer membrane virulence protein within the TonB-dependent receptor (TBDR) family.<sup>28</sup> TBDRs mediate substrate-specific transport across the outer membrane and are involved in the uptake and utilization of several nutrients including chelated iron and vitamin B<sub>12</sub>.<sup>27</sup> A previous study by Payne et al. found that the *tonB* mutant of the UPEC strain CFT073 was attenuated for infection of the bladder and kidney, indicating that CFT073 requires TonB *in vivo* to mediate the uptake of iron during colonization and multiplication within the urinary tract.<sup>29</sup> Our

proteomic analysis found that c5174 was significantly downregulated in both the *cpxA* mutant and compound-treated CFT073 cells. The gene encoding the iron uptake system component EfeO (*ycdO*) was also significantly downregulated in the two groups. This, along with evidence that the *efeUOB* operon is shown to be induced by acid in a CpxRA-dependent manner driving iron import,<sup>30</sup> suggests that the mechanism behind UPEC fitness impairment by the CpxRA 2CSTS is associated with iron transport and sequestration.

**Table 2.1. Downregulated proteins in both the *cpxA* mutant and compound treated WT.**

Ensembl Gene ID	Gene Symbol	Protein Function <sup>31</sup>
Ion Transport Proteins		
c1816	<i>zntB</i>	Mediates efflux of zinc ions
c3450	<i>ygeY</i>	Metal-binding (Zn <sup>2+</sup> , Co <sup>2+</sup> )
c5174	c5174	Putative iron-regulated outer membrane virulence protein
c1156	<i>ycdO</i>	Iron uptake system component EfeO
Membrane Proteins		
c0726	<i>mrda</i>	Catalyzes cross-linking of the peptidoglycan cell wall
c4364	<i>yhjW</i>	Sulfatase and phosphatase activity
Uncharacterized Proteins		
c4731	<i>yigA</i>	
c0886	<i>ybiJ</i>	

### 2.3 Conclusions and future directions

Urinary tract infection (UTI) is the most common form of extraintestinal infection due to *E. coli*, and *E. coli* is one of the most common causative agents of all types of UTIs with approximately 80% of uncomplicated UTIs in the United States caused by uropathogenic *E. coli* (UPEC).<sup>32</sup> UPEC strains expressing extended-spectrum  $\beta$ -lactamase and quinolone resistance are becoming more prevalent, raising the possibility that ordinary infections may soon become untreatable by our current arsenal of antibiotics. Given that conventional approaches to develop

new antibiotics have yielded few new drugs, the potential reward of exploring novel targets and mechanisms is very high.

Bacterial 2CSTS are major players in organismal pathogenicity, fitness, communication, biofilm formation, and antibacterial resistance making them attractive targets. Unfortunately, most of what we know about these systems has been revealed through genetic manipulation or small molecule inhibitors of such systems, which is not always indicative of therapeutic potential. As such, there is an increasing interest in developing small molecule probes that can be used to activate these systems to uncover new biology that may translate to new antibacterial approaches. Along these lines, we aimed to improve the activity of **2.1**, a newly identified CpxA phosphatase inhibitor that indirectly activates the CpxRA signaling pathway through increasing the lifetime of CpxR-P. Leveraging three different structural modification approaches, we identified compound **2.26** ( $EC_{50} = 1.1 \mu\text{M}$ ), which exhibits ~30-fold improvement in CpxA phosphatase inhibition over the initial hit **2.1** as determined in a cellular *lacZ* reporter assay. The stereochemical and conformational requirements found for the primary amine within this chemotype illustrates its importance in target engagement and involvement in membrane permeation and protection against efflux in *E. coli*.

With compound **2.26** as lead CpxA phosphatase inhibitor, its efficacy in mouse UTI models was explored. Compound **2.26** was found to be as active as ciprofloxacin in reducing pathogen fitness in urine, bladder, and kidney samples. Notably, the CFT073 $\Delta$ *cpxA* mutant grew in the same densities as CFT073 in the urine, bladder, and kidneys, while **2.26**-treated CFT073 had significantly lower recoverable CFU in all three compartments. The proteome profiles of *E. coli* CFT073-UPEC grown in urine were sequenced and analyzed in three groups: wild-type cells treated with compound **2.26**, *cpxA* deletion mutant, and wild-type cells treated with empty vector.



When comparing protein expression between the constitutively active CpxRA mutant cells (genetic modification) and the **2.26**-activated CpxRA cells (pharmacological activation), a decrease in the expression of metal-transport machinery was found in both. This commonality in the proteomes signifies that UPEC fitness impairment by the CpxRA 2CSTS is associated with iron transport and sequestration, a potential mechanism of action. In contrast, the CFT073 $\Delta$ cpxA mutant did not increase the expression of CpxR or CpxR-P, while CpxR and CpxR-P levels were significantly higher in **2.26**-treated CFT073. This led us to hypothesize that CpxA acts as a net kinase *in vivo* as **2.26** fosters accumulation of CpxR-P and downregulates virulence determinants. Since treatment of CFT073 by **2.26** does not inhibit bacterial growth but still alters UPEC fitness and expression of virulence factors, we have demonstrated that CpxA phosphatase inhibitors may be useful in treating UTIs caused by UPEC.

Although we have shown that chemo-modulation of the CpxRA 2CSTS is possible and has therapeutic relevance *in vivo*, we do not know general selectivity of the chemotype developed. Future studies will address the selectivity of the inhibitors and their pharmacokinetics. Nonetheless, this work provides useful SAR and a foundation for which to advance the utility of 2,3,4,9-tetrahydro-1*H*-carbazol-1-amines as chemical probes to uncover new biology and further understand the biological significance and therapeutic potential of CpxRA and 2CSTS in general.

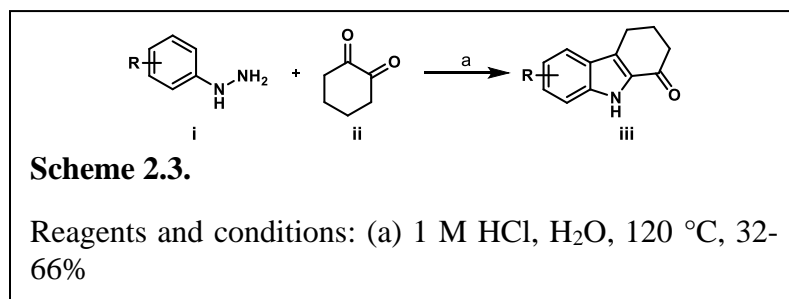
## **2.4 Experimental**

### **2.4.1 General Chemistry Methods**

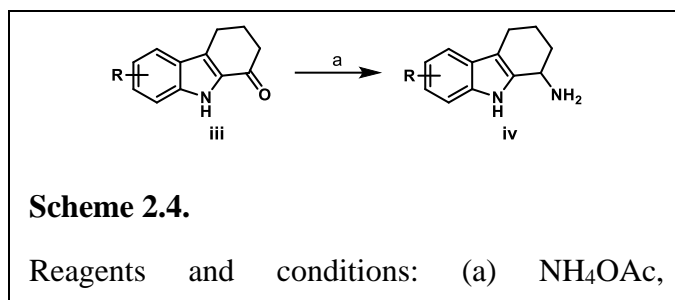
All commercial reagents were used without further purification. Distilled water was used for all water necessities in synthetic procedures (e.g., reagent, solvent, work-up). Flash column chromatography was performed with silica gel 60. TLC analyses were completed with EMD

Millipore silica gel coated (250  $\mu$ M) F254 glass plates and visualized with UV light. NMR samples were prepared in 5 mm tubes with 0.6 mL deuterated solvent. NMR data were all collected on a 300, 400, or 500 MHz (specified below) Varian VNMRs Direct Drive spectrometer equipped with an indirect detection probe. Data was collected at 25  $^{\circ}$ C unless otherwise indicated. Pulse sequences were used as supplied by Varian VNMRJ 4.2 software. All NMR data was processed in MestreNova v10. Peak positions are reported after reference centering on deuterated solvent of relevance.

### 2.4.2 Synthetic Procedures



**General procedure to prepare ketones iii.** A mixture of a substituted phenylhydrazine **i** (3.0 mmol), 1,2-cyclohexanedione **ii** (6.0 mmol), and water (50 mL) was stirred at room temperature (23  $^{\circ}$ C) in a 250 mL round bottom flask. After 16 h, 10 mL of aqueous 1 M HCl was added and the reaction was heated to reflux. After 12 h, the reaction was refrigerated to induce crystallization. The resulting solid was filtered and air dried to provide the crude product. The desired product was purified by flash column chromatography (SiO<sub>2</sub>) using 20-30% ethyl acetate in hexanes as the eluent. <sup>1</sup>H and <sup>13</sup>C NMR spectra for products were compared to literature values to confirm structure.



**General procedure to prepare racemic amines iv (2.1 - 2.20).** Solid  $\text{NH}_4\text{OAc}$  (5.0 mmol) was added to a stirring solution of requisite ketone **iii** (0.5 mmol) dissolved in 20 mL solvent grade  $\text{CH}_3\text{OH}$ , and this mixture was allowed to stir at room temperature (23 °C) for 3-6 h. Upon complete consumption of **iii**, as determined by thin layer chromatography, solid  $\text{NaCNBH}_3$  (2.5 mmol) was added and the temperature was raised to 60 °C. After stirring 12-16 h, the reaction was cooled to room temperature (23 °C) and treated with an aqueous 1 M  $\text{HCl}$  solution. The mixture was extracted with ethyl acetate, and the combined organic layers were washed with brine and dried over anhydrous  $\text{Na}_2\text{SO}_4$ , filtered, and concentrated under reduced pressure to afford the crude product. The desired product was purified by flash column chromatography ( $\text{SiO}_2$ ) using  $\text{CH}_2\text{Cl}_2$  and  $\text{CH}_3\text{OH}$  as the eluent.  $^1\text{H}$  and  $^{13}\text{C}$  NMR spectra for products were compared to literature values to confirm structure except as included below.

**6-fluoro-2,3,4,9-tetrahydro-1H-carbazol-1-amine (2.6):** Yield 26%, white amorphous solid.  $^1\text{H}$  NMR (400 MHz, Methanol- $d_4$ )  $\delta$  7.29 – 7.20 (m, 1H), 7.05 (dd,  $J = 9.8, 2.5$  Hz, 1H), 6.82 (ddd,  $J = 9.6, 8.7, 2.5$  Hz, 1H), 4.10 (dd,  $J = 7.1, 5.5$  Hz, 1H), 2.74 – 2.60 (m, 3H), 2.25 – 2.13 (m, 1H), 2.13 – 2.00 (m, 1H), 1.91 – 1.67 (m, 2H).  $^{13}\text{C}$  NMR (101 MHz, Methanol- $d_4$ )  $\delta$  158.9 (d,  $J = 232.0$  Hz), 140.0, 134.3, 128.9 (d,  $J = 9.3$  Hz), 112.4 (d,  $J = 9.7$  Hz), 111.4 (d,  $J = 5.2$  Hz), 110.0 (d,  $J = 26.4$  Hz), 103.7 (d,  $J = 23.3$  Hz), 46.6, 34.1, 22.2, 22.0.

**5-fluoro-2,3,4,9-tetrahydro-1H-carbazol-1-amine (2.14):** Yield 49%, white amorphous solid.  $^1\text{H}$  NMR (500 MHz, Methanol- $d_4$ )  $\delta$  7.20 (d,  $J = 8.2$  Hz, 1H), 7.10 (td,  $J = 8.0, 5.1$  Hz, 1H),

6.70 (dd,  $J = 11.0, 7.8$  Hz, 1H), 4.62 (t,  $J = 5.0$  Hz, 1H), 3.03 (dt,  $J = 16.4, 5.3$  Hz, 1H), 2.95 – 2.85 (m, 1H), 2.33 – 2.22 (m, 1H), 2.14 – 1.94 (m, 3H).  $^{13}\text{C}$  NMR (126 MHz, Methanol- $d_4$ )  $\delta$  158.8 (d,  $J = 245.1$  Hz), 140.8 (d,  $J = 11.5$  Hz), 129.1, 124.4 (d,  $J = 7.8$  Hz), 116.6 (d,  $J = 20.7$  Hz), 113.3 (d,  $J = 2.3$  Hz), 108.8 (d,  $J = 3.5$  Hz), 105.2 (d,  $J = 19.1$  Hz), 45.8, 29.0, 23.0, 20.2.

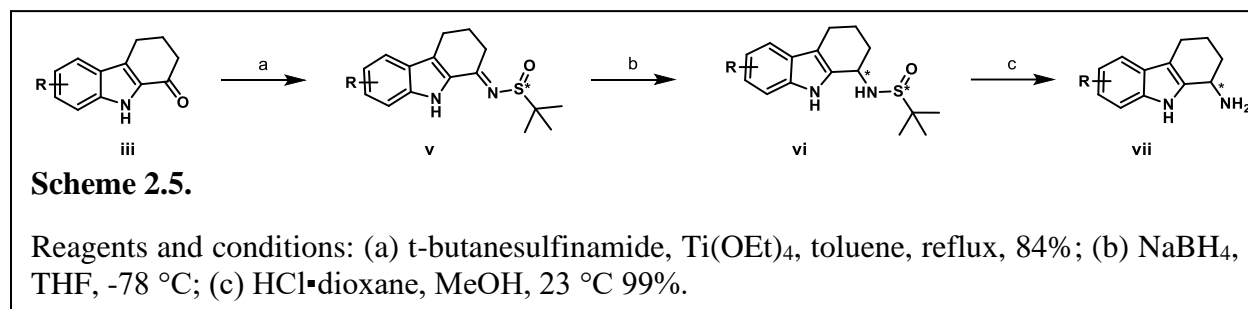
**5-(trifluoromethyl)-2,3,4,9-tetrahydro-1H-carbazol-1-amine (2.15):** Yield 67%, white amorphous solid.  $^1\text{H}$  NMR (500 MHz, Methanol- $d_4$ )  $\delta$  7.69 (dt,  $J = 8.2, 0.8$  Hz, 1H), 7.43 (dt,  $J = 7.4, 0.8$  Hz, 1H), 7.29 (ddd,  $J = 8.2, 7.5, 0.8$  Hz, 1H), 4.71 (t,  $J = 5.2$  Hz, 1H), 2.97 (dt,  $J = 16.5, 5.4$  Hz, 1H), 2.87 – 2.77 (m, 1H), 2.34 – 2.24 (m, 1H), 2.16 – 1.95 (m, 3H).  $^{13}\text{C}$  NMR (151 MHz, Methanol- $d_4$ )  $\delta$  139.2, 131.6, 126.3 (q,  $J = 270.6$  Hz), 123.2, 122.7, 122.3 (q,  $J = 65.5, 32.7$  Hz), 118.5 (q,  $J = 6.3$  Hz), 117.0, 113.6, 46.0, 28.71 23.2, 20.3.

**7-fluoro-2,3,4,9-tetrahydro-1H-carbazol-1-amine (2.16):** Yield 39%, white amorphous solid.  $^1\text{H}$  NMR (500 MHz, Methanol- $d_4$ )  $\delta$  7.45 (dd,  $J = 8.6, 5.3$  Hz, 1H), 7.11 (dd,  $J = 9.9, 2.3$  Hz, 1H), 6.88 – 6.79 (m, 1H), 4.63 (t,  $J = 5.1$  Hz, 1H), 2.84 (dt,  $J = 16.0, 5.3$  Hz, 1H), 2.77 – 2.66 (m, 1H), 2.33 – 2.22 (m, 1H), 2.15 – 1.93 (m, 3H).  $^{13}\text{C}$  NMR (126 MHz, Methanol- $d_4$ )  $\delta$  161.7 (d,  $J = 236.8$  Hz), 138.3 (d,  $J = 12.6$  Hz), 129.5, 124.6, 120.7 (d,  $J = 10.4$  Hz), 115.3, 108.9 (d,  $J = 25.0$  Hz), 98.5 (d,  $J = 26.3$  Hz), 45.9, 29.3, 21.4, 20.2.

**7-(trifluoromethyl)-2,3,4,9-tetrahydro-1H-carbazol-1-amine (2.17):** Yield 85%, white amorphous solid.  $^1\text{H}$  NMR (600 MHz, Methanol- $d_4$ )  $\delta$  7.74 – 7.70 (m, 1H), 7.64 (d,  $J = 8.4$  Hz, 1H), 7.29 (d,  $J = 8.3$  Hz, 1H), 4.68 – 4.63 (m, 1H), 2.90 – 2.83 (m, 1H), 2.76 (dt,  $J = 15.3, 6.8$  Hz, 1H), 2.33 – 2.24 (m, 1H), 2.14 – 1.95 (m, 3H).  $^{13}\text{C}$  NMR (151 MHz, Methanol- $d_4$ )  $\delta$  137.1, 132.2, 130.2, 126.7 (d,  $J = 270.9$  Hz), 125.8 (d,  $J = 32.7$  Hz), 120.4, 116.8 (d,  $J = 3.9$  Hz), 115.4, 110.0 (d,  $J = 4.7$  Hz), 45.8, 29.2, 21.3, 20.1.

**8-fluoro-2,3,4,9-tetrahydro-1H-carbazol-1-amine (2.18):** Yield 55%, white amorphous solid.  $^1\text{H}$  NMR (500 MHz, Methanol- $d_4$ )  $\delta$  7.34 – 7.28 (m, 1H), 7.01 (td,  $J = 7.9, 4.7$  Hz, 1H), 6.96 – 6.88 (m, 1H), 4.67 (t,  $J = 5.2$  Hz, 1H), 2.91 – 2.81 (m, 1H), 2.81 – 2.70 (m, 1H), 2.37 – 2.25 (m, 1H), 2.16 – 1.95 (m, 3H).  $^{13}\text{C}$  NMR (126 MHz, Methanol- $d_4$ )  $\delta$  151.0 (d,  $J = 243.2$  Hz), 131.7 (d,  $J = 5.5$  Hz), 130.2, 126.2 (d,  $J = 13.3$  Hz), 120.8 (d,  $J = 6.0$  Hz), 116.0 (d,  $J = 2.4$  Hz), 115.8 (d,  $J = 3.4$  Hz), 108.5 (d,  $J = 16.3$  Hz), 46.0, 29.3, 21.5, 20.3.

**8-(trifluoromethyl)-2,3,4,9-tetrahydro-1H-carbazol-1-amine (2.19):** Yield 99%, yellow amorphous solid.  $^1\text{H}$  NMR (400 MHz, Methanol- $d_4$ )  $\delta$  7.55 (d,  $J = 7.8$  Hz, 1H), 7.29 (d,  $J = 7.5$  Hz, 1H), 7.01 (t,  $J = 7.7$  Hz, 1H), 4.03 (t, 1H), 2.61 (dt,  $J = 9.6, 3.5$  Hz, 2H), 2.17 – 2.04 (m, 1H), 2.02 – 1.86 (m, 1H), 1.80 – 1.58 (m, 2H).  $^{13}\text{C}$  NMR (101 MHz, Methanol- $d_4$ )  $\delta$  139.5, 132.8, 130.3, 126.6 (q,  $J = 270.7$  Hz), 123.4, 119.5 (q,  $J = 4.8$  Hz), 119.0, 113.9 (q,  $J = 32.5$  Hz), 112.0, 46.3, 33.8, 22.1, 21.8.



**General procedure to prepare enantiopure amines vii (2.23, 2.24, and 2.26).** Titanium (IV) ethoxide was added to a stirring mixture of requisite ketone **iii** (0.5 mmol) and *t*-butyl sulfinamide (0.5 mmol) in 10 mL toluene. The heterogeneous mixture was heated at reflux and stirred for 12 h before cooling to room temperature ( $23$  °C). The reaction was quenched with brine and filtered over celite. The filtrate was extracted with  $\text{CH}_2\text{Cl}_2$  and the organics were combined, dried over anhydrous  $\text{Na}_2\text{SO}_4$ , filtered, and concentrated in vacuo. The crude product was purified by flash column chromatography ( $\text{SiO}_2$ ) using 10-50% ethyl acetate in hexanes as the eluent, to

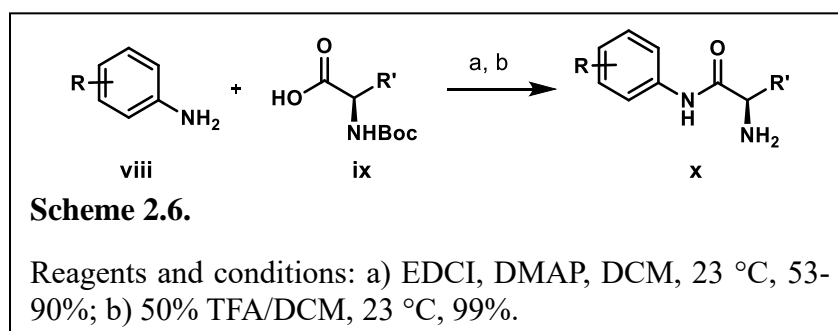
afford pure compound **v**. Compound **v** was dissolved in anhydrous THF under nitrogen atmosphere and cooled to -78 °C. Solid NaBH<sub>4</sub> (1.5 mmol) was added, and the mixture was stirred at -78 °C for 4 h, warmed to 0 °C and stirred 8-12 h. The reaction was quenched with saturated aqueous NH<sub>4</sub>Cl and extracted with CH<sub>2</sub>Cl<sub>2</sub>. The organics were combined, dried over anhydrous Na<sub>2</sub>SO<sub>4</sub>, filtered, and concentrated in vacuo to afford **vi**. To remove Ellman's chiral auxiliary, **vi** was dissolved in 2 mL anhydrous CH<sub>3</sub>OH and 4 M HCl in dioxane (3.0 mmol) was added at room temperature (23 °C), stirred for 16 h, and the solvent was removed by evaporation under reduced pressure. An aqueous 2 M HCl solution was added to the remaining residue, and the mixture was extracted with ethyl acetate. The aqueous layer was basified with an aqueous buffer solution of NH<sub>3</sub>/NH<sub>4</sub>Cl and extracted with CH<sub>2</sub>Cl<sub>2</sub> to afford final enantiopure compound **vii**.

**(R)-6-fluoro-2,3,4,9-tetrahydro-1H-carbazol-1-amine (2.23):** Yield 26%, white amorphous solid. <sup>1</sup>H NMR (400 MHz, Methanol-*d*<sub>4</sub>) δ 7.29 – 7.20 (m, 1H), 7.05 (dd, *J* = 9.8, 2.5 Hz, 1H), 6.82 (ddd, *J* = 9.6, 8.7, 2.5 Hz, 1H), 4.10 (dd, *J* = 7.1, 5.5 Hz, 1H), 2.74 – 2.60 (m, 3H), 2.25 – 2.13 (m, 1H), 2.13 – 2.00 (m, 1H), 1.91 – 1.67 (m, 2H). <sup>13</sup>C NMR (101 MHz, Methanol-*d*<sub>4</sub>) δ 158.9 (d, *J* = 232.0 Hz), 140.0, 134.3, 128.9 (d, *J* = 9.3 Hz), 112.4 (d, *J* = 9.7 Hz), 111.4 (d, *J* = 5.2 Hz), 110.0 (d, *J* = 26.4 Hz), 103.7 (d, *J* = 23.3 Hz), 46.6, 34.1, 22.2, 22.0. [α] = +2.5 (c = 2.0 mg/mL, CH<sub>3</sub>OH)

**(S)-6-fluoro-2,3,4,9-tetrahydro-1H-carbazol-1-amine (2.24):** Yield 26%, white amorphous solid. <sup>1</sup>H NMR (400 MHz, Methanol-*d*<sub>4</sub>) δ 7.29 – 7.20 (m, 1H), 7.05 (dd, *J* = 9.8, 2.5 Hz, 1H), 6.82 (ddd, *J* = 9.6, 8.7, 2.5 Hz, 1H), 4.10 (dd, *J* = 7.1, 5.5 Hz, 1H), 2.74 – 2.60 (m, 3H), 2.25 – 2.13 (m, 1H), 2.13 – 2.00 (m, 1H), 1.91 – 1.67 (m, 2H). <sup>13</sup>C NMR (101 MHz, Methanol-*d*<sub>4</sub>) δ 158.9 (d, *J* = 232.0 Hz), 140.0, 134.3, 128.9 (d, *J* = 9.3 Hz), 112.4 (d, *J* = 9.7 Hz), 111.4 (d, *J* =

5.2 Hz), 110.0 (d,  $J = 26.4$  Hz), 103.7 (d,  $J = 23.3$  Hz), 46.6, 34.1, 22.2, 22.0.  $[\alpha] = -2.25$  ( $c = 1.33$  mg/mL, CH<sub>3</sub>OH)

**(R)-6,7-difluoro-2,3,4,9-tetrahydro-1H-carbazol-1-amine (2.26):** Yield 72%, yellow amorphous solid. <sup>1</sup>H NMR (500 MHz, Methanol-*d*<sub>4</sub>)  $\delta$  7.37 – 7.25 (m, 2H), 4.62 (t,  $J = 5.0$  Hz, 1H), 2.82 (dt,  $J = 16.0, 5.3$  Hz, 1H), 2.75 – 2.65 (m, 1H), 2.33 – 2.22 (m, 1H), 2.15 – 1.94 (m, 3H). <sup>13</sup>C NMR (126 MHz, Methanol-*d*<sub>4</sub>)  $\delta$  148.3 (dd,  $J = 239.8, 15.8$  Hz), 146.2 (dd,  $J = 236.9, 15.1$  Hz), 132.0 (d,  $J = 10.6$  Hz), 129.4 (d,  $J = 3.8$  Hz), 121.8 (d,  $J = 8.2$  Hz), 114.0 (d,  $J = 4.7$  Hz), 104.9 (d,  $J = 18.6$  Hz), 99.0 (d,  $J = 22.0$  Hz), 44.4, 27.8, 19.9, 18.6.  $[\alpha] = -3.75$  ( $c = 0.53$  mg/mL, CH<sub>3</sub>OH)



**General procedure to prepare amides x (2.27 - 2.32).** Aniline **viii** (0.5 mmol) was added to stirring solution of Boc-protected amino acid **ix** (0.5 mmol) dissolved in DCM (5 mL). 1-Ethyl-3-(3-dimethylaminopropyl)carbodiimide (0.6 mmol) was added, followed by 4-dimethylaminopyridine (0.6 mmol). After stirring at 23 °C for 8-12 h, the reaction mixture was extracted with ethyl acetate and the organics were combined, washed with 10% aqueous citric acid, water, and brine. The organic layer was dried over anhydrous Na<sub>2</sub>SO<sub>4</sub>, filtered, and concentrated under vacuum to afford the crude product, which were purified by flash column chromatography (SiO<sub>2</sub>) using 15-35% ethyl acetate in hexanes. The isolated product was subjected to 50% TFA/CH<sub>2</sub>Cl<sub>2</sub>, to afford the desired amide.

**(R)-2-amino-N-(3,4-difluorophenyl)propenamide (2.27):** Yield 91%, amber oil.  $^1\text{H}$  NMR (500 MHz, Methanol- $d_4$ )  $\delta$  7.64 – 7.56 (m, 2H), 7.14 – 7.05 (m, 2H), 4.05 (q,  $J = 7.0$  Hz, 1H), 1.60 (d,  $J = 7.1$  Hz, 3H).  $^{13}\text{C}$  NMR (151 MHz, Methanol- $d_4$ )  $\delta$  169.1, 161.0 (d,  $J = 243.4$  Hz), 135.3, 123.1 (d,  $J = 7.9$  Hz), 116.5 (d,  $J = 22.7$  Hz), 50.8, 17.6. HRMS calcd for  $\text{C}_9\text{H}_{11}\text{FN}_2\text{O}$   $[\text{M}+\text{H}]^+$ : 183.09, found: 183.0925.

**(R)-2-amino-N-(4-fluorophenyl)-3-methylbutanamide (2.28):** Yield 70%, yellow oil.  $^1\text{H}$  NMR (500 MHz, Methanol- $d_4$ )  $\delta$  7.65 – 7.57 (m, 2H), 7.15 – 7.06 (m, 2H), 3.77 (d,  $J = 6.0$  Hz, 1H), 2.35 – 2.24 (m, 1H), 1.12 (dd,  $J = 12.8, 6.9$  Hz, 6H).  $^{13}\text{C}$  NMR (151 MHz, Methanol- $d_4$ )  $\delta$  167.9, 161.1 (d,  $J = 242.4$  Hz), 135.1, 123.2 (d,  $J = 8.0$  Hz), 116.5 (d,  $J = 22.7$  Hz), 60.4 (d,  $J = 2.4$  Hz), 31.7, 18.9, 17.9. HRMS calcd for  $\text{C}_{11}\text{H}_{15}\text{FN}_2\text{O}$   $[\text{M}+\text{H}]^+$ : 211.12, found: 211.1238.

**(2R)-2-amino-N-(4-fluorophenyl)-3-methylpentanamide (2.29):** Yield 92%, yellow oil.  $^1\text{H}$  NMR (500 MHz, Methanol- $d_4$ )  $\delta$  7.64 – 7.56 (m, 2H), 7.14 – 7.05 (m, 2H), 3.80 (d,  $J = 6.0$  Hz, 1H), 2.08 – 1.96 (m, 1H), 1.71 – 1.59 (m, 1H), 1.34 – 1.21 (m, 1H), 1.10 (d,  $J = 6.9$  Hz, 3H), 1.00 (t,  $J = 7.4$  Hz, 3H).  $^{13}\text{C}$  NMR (600 MHz, Methanol- $d_4$ )  $\delta$  168.0, 161.1 (d,  $J = 242.3$  Hz), 135.1, 123.3 (d,  $J = 8.1$  Hz), 116.5 (d,  $J = 22.7$  Hz), 59.6, 38.2, 25.5, 15.2, 11.5. HRMS calcd for  $\text{C}_{12}\text{H}_{17}\text{FN}_2\text{O}$   $[\text{M}+\text{H}]^+$ : 225.14, found: 225.1390.

**(R)-2-amino-N-(4-fluorophenyl)-3-phenylpropanamide (2.30):** Yield 55%, white amorphous solid.  $^1\text{H}$  NMR (500 MHz, Methanol- $d_4$ )  $\delta$  7.53 – 7.45 (m, 2H), 7.41 – 7.34 (m, 2H), 7.32 (tt,  $J = 7.9, 1.5$  Hz, 3H), 7.12 – 7.03 (m, 2H), 4.16 (td,  $J = 7.4, 1.3$  Hz, 1H), 3.29 (dd,  $J = 13.8, 7.1$  Hz, 1H), 3.16 (dd,  $J = 13.9, 7.7$  Hz, 1H).  $^{13}\text{C}$  NMR (151 MHz, Methanol- $d_4$ )  $\delta$  167.9, 161.1 (d,  $J = 243.6$  Hz), 135.6, 134.9, 130.5, 130.1, 128.9, 123.3 (d,  $J = 8.0$  Hz), 116.4 (d,  $J = 22.9$  Hz), 56.4, 38.8. HRMS calcd for  $\text{C}_{15}\text{H}_{15}\text{FN}_2\text{O}$   $[\text{M}-\text{H}]^-$ : 257.12, found: 257.1090.



**(R)-2-amino-N-(4-fluorophenyl)propenamide (2.31):** Yield 53%, amber oil.  $^1\text{H}$  NMR (500 MHz, Methanol- $d_4$ )  $\delta$  7.78 – 7.70 (m, 1H), 7.30 – 7.18 (m, 2H), 4.05 (qd,  $J = 7.1, 1.4$  Hz, 1H), 1.59 (d,  $J = 7.1$  Hz, 3H).  $^{13}\text{C}$  NMR (151 MHz, Methanol- $d_4$ )  $\delta$  169.5, 151.2 (dd,  $J = 245.1, 13.2$  Hz), 148.3 (dd,  $J = 243.9, 12.7$  Hz), 136.1 (d,  $J = 7.5$  Hz), 118.4 (d,  $J = 18.3$  Hz), 117.4 – 116.9 (m), 110.5 (d,  $J = 22.2$  Hz), 50.9, 17.5. HRMS calcd for  $\text{C}_9\text{H}_{10}\text{F}_2\text{N}_2\text{O}$   $[\text{M}+\text{H}]^+$ : 201.08, found: 201.0830.

**(R)-2-amino-N-(3,4-difluorophenyl)-3-methylbutanamide (2.32):** Yield 57%, red oil.  $^1\text{H}$  NMR (500 MHz, Methanol- $d_4$ )  $\delta$  7.80 – 7.72 (m, 1H), 7.33 – 7.21 (m, 2H), 3.78 (dt,  $J = 5.9, 1.2$  Hz, 1H), 2.34 – 2.24 (m, 1H), 1.11 (dd,  $J = 15.0, 6.9$  Hz, 6H).  $^{13}\text{C}$  NMR (151 MHz, Methanol- $d_4$ )  $\delta$  168.1, 151.2 (dd,  $J = 245.8, 13.6$  Hz), 148.3 (dd,  $J = 245.0, 12.9$  Hz), 135.8 (d,  $J = 3.4$  Hz), 118.5 (d,  $J = 18.7$  Hz), 117.2 (dd,  $J = 6.0, 3.7$  Hz), 110.6 (d,  $J = 21.9$  Hz), 60.4, 31.7, 18.9, 17.8. HRMS calcd for  $\text{C}_{11}\text{H}_{14}\text{F}_2\text{N}_2\text{O}$   $[\text{M}-\text{H}]^-$ : 227.11, found: 227.0997

### 2.4.3 Biological evaluation

**Detection of phosphorylated CpxR.** Wild-type and  $\Delta\text{cpxA}$  bacteria were grown overnight in side-arm flasks in TB7 broth without glucose, then diluted to  $\text{OD}_{600}$  of about 0.1 in 1.7X TB7 supplemented with glucose; To each well of a 384-well plate, 30  $\mu\text{L}$  of this dilution was added to 20  $\mu\text{L}$  of compound D13 (10  $\mu\text{M}$ ) dissolved in DMSO or DMSO alone (192 wells for each strain/treatment). After 5 hours incubation at 37  $^\circ\text{C}$ , the wells were pooled and harvested by centrifugation. All processing was carried out at 4  $^\circ\text{C}$ . The cells were washed once in phosphate-buffered saline, pH 7.4 and suspended in 2X Laemmli lysis buffer, according to bacterial pellet weight. As controls, 10  $\mu\text{M}$  His6-CpxR, expressed and purified as previously described,<sup>33</sup> was incubated with 0 or 20 mM AcP at 30  $^\circ\text{C}$  for 15 min. Respectively, 5  $\mu\text{L}$  and 10  $\mu\text{L}$  aliquots of each cell lysate and AcP treatment were separated on a Phos-Tag<sup>TM</sup> gel, which was prepared

according to Lima and colleagues<sup>33</sup> and the manufacturer's protocol with some modifications. Phos-tag acrylamide was purchased from Wako. The stacking gel contained 4% acrylamide:bis-acrylamide prepared in 350 mM bis-tris, pH 6.8. The separating gel contained 10% acrylamide/bis-acrylamide, 25  $\mu$ M Phos-tag acrylamide and 50  $\mu$ M Zn(NO<sub>3</sub>) prepared in 350 mM bis-tris, pH 6.8, and was de-gassed with stirring for 2 minutes prior to pouring. The gel was run at 4 °C in MOPS buffer (0.1 M MOPS, 0.1 M Tris, 5 mM sodium bisulfite and 0.1% SDS) for 2 hours at 40 mAMPs, and the buffer was refreshed each hour. The gel was washed for 15 min in Towbin transfer buffer containing 1 mM EDTA, then for 30 min in standard Towbin transfer buffer. Proteins were transferred to polyvinylidene difluoride membrane using a wet transfer method. Tris-buffered saline containing 0.1% Tween-20 (TBST) was used for washing and TBST supplemented with 5% skim milk was used for blocking and antibody incubations. The membrane was blocked for 1 hour and probed overnight at 4 °C with 1:30,000 anti-MBP/CpxR antibody. The secondary antibody goat anti-rabbit IgG-horseradish peroxidase conjugate was used at a 1:5,000 dilution for 1 hour at room temperature. Densitometry values were determined using Photoshop, and the ratio of CpxR-P to CpxR was analyzed by one way ANOVA .

**Intracellular accumulation of compounds.** *E. coli* BW attTn7::araC-fhuA (WT-Pore) and BW  $\Delta$ TolC attTn7::PLAC-fhuA ( $\Delta$ TolC-Pore ) strains<sup>21</sup> were grown in MOPS-M9 (pH 7.2) medium overnight. The next morning, cells were subcultured into 200 mL of fresh medium and incubated until OD<sub>600</sub> reached ~ 0.2. The cell cultures were split into two flasks, 100 mL each, and L-arabinose, the inducer of the Pore was added to one of the culture flask at 0.1% (w/v) final concentration. Cells were grown for additional four hours, pelleted by centrifugation at room temperature (RT), washed twice in MOPS-M9 medium and concentrated ten-fold. For accumulation assays, cells were incubated with 16, 32, 64 and 128  $\mu$ g/mL of compounds and after

1 and 40 min incubation at RT, 100  $\mu$ L cell aliquots were collected by vacuum filtration onto 1.0  $\mu$ m Glass Fiber Type B filters. Filters were washed twice with 10 mM Tris-HCl (pH 8.0), dried and placed into 100% methanol at -80 °C for at least 10 min. Intracellular material was extracted by water bath sonication for 1 min. Cell and filter debris were separated by ultracentrifugation at 100,000xg for 8 min at 16 °C and the pellet re-extracted with 80% methanol in water by sonication for 15 min followed by ultracentrifugation at the same conditions. Supernatants from two extractions were combined and stored at -80 °C until needed. For compound quantification, 5  $\mu$ L of solution was analyzed in triplicates. The calibration curves for compounds were generated in the same experiment by mixing compounds at increasing concentrations with the sonicated *E. coli* cell extracts.

An Agilent 1290 Infinity II ultrahigh-pressure liquid chromatography (UHPLC) system and 6545 quadrupole/time-of-flight (Q/TOF) system (Agilent Technologies) were used to quantify intracellular concentrations of compounds. A Zorbax Rapid Resolution High Definition column (RRHD, 2.1x50mm, 1.8  $\mu$ m) was used for the separation with a flow rate of 0.65 mL/min. The initial concentration of 5% MS grade Acetonitrile was maintained for 1 min, and this was followed by a linear gradient to 80% over 3 min, and then by 100% over 1.1 min which was maintained for an additional 1.2 min. HPLC solvent mixtures contained 0.1% HPLC grade formic acid (SigmaAldrich) to improve ionization efficiency. MS parameters were as follows: gas temperature, 325 °C; capillary voltage, 4000V; fragmentor voltage, 175V; m/z range, 50–1100; detector signal acquisition rate, 4GHz; and spectrum storage rate, 2s<sup>-1</sup>. MassHunter qualitative and quantitative analysis B8.0 was used to quantify compound concentrations using the calibration curve.

**Murine infection experiments.** Animal experiments were conducted according to the guidelines of the University of Michigan Institutional Animal Care and Use Committee. For the

animal infection experiments, bacterial strains were cultured at 37 °C in LB medium overnight with shaking.<sup>14</sup> Female CBA/J mice (Jackson Laboratories, Bar Harbor, ME) were inoculated transurethrally with a target dose of  $\sim 10^8$  CFU of CFT073 or CFT073 $\Delta cpxA::cat$ . Mice were subsequently treated 12 h later either with the vehicle, ciprofloxacin hydrochloride (PanReac AppliChem ITW Reagents, Jade Scientific), compound **2.1**, compound **2.6**, or compound **2.26** as described in the results and euthanized 4 h after the last treatment. Bacterial loads of each strain were calculated from the urine, bladder, and kidneys of mice, as previously described; the limits of detection for these assays were 100 CFU/ml or 100 CFU/g of urine and tissue, respectively.<sup>34</sup> Values of 50 CFU/ml or 50 CFU/g were assigned to specimens whose yields were below the limit of detection. Due to the extreme skewness of the data, natural log transformation was used before the data were analyzed statistically. Descriptive statistics were calculated for all the log transformed variables. Statistical comparisons were done using Analysis of Variance (ANOVA) with follow-up pairwise tests adjusted for multiple comparisons using the Tukey procedure.

#### **2.4.5 Proteomic analysis**

**Sample preparation.** Samples (cell pellets) were lysed with a lysis buffer (8 M urea, 1 mM sodium orthovanadate, 20 mM HEPES, 2.5 mM sodium pyrophosphate, 1 mM  $\beta$ -glycerophosphate, pH 8.0, 20 min, 4 °C) followed by sonication at 40% amplification by using a microtip sonicator (QSonica, LLC, Model no. Q55) and cleared by centrifugation (14 000  $\times$  g, 15 min, 15 °C). Protein concentration was measured (Pierce BCA Protein Assay, Thermo Fisher Scientific, IL, USA). A total of 50  $\mu$ g of protein per sample was subjected for trypsin digestion. One  $\mu$ g of BSA was included in each sample prior in-solution digestion to investigate the proper digestion performance and downstream LC-MS/MS analysis.

In-solution digestion with trypsin/LysC (V5071, Promega) was performed according to the manufacturer protocol. Tryptic peptides were desalted using C18 Sep-Pak plus cartridges (Waters, Milford, MA) and were lyophilized for 8 hours to dryness. The dried peptides were reconstituted with 100  $\mu$ l buffer A (0.1 % formic acid). The final concentration of the peptide samples 0.5  $\mu$ g/ $\mu$ l and 4  $\mu$ l (2  $\mu$ g)/sample was injected for LC-MS/MS analysis.

**LC-MS/MS identification and label-free quantitation.** The LC-MS/MS was performed on a fully automated proteomic platform that includes a Dionex UltiMate <sup>®</sup> 3000 (Thermo Fisher Scientific, USA) system connected to a Q Exactive HF-X mass spectrometer (Thermo Fisher Scientific, Waltham, MA). The MS/MS analysis was performed according to the earlier published protocol.<sup>35</sup>

Peptide spectrum matching of MS/MS spectra of each file was searched against the UniProt E Coli CFT073-UPEC database (TaxID:199310) using the Sequest algorithm within Proteome Discoverer v 2.4 software (Thermo Fisher Scientific, San Jose, CA). The Sequest database search was performed with the following parameters: trypsin enzyme cleavage specificity, 2 possible missed cleavages, 10 ppm mass tolerance for precursor ions, 0.02 Da mass tolerance for fragment ions. Search parameters permitted dynamic modification of methionine oxidation (+15.9949 Da) and static modification of carbamidomethylation (+57.0215 Da) on cysteine. Peptide assignments from the database search were filtered down to a 1% FDR. The relative label-free quantitative and comparative among the samples were performed using the Minora algorithm and the adjoining bioinformatics tools of the Proteome Discoverer (PD) 2.4 software. A recent comparative analysis between the two most popular proteomic data analysis software MaxQuant (MQ) and PD showed that PD outperformed MQ in terms of protein/peptide quantification yield, dynamic range, and reproducibility. In addition, Minora algorithm methods including normalization were the most

accurate in estimating the abundance ratio between groups and the most sensitive when comparing groups with a narrow abundance ratio.<sup>36</sup>

## 2.5 References for Chapter 2

- (1) Li, Y.; Gardner, J. J.; Fortney, K. R.; Leus, I. V.; Bonifay, V.; Zgurskaya, H. I.; Pletnev, A. A.; Zhang, S.; Zhang, Z.-Y.; Gribble, G. W.; Spinola, S. M.; Duerfeldt, A. S. First-Generation Structure-Activity Relationship Studies of 2,3,4,9-Tetrahydro-1H-Carbazol-1-Amines as CpxA Phosphatase Inhibitors. *Bioorganic & Medicinal Chemistry Letters* **2019**, *29* (14), 1836–1841. <https://doi.org/10.1016/j.bmcl.2019.05.003>.
- (2) Fortney, K. R.; Smith, S. N.; van Rensburg, J. J.; Brothwell, J. A.; Gardner, J. J.; Katz, B. P.; Ahsan, N.; Duerfeldt, A. S.; Mobley, H. L. T.; Spinola, S. M. CpxA Phosphatase Inhibitor Activates CpxRA and Is a Potential Treatment for Uropathogenic Escherichia Coli in a Murine Model of Infection. *Microbiology Spectrum* *0* (0), e02430-21. <https://doi.org/10.1128/spectrum.02430-21>.
- (3) Boucher, H. W.; Talbot, G. H.; Bradley, J. S.; Edwards, J. E.; Gilbert, D.; Rice, L. B.; Scheld, M.; Spellberg, B.; Bartlett, J. Bad Bugs, No Drugs: No ESKAPE! An Update from the Infectious Diseases Society of America. *Clin Infect Dis* **2009**, *48* (1), 1–12. <https://doi.org/10.1086/595011>.
- (4) Coates, A. R. M.; Hu, Y. Novel Approaches to Developing New Antibiotics for Bacterial Infections: Novel Approaches for Making New Antibiotics. *British Journal of Pharmacology* **2007**, *152* (8), 1147–1154. <https://doi.org/10.1038/sj.bjp.0707432>.

- (5) Coates, A. R.; Halls, G.; Hu, Y. Novel Classes of Antibiotics or More of the Same? *British Journal of Pharmacology* **2011**, *163* (1), 184–194. <https://doi.org/10.1111/j.1476-5381.2011.01250.x>.
- (6) Spellberg, B.; Powers, J. H.; Brass, E. P.; Miller, L. G.; Edwards, J. E. Trends in Antimicrobial Drug Development: Implications for the Future. *Clinical Infectious Diseases* **2004**, *38* (9), 1279–1286. <https://doi.org/10.1086/420937>.
- (7) Högberg, L. D.; Heddini, A.; Cars, O. The Global Need for Effective Antibiotics: Challenges and Recent Advances. *Trends in Pharmacological Sciences* **2010**, *31* (11), 509–515. <https://doi.org/10.1016/j.tips.2010.08.002>.
- (8) Rasko, D. A.; Sperandio, V. Anti-Virulence Strategies to Combat Bacteria-Mediated Disease. *Nat Rev Drug Discov* **2010**, *9* (2), 117–128. <https://doi.org/10.1038/nrd3013>.
- (9) Stock, A. M.; Robinson, V. L.; Goudreau, P. N. Two-Component Signal Transduction. *Annu. Rev. Biochem.* **2000**, *69* (1), 183–215. <https://doi.org/10.1146/annurev.biochem.69.1.183>.
- (10) Raivio, T. L.; Silhavy, T. J. Transduction of Envelope Stress in Escherichia Coli by the Cpx Two-Component System. *J Bacteriol* **1997**, *179* (24), 7724–7733. <https://doi.org/10.1128/jb.179.24.7724-7733.1997>.
- (11) Humphreys, S.; Rowley, G.; Stevenson, A.; Anjum, M. F.; Woodward, M. J.; Gilbert, S.; Kormanec, J.; Roberts, M. Role of the Two-Component Regulator CpxAR in the Virulence of *Salmonella Enterica* Serotype Typhimurium. *Infect Immun* **2004**, *72* (8), 4654–4661. <https://doi.org/10.1128/IAI.72.8.4654-4661.2004>.
- (12) Spinola, S. M.; Fortney, K. R.; Baker, B.; Janowicz, D. M.; Zwickl, B.; Katz, B. P.; Blick, R. J.; Munson, R. S. Activation of the CpxRA System by Deletion of *CpxA* Impairs the Ability

- of *Haemophilus Ducreyi* To Infect Humans. *Infect Immun* **2010**, 78 (9), 3898–3904.  
<https://doi.org/10.1128/IAI.00432-10>.
- (13) Gangaiah, D.; Raterman, E. L.; Wu, H.; Fortney, K. R.; Gao, H.; Liu, Y.; Jerse, A. E.; Spinola, S. M. Both MisR (CpxR) and MisS (CpxA) Are Required for *Neisseria Gonorrhoeae* Infection in a Murine Model of Lower Genital Tract Infection. *Infect Immun* **2017**, 85 (9).  
<https://doi.org/10.1128/IAI.00307-17>.
- (14) Dbeibo, L.; van Rensburg, J. J.; Smith, S. N.; Fortney, K. R.; Gangaiah, D.; Gao, H.; Marzoo, J.; Liu, Y.; Mobley, H. L. T.; Spinola, S. M. Evaluation of CpxRA as a Therapeutic Target for Uropathogenic *Escherichia Coli* Infections. *Infect Immun* **2018**, 86 (3).  
<https://doi.org/10.1128/IAI.00798-17>.
- (15) Gotoh, Y.; Eguchi, Y.; Watanabe, T.; Okamoto, S.; Doi, A.; Utsumi, R. Two-Component Signal Transduction as Potential Drug Targets in Pathogenic Bacteria. *Current Opinion in Microbiology* **2010**, 13 (2), 232–239. <https://doi.org/10.1016/j.mib.2010.01.008>.
- (16) Schreiber, M.; Res, I.; Matter, A. Protein Kinases as Antibacterial Targets. *Current Opinion in Cell Biology* **2009**, 21 (2), 325–330. <https://doi.org/10.1016/j.ceb.2009.01.026>.
- (17) van Rensburg, J. J.; Fortney, K. R.; Chen, L.; Krieger, A. J.; Lima, B. P.; Wolfe, A. J.; Katz, B. P.; Zhang, Z.; Spinola, S. M. Development and Validation of a High-Throughput Cell-Based Screen To Identify Activators of a Bacterial Two-Component Signal Transduction System. *Antimicrob. Agents Chemother.* **2015**, 59 (7), 3789–3799.  
<https://doi.org/10.1128/AAC.00236-15>.
- (18) Robinson, B. The Fischer Indole Synthesis. *Chem. Rev.* **1963**, 63 (4), 373–401.  
<https://doi.org/10.1021/cr60224a003>.

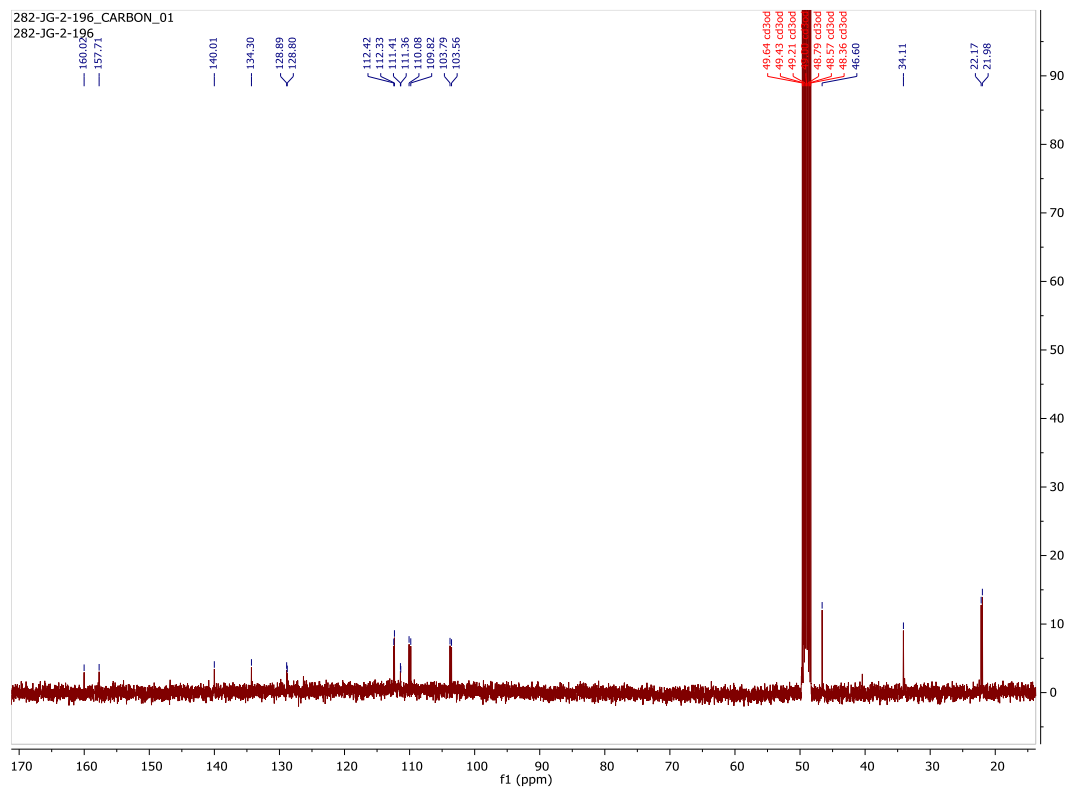
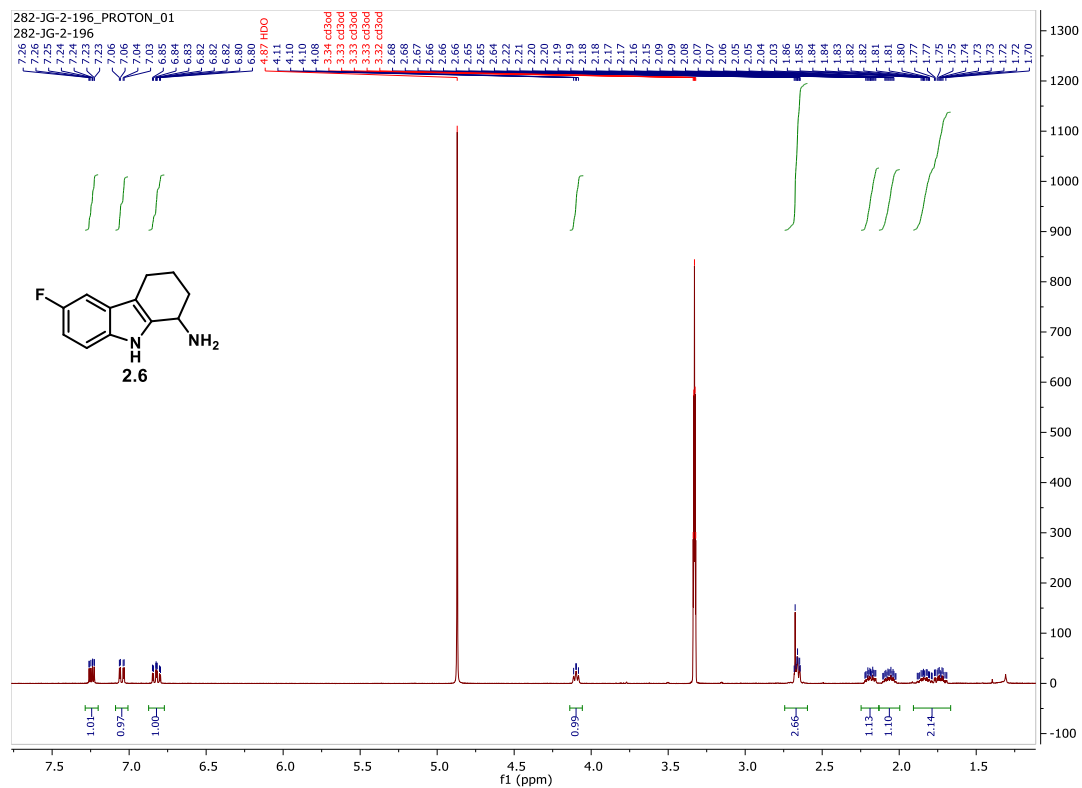


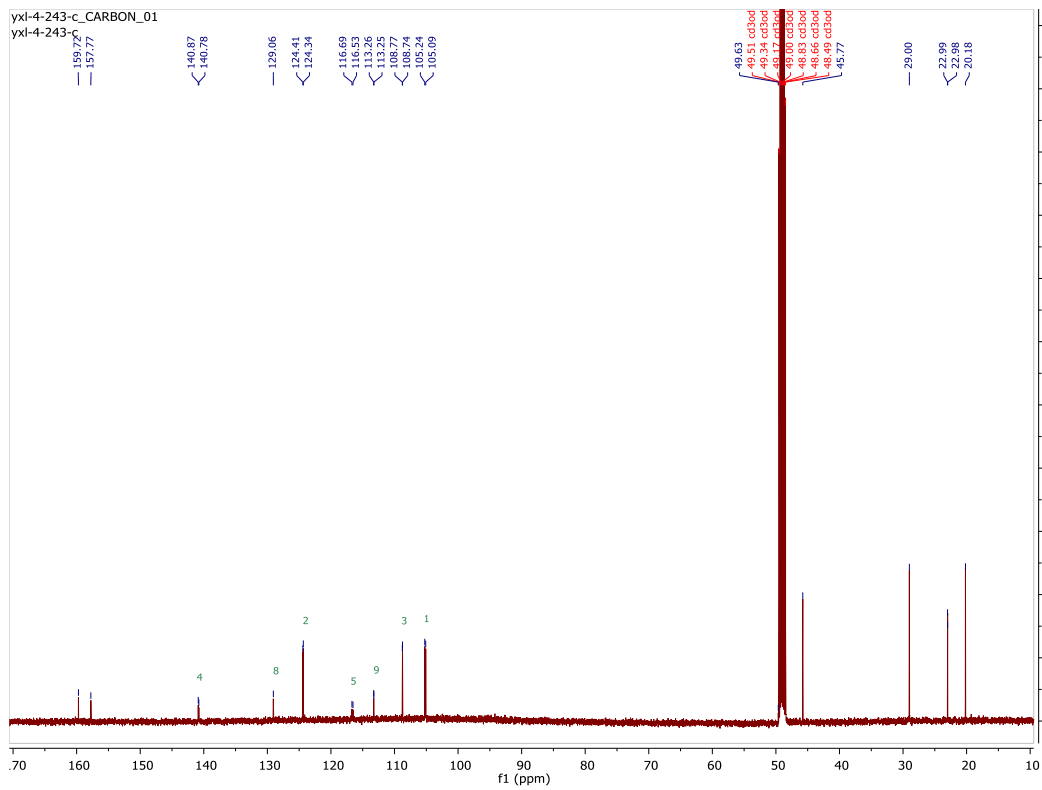
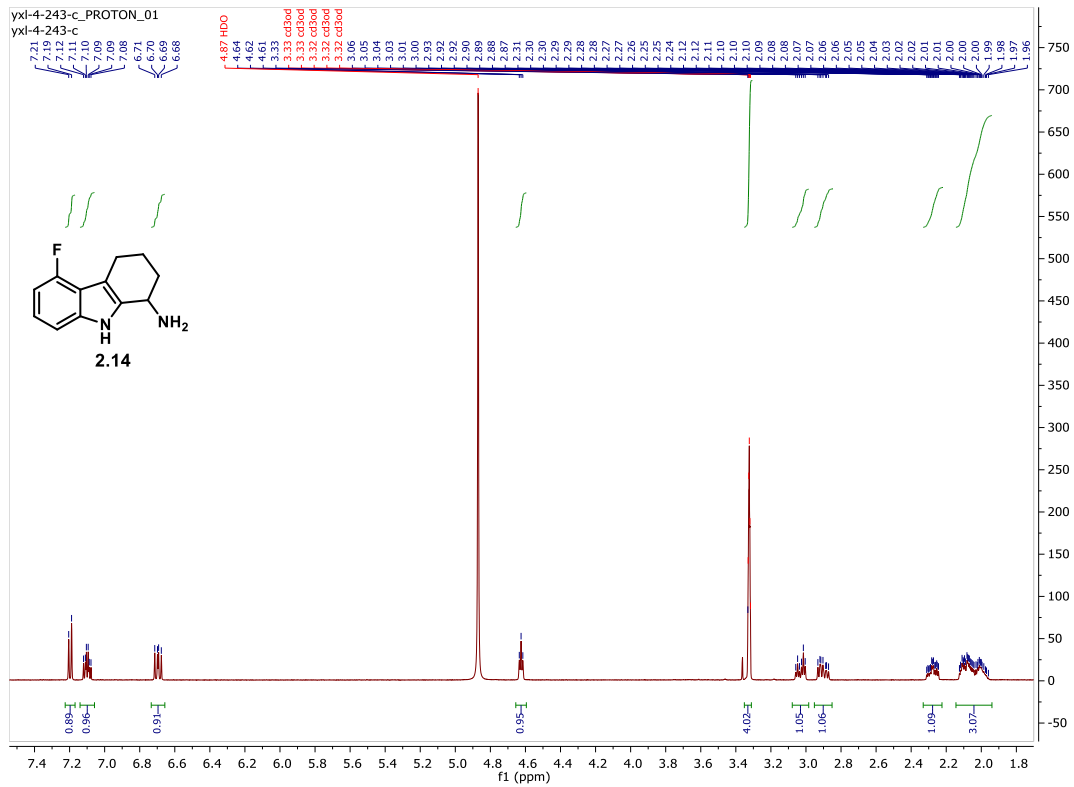
- (19) Scherer, G.; Kramer, M. L.; Schutkowski, M.; Reimer, U.; Fischer, G. Barriers to Rotation of Secondary Amide Peptide Bonds. *J. Am. Chem. Soc.* **1998**, *120* (22), 5568–5574. <https://doi.org/10.1021/ja980181t>.
- (20) Richter, M. F.; Drown, B. S.; Riley, A. P.; Garcia, A.; Shirai, T.; Svec, R. L.; Hergenrother, P. J. Predictive Compound Accumulation Rules Yield a Broad-Spectrum Antibiotic. *Nature* **2017**, *545* (7654), 299–304. <https://doi.org/10.1038/nature22308>.
- (21) Krishnamoorthy, G.; Wolloscheck, D.; Weeks, J. W.; Croft, C.; Rybenkov, V. V.; Zgurskaya, H. I. Breaking the Permeability Barrier of Escherichia Coli by Controlled Hyperporination of the Outer Membrane. *Antimicrob Agents Chemother* **2016**, *60* (12), 7372–7381. <https://doi.org/10.1128/AAC.01882-16>.
- (22) Krcmery, S.; Naber, K. G. Ciprofloxacin Once versus Twice Daily in the Treatment of Complicated Urinary Tract Infections. *International Journal of Antimicrobial Agents* **1999**, *11* (2), 133–138. [https://doi.org/10.1016/S0924-8579\(98\)00088-0](https://doi.org/10.1016/S0924-8579(98)00088-0).
- (23) Oliphant, C.; Green, G. Quinolones: A Comprehensive Review. *Am Fam Physician* **2002**, *65* (3), 455–465.
- (24) Zhang, G.-F.; Liu, X.; Zhang, S.; Pan, B.; Liu, M.-L. Ciprofloxacin Derivatives and Their Antibacterial Activities. *European Journal of Medicinal Chemistry* **2018**, *146*, 599–612. <https://doi.org/10.1016/j.ejmech.2018.01.078>.
- (25) Lau, C. K. Y.; Krewulak, K. D.; Vogel, H. J. Bacterial Ferrous Iron Transport: The Feo System. *FEMS Microbiology Reviews* **2016**, *40* (2), 273–298. <https://doi.org/10.1093/femsre/fuv049>.
- (26) Behnsen, J.; Raffatellu, M. Siderophores: More than Stealing Iron. *mBio* **7** (6), e01906-16. <https://doi.org/10.1128/mBio.01906-16>.

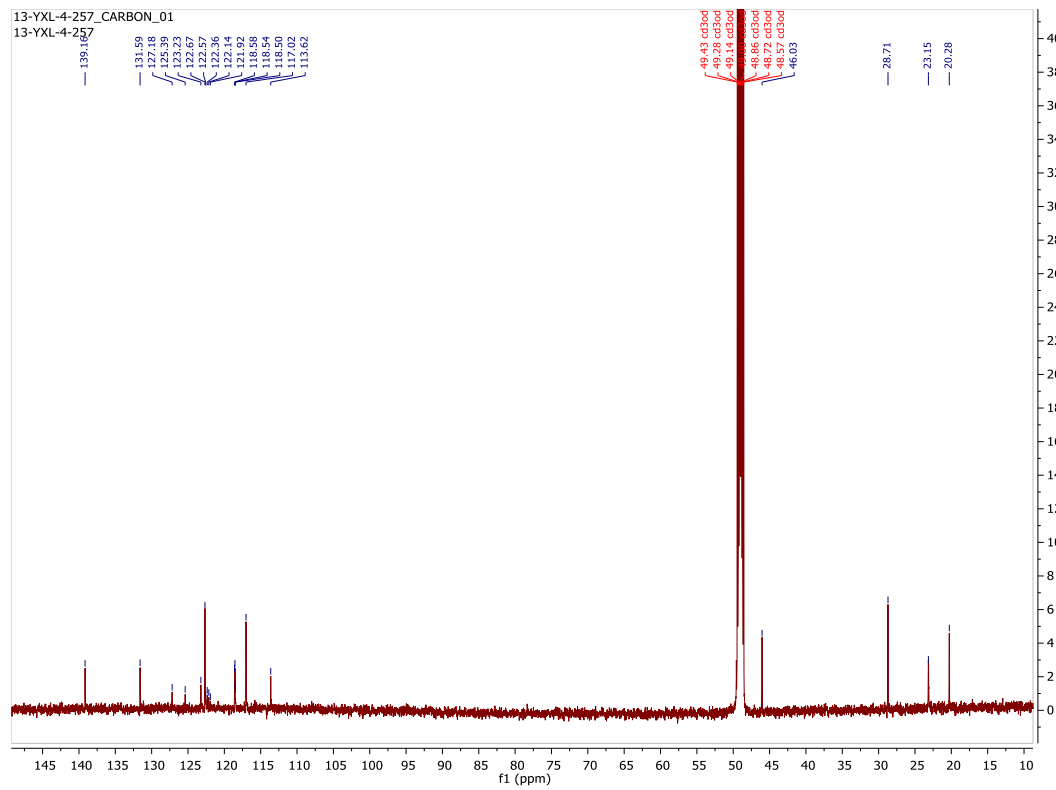
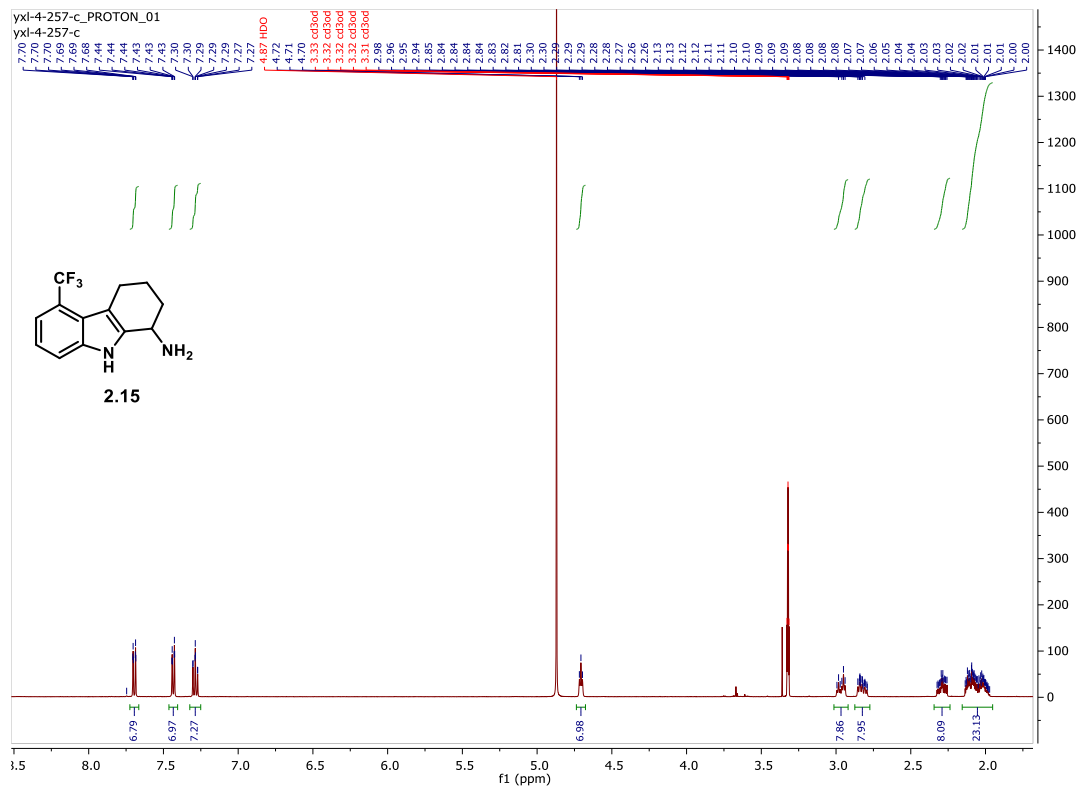
- (27) Braun, V. Energy-Coupled Transport and Signal Transduction through the Gram-Negative Outer Membrane via TonB-ExbB-ExbD-Dependent Receptor Proteins. *FEMS Microbiol Rev* **1995**, *16* (4), 295–307. <https://doi.org/10.1111/j.1574-6976.1995.tb00177.x>.
- (28) Fujita, M.; Mori, K.; Hara, H.; Hishiyama, S.; Kamimura, N.; Masai, E. A TonB-Dependent Receptor Constitutes the Outer Membrane Transport System for a Lignin-Derived Aromatic Compound. *Commun Biol* **2019**, *2* (1), 1–10. <https://doi.org/10.1038/s42003-019-0676-z>.
- (29) Torres, A. G.; Redford, P.; Welch, R. A.; Payne, S. M. TonB-Dependent Systems of Uropathogenic Escherichia Coli: Aerobactin and Heme Transport and TonB Are Required for Virulence in the Mouse. *Infect Immun* **2001**, *69* (10), 6179–6185. <https://doi.org/10.1128/IAI.69.10.6179-6185.2001>.
- (30) Cao, J.; Woodhall, M. R.; Alvarez, J.; Cartron, M. L.; Andrews, S. C. EfeUOB (YcdNOB) Is a Tripartite, Acid-Induced and CpxAR-Regulated, Low-PH Fe<sup>2+</sup> Transporter That Is Cryptic in Escherichia Coli K-12 but Functional in E. Coli O157:H7. *Molecular Microbiology* **2007**, *65* (4), 857–875. <https://doi.org/10.1111/j.1365-2958.2007.05802.x>.
- (31) Welch, R. A.; Burland, V.; Plunkett, G.; Redford, P.; Roesch, P.; Rasko, D.; Buckles, E. L.; Liou, S.-R.; Boutin, A.; Hackett, J.; Stroud, D.; Mayhew, G. F.; Rose, D. J.; Zhou, S.; Schwartz, D. C.; Perna, N. T.; Mobley, H. L. T.; Sonnenberg, M. S.; Blattner, F. R. Extensive Mosaic Structure Revealed by the Complete Genome Sequence of Uropathogenic Escherichia Coli. *PNAS* **2002**, *99* (26), 17020–17024. <https://doi.org/10.1073/pnas.252529799>.
- (32) Johnson, J. R. Virulence Factors in Escherichia Coli Urinary Tract Infection. *Clin Microbiol Rev* **1991**, *4* (1), 80–128. <https://doi.org/10.1128/CMR.4.1.80>.

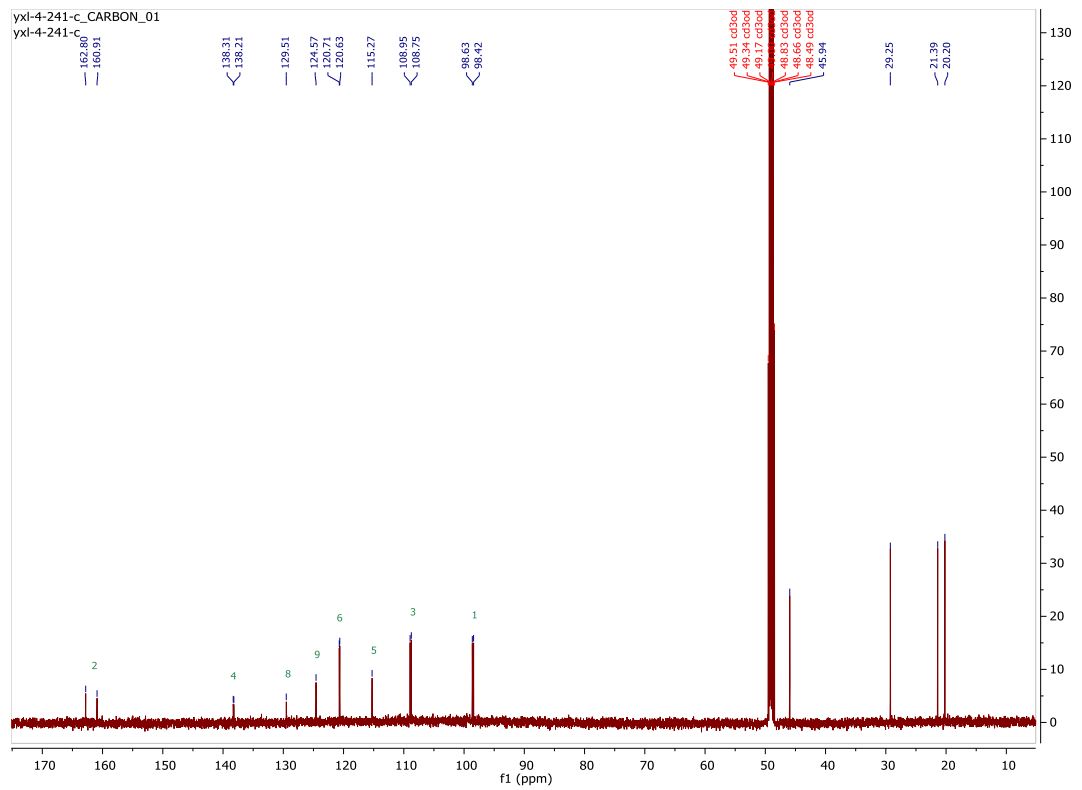
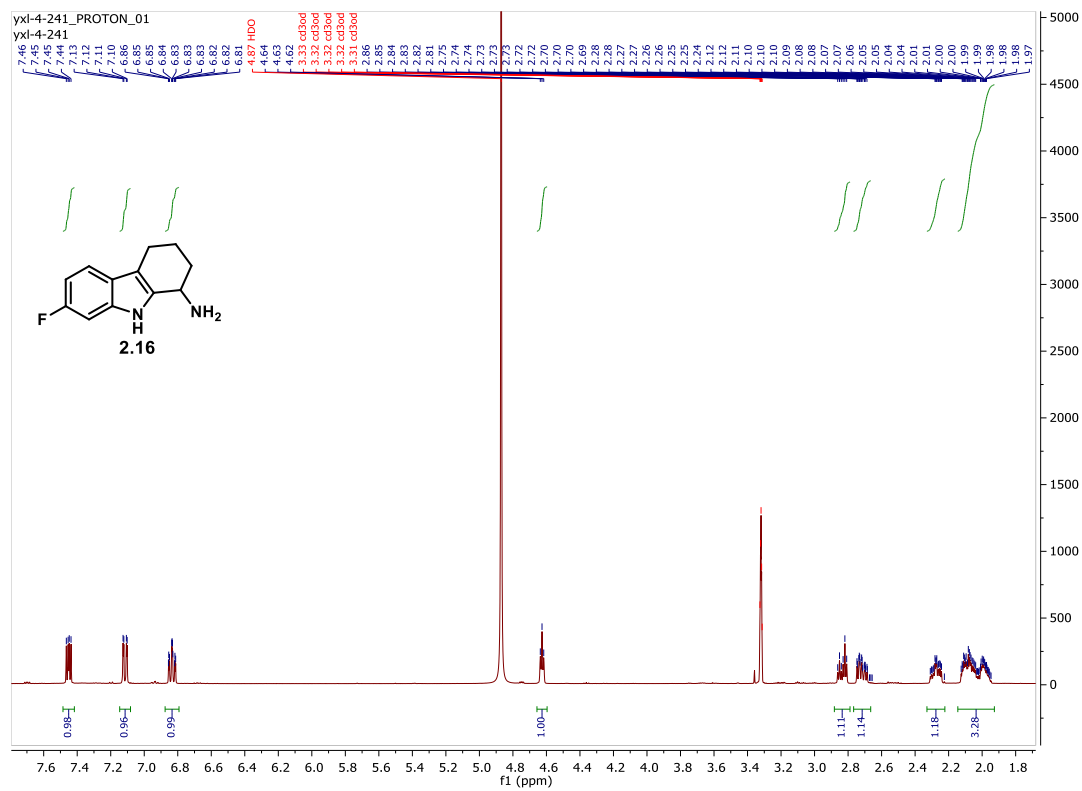
- (33) Lima, B. P.; Thanh Huyen, T. T.; Bäsell, K.; Becher, D.; Antelmann, H.; Wolfe, A. J. Inhibition of Acetyl Phosphate-Dependent Transcription by an Acetylatable Lysine on RNA Polymerase. *Journal of Biological Chemistry* **2012**, *287* (38), 32147–32160. <https://doi.org/10.1074/jbc.M112.365502>.
- (34) Alteri, C. J.; Hagan, E. C.; Sivick, K. E.; Smith, S. N.; Mobley, H. L. T. Mucosal Immunization with Iron Receptor Antigens Protects against Urinary Tract Infection. *PLoS Pathog* **2009**, *5* (9), e1000586. <https://doi.org/10.1371/journal.ppat.1000586>.
- (35) Bishop, C. E.; Shadid, T.; Lavey, N. P.; Kempfer, M. L.; Ahsan, N.; Ballard, J. D.; Duerfeldt, A. S. *Loss of ClpP Function in Clostridioides Difficile 630 Significantly Impacts Sporulation Systems*; preprint; Microbiology, 2021. <https://doi.org/10.1101/2021.02.05.429978>.
- (36) Palomba, A.; Abbondio, M.; Fiorito, G.; Uzzau, S.; Pagnozzi, D.; Tanca, A. Comparative Evaluation of MaxQuant and Proteome Discoverer MS1-Based Protein Quantification Tools. *J. Proteome Res.* **2021**, *20* (7), 3497–3507. <https://doi.org/10.1021/acs.jproteome.1c00143>.

## **Appendix I. Spectra Relevant to Chapter 2**

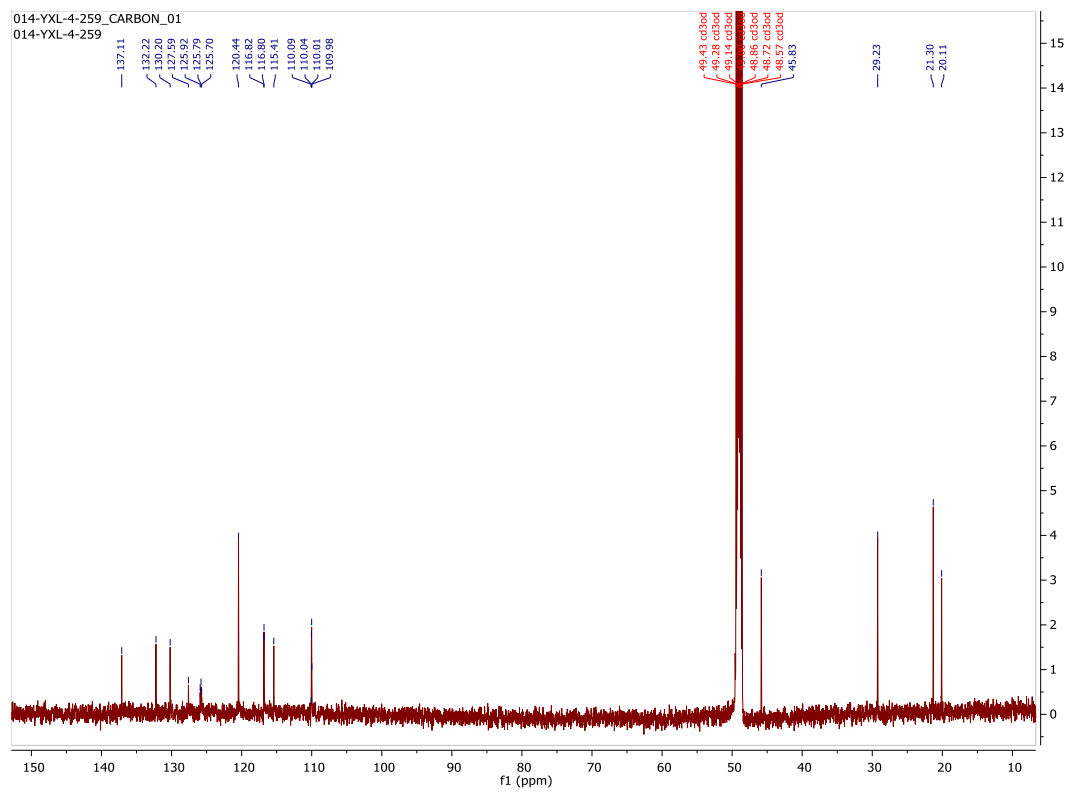
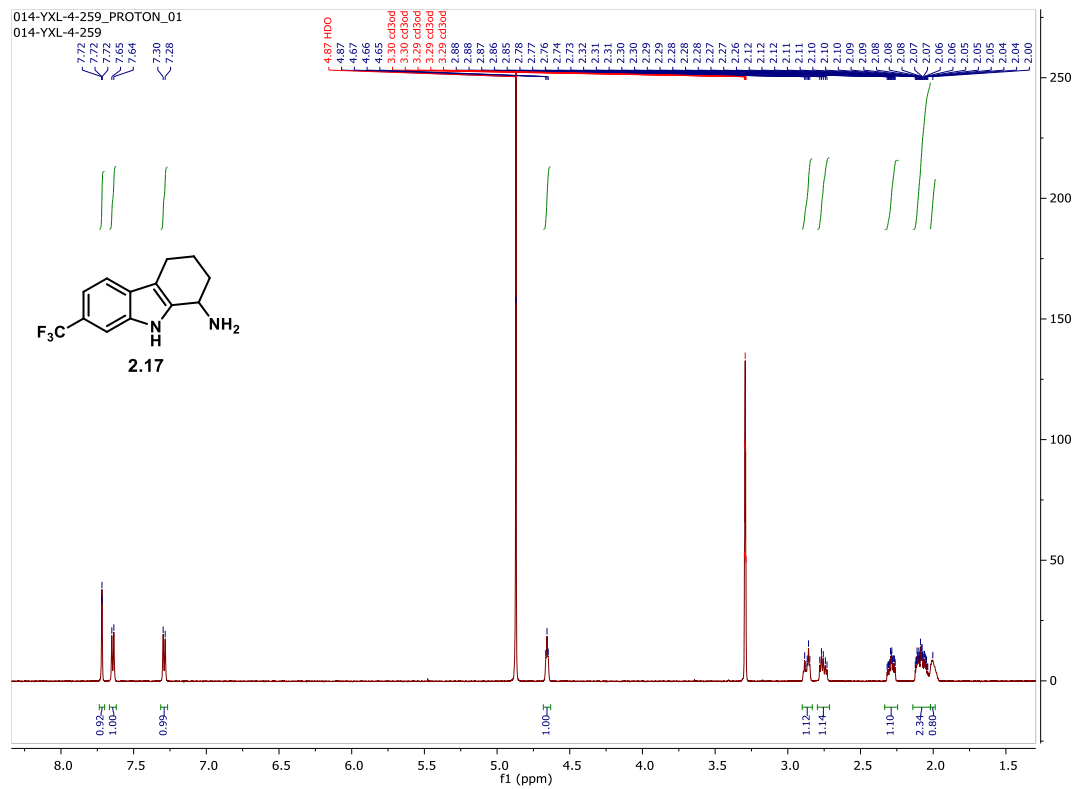




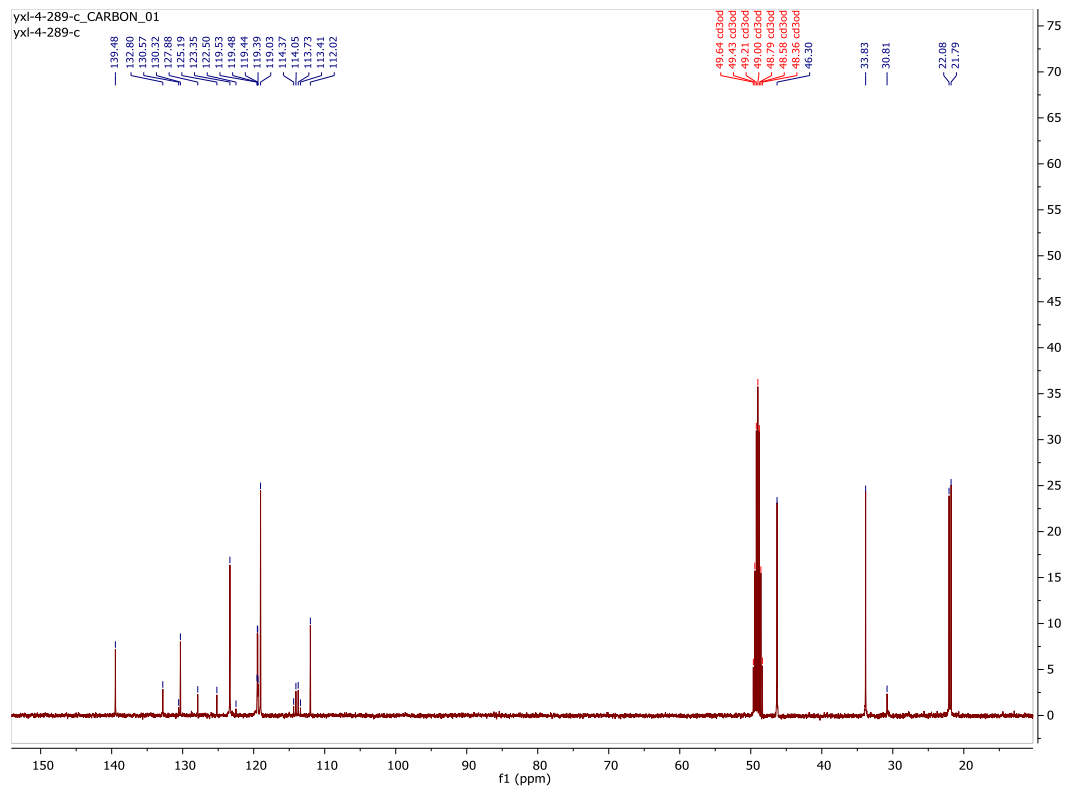
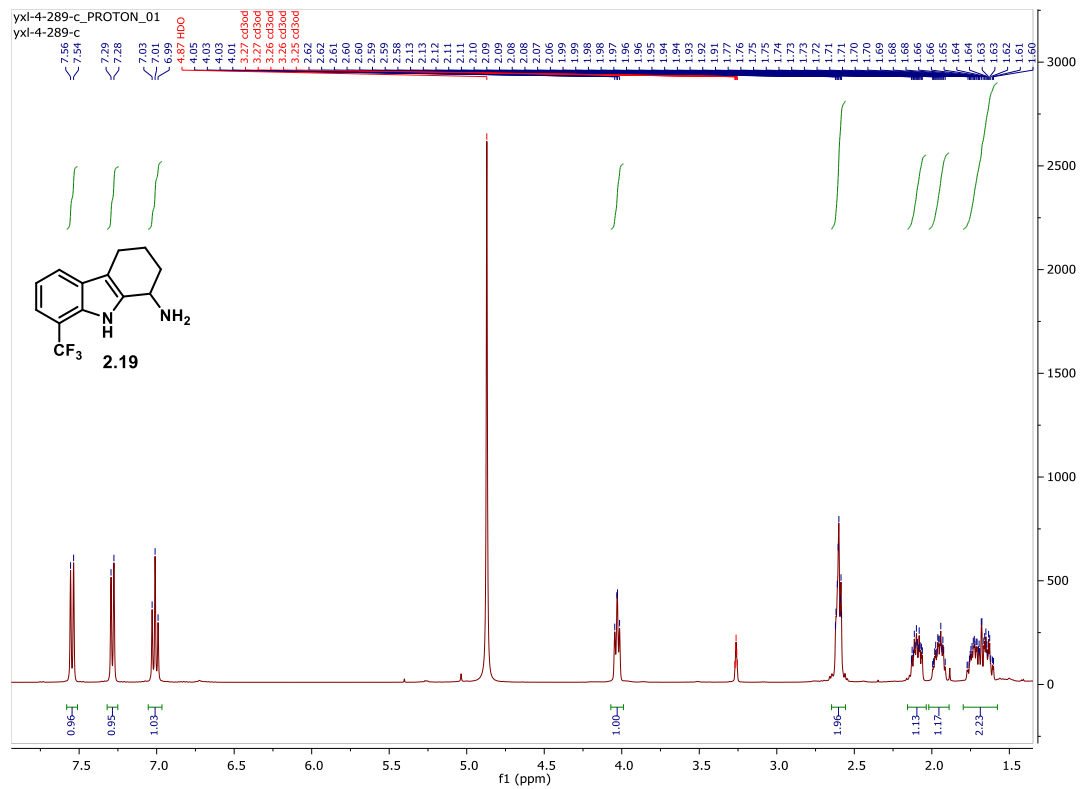


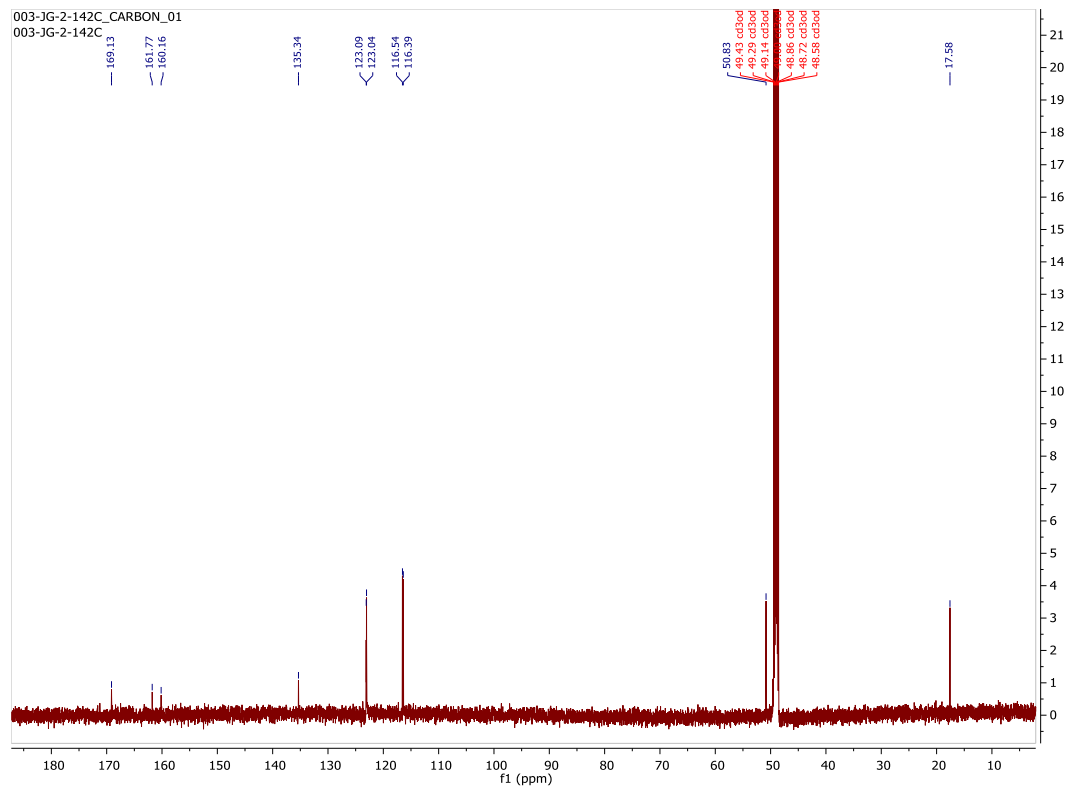
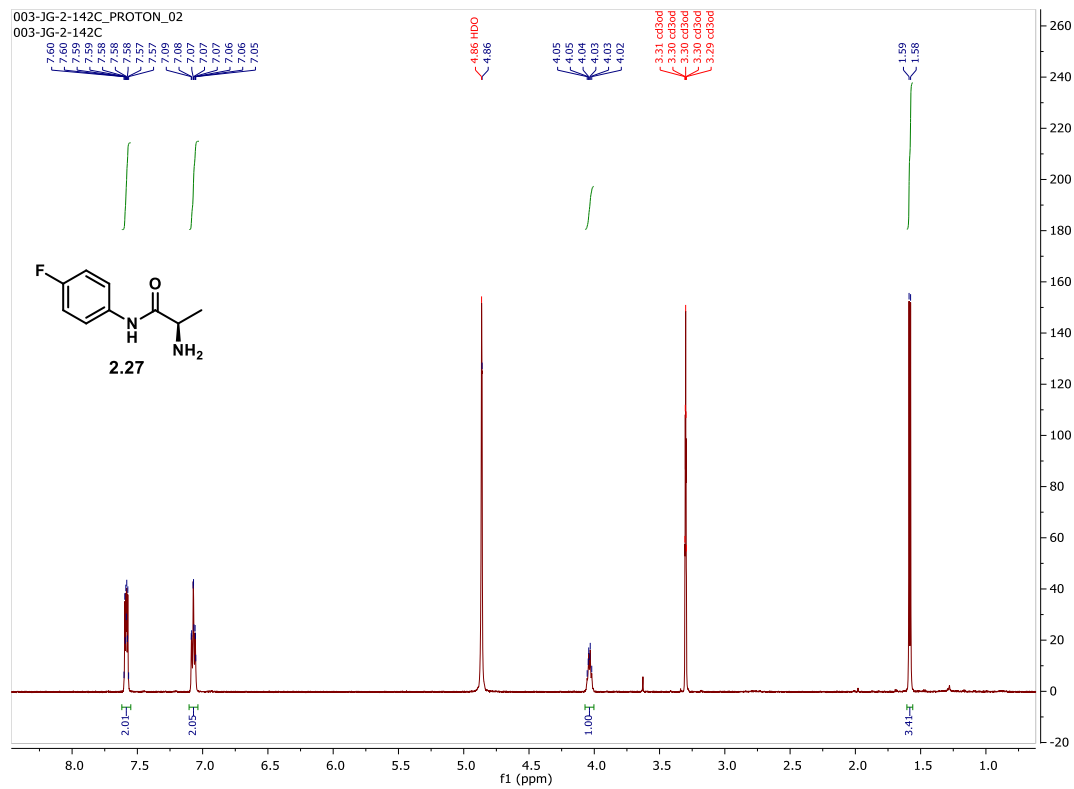


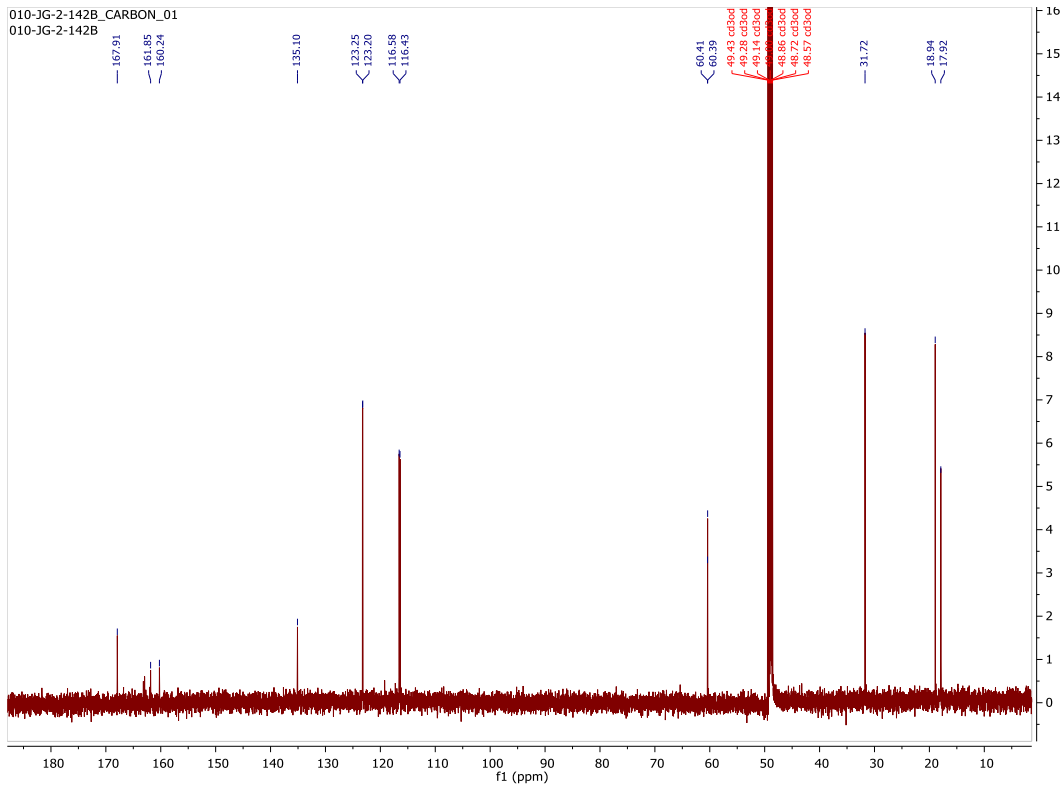
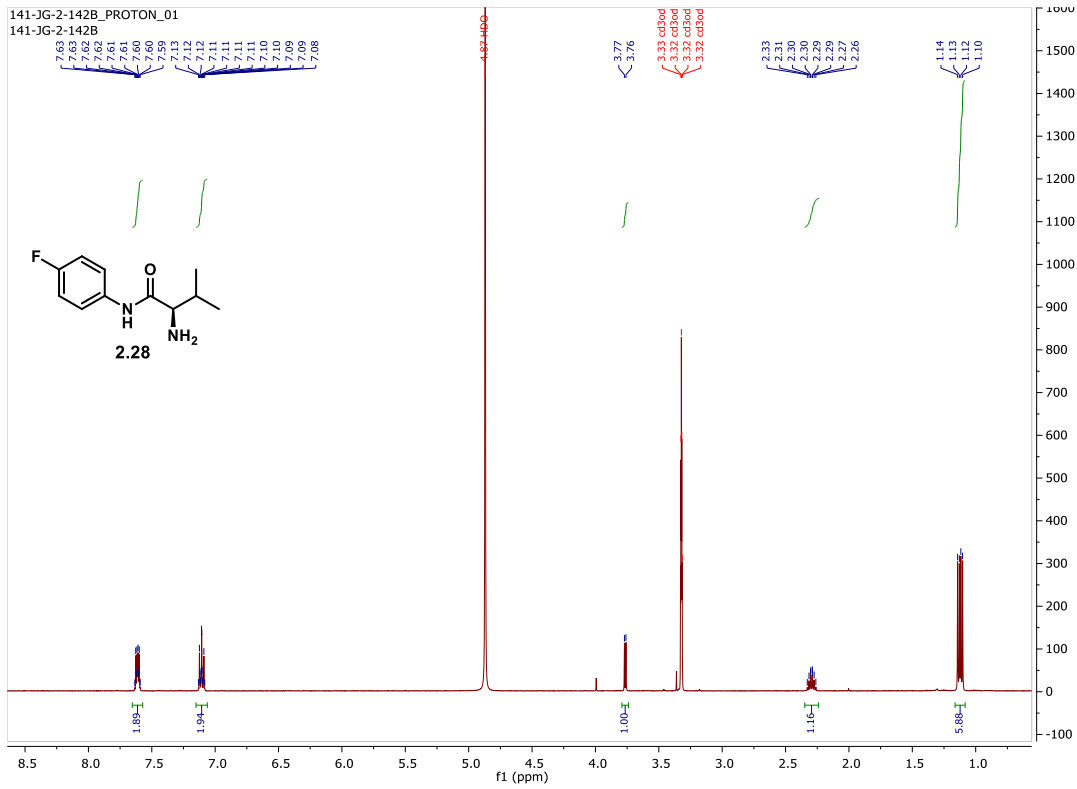


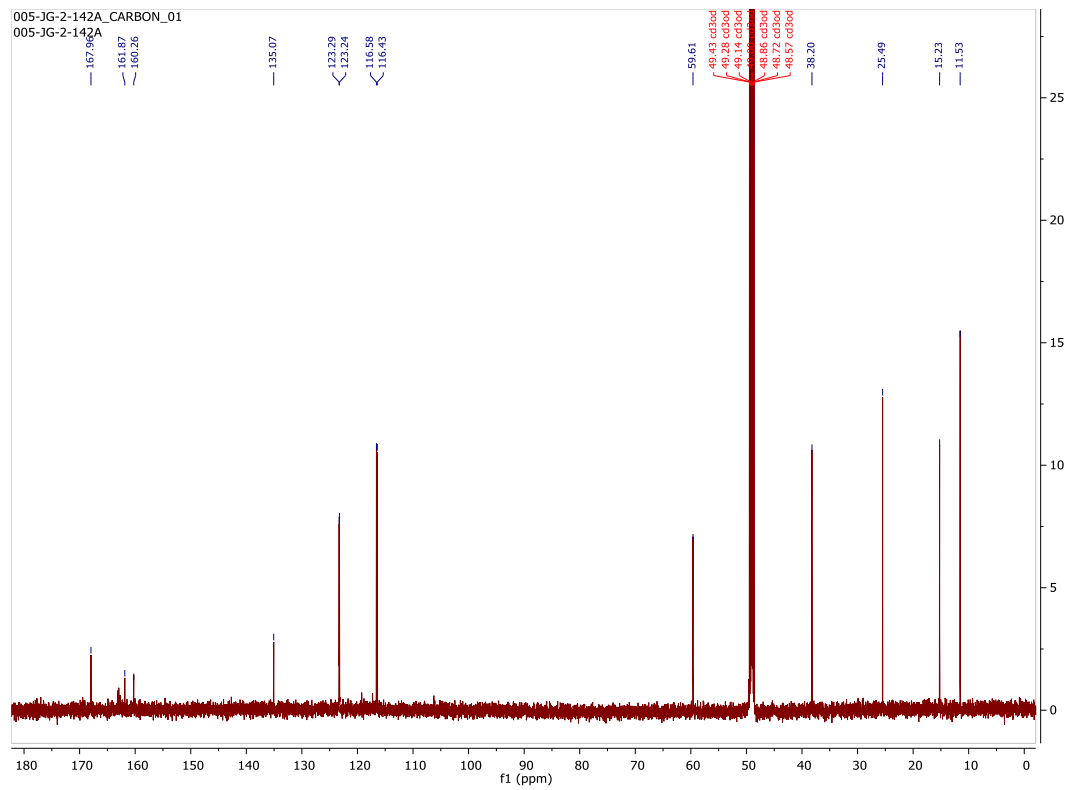
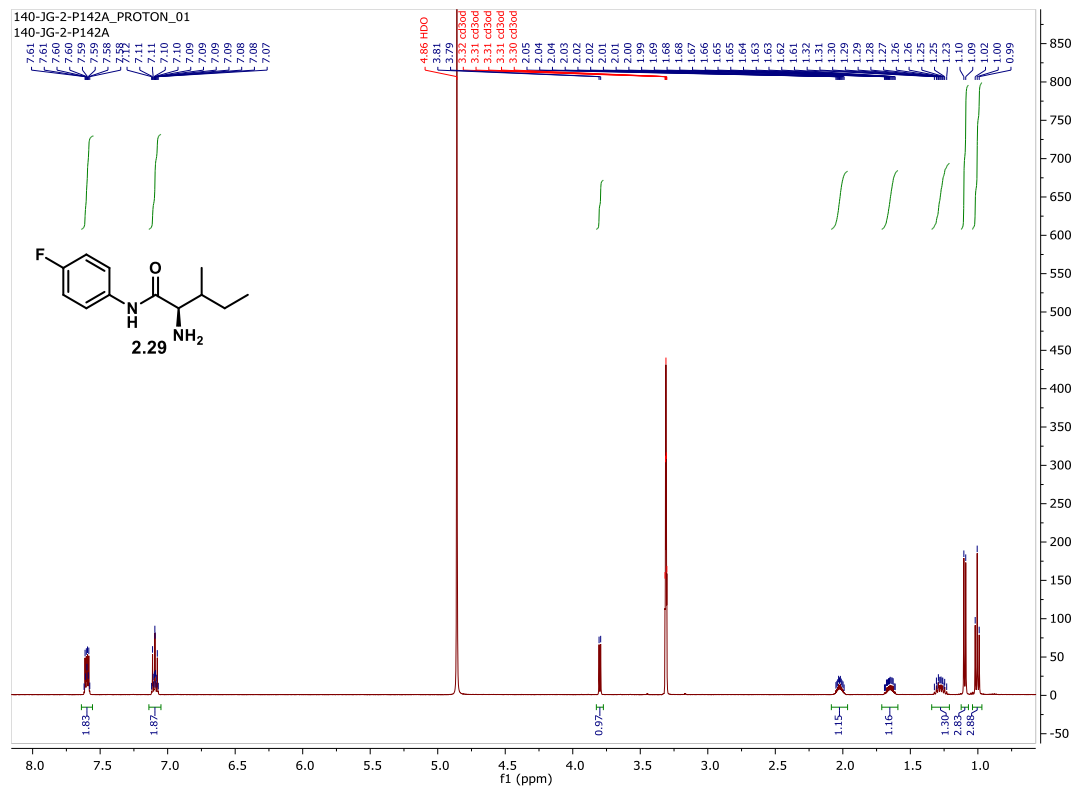


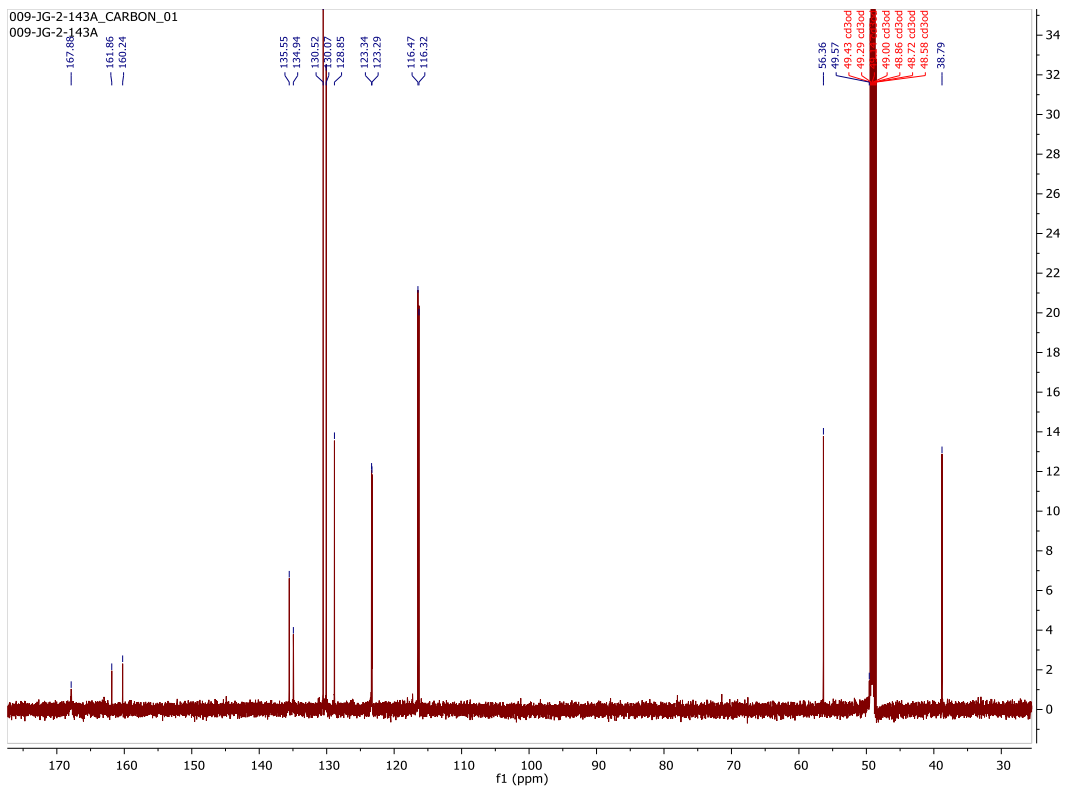
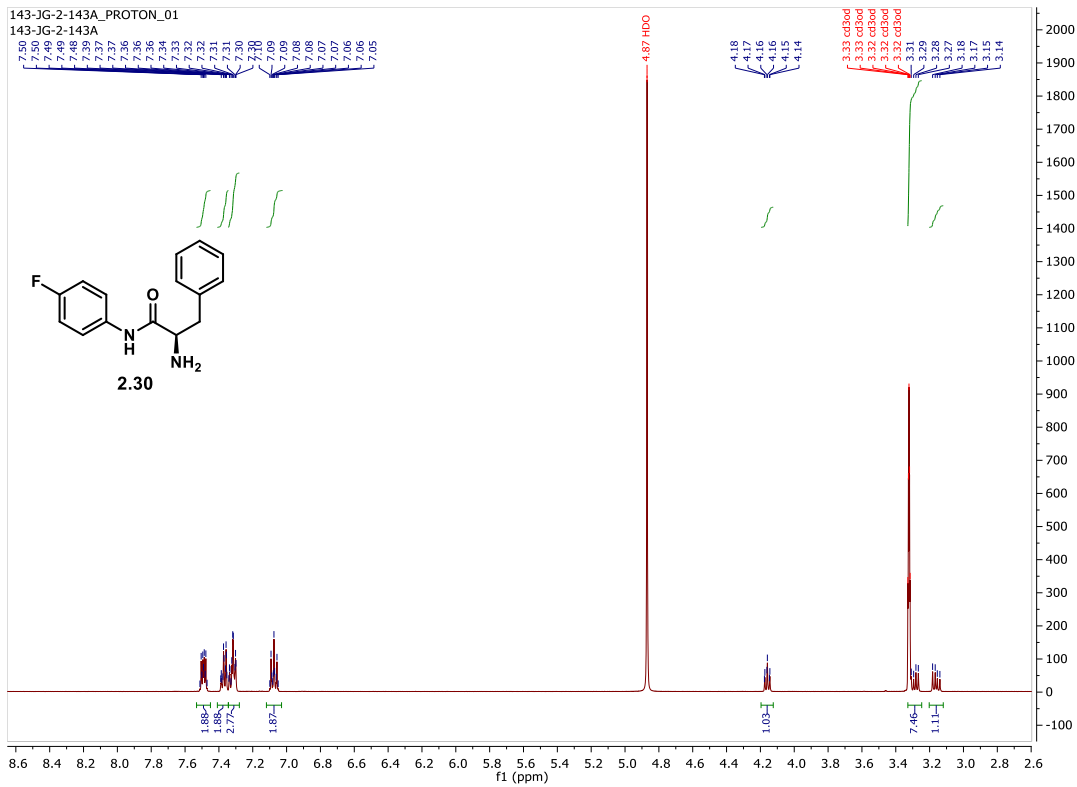






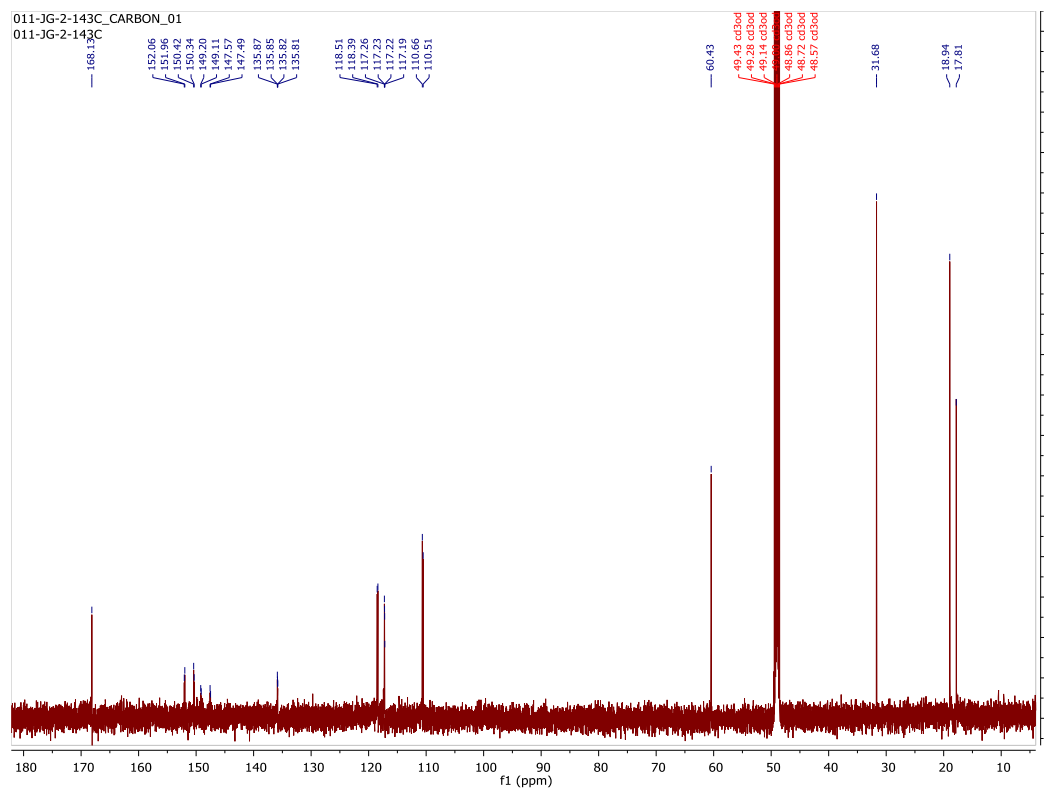
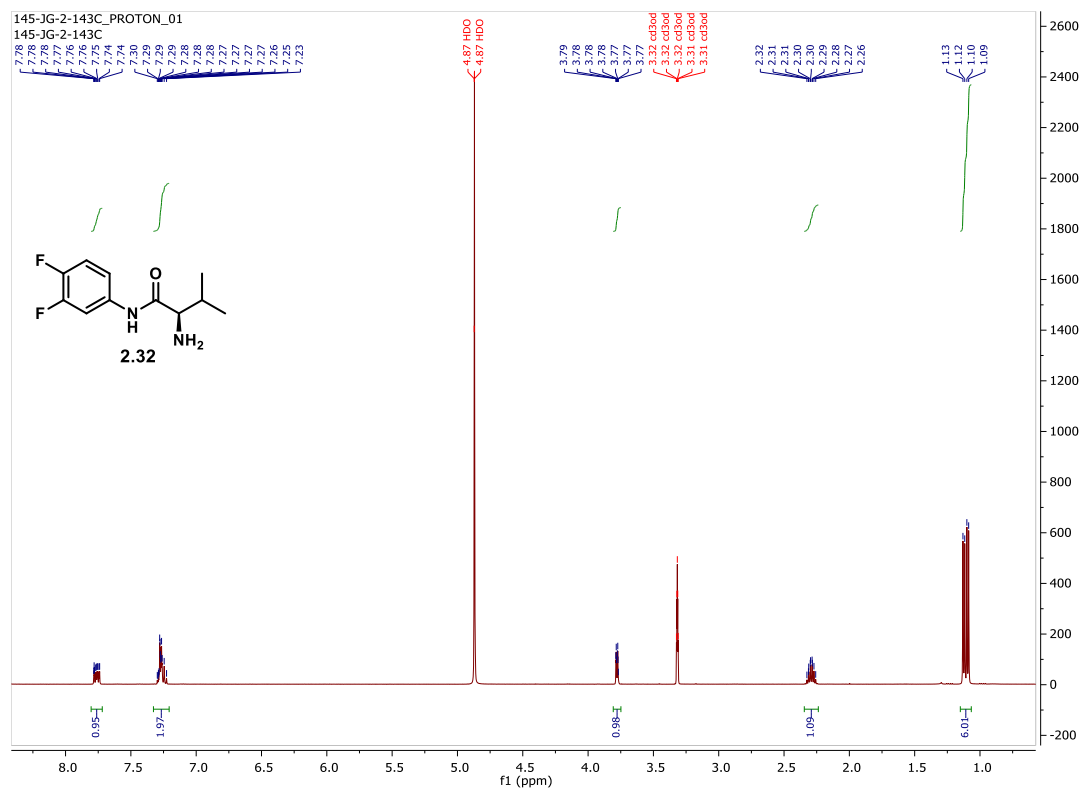


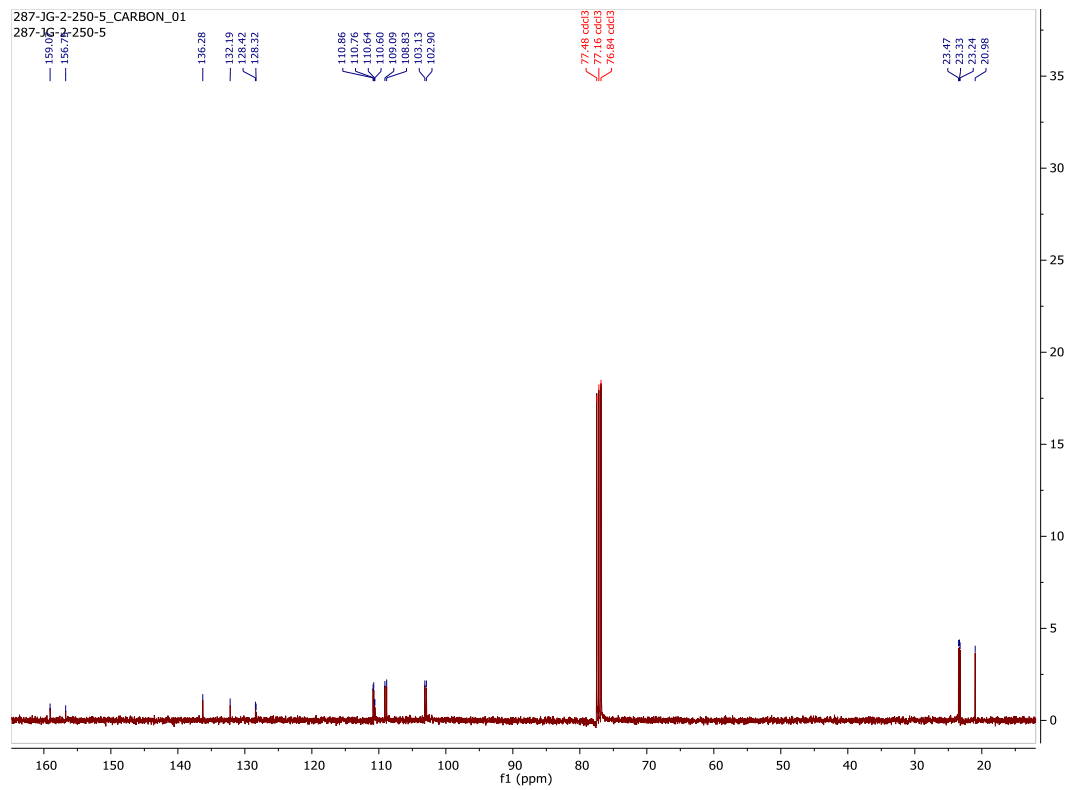
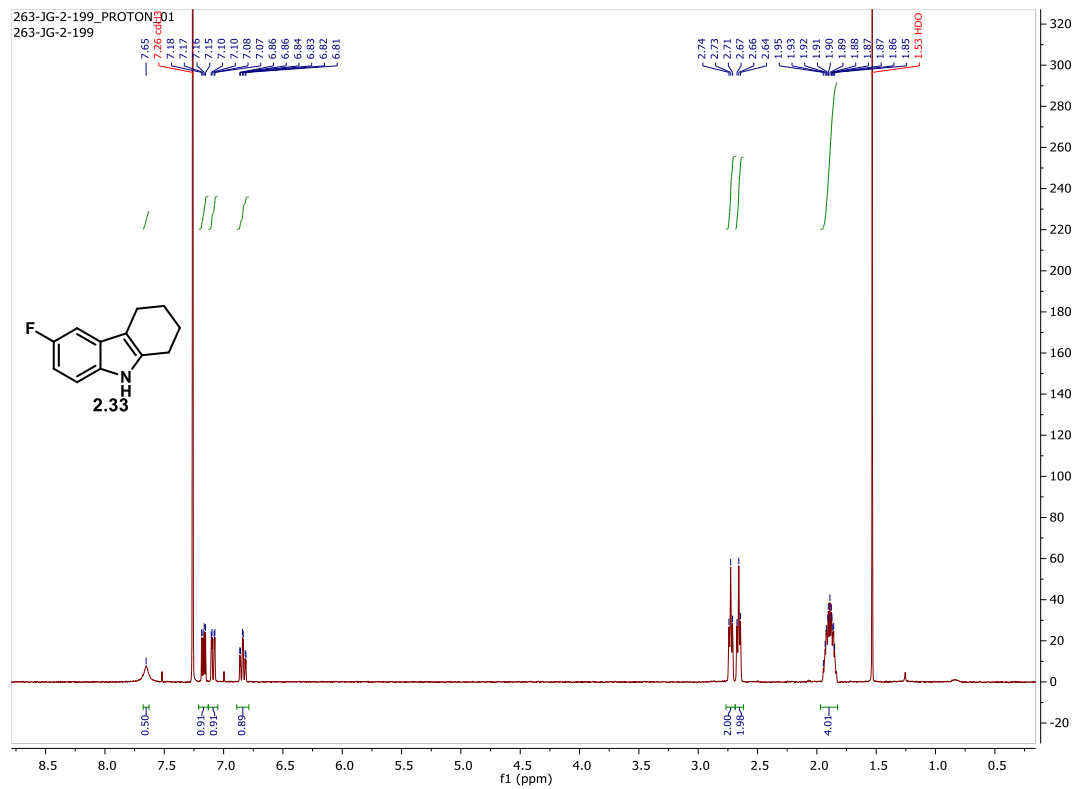










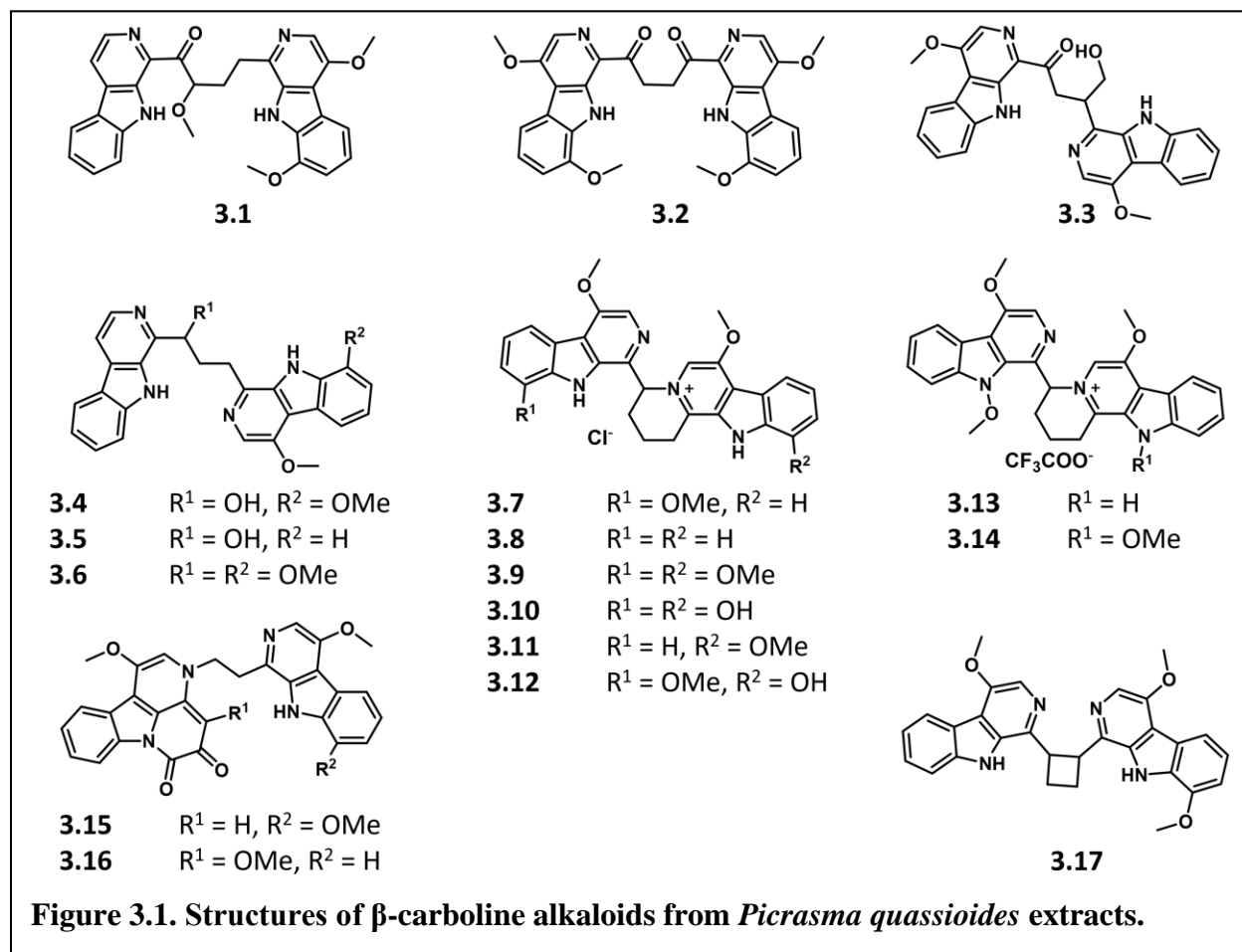


### Chapter 3: $\beta$ -carboline synthesis and functionalization for studies toward the total synthesis of picrasidine alkaloids

**Abstract.** The stem and root bark from *Picrasma quassioides* have been used historically in China, India, and the Himalayas as a traditional herbal medicine to treat a wide variety of illnesses such as fever, gastric discomfort, and pediculosis, or head lice infestation. As such, several research studies have been conducted in China and Japan to assess the efficacy of quassia-based medicines, leading to the identification and structural characterization of the *Picrasma* alkaloids. The *Picrasma* natural products are a large (approx. 94 phytochemicals) class of structurally diverse compounds with a wide array of biological activities, but the  $\beta$ -carboline alkaloids will be the focus of this chapter. Specifically, our lab is interested in picrasidine C (**1**) and its demonstrated efficacy for subtype selective PPAR $\alpha$  agonism as a promising treatment for diabetic retinopathy. The original aim was to complete the total synthesis of **1** and design analogs in order to probe structure-activity relationships (SAR) and explore the therapeutic potential of this chemotype. Two approaches were considered for this total synthesis: (1) building the heterocycle from structural fragments or (2) functionalizing an existing  $\beta$ -carboline ring. While the total synthesis of **1** was unsuccessful, six new *Picrasma* alkaloid analogs, two mono- and four bis- $\beta$ -carboline, were synthesized. These analogs have the capacity to serve as synthetic building blocks for  $\beta$ -carboline natural products because of their reactive functional groups (enamine, carbonyl, epoxide). Furthermore, a novel, metal-free acid-catalyzed Pictet-Spengler enamine cyclization cascade was discovered, providing efficient access to indoloquinolizine heterocycles.

### 3.1 Introduction to *Picrasma* alkaloids

#### 3.1.1 *Picrasma* alkaloids in traditional medicine.



*Picrasma quassioides* of the Simaroubaceae family is a deciduous bitterwood tree, native to temperate regions of southern Asia.<sup>1</sup> The stem and bark of these plants have been used historically in China, India, and the Himalayas as traditional herbal medicine to treat a wide variety of illnesses such as fever,<sup>2</sup> gastric discomfort,<sup>3</sup> and pediculosis, or head lice infestation. Although there is no evidence for inhibition of louse growth, one study observed that among 454 patients, 99% reported reduced irritation associated with pediculosis, when ground quassia powders were administered topically.<sup>4</sup> Moreover, quassia tinctures were historically consumed orally to treat infections such as the common cold, infections of the upper respiratory tract, and diarrhea,

demonstrating a broad pharmacological profile. As such, several research studies have been conducted in China and Japan to not only assess the efficacy of quassia-based medicines but also to identify and structurally characterize the natural products responsible for such biological activities. These efforts led to the discovery of the *Picrasma* alkaloids (examples in **Figure 3.1**).<sup>5</sup>

**Table 3.1 Source and biological relevance of bis- $\beta$ -carboline alkaloids from *Picrasma quassioides* plant extracts.**

Compound No.	Compound Name	Extract Source	Significance or Activity
<b>3.1</b>	Picrasidine C	Stem or bark	Glucose and lipid homeostasis <sup>6</sup>
<b>3.2</b>	Picrasidine R	Root bark	Unknown <sup>7</sup>
<b>3.3</b>	Picrasidine H	Root bark	Unknown <sup>7</sup>
<b>3.4</b>	Quassidine B	Stem	Anti-inflammatory <sup>8</sup>
<b>3.5</b>	Quassidine C	Stem	Anti-inflammatory <sup>8</sup>
<b>3.6</b>	Quassidine D	Stem	Anti-inflammatory <sup>8</sup>
<b>3.7</b>	Picrasidine F	Stem or bark	Antibacterial <sup>9</sup>
<b>3.8</b>	Picrasidine G	Stem or bark	Antibacterial <sup>9</sup> , Cytotoxic <sup>10</sup>
<b>3.9</b>	Picrasidine S	Stem or bark	Antibacterial <sup>9</sup>
<b>3.10</b>	Picrasidine T	Bark	Synthetically relevant <sup>11</sup>
<b>3.11</b>	Quassidine I	Stem	Cytotoxic <sup>12</sup>
<b>3.12</b>	Quassidine J	Stem	Cytotoxic <sup>12</sup>
<b>3.13</b>	NMCA 1	Stem	Neuroprotection <sup>13</sup>
<b>3.14</b>	NMCA 2	Stem	Neuroprotection <sup>13</sup>
<b>3.15</b>	Picrasidine M	Root bark	Unknown <sup>14</sup>
<b>3.16</b>	Picrasidine N	Root bark	Glucose and lipid homeostasis <sup>15</sup>
<b>3.17</b>	Quassidine A	Stem	Anti-inflammatory <sup>8</sup>

NMCA = N-methoxy- $\beta$ -carboline alkaloids

The various pharmacological benefits exhibited by *P. quassioides* extracts are attributed to approximately 94 distinct phytochemicals<sup>5</sup> that are structurally categorized as quassinoids,<sup>16</sup>  $\beta$ -carbolines,<sup>9,17</sup> canthinones,<sup>18</sup> and neolignans,<sup>19</sup> among others. This chapter will focus on the bis- $\beta$ -carboline-containing alkaloids (**3.1 – 3.17**). Representative structures and biological relevance of such compounds are shown in **Figure 3.1** and **Table 3.1**, respectively. It is important to note

that while compounds **3.15** and **3.16** contain a bis- $\beta$ -carboline-type system, they are structurally categorized as canthinones because of their distinct diketo ring fused to the  $\beta$ -carboline skeleton.

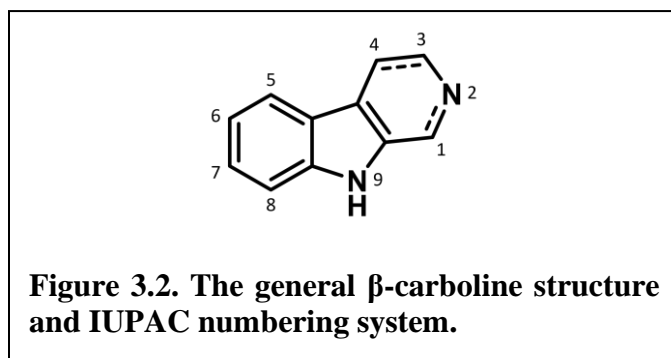
Interestingly, both picrasidine C (**3.1**) and N (**3.16**) were found to modulate lipid and glucose homeostasis via peroxisome proliferator-activated receptor (PPAR) agonism. They differ in subtype-selectivity, however, as **3.1** promotes PPAR $\alpha$  transcriptional activity<sup>6</sup> while **3.16** is a selective PPAR $\beta/\delta$  agonist.<sup>15</sup> PPARs regulate the expression of genes involved in numerous cellular functions including insulin sensitivity, fatty acid oxidation, inflammation, and cell proliferation, differentiation and survival.<sup>20</sup> PPAR subtypes localize in differing concentrations depending on the tissue type.<sup>21</sup> As such, selectively targeting PPAR subtypes is believed to be important for triggering specific responses while avoiding harmful side effects.<sup>22</sup> Consequently, tuning target specificity is contingent on structural differences between chemo-modulators.

Structure-activity relationship (SAR) studies within the *Picrasma* alkaloid class are integral to identifying structural motifs that dictate biological activity and target specificity. Stemming from our lab's interest in **3.1** as a PPAR $\alpha$  agonist<sup>6</sup> and in the demonstrated efficacy for PPAR $\alpha$  agonism as a promising treatment for diabetic retinopathy,<sup>23</sup> the original aim was to complete the total synthesis of **3.1** and design analogues in order to probe SAR and explore the therapeutic potential of this chemotype. This work has since evolved into a synthetic investigation towards several members of the *Picrasma* alkaloid family and my efforts towards the total synthesis of **3.1** and related *Picrasma* alkaloids will be discussed herein.

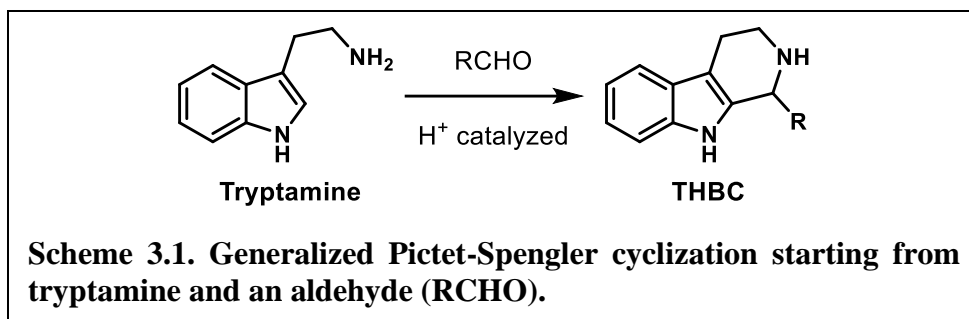
### **3.1.2 Overview of $\beta$ -carbolines and existing synthetic methods.**

Establishment of methods for the synthesis of *Picrasma* alkaloids is of pharmaceutical importance for several reasons. First, poor isolation yields from natural sources is not sufficient for intensive biological evaluation or SAR campaigns. For example, only 5.6 mg of **3.1** can be

isolated from 100 kg of *P. quassioides* stems, using current extraction methods.<sup>8</sup> Synthetic studies would also help to determine absolute stereochemistry, since the assignment of stereocenters for *Picrasma* alkaloids are often absent<sup>24</sup> or ambiguously<sup>25,26</sup> presented within literature. Further, total synthesis would provide a foundation for the development of synthetic analogues, especially when the synthetic approach is designed to enable facile diversification. The total synthesis of compounds within this natural product family is necessary to deconvolute the structural contributions to biological activity and to enable structural optimization of the family for diverse therapeutic interests.

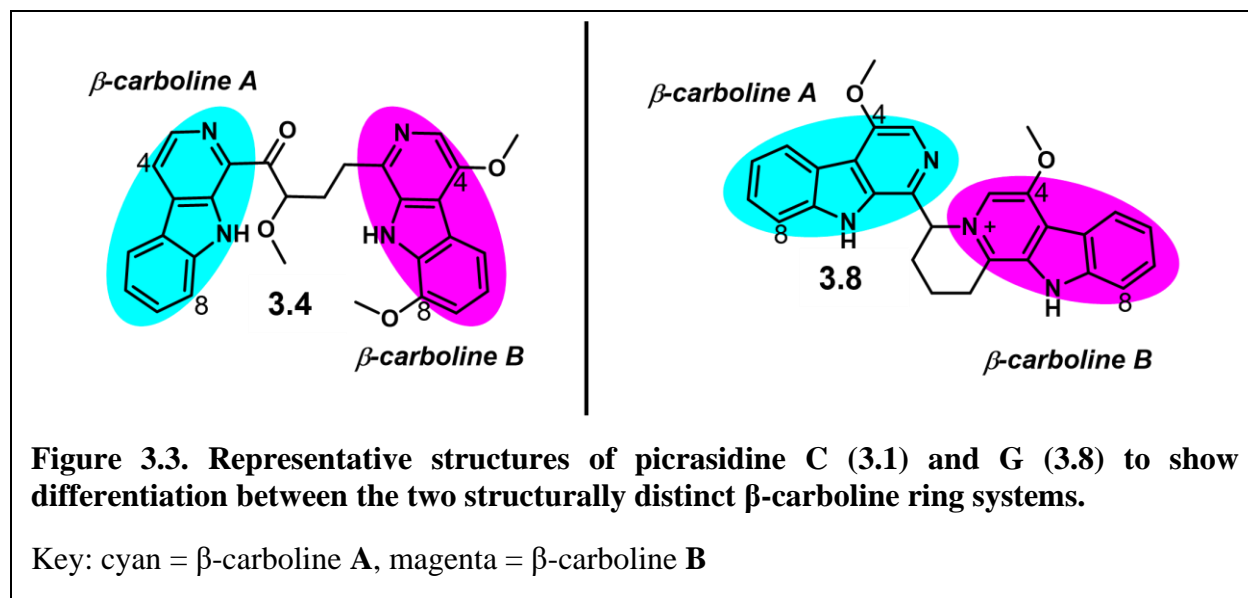


Completing the total synthesis of the  $\beta$ -carboline-containing *Picrasma* alkaloids hinges on the ability to construct a properly substituted tricyclic ring system, which consists of an indole skeleton fused to a pyridine. Currently, the most common route to generate the  $\beta$ -carboline heterocycle and its saturated tetrahydro- $\beta$ -carboline (THBC) congener (**Figure 3.2**) includes the condensation of tryptamine with an aldehyde or ketone.<sup>27</sup> Named the Pictet-Spengler reaction (PSR), its multifunctionality has significant synthetic value since the amine and aldehyde components can vary widely, allowing for the construction of structurally diverse THBC ring systems (**Scheme 3.1**). The driving force of this reaction is the electrophilicity of the intermediate iminium ion, which can be enhanced by acidic conditions.<sup>28</sup>

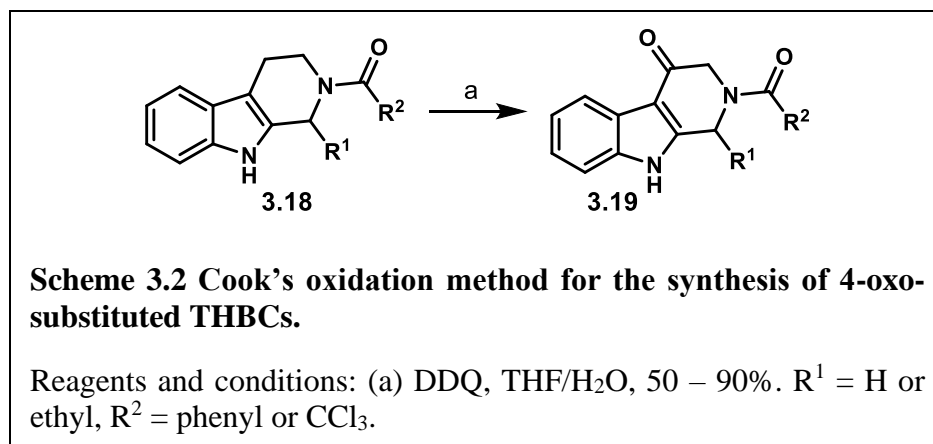


The *Picrasma* family of alkaloids are unique in their asymmetrical bis- $\beta$ -carboline structure and widely varying oxidation patterns. For example, picrasidine C (**3.1**) contains two distinct  $\beta$ -carboline systems, with the first unsubstituted (denoted as  $\beta$ -carboline A, **Figure 3.3**) and the second containing two methoxy groups, at the 4- and 8-positions (denoted as  $\beta$ -carboline B, **Figure 3.3**). Picrasidines C (**3.1**), R (**3.2**), and H (**3.3**), and quassidines A (**3.17**) B (**3.4**), C (**3.5**), and D (**3.6**) each contain a three- or four-carbon linker region connecting the two heterocycles, although the carbon skeletons and oxidation patterns differ between the structures. The pyridinium-type salts, including picrasidines F (**3.7**), G (**3.8**), S (**3.9**), and T (**3.10**), quassidines I (**3.11**) and J (**3.12**), and the N-methoxy- $\beta$ -carboline alkaloids (NMCA) **3.13** and **3.14**, stand apart structurally due to the presence of a four-carbon linker lacking oxidation and inclusion of a fourth fused ring to create a pyridinium-type ionic species.

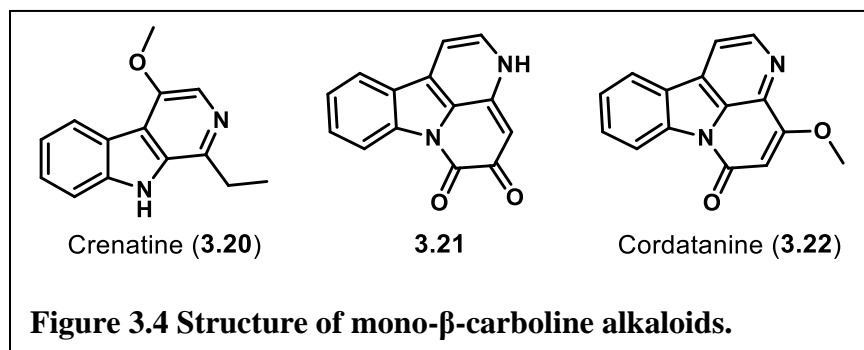




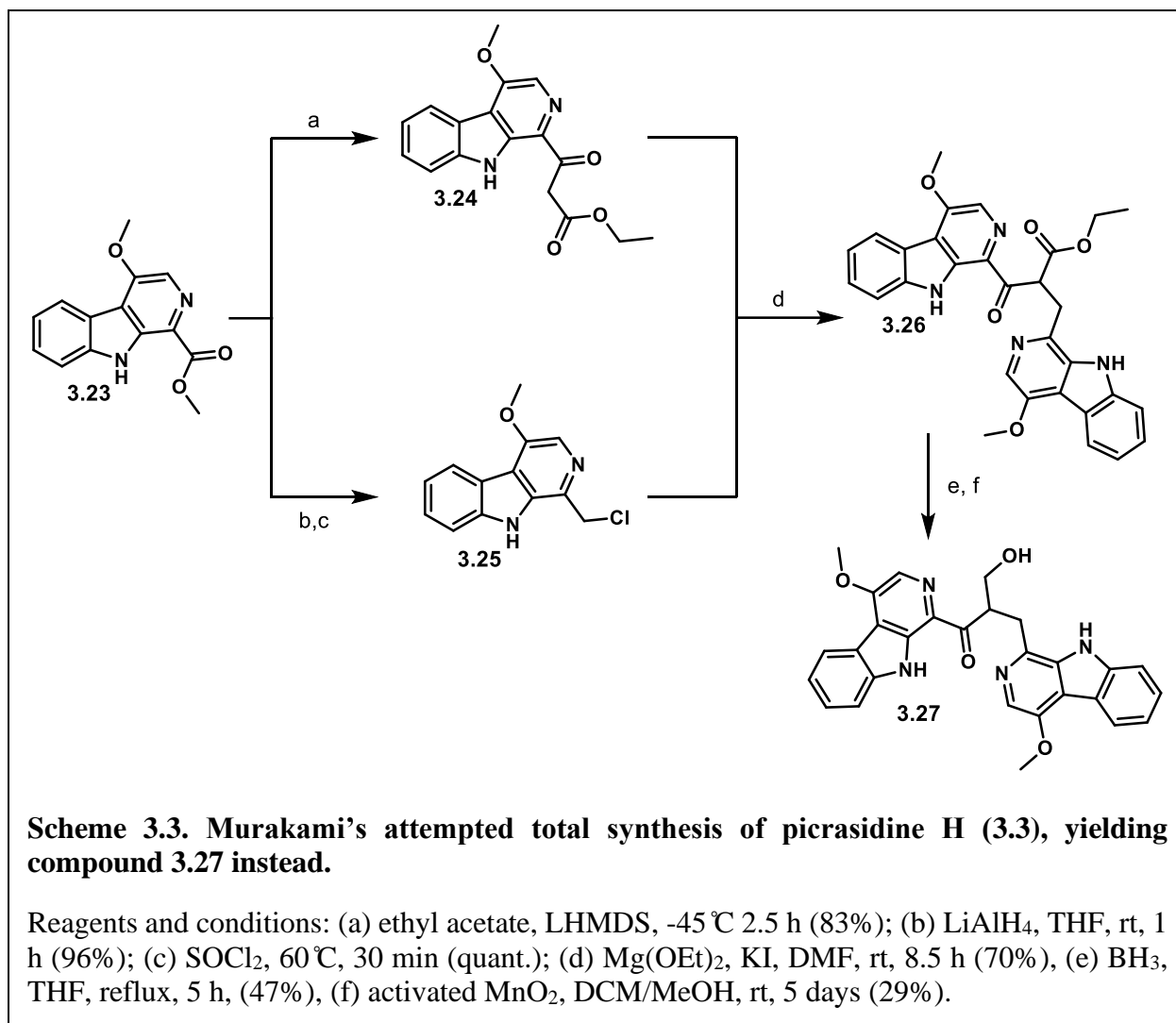
Despite the varying oxidation patterns within the *Picrasma* alkaloid family, at least one 4-oxygenated  $\beta$ -carboline structure remains consistent in each family member. Synthesis of the 4-oxygenated  $\beta$ -carboline structure is reportedly problematic, because the classical Bischler-Napieralski<sup>29</sup> or Pictet-Spengler cyclization reactions of tryptamines are not compatible with the construction of these analogs.<sup>30</sup> Notably, one method devised by Cook et al. in 1989<sup>31</sup> found dichlorodicyanobenzoquinone (DDQ) to be an appropriate oxidizing agent for transforming THBCs **3.18** into their 4-oxo counterparts **3.19** (Scheme 3.2). Though this site-specific oxidation method has found some utility in  $\beta$ -carboline chemistry,<sup>32,33</sup> its suitability for the general synthesis of *Picrasma* alkaloids is limited, as it requires the presence of an objective substituent on the 1-position of the  $\beta$ -carboline during early stages of synthesis.<sup>34</sup>



While some mono- $\beta$ -carboline alkaloids have been successfully synthesized, such as crenatine (**3.20**),<sup>35</sup> canthinone-type alkaloids (**3.21**),<sup>36</sup> and cordatanine (**3.22**)<sup>37</sup> (structures shown in **Figure 3.4**), there are currently no synthetic routes reported for the bis- $\beta$ -carboline *Picrasma* alkaloids. The total synthesis of picrasidine H (**3.3**) has been attempted by Murakami et al. in 1997, although only the synthesis of its regioisomer **3.27** was achieved, creating confusion around true structure of Picrasidine H (**Scheme 3.3**).<sup>38</sup> Despite Murakami's efforts, the total synthesis of **3.3** has not yet been reported.



Although the work by Murakami provides inspiration for bis- $\beta$ -carboline syntheses, the approach is contingent on the coupling of two in-tact  $\beta$ -carboline heterocycles, limiting linker structure and connectivity. A more flexible synthetic design would allow for structural diversification, the possibilities of which will be discussed in this chapter.



## 3.2 Retrosynthetic analysis

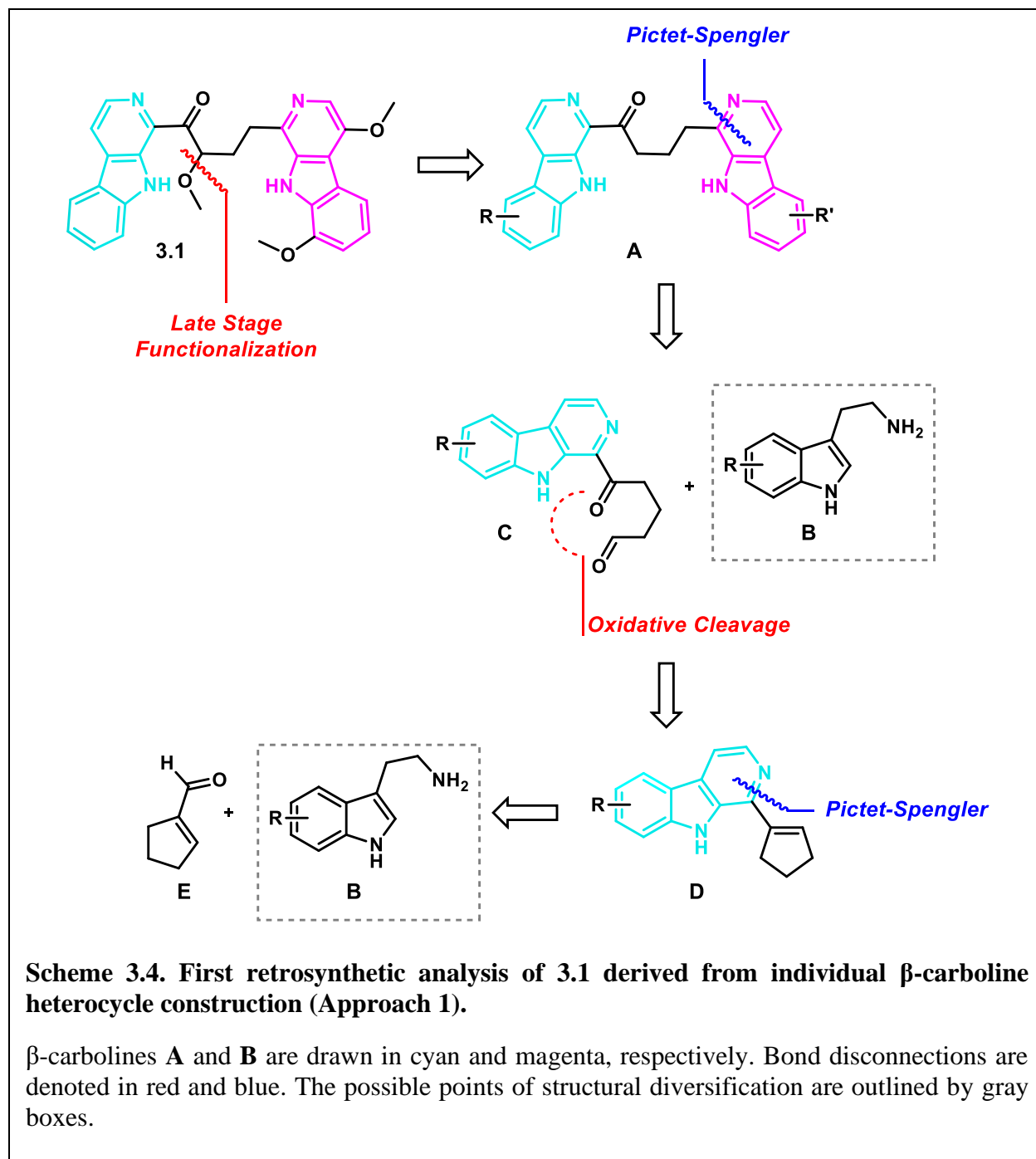
I primarily envisioned two approaches for accessing  $\beta$ -carboline-containing molecules: (1) building the heterocycle from structural fragments or (2) functionalizing an existing  $\beta$ -carboline ring. Efforts to employ each strategy are the focus of this chapter.

### 3.2.1 Iterative $\beta$ -carboline ring construction (Approach 1).

The first strategy for the total synthesis of **3.1** relied on the individual construction of both  $\beta$ -carboline A (cyan) and B (magenta) ring systems (**Scheme 3.**). The first bond disconnection was

made at the methoxy substituent in the linker to enable late-stage functionalization of synthon **A**. Relying on the historic utility of the Pictet-Spengler cyclization for the construction of both  $\beta$ -carboline **A** and **B**, synthon **C** was envisioned to allow for one PSR with substituted tryptamines **B** to form  $\beta$ -carboline **B**. Synthon **C** also contains the linker atoms and the important aldehyde component for the PSR. The linker was envisioned to arise from an oxidative cleavage of a cyclic olefin, such as synthon **D**, which could be synthesized via another PSR.

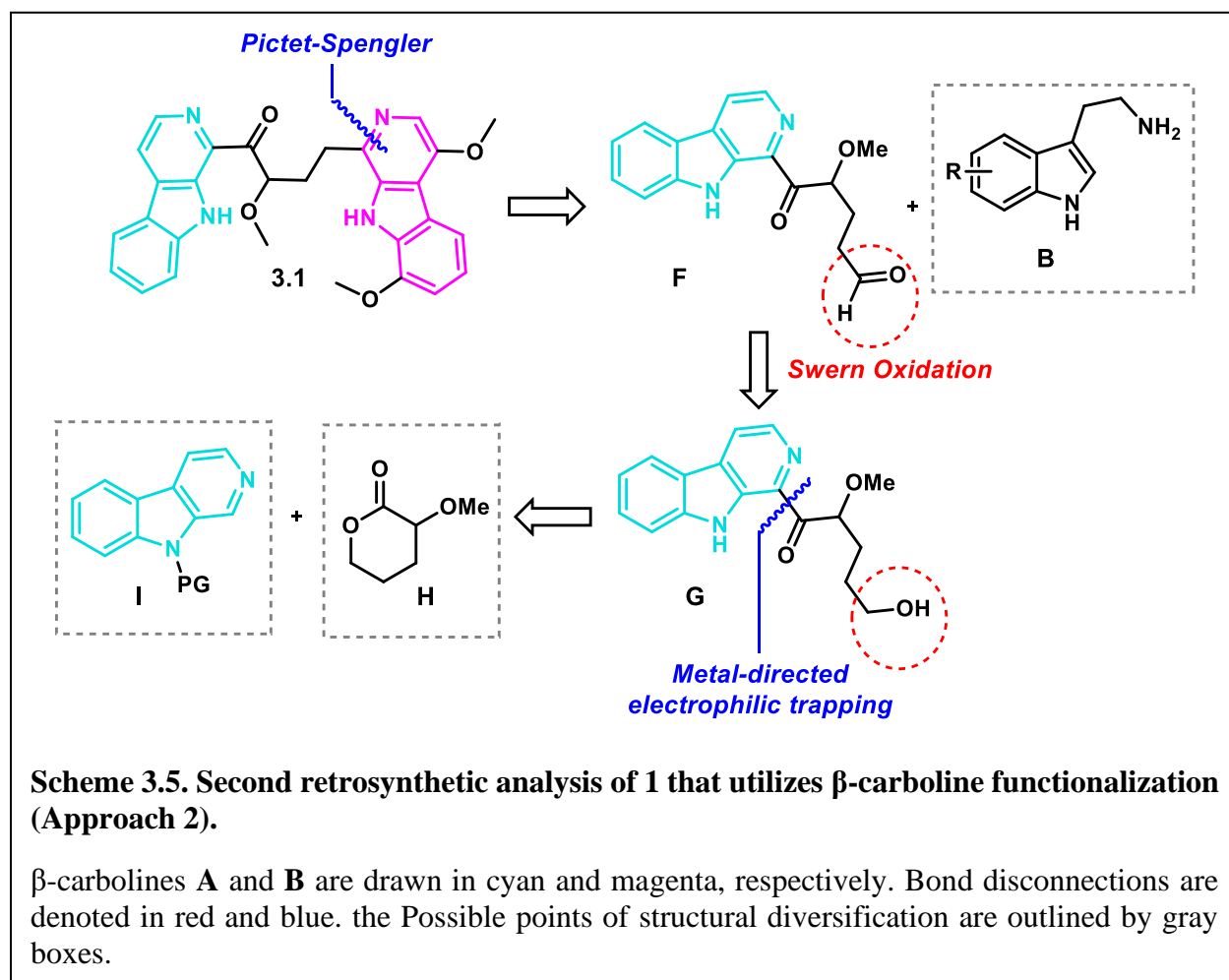
This route employs inexpensive and commercially available tryptamine starting materials **B**. With 1-cyclopentene-1-carbaldehyde (**E**) as the PSR carbonyl component for  $\beta$ -carboline **A**, after oxidative aromatization, the resulting olefin **D** is poised for oxidative cleavage to continue the total synthesis as envisioned by the retrosynthetic analysis. The olefin in **D** also provides a synthetic handle for functionalization or eventual diversification, with potential to investigate new chemical space within the Picrasma alkaloids. Another location in this plan that allows for possible structural diversification is the  $\alpha$ -keto position on synthon **A**. Specifically, oxidation and alkylation to install an  $\alpha$ -keto-methoxy group would result in the total synthesis of **3.1**. Additional analogs were envisioned to be accessible through enolate trapping of synthon **A**. Further, if stereoselective  $\alpha$ -keto functionalization is possible, then both enantiomers of **3.1** can be synthesized individually to help elucidate the absolute stereochemistry of the natural product. Two other points of diversification exist in both PSR steps where substituted tryptamines **B** would provide  $\beta$ -carboline molecules with a variety of substitution patterns (points of diversification denoted by intermediates in dashed-line boxes in **Scheme 3**).



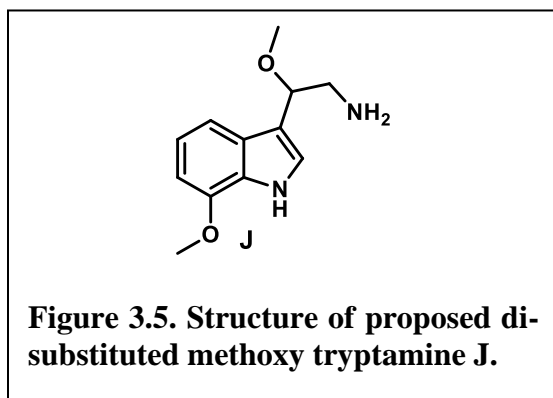
### 3.2.2 β-carboline functionalization (Approach 2).

This approach only employs one PSR for the formation of β-carboline **B** (magenta, **Scheme 3.**) from an aldehyde such as **F**. Synthon **F** contains an already in-tact β-carboline **A** heterocycle (cyan, **Scheme 3.**) and a linker with the correct oxidation pattern present in **3.1**. The formation of

synthon **F** could arise from Swern oxidation<sup>39</sup> of alcohol **G**. The formation of synthon **G** is anticipated to be a difficult step in this retrosynthetic analysis, because it relies on the ability to create a nucleophilic 1-position on  $\beta$ -carboline **A**. The synthesis of  $\beta$ -carboline synthon **G** was envisioned to arise from ring metalation,<sup>40</sup> C-H activation,<sup>41</sup> or radical functionalization at the 1-position of the  $\beta$ -carboline in synthon **I**.<sup>42</sup> If the substituted  $\delta$ -valerolactone synthon **H** is an adequate electrophile, then the linker can be directly attached with the proper oxidation pattern of the linker in compound **3.1**. Ideally, the terminal carbon on the linker would be captured in a final PSR as C1 in  $\beta$ -carboline **B** (magenta, **Scheme 3**).



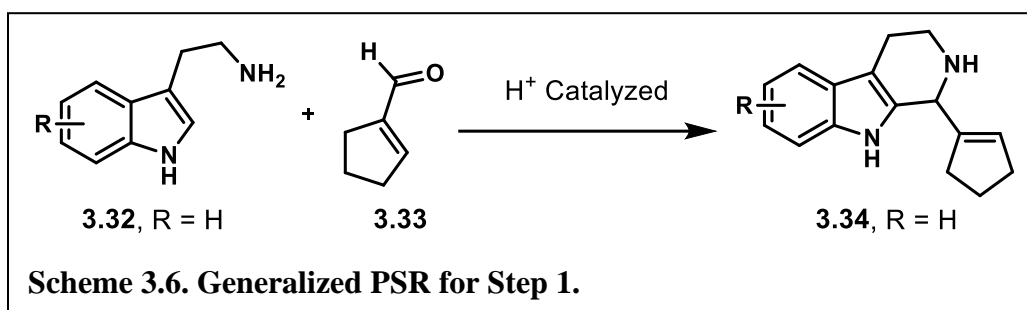
This synthetic approach allows for structural diversification at three different points, denoted by the intermediates highlighted with dashed-lined boxes in **Scheme 3.** Depending on the substitution pattern of various  $\beta$ -carbolines (**I**) and the corresponding effects to the metalation chemistry, the initial coupling reaction of compounds **I** and **H** is expected to provide the first point of diversification. This would allow for diversification of both  $\beta$ -carboline **A** and the linker. Alternatively, differently substituted tryptamines in the final PSR are expected to enable diversification of  $\beta$ -carboline **B**. For example, if tryptamine **J** (**Figure 3.5**) was employed in the PSR with aldehyde **A** (**Scheme 3.5**), then the total synthesis of **3.1** would be achieved. As such, this synthetic approach provides a valuable opportunity to develop a Picrasma alkaloid library to interrogate the SAR of Picrasidine C and related congeners.



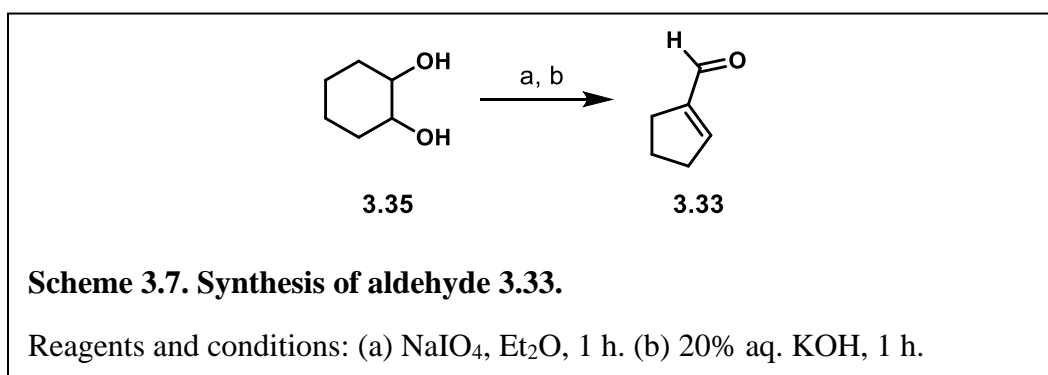
### 3.3 Results and discussion for Approach 1

The iterative  $\beta$ -carboline construction approach was explored more extensively between the two approaches. The PSR is the pivotal reaction of this approach as it is utilized for the assembly of both  $\beta$ -carbolines **A** and **B**, and each PSR step required individual optimization. **Approach 1** can be generalized and broken down into four steps: (1) PSR1, (2) oxidative aromatization, (3) oxidative cleavage, and (4) PSR2. The investigation, optimization, and application of each of these steps in the efforts to synthesize **3.1** are discussed in this section.

### 3.3.1 Step 1: Pictet-Spengler cyclization with cyclopentene-1-aldehyde for the formation of THBC 3.34 (PSR1).



The first Pictet-Spengler reaction, hereby denoted as **PSR1** or **Step 1**, was integral to the retrosynthetic plan, because it would provide the carbon and nitrogen skeleton of both  $\beta$ -carboline **A** and the linker. To achieve this, **PSR1** was envisaged from starting materials tryptamine **3.32** and cyclopentene-1-aldehyde **3.33**, where substituted tryptamines might also be used during future diversification of THBC **3.34** (**Scheme 3.**). This reaction was more challenging than predicted, thus this subsection will describe the work towards accomplishing **Step 1** and its optimization.



Aldehyde compound **3.33** is a colorless, volatile liquid. It is commercially available and relatively expensive, however supply chain issues and material limitations (<5 g available at a time) inspired me to synthesize it in-house. As in the typical case of  $\alpha,\beta$ -unsaturated aldehydes,<sup>43</sup> **3.33** is also rather unstable, as it polymerizes under mildly basic conditions or in an aqueous environment. Thus, **3.33** was freshly synthesized each time before executing **PSR1**. The synthesis



of **3.33** was achieved through oxidation of *cis*-1,2-cyclohexanediol (**3.35**) with sodium (meta)periodate (NaIO<sub>4</sub>) followed by base-promoted ring-opening with potassium hydroxide (KOH). This reaction is performed in a biphasic mixture of water and diethyl ether at room temperature (**Scheme 3**). Since **3.33** is a low molecular weight liquid and is highly volatile, purification is best achieved using a Kugelrohr distillation apparatus. Purification was circumvented, however, and the crude product in ether was used immediately for the Pictet-Spengler cyclization reaction. Notably, yields of the following PSR were not affected by purity of the aldehyde solution.

The PSR is generally performed under acidic conditions at refluxing temperatures in a variety of solvents.<sup>27</sup> In order to assess the best conditions for this reaction to occur with the cyclopentene-1-aldehyde substrate, methanol, dichloroethane (DCE), dichloromethane (DCM), and diethyl ether (Et<sub>2</sub>O) were employed (**Table 3.2**). Following typical PSR procedures,<sup>27</sup> the reaction was first attempted in methanol at 80 °C with one equivalent of glacial acetic acid, which resulted in no observable product formation (**Table 3.2**, entry 1). Likewise, heating to 110 °C in DCE and TFA failed to provide the desired product (**Table 3.2**, entry 2). Finally, two equivalents of TFA in DCM at room temperature (~23 °C) resulted in product formation, albeit in 18% yield (**Table 3.2**, entry 3). Interestingly, yields for this reaction, when repeating the same conditions, were inconsistent and ranged from 18 – 39%.

Based on results by TLC, all reactions independent of solvent or temperature form one very polar product, which appears at baseline and remains immobile in a 5 – 20% methanol/ethyl acetate eluent. Unsuccessful attempts were made to isolate and characterize this product, but it is presumed to be a polymerization product from either the aldehyde, tryptamine, or a combination of the two. Qualitatively, the formation of the putative polymerization product can be observed as a brownish

amber sticky oil as the reaction occurs. I also believe that the formation of this by-product continuously diminishes the yield of the desired product **3.34**, so that once the polymer starts to form, the production of the desired product stalls. Practically speaking, when the reaction turns dark brown or a brown tar collects on the side of the reaction flask, I could assume a poor yielding reaction.

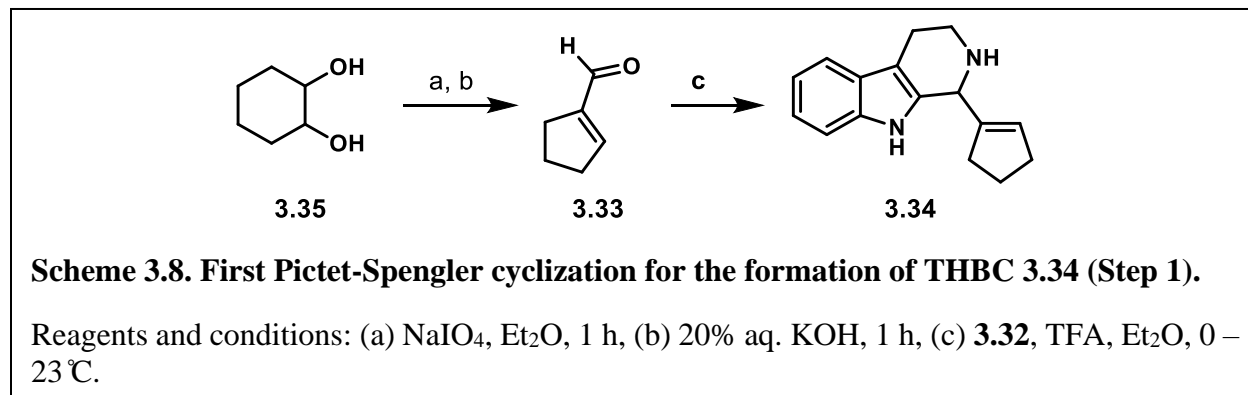
**Table 3.2. Optimization table for PSR1.**

Entry	Acid	Solvent	Additive	Method	Temp (°C)	Yield (%)
1	AcOH	Methanol	None	A	80	0
2	TFA	DCE	None	A	110	0
3	TFA	DCM	None	A	23	18
4	TFA	DCM	Na <sub>2</sub> SO <sub>4</sub>	A	0 – 23	39
5	TFA	DCM	Na <sub>2</sub> SO <sub>4</sub>	B	0 – 23	46
6	TFA	DCM	Na <sub>2</sub> SO <sub>4</sub>	C	0 – 23	65
7	TFA	Et <sub>2</sub> O	Na <sub>2</sub> SO <sub>4</sub> or MS	C	23	18
8	TFA	Et <sub>2</sub> O	MS	C	0 – 23	87

MS = molecular sieves. Method varies by acid addition: (A) Acid added dropwise. (B) Acid added dropwise slowly over the course of 10 minutes. (C) Acid added dropwise slowly over the course of 1 hour.

Since polymerization was believed to be the issue, focus shifted towards altering conditions to prevent the formation of polymerization side-products. The most obvious approach for circumventing polymerization is to decrease the reaction concentration. As such, the solvent volume was doubled for the remaining trials. Notably, the water formed as a by-product during this PSR can hinder reaction progress, since aldehyde **3.33** polymerizes in the presence of water. Therefore, water adsorption additives were used in attempts to prevent unwanted side reactions. Sodium sulfate was adequate as a desiccant (**Table 3.2**, entries 4 – 6), but molecular sieves worked best (**Table 3.2**, entry 8). While the brown resin assumed to be polymerization products can be

seen accumulating around the solid desiccants, yields improved. Next, lower temperatures were investigated. As mentioned previously, high temperatures are typically necessary for the PSR cyclization to occur, but high temperatures also promote polymerization.<sup>44</sup> It was found that starting the reaction over an ice bath and gradually warming to room temperature provided more reliable product formation (**Table 3.2**, entries 6 and 8).

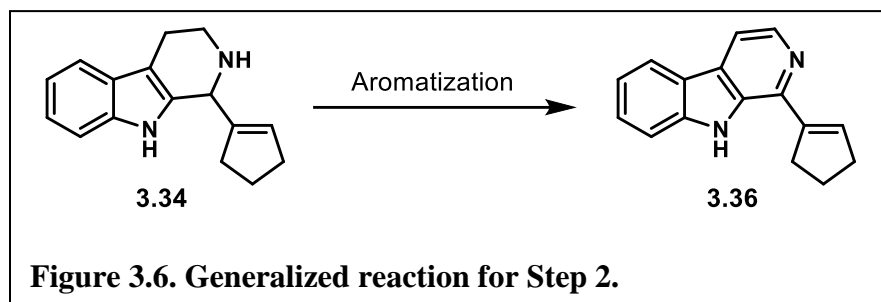


This gradual temperature increase improved the yield significantly, more than double compared to the room temperature reaction (**Table 3.2**, entry 4). Upon this discovery, I then tried slowing the addition of the acid, adding the TFA dropwise over the course of 0, 10, or 60 minutes (**Table 3.2**, entries 4 – 6), resulting in a significant yield increase to 65% (**Table 3.2**, entry 6), a ~3-fold improvement from the initial conditions. These newfound reaction conditions were standard for most of the total synthesis process: two equivalents of TFA added dropwise over one hour in DCM at 0 °C. Yields remained modest (55 – 65%), however, and it was not until a serendipitous change of solvent to diethyl ether when yields improved significantly to >85% (**Table 3.2**, entry 8). I chose to try ether as an alternative solvent simply because the previous reaction to form aldehyde **3.33** was unintentionally diluted with twice the amount of ether than usual and adding DCM would have necessitated a larger reaction vessel. Thusly, the optimized reaction conditions for the first step of this total synthesis were identified as requiring slow addition of TFA into a mixture of compound **3.33** and tryptamine **3.32** in ether at 0 °C, followed by gradual

warming to ambient temperature until full conversion of the tryptamine starting material was observed by TLC (**Scheme 3**).

### 3.3.2 Step 2: Oxidative aromatization of THBC 3.34.

While **Step 1** provided the THBC skeleton for  $\beta$ -carboline **A**, it was speculated that aromatization must be completed before the envisioned upcoming oxidative cleavage of the olefin, because the free secondary amine present in THBC **3.34** might provide problematic side products. The aromatization reaction for the formation of  $\beta$ -carboline **3.36** will be referred to as **Step 2** hereafter (**Figure 3.6**). Despite the extensive amount of oxidative or dehydrogenative conditions available and attempted for this aromatization reaction, the best obtainable yields for **Step 2** were found to be rather humbling. Therefore, the success of this reaction was measured not only based on reproducible yields but also for the ability to recover the THBC starting material, especially when the THBC emerged from expensive or difficult to obtain tryptamines.



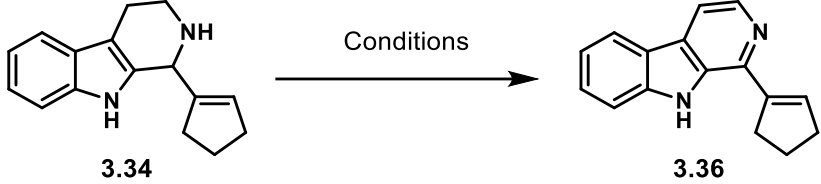
Dehydrogenative aromatization reactions of THBCs are generally mediated by stoichiometric oxidants such as sulfur,<sup>45</sup> potassium permanganate (KMnO<sub>4</sub>), manganese dioxide (MnO<sub>2</sub>), selenium dioxide (SeO<sub>2</sub>),<sup>46</sup> hydrogen peroxide (H<sub>2</sub>O<sub>2</sub>),<sup>47</sup> hypervalent iodine species such as iodosobenzene or iodoxybenzoic acid (IBX),<sup>16</sup> N-bromosuccinimide (NBS),<sup>49</sup> palladium on carbon (Pd/C),<sup>50</sup> or dichlorodicyanobenzoquinone (DDQ).<sup>51</sup> For this specific THBC substrate **3.34**, however, most of these oxidative conditions did not provide any product and the starting material remained unchanged in the reaction vessel. Even under elevated temperatures or after

several hours of reaction time (**Table 3.3**, entries 2 – 11) these traditional methods failed to produce product in isolable quantities. Notably, reactions with DDQ (**Table 3.3**, entries 12 – 15) or Pd/C (**Table 3.3**, entries 23 – 25) did provide aromatized product **3.36** at yields between 8 – 26%, although inconsistently and with unrecoverable starting material.

Precious metal or metal oxide catalysis are often energy- and resource-intensive. This prompted the development of alternative, metal-free methods to support sustainable chemistry<sup>52</sup> and gave rise to base-mediated dehydrogenative aromatization methods for the synthesis of heterocycles.<sup>53–55</sup> In this context, the study of organic base-promoted aromatization of THBCs into  $\beta$ -carbolines under air suggested a greener and more practical approach,<sup>56</sup> which inspired the use of 1,5-diazabicyclo[4.3.0]non-5-ene (DBN) and 1,8-diazabicyclo[5.4.0]undec-7-ene (DBU) in the aromatization trials for **Step 2**. Utilizing oxygen gas (O<sub>2</sub>) from the air as a clean oxidant is the ultimate goal of oxidation reactions, as it is readily available and environmentally friendly. Encouragingly, I found that DBN and DBU promoted the aromatization of THBC **3.34**, providing the desired product **3.36**, albeit in low yields ( $\leq 10\%$ ). Specifically, use of DBN in superstoichiometric amounts or as the solvent at high temperatures using air as the oxidant (**Table 3.3**, entry 16) proved to be reproducible. These DBN and DBU reactions (**Table 3.3**, entries 15, 16, and 19) were notable because the unreacted starting material remained intact and recoverable via column chromatography, which was especially helpful in maximizing the use of **3.34**. This was followed by the exploration of copper salt additives in attempts to increase reaction yield, as copper is a cost-effective transition metal with low toxicity that is compatible with air.<sup>57</sup> While adding CuCl<sub>2</sub> seemed to double the yield of the DBN and DBU reactions (**Table 3.3**, entries 17 and 21), it also rendered the unreacted starting material unrecoverable, presumably because of the ability

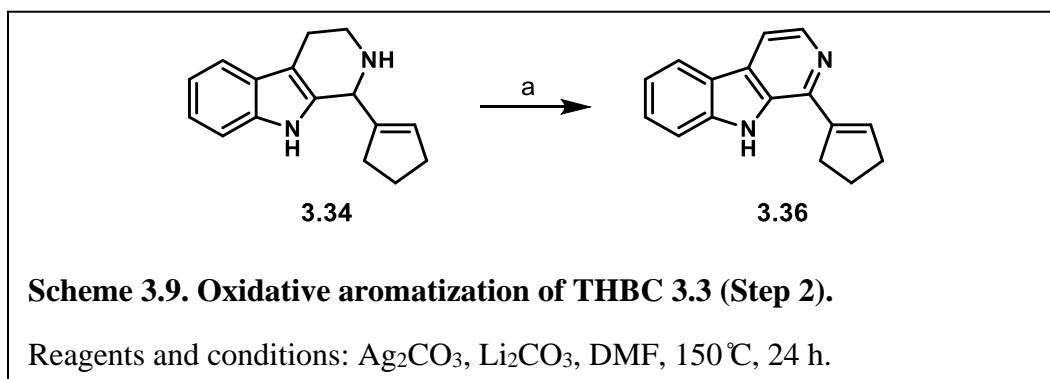
of nitrogen heterocycles to create aggregates with Cu<sup>2+</sup> ions.<sup>58</sup> Therefore, further investigation into other aromatization conditions was necessary.

**Table 3.3. Conditions screen and optimization table for oxidative aromatization of 3.34.**

							
Entry	Reagent(s)	Solvent	Temp (°C)	Time (h)	3.34 Consumed <sup>a</sup>	3.36 Formed <sup>a</sup>	Yield (%) <sup>b</sup>
1	-	MeOH	23	48	N	N	0
2	activated charcoal	neat	150	48	N	Y	ND
3	PhI(OAc) <sub>2</sub>	DMF	23	2	N	Y	ND
4	S	xylenes	120	12	N	N	0
5	I <sub>2</sub> , H <sub>2</sub> O <sub>2</sub>	DMSO	60	8	N	N	0
6	MnO <sub>2</sub>	p-xylene	150	12	N	N	0
7	IBX	DMSO	150	12	N	N	0
8	I <sub>2</sub>	DMSO	150	12	N	N	0
9	SeO <sub>2</sub>	dioxane	98	14	N	N	0
10	SeO <sub>2</sub>	p-xylene	150	12	N	N	0
11	NBS	toluene	23	12	N	N	ND
12	DDQ	DCM	23	12	Y	Y	20
13	DDQ, MS	DCM	23	48	Y	Y	19.5
14	DDQ, MnO <sub>2</sub>	MeCN	23	48	Y	Y	8.6
15	DDQ, mol. sieves	DCM	45	4	N	N	0
16	DBN	neat	110	48	N	Y	10
17	DBN	toluene	150	36	N	Y	9
18	DBN, CuCl <sub>2</sub>	toluene	120	48	N	Y	17
19	DBN, CuCl <sub>2</sub>	MeCN	23	24	N	Y	ND
20	DBU	neat	110	24	N	Y	5
21	DBU, CuCl <sub>2</sub>	MeCN	23	48	N	Y	19.5
22	DBU, CuCl <sub>2</sub>	MeCN	90	48	N	Y	1.6
23	Pd/C	neat	150	18	N	Y	26.5
24	Pd/C	xylenes	145	24	N	N	0
25	Pd/C	tol/BuOH	150	3	N	Y	12
26	Pd/C, Li <sub>2</sub> CO <sub>3</sub>	tol/BuOH	150	12	N	N	0
27	Ag <sub>2</sub> CO <sub>3</sub> , Li <sub>2</sub> CO <sub>3</sub>	DMF	155	48	Y	Y	30

ND = no data. <sup>a</sup> Qualitative result based on thin layer chromatography (TLC). <sup>b</sup> Isolated yield after column chromatography.

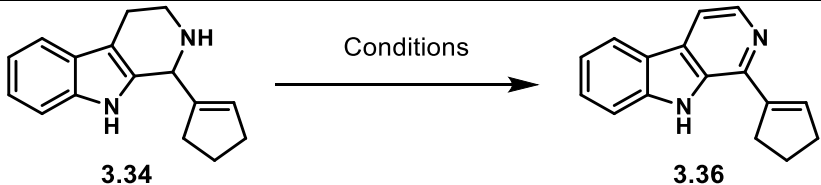
Interestingly, a recent communication in *Tetrahedron Letters* reported in the commentary that a researcher mistakenly selected silver carbonate ( $\text{Ag}_2\text{CO}_3$ ) instead of a traditional hydrogenation metal while running a reaction, and serendipitously discovered a silver-mediated oxidation THBCs into their aromatic counterparts.<sup>59</sup> This mistake was a fortunate one for me, because a mixture of  $\text{Ag}_2\text{CO}_3$  and lithium carbonate ( $\text{Li}_2\text{CO}_3$ ) in refluxing dimethylformamide (DMF) for 24 – 48 h provided the desired  $\beta$ -carboline **3.36** at a humble yet fortuitous 30% yield (**Table 3.3**, entry 26). This reaction still has its limitations, however, as 1) the silver reagent must be used in stoichiometric or super-stoichiometric amounts, 2) it requires harsh reaction temperatures of 150 – 175 °C, and 3) the reaction must be exceptionally anhydrous. As such, the aromatization step to form  $\beta$ -carboline **3.36** acts as a bottle-neck step due to low yields. Despite the less than optimal ecological and economic consequences, two equivalents of  $\text{Li}_2\text{CO}_3$ , one equivalent of  $\text{Ag}_2\text{CO}_3$  in degassed DMF and refluxing for 2 d became the standard reaction conditions for the aromatization of THBC **3.34** (**Scheme 3**).



With the disappointing yields and burdensome reaction times of this oxidative aromatization step, attempts to optimize this reaction continued. Microwave-assisted chemical reactions, has emerged as a valuable alternative in organic synthesis and are now well-established practices in the laboratory setting.<sup>60</sup> The microwave-mediated aromatization of THBCs had been previously reported, utilizing catalytic Pd/C in a 75:25 mixture of toluene and n-butanol.<sup>61</sup> This

method, however, failed to prove useful for this specific THBC substrate **3.34**, as no product formation was observed (**Table 3.4**, entry 1). Addition of acetic acid or  $\text{Li}_2\text{CO}_3$  also resulted in no reaction (**Table 3.4**, entries 2 – 3). The silver and lithium salt mixture from the earlier optimized conditions were also tried under microwave radiation (**Table 3.4**, entries 5 – 7). Notably, while the microwave-assisted reaction under the optimized conditions did provide some usable product **3.36** in only 8 h, as compared to the 24 h required for traditional heating, microwave methods failed to improve the yield. Furthermore, the specific microwave reactor available to me only operated with a maximum volume of 35 mL, limiting the scale of reaction possible. As such, the conditions in **Scheme 3**. remained the best option for **Step 2** in this total synthesis.

**Table 3.4. Aromatization reactions inside microwave reactor**

							
Entry	Reagent(s)	Solvent	Temp (°C)	Time (h)	3.34 Consumed <sup>a</sup>	3.36 Formed <sup>a</sup>	Yield (%) <sup>b</sup>
1	Pd/C	tol/BuOH	175	5	N	N	0
2	Pd/C, AcOH	p-xylene	150	12	N	N	0
3	Pd/C, $\text{Li}_2\text{CO}_3$	tol/BuOH	150	3.5	N	N	0
4	Pd/C, $\text{Li}_2\text{CO}_3$ , $\text{Ag}_2\text{CO}_3$	tol/BuOH	200	3.5	ND <sup>c</sup>	ND <sup>c</sup>	ND <sup>c</sup>
5	$\text{Ag}_2\text{CO}_3$ , $\text{Li}_2\text{CO}_3$	DMF	150	6	Y	Y	15
6	$\text{Ag}_2\text{CO}_3$ , $\text{Li}_2\text{CO}_3$	DMF	150	8	Y	Y	27.7
7	$\text{Ag}_2\text{CO}_3$ , $\text{Li}_2\text{CO}_3$	DMF	175	8	Y	Y	9.9

ND = no data.

<sup>a</sup> Qualitative result based on thin layer chromatography (TLC).

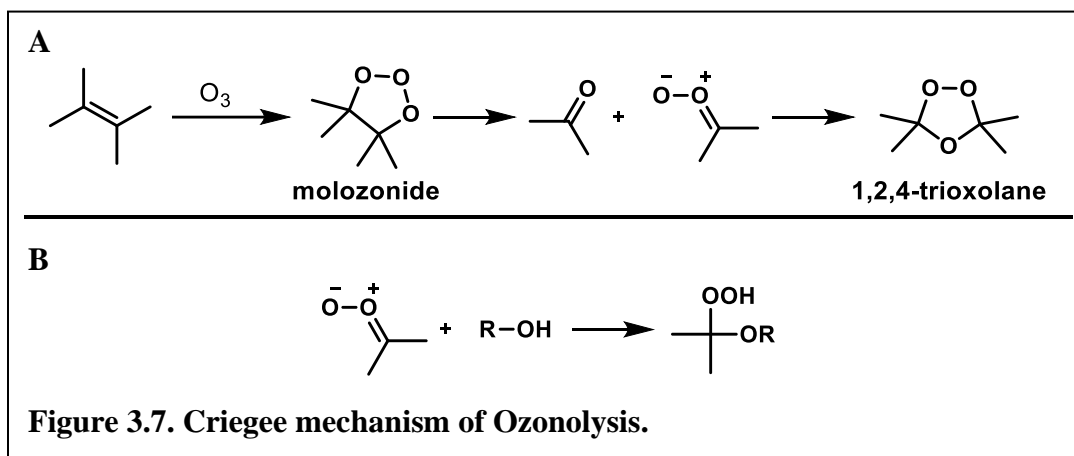
<sup>b</sup> Isolated yield after column chromatography.

<sup>c</sup> Reaction vessel broke inside microwave reactor, so data was un-obtainable.



### 3.3.3 Step 3: Oxidative cleavage to construct the linker region

The alkene present in the  $\beta$ -carboline intermediate **3.36** provides a functionalizable handle for the progression of this total synthesis. I had envisaged the cleaving of said olefin into a dicarbonyl compound where the aldehyde would be poised for a second Pictet-Spengler cyclization to form the second  $\beta$ -carboline heterocycle ( $\beta$ -carboline **B**). This oxidative cleavage step will hereby be referred to as **Step 3**.

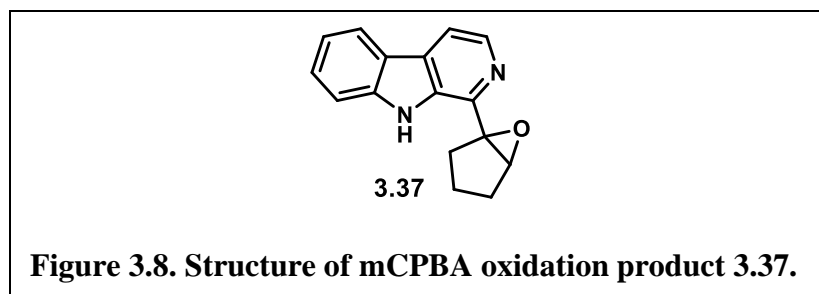


Cleavage of carbon-carbon double bonds to obtain dicarbonyl compounds (ketones and/or aldehydes) is a key reaction in synthetic organic chemistry<sup>62</sup> as it provides access to a wide but controllable range of products.<sup>63</sup> The mechanism of ozonolysis has been thoroughly studied, with the three-step Criegee mechanism being the most widely accepted.<sup>64</sup> Generally, ozone ( $\text{O}_3$ ) undergoes a 1,3-dipolar cycloaddition with the alkene, leading to the primary ozonide (molozonide), which decomposes to give a carbonyl compound and carbonyl oxide (**Figure 3.7A**).<sup>65</sup> This is a fascinating reaction in practice as it can be qualitatively monitored. Gaseous  $\text{O}_3$  is passed through a cold solution (usually  $-78 - 0^\circ\text{C}$ ) until a blue color is observed, indicating the consumption of the double bond and formation of the ozonide intermediates. The reaction is then halted when the ozone is forced to dissipate via sparging with nitrogen gas, followed by a reductive or oxidative workup, the choice of which typically determining product structure. In the presence

of alcohols, addition to the carbonyl oxide is possible affording geminal methoxyhydroperoxides (**Figure 3.7B**).

While ozone gas is a clean and effective choice that allows cleavage of the olefin under extremely mild conditions and efficient atom economy, several newer methodologies have been developed to avoid the risk of respiratory illness<sup>66</sup> due to acute and chronic ozone exposure. For example, the hypervalent iodine species iodosylbenzene in combination with fluoroboric acid (aqueous  $\text{HBF}_3$ ) in hexafluoroisopropanol (HFIP) were found to be a safer ozonolysis substitute, efficiently providing dicarbonyl compounds from alkenes.<sup>67</sup> This method is interesting because of its environmentally friendly nature and high selectivity. Alternatively, metal-based methods (potassium permanganate ( $\text{KMnO}_4$ ), ruthenium oxides, ceric ammonium nitrate (CAN), and chromium reagents), electrocatalytic anodic cleavage, singlet oxygen, and enzymatic methods are available for alkene cleavage.<sup>68</sup>

Perhaps the most effective ozone alternative, however, involves catalytic amounts of osmium tetroxide ( $\text{OsO}_4$ ). In this reaction, the combination of  $\text{OsO}_4$  dihydroxylation of an olefin and subsequent periodate (or other oxidant) cleavage of a 1,2-glycol mimics ozonolysis.<sup>69</sup> Namely, the Lemieux-Johnson oxidation<sup>70</sup> was an attractive method for this total synthesis for a few reasons. Firstly, catalytic amounts of the osmium reagent are sufficient because the periodate oxidizes osmium in its lower valence forms to the tetroxide, thus regenerating the hydroxylating agent.<sup>71</sup> Second, the catalytic nature of this reaction permits the use of relatively small amounts of the very expensive and poisonous osmium reagent. Finally, the periodate cleavage should cease at the aldehyde stage of the oxidation, providing the only the desired aldehyde intermediate **3** without further oxidation into the corresponding carboxylic acid.



Fortunately,  $\beta$ -carboline **3.36** was a suitable substrate for oxidative cleavage and **Step 3** proceeded without introducing any major problems. A simple condition screen of ozonolysis conditions including ozone gas ( $O_3$ ), meta-chloroperoxybenzoic acid (mCPBA), iodosobenzene diacetate, iodosylbenzene, and potassium permanganate ( $KMnO_4$ ) was performed (**Table 3.5**). Predictably,<sup>72</sup> mCPBA only afforded the epoxide product **3.37** (**Figure 3.8**), which has potential as a picrasidine building block and diversification point to explore in future studies.<sup>73</sup>

**Table 3.5. Screening conditions for oxidative cleavage Step 3.**

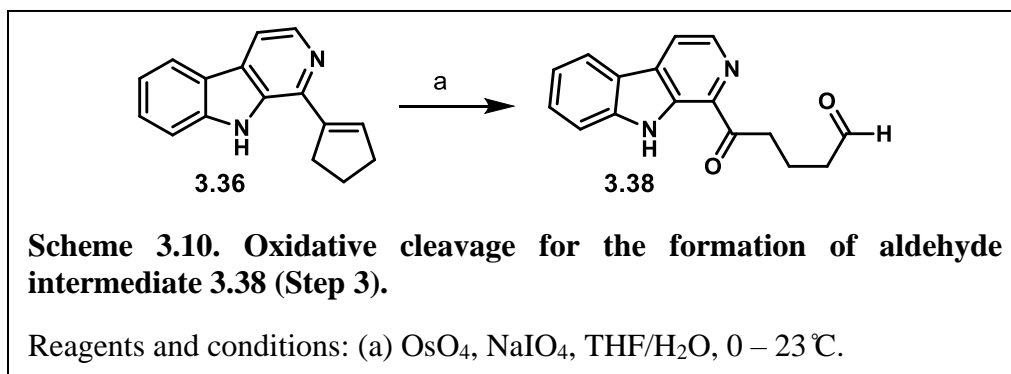
Entry	Reagent(s)	Solvent	Temp (°C)	Time (h)	Product	Yield (%) <sup>a</sup>
1	$O_3$	MeOH	0	1	NP	-
2	mCPBA	DCM	-78 – 23	1	3.37	12
3	$PhI(OAc)_2$	MeOH/ $H_2O$	0 – 23	25	NP	-
4	$KMnO_4$ , AcOH	DCM	23	21	NP	-
5	$PhIO$ , $HBF_4$	DCM/HFIP/ $H_2O$	23	4	NP	-
6	$OsO_4$ , NMO	THF/ $H_2O$	0 – 23	2	3.38	60
7	$OsO_4$ , $NaIO_4$	THF/ $H_2O$	0 – 23	3	3.38	85

NP = no product.

<sup>a</sup> Isolated yield after column chromatography.

After screening several oxidative cleavage conditions, only catalytic  $OsO_4$  in combination with either N-methylmorpholine-N-oxide (NMO) or sodium metaperiodate ( $NaIO_4$ ) additives provided product. I found that subjecting compound **3.36** to catalytic amounts (0.1 equivalents) of

OsO<sub>4</sub> and two equivalents of NMO in tetrahydrofuran (THF) and water (3:1) over an ice bath (0°C), afforded the key aldehyde intermediate **3.3** with a 60% yield. Eventually, replacing NMO with NaIO<sub>4</sub>, and allowing substrate exposure to the osmium catalyst for 1 h before adding the oxidant, provided a significant improvement in yield 85%. The optimized oxidative cleavage conditions for **Step 3** are shown in **Scheme 3**.

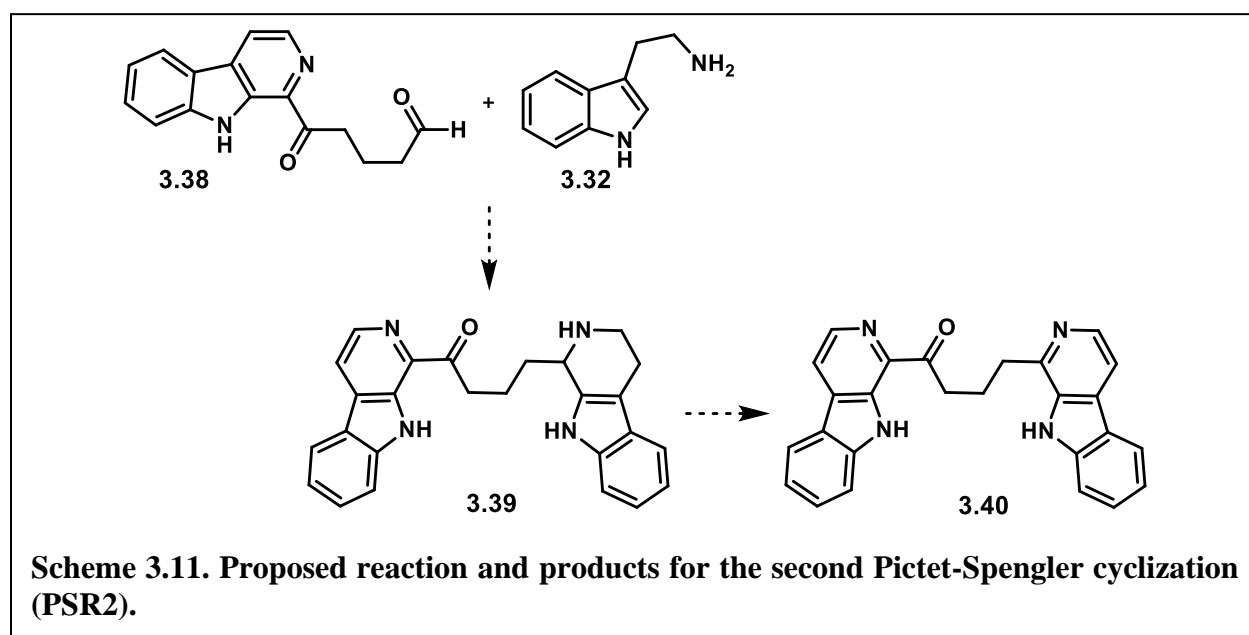


#### 3.3.4 Step 4: Generating the second $\beta$ -carboline system from key aldehyde intermediate **3.38** via Pictet-Spengler cyclization (PSR2).

After successfully optimizing the oxidative cleavage for **Step 3**, compound **3.38** was presumed to be an adequate substrate for a second PSR wherein the reactive aldehyde functional group would undergo acid-catalyzed imine formation with tryptamine **3.32** to assemble THBC **3.39**, thus conceptualizing **Step 4**, which is hereby denoted as **PSR2**. The original plan and hypothesized THBC-containing product **3.39** for **PSR2** is shown in **Scheme 3**. At this point, I believed that oxidative aromatization of **3.39** would provide compound **3.40**, comparable to **Step 2**, providing the scaffolding of picrasidine C.

To test this hypothesis, typical TFA catalysis conditions were first employed (**Table 3.6**, entry 1) on small scale (0.02 mmol). Initial results, qualitatively determined by TLC, showed the formation of inseparable products, in addition to an indeterminable nuclear magnetic resonance (NMR) spectroscopic analysis of the crude sample. Subsequently, conditions were screened in

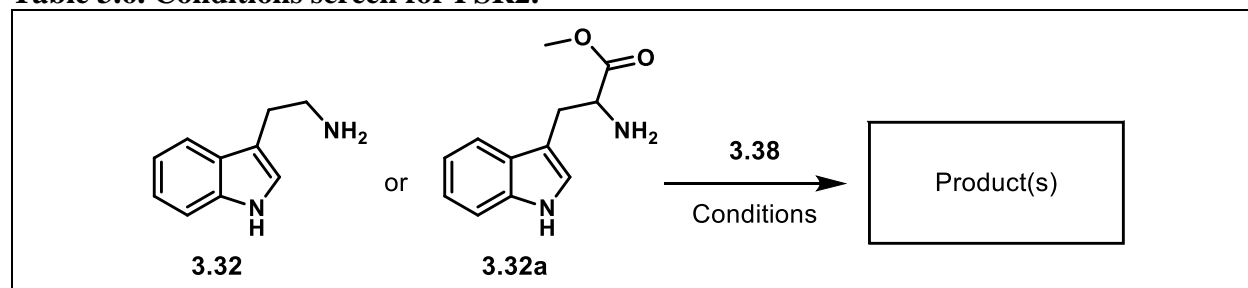
attempts to find the best method for the construction of compound **3.39**. Tryptamine **3.32** or tryptophan methyl ester **3.32a** was reacted with aldehyde **3.38** under acidic conditions (TFA or HCl) with various desiccant additives ( $\text{Na}_2\text{SO}_4$  or MS) and solvents (DCM or MeOH), starting at  $0^\circ\text{C}$  and warming to room temperature ( $23^\circ\text{C}$ ) while monitoring reaction progress by TLC (**Table 3.6**, entries 2 – 5). Notably, triethylamine ( $\text{Et}_3\text{N}$ ) was utilized, as previous evidence by Sharma et al. suggested a successful PSR under aprotic conditions.<sup>74</sup> For this specific substrate however, these conditions failed to provide the desired product (**Table 3.6**, entry 3).



From this initial screen, still conducted at a small scale (0.02 mmol), I found HCl in MeOH to provide the cleanest reaction mixture, from which a single product was visible by TLC (**Table 3.6**, entry 4). Upon initial scale-up (0.27 mmol), the HCl (2 M aqueous solution) in the presence of molecular sieves as a desiccant provided a modest 21% yield of a single product (**Table 3.6**, entry 6). Unable to fully characterize the structure of the product due to the low mass of the sample, I repeated the reaction in anhydrous conditions. Use of HCl gas in methanol provided a 74% yield

and enough product to conduct multiple 2D NMR analyses (see **Appendix II**), which revealed the product as compound **3.41** rather than the target compound **3.40**.

**Table 3.6. Conditions screen for PSR2.**



Entry	Amine	Reagent(s)	Solvent	Additive	Temp (°C)	Product	Yield (%) <sup>a</sup>
1	3.32	TFA	Et <sub>2</sub> O	-	23	CM <sup>b</sup>	-
2	3.32a	TFA	DCM	Na <sub>2</sub> SO <sub>4</sub>	0 – 23	CM <sup>b</sup>	-
3	3.32a	Et <sub>3</sub> N	DCM	Na <sub>2</sub> SO <sub>4</sub>	0 – 23	NR	-
4	3.32	HCl (aq.)	MeOH	-	0 – 23	One <sup>b</sup>	-
5	3.32a	HCl (aq.)	MeOH	-	0 – 23	CM <sup>b</sup>	-
6	3.32	HCl (aq.)	MeOH	MS	23	3.41	21
7	3.32	HCl <sup>c</sup>	MeOH	-	0 – 23	3.41	74

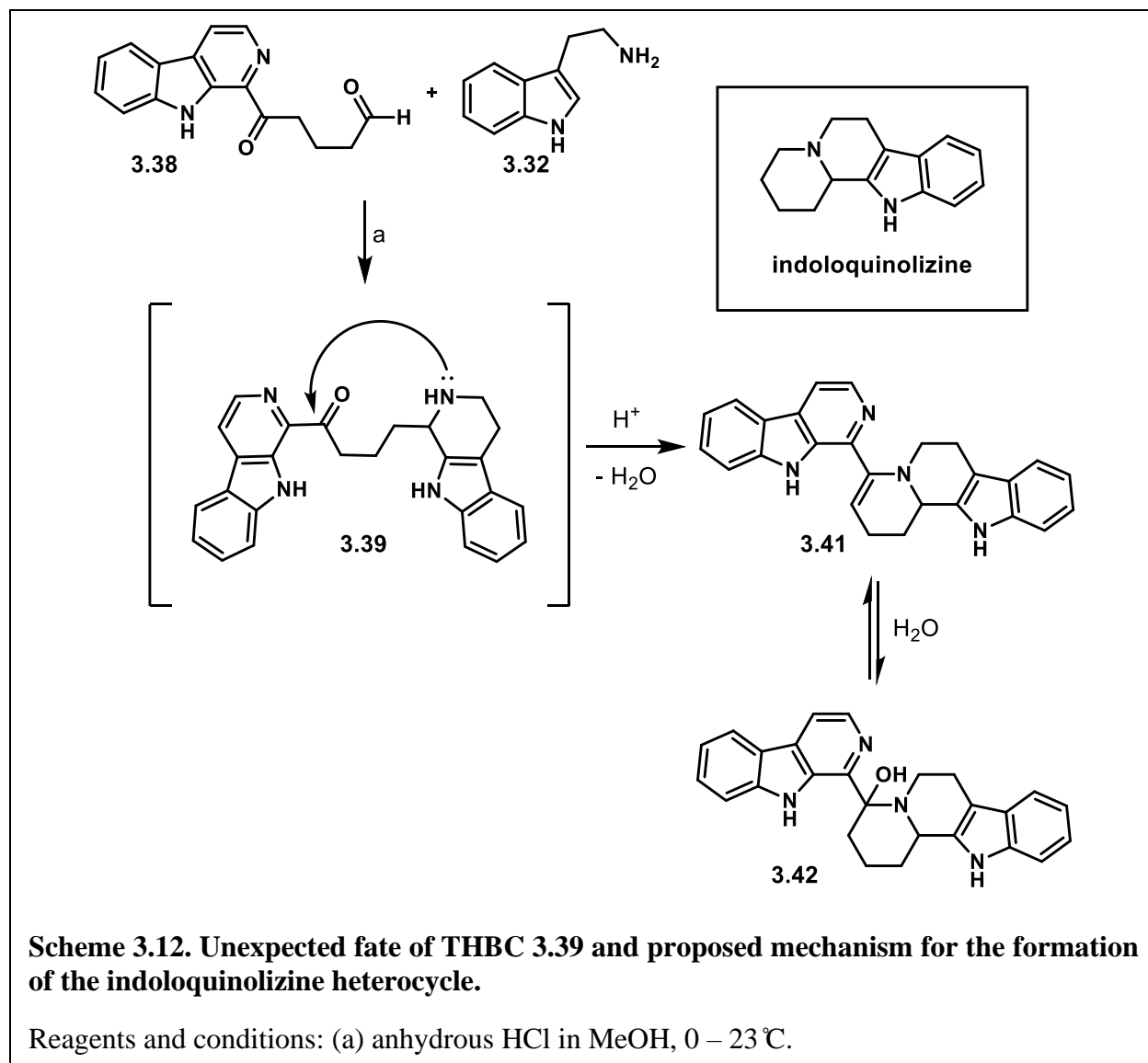
CM = complex mixture. NR = no reaction. One = one product formed. MS = molecular sieves.

<sup>a</sup> Isolated yield after column chromatography.

<sup>b</sup> Qualitative result based on TLC.

<sup>c</sup> Hydrochloric acid as anhydrous solution in methanol.

The formation of compound **3.41** is predicted to arise by the mechanism proposed in **Scheme 3**. Based on the accepted mechanism of the PSR,<sup>75</sup> this reaction is surmised to first form the desired THBC **3.39**. This product, however, contains a ketone that is likely protonated within the acidic solution and readily attacked by the secondary amine of the THBC to form the indoloquinolizine ring system (**Scheme 3**). This novel, metal-free acid-catalyzed Pictet-Spengler enamine cyclization cascade sequence serendipitously provides efficient access to indoloquinolizine heterocycles, a common building block in several natural products and pharmaceuticals (see **Section 3.5.2** for more details about indoloquinolizines).



### 3.3.5 Exploring the enamine reactivity of compound 3.41.

The elucidation of structure **3.41** was perhaps serendipitous, since the enamine functional group provides a reactive synthetic handle, thus prompting the investigation of enamine functionalization reactions. Specifically, oxidation, reduction, bromination, and hydrolysis reactions with compound **3.41** were investigated (**Table 3.7**). Bromination with NBS was unsuccessful, even with the presence of the radical initiator azobisisobutyronitrile (AIBN) (**Table 3.7**, entries 5 and 6). Sodium borohydride (NaBH<sub>4</sub>) was employed in attempts to reduce the

enamine double bond (**Table 3.7**, entry 8), but the resulting product mixture was too complex to pursue spectroscopic characterization. Stronger reducing agents such as lithium aluminum hydride (LAH)<sup>76</sup> might be necessary to reduce the fully conjugated double bond of the enamine. This reaction was not pursued, however, because **3.41** was more reactive under oxidation conditions and thus my focus shifted to the interrogation of oxidation chemistry.

**Table 3.7. Reaction screen for the functionalization of enamine compound 3.41.**

Entry	Reagent(s)	Solvent	Temp (°C)	Product	Yield (%) <sup>a</sup>
1	HCl (aq.)	MeOH	23	3.42	ND
2	Et <sub>3</sub> N	DCM	23	NR	-
3	NaOH (aq.)	MeOH	23	NR	-
4	mCPBA	DCM	0	3.43	7
5	NBS	DCM	23 – 40	NR	-
6	NBS, AIBN	DCM	23 – 40	NR	-
7	DDQ	DCM	23	3.44	37
8	NaBH <sub>4</sub> , AcOH	THF	0 – 23	CM	-

ND = no data. NR = no reaction, starting material unchanged. CM = Complex mixture.

<sup>a</sup> Isolated yield after column chromatography.

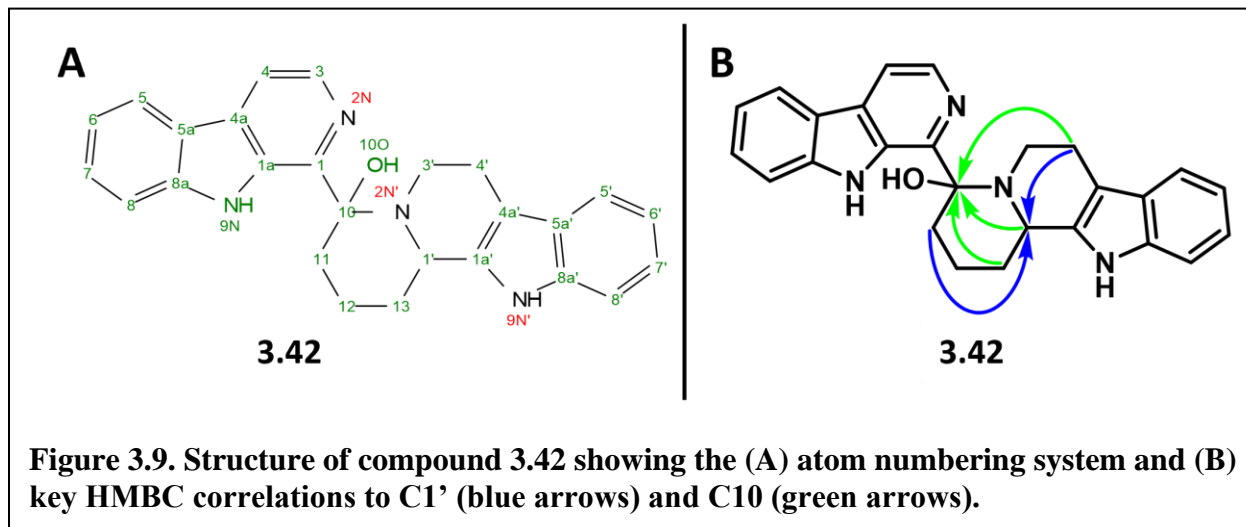
Treating **3.41** with aqueous sodium hydroxide in attempts at base-promoted hydrolysis was unsuccessful, (**Table 3.7**, entry 3). The organic base triethylamine under anhydrous conditions also resulted in no reaction (**Table 3.7**, entry 2). Enamine **3.41** also proved to be recalcitrant to acid-promoted hydrolysis (**Table 3.7**, entry 1), instead giving rise to the hydrate **3.42** (**Scheme 3**). No yield was calculated for the formation of **3.42** due to the inability to reproduce results on multiple occasions.



The emergence of **3.42** was puzzling at first, because I was under the impression that I was isolating **3.41** after a **PSR2** reaction, and TLCs of the resulting fractions showed only one compound spot, so I was expecting a pure NMR. During typical NMR analysis for compound **3.41**, I consider the proton peak for C1' as the diagnostic peak, which usually appears at about 4.58 ppm as a doublet (see

**Table 3.8).** This specific sample also produced a new triplet proton peak at about 6.02 ppm, and I found that the single TLC spot was actually two compounds with equal Rf values: **3.41** and an unknown. After producing a pure sample of this unknown, I ran a detailed NMR analysis including proton ( $^1\text{H}$ ) and carbon ( $^{13}\text{C}$ ) 1D NMR, COSY, HSQC, and HMBC experiments (see **Appendix II**). By HSQC, the  $^1\text{H}$  at 6.02 ppm is correlated to the  $^{13}\text{C}$  at 69.8 ppm which is assigned to C1'. In the HMBC spectrum, H1', H4', and H13 showed correlations to C10 ( $\delta_{\text{C}}$  84.2). In addition, H11 and H4' showed correlations to C1' ( $\delta_{\text{C}}$  69.8). These key HMBC correlations are shown in **Figure 3.9**. Upon deeper inspection of the spectra, I assigned the structure of the unknown compound to **3.42**, the hydrate of **3.41** (see spectral assignments in

Table 3.8).



The formation of **3.42** is generally unpredictable, as **PSR2** produces mixtures **3.41** and **3.42** in varying quantities of each depending on the batch. I believe that if the HCl/MeOH solution used in **PSR2** is not completely anhydrous, then the formation of **3.42** becomes more prevalent. Compound **3.42** also seems to form after column purification if the silica is not deactivated by a base such as triethylamine. These two compounds more than likely participate in a dynamic equilibrium, especially when water is present. Notably, the mass for both compounds **3.41** and **3.42** will appear after high-resolution mass spectrometry (HRMS) analysis, even if the sample shows pure compound **3.41** by NMR. Compounds **3.41** and **3.42** are inseparable by HPLC, presumably because of their dynamic equilibrium, which may occur in the acidic, aqueous eluent (0.1% TFA in water/acetonitrile). Eventually, I found that the change in chemical shift of C10 provides a diagnostic to distinguish between compound **3.41** and its hydrate **3.42** (red text in

**Table 3.8**), which is easily visible on the HMBC spectra.

Fortunately, enamine functionalization was found possible under oxidizing conditions with mCPBA, giving epoxide product **3.43** (structure shown in **Figure 3.10**), albeit at a poor 7% yield (**Table 3.7**, entry 4). Reactions employing DDQ (**Table 3.7**, entry 7) were also investigated, as these oxidizing conditions consistently gave a single, easily isolatable product. The extensive spectroscopic characterization experiments of the DDQ reaction major product (**3.44**) will be discussed in section **3.3.6**.

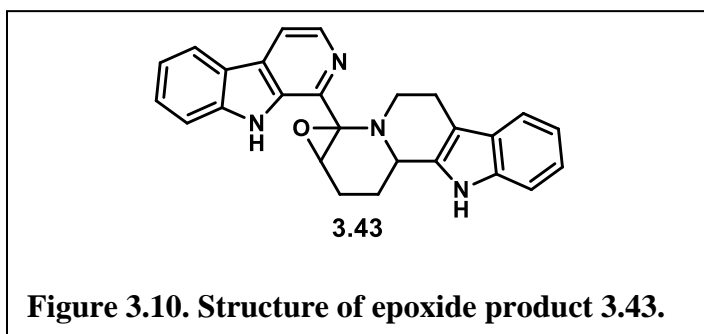
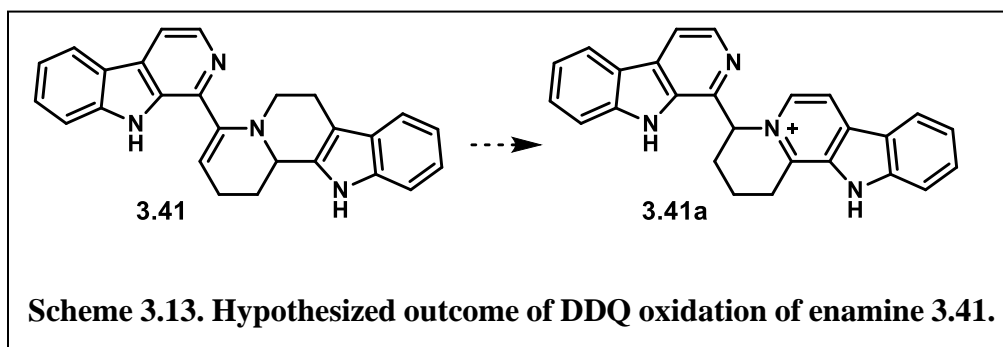


**Table 3.8. NMR assignments for compounds 3.41 and 3.42 (d<sub>6</sub>-DMSO)**

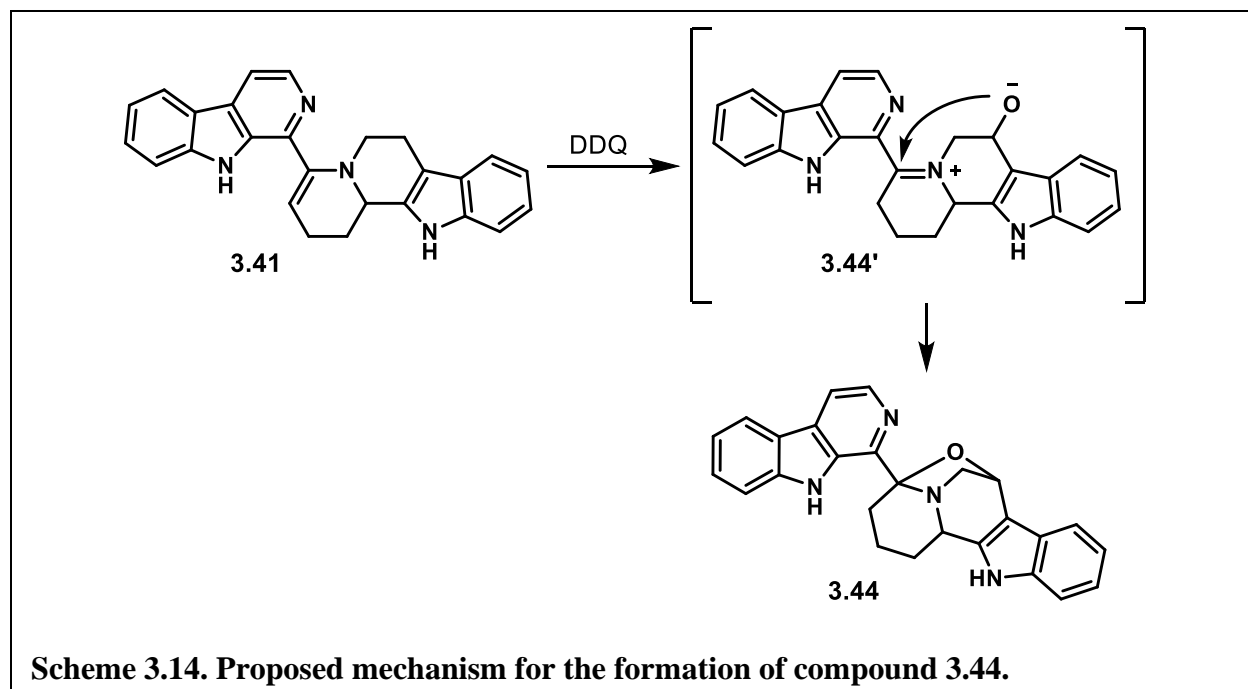
		Enamine 3.41		Enamine-OH 3.42	
Segment	Position	$\delta$ C (ppm), type	$\delta$ H (ppm)	$\delta$ C (ppm), type	$\delta$ H (ppm)
$\beta$ -carboline A	1	132.8, C	-	133.6, C	-
	1a	145.4, C	-	144.3, C	-
	3	137.7, CH	8.32 (d)	137.9, CH	8.28 (d)
	4	121.3, CH	8.21 (d)	114.1, CH	7.94 (d)
	4a	140.4, C	-	139.3, C	-
	5	113.7, CH	8.05 (d)	122.5, CH	8.22 (d)
	5a	141.1, C	-	141.7, C	-
	6	117.4, CH	7.37 (t)	119.7, CH	7.26 (m)
	7	127.7, CH	7.49 (ddd)	128.3, CH	7.58 (m)
	8	112.5, CH	7.67 (d)	110.0, CH	7.70 (d)
	8a	128.1, C	-	121.0, C	-
	9N	-	10.99 (s)	-	10.64 (s)
$\beta$ -carboline B	1'	53.5, CH	4.58 (d)	69.8, CH	6.02 (t)
	1a'	136.1, C	-	136.1, C	-
	3'	45.3, CH <sub>2</sub>	2.93 (m), 2.99 (m)	25.2, CH <sub>2</sub>	2.87 (m), 2.97 (m)
	4'	21.4, CH <sub>2</sub>	2.71 (m), 2.53 (m)	46.6, CH <sub>2</sub>	1.85 (m), 3.21 (m)
	4a'	118.3, C	-	112.4, C	-
	5'	119.2, CH	7.22 (t)	122.2, CH	6.99 (m)
	5a'	135.8, C	-	111.2, C	-
	6'	111.0, CH	7.35 (t)	118.2, CH	7.31 (d)
	7'	118.1, CH	6.96 (t)	117.7, C	6.78 (t)
	8'	120.5, CH	7.05 (m)	120.7, CH	6.95 (m)
	8a'	126.6, C	-	127.0, C	-
	9N'	-	10.99 (s)	-	10.64 (s)
Linker	10	107.3, C	-	84.2, C	-
	11	110.3, CH	5.61 (m)	39.1, CH <sub>2</sub>	1.88 (m), 2.08 (m)
	12	22.9, CH <sub>2</sub>	2.32 (m), 2.42 (m)	18.5, CH <sub>2</sub>	0.69 (m), 1.59 (d)
	13	24.4, CH <sub>2</sub>	1.97 (m), 2.28 (m)	30.5, CH <sub>2</sub>	1.97 (d), 2.13 (m)

### 3.3.6 Discovery and structural characterization of compound 3.44.

An attempt was made to oxidize **3.41** into its aromatic congener **3.41a** (Scheme 3.), which contains the carbon and nitrogen scaffold of *Picrasma* alkaloids **3.7** – **3.12**. Since DDQ exhibited some success in the oxidative aromatization in **Step 2** (see section 3.3.2), and is known to assist in aromatization reactions of nitrogen heterocycles,<sup>51,77,78</sup> I expected DDQ to aromatize  $\beta$ -carboline **B** in **3.41** to provide the charged species **3.41a**.



The reaction of **3.41** with DDQ in DCM at 23 °C for 12 h provides a single product that is easily purified with silica gel chromatography. These results were encouraging at first, because of the straightforward purification and when analyzing this product by HRMS, the mass ES+  $m/z$  389.176 (calculated for  $C_{26}H_{21}N_4^+$  is 389.18) was found. The mass ES+  $m/z$  407.187 was also found, however, which was originally thought to evidence for the presence of a **3.41a**-hydrate. Upon NMR analysis, however, it was clear that the sample contained a mixture of diastereomers, while **3.41a** should only have been a racemic mixture, and the structure of **3.41a** was not confirmed by the NMR spectra. This prompted an extensive literature review of DDQ reactions and some mechanistic brainstorming.



Benzylic C-H bond oxidations are known to occur with DDQ reactions,<sup>79</sup> and DDQ is known to oxidize the THBC 4-position to form 4-oxo-THBC.<sup>31</sup> There is also evidence of the ability of DDQ to promote oxidative cyclizations.<sup>78</sup> Thus, the mechanism for the formation of **3.44** is proposed in **Scheme 3.14**. Briefly, oxidation of the indoloquinolizine at the pseudo-benzylic position in addition to enamine tautomerization to the iminium ion **3.44'** would allow for cyclization and the formation of a fused 5-membered ring. At first glance, the structure of **3.44** appears sterically strained and unstable due to the hemiaminal that is formed. However, the (6-6-5)-fused heterocyclic octahydro-2*H*-3,6-epoxyquinolizine skeleton is found in the iboga class of natural products<sup>80</sup> which contradicts its unstable appearance. The existence of **3.44** is also corroborated with the aforementioned HRMS data. This, along with the thorough NMR analysis provided below, is evidence of the formation of compound **3.44**.

The structure of **3.44** was confirmed by <sup>1</sup>H and <sup>13</sup>C 1D NMR, HSQC, HMBC, HSQC-TOCSY, and TOCSY 2D NMR, and HRMS. Key COSY, HSQC, and TOCSY correlations are shown in **Figure 3.11**. Focusing on the aliphatic region where the chemistry most likely occurred,

the linker carbons ( $\delta_C$  34.4, C11; 18.1, C12; 30.7, C13) and their corresponding protons were identified with COSY correlations indicating their connectivity. COSY correlations also showed a single proton ( $\delta_H$  5.07, H4') connected to two diastereotopic protons ( $\delta_H$  2.77 and 3.28, H3'). TOCSY and HSQC-TOCSY showed C4' and C3' in an isolated spin system. Additionally, C10 ( $\delta_C$  90.9) showed correlations to H1' and H3' in the HMBC spectrum. The carbon shift of 90.9 ppm, too low for  $sp^2$  carbons and too high for a typical oxygen-bonded carbon, suggested more complexity to C10. This spectroscopic data along with the mechanistic rationale above, arrived at the structure of compound **3.44**. Two diastereomers of **3.44** were found by NMR in 3:2 ratio, but absolute stereochemistry is unknown. The final NMR assignments are shown in



Table 3.9.

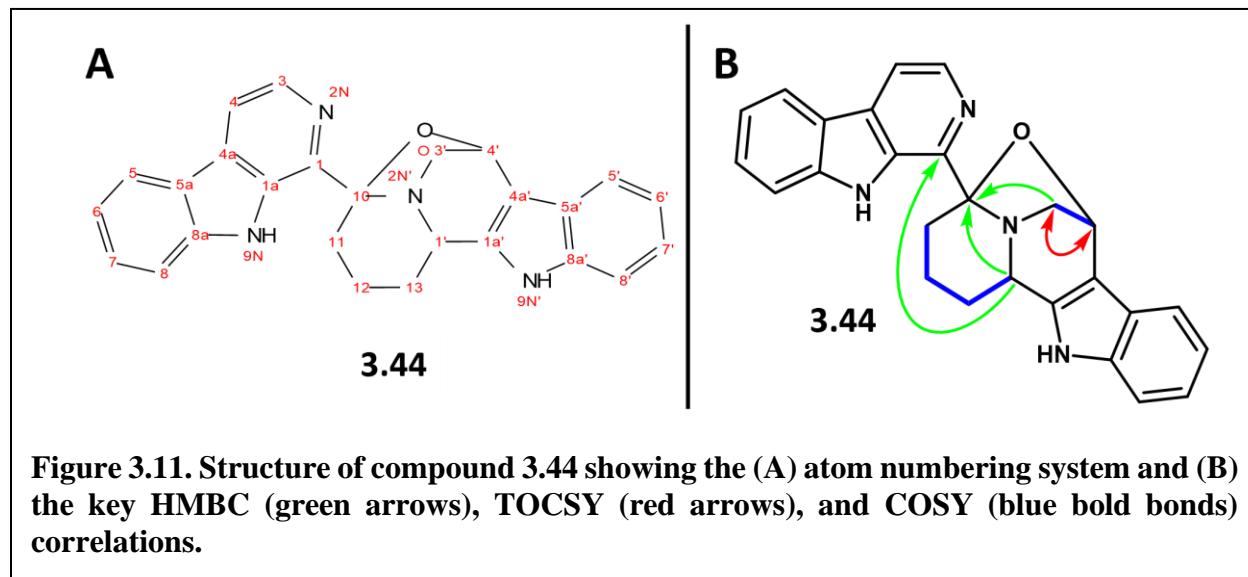
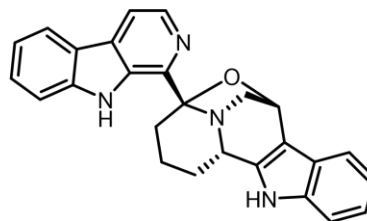
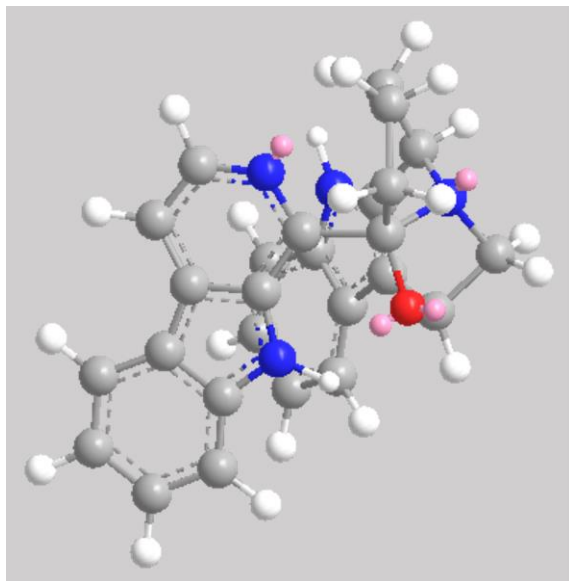


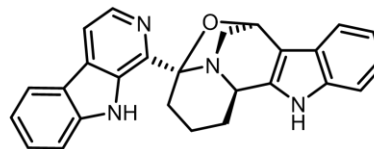
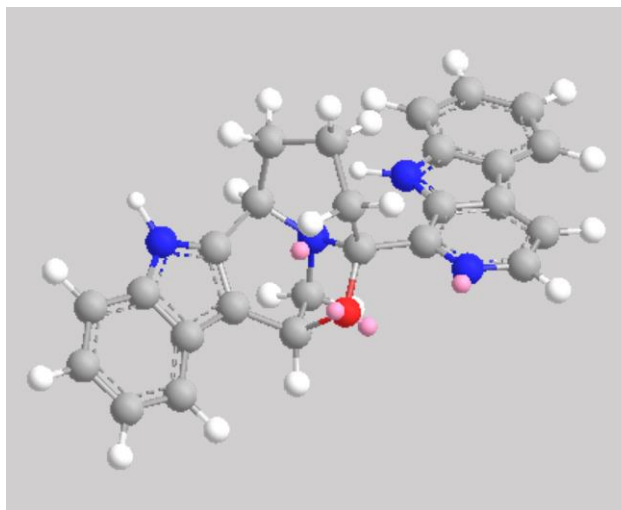
**Table 3.9. NMR assignments for compound 3.44 (d6-DMSO).**

Segment	Position	$\delta C$ (ppm), type	$\delta H$ (ppm)
$\beta$ -carboline A	1	134.0, C	-
	1a	142.8, C	-
	3	139.0, CH	8.39 (d)
	4	114.5, CH	8.03 (d)
	5	124.2, CH	7.33 (d)
	6	121.4, CH	7.12 (ddd)
	7	118.8, CH	7.05 (m)
	8	114.3, CH	7.99 (m)
	9N	-	10.97 (s)
$\beta$ -carboline B	1'	66.7, CH	6.19 (q)
	3'	51.1, CH <sub>2</sub>	2.77 (t), 3.28 (dd)
	4'	71.1, CH	5.07 (dd)
	5'	110.2, CH	7.73 (dd)
	6'	128.0, CH	7.61 (m)
	7'	119.4, CH	7.29 (m)
	8'	122.7, CH	8.27 (dd)
	9N'	-	10.85 (s)
Linker Region	10	90.9, C	-
	11	34.4, CH <sub>2</sub>	2.12 (m)
	12	18.1, CH <sub>2</sub>	0.69 (m), 1.73 (t)
	13	30.7, CH <sub>2</sub>	1.96 (m), 2.24 (m)

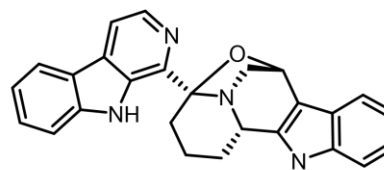
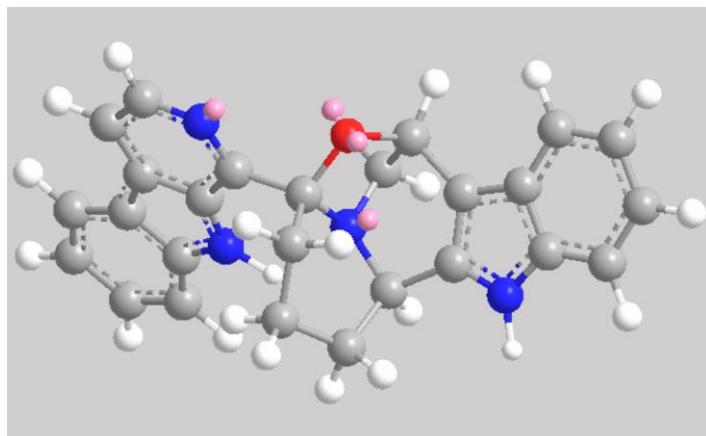
Interestingly, this DDQ reaction resulted in a tandem oxidation-cyclization for the formation of a complex pentacyclic system while generating two new stereogenic centers. Some qualitative structural analysis using Spartan was completed to visualize the 3D structure of **3.44**. Its three chiral centers provide six possible diastereomers, three of which are shown in **Figure 3.12** at their lowest energy states as calculated by the Spartan program.



**3.44a**



**3.44b**



**3.44c**

**Figure 3.12. Structures and 3D models for three diastereomers of compound 3.44.**

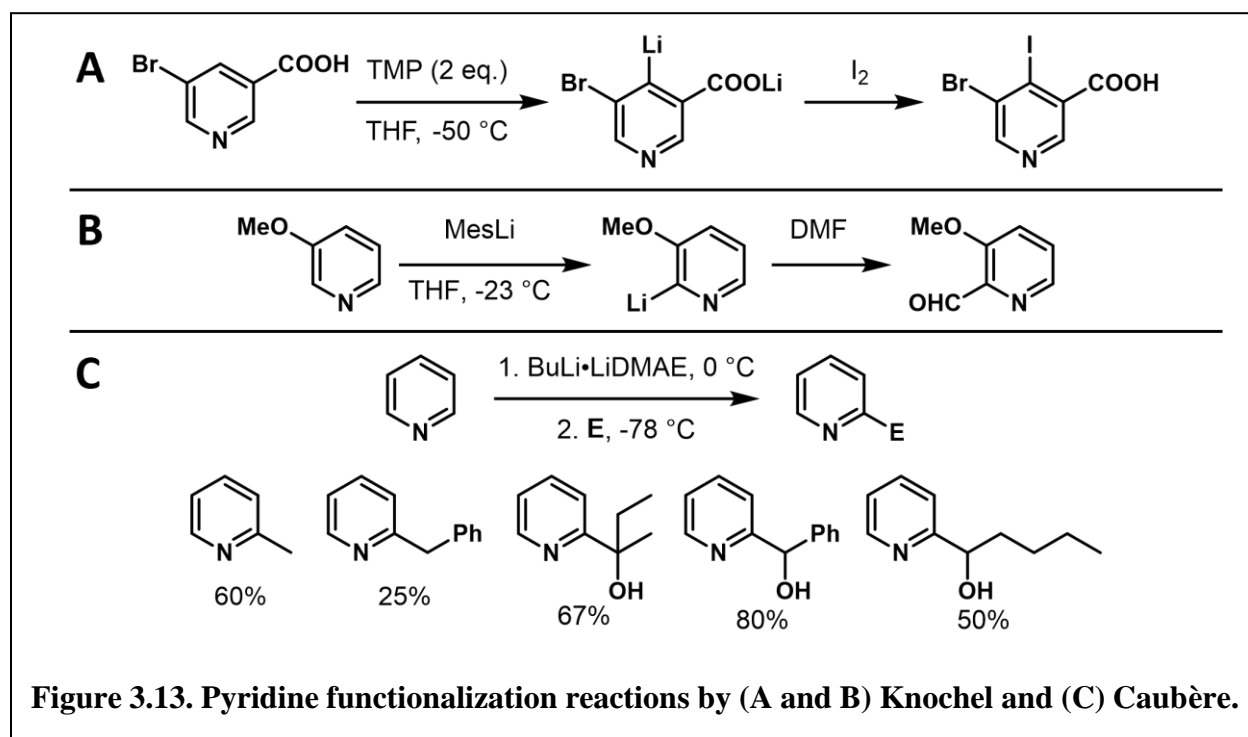
### 3.4 Results and discussion for Approach 2

During the investigation of the reactivity of **3.41**, the direct functionalization of the  $\beta$ -carboline 1-position was explored via C-H metalation followed by electrophilic trapping (**Approach 2**). The directed metalation of aromatic substrates is an increasingly important strategy for the synthesis of natural products and new drug entities. A notable example is the ortho metalation of thiophene, furan, pyrrole, and pyridine rings with tetramethylethylenediamine (TMEDA) or *sec*-butyllithium allows for the installation of nitrile, halo, and methoxy groups.<sup>81</sup> While successful pyridine lithiation for electrophilic aromatic substitution reactions have previously been reported,<sup>82</sup> the analogous quinoline metalation was found to be much more laborious, presumably due to the less reactive lithium-pyridine species.<sup>40</sup> To the best of my knowledge, there is no existing methodology for creating a carbon nucleophile on any position of the  $\beta$ -carboline ring. Preliminary work towards selective lithiation of C1 on the  $\beta$ -carboline is described in this section.

#### 3.4.1 A preliminary study on $\beta$ -carboline functionalization, with inspiration from pyridine chemistry.

Complex methodologies for the synthesis of pyridines have been extensively studied, particularly directed metalations for regioselective substitutions. For example, lithium 2,2,6,6-tetramethylpiperidide (TMP) is a powerful base, especially for the deprotonation of pyridine such as for the iodation reaction in **Figure 3.13A**.<sup>83</sup> Sterically hindered aryl-lithium reagents such as mesityl-lithium (MesLi) can provide 2-lithiated pyridines irreversibly (**Figure 3.13B**),<sup>84</sup> while lithium amides such as lithium diisopropylamide (LDA) can be expected to perform reversible lithiation reactions on electron-rich pyridines like 3-methoxypyridine (**Figure 3.13B**).<sup>82</sup> Further, the use of mixed aggregates of *n*-butyllithium (*n*-BuLi) with aminoalkoxides such as lithium 2-

dimethylaminoethanolate (LiDMAE) has also been shown to perform highly regioselective lithiations on pyridine substrates (**Figure 3.13C**).<sup>40</sup>



These examples, along with inspiration from a review on regioselective functionalizations of pyridines by the Knochel group,<sup>82,85,86</sup> the lithiation of  $\beta$ -carboline was hypothesized to occur under similar conditions. It was predicted that an excess of basic, sterically hindered organolithium reagents could allow for  $\beta$ -carboline lithiation with possible regioselectivity on the 1-position. To explore this idea, an attempt at forming  $\beta$ -carboline nucleophiles from **D1** – **D3** for electrophilic trapping by methyl ethyl ketone (**3.45**) was attempted (**Table 3.10**).

Tried first were the lithium bases *n*-BuLi, LDA, lithium hexamethyldisilazide (LiHMDS), or the complex base LiDMAE with  $\beta$ -carboline **D1** (no N-protecting group), all resulting in no reaction with **3.28** as the electrophile (**Table 3.10**, entries 2, 4, 6, and 7). Afterwards, boron trifluoride etherate (BF<sub>3</sub>OEt<sub>2</sub>) was tried as an additive, assuming the boron would coordinate with the sp<sup>2</sup> nitrogen to change the reactivity of the C1-H bond. The reaction of **D1** with LiHMDS and

BF<sub>3</sub>OEt<sub>2</sub> produced a trace product that I was unable to characterize (**Table 3.10**, entry 3). N-protected β-carbolines **D2** (*tert*-butyloxycarbonyl, boc) and **D3** (tosyl) also resulted in no reaction (**Table 3.10**, entries 8 – 10). Interestingly, the reaction of **D1** with *n*-BuLi and BF<sub>3</sub>OEt<sub>2</sub> produced product **3.47** (structure shown in **Figure 3.15**), where the tetrahydrofuran (THF) solvent was incorporated onto the β-carboline C1 (**Table 3.10**, entry 5). This reaction will be discussed in more detail in section 3.4.2. Compound **3.46** was never formed.

**Table 3.10. β-carboline substitution reaction conditions screen.**

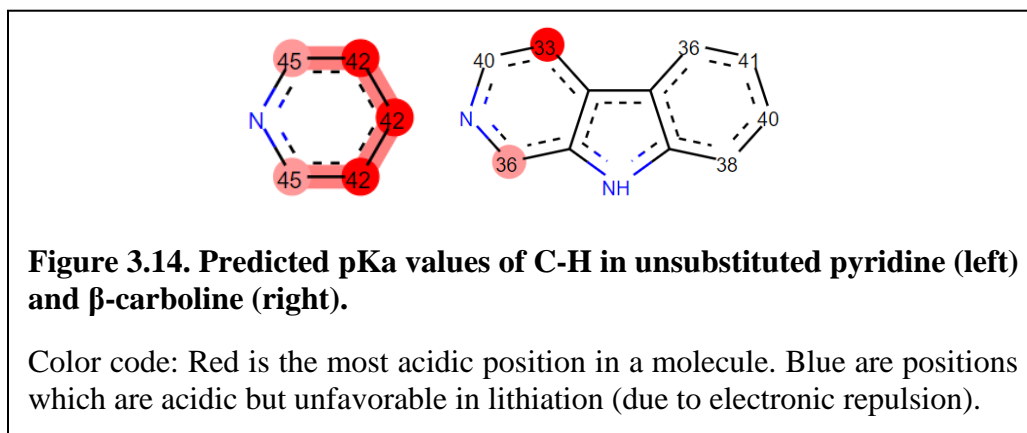
Entry	D	Protecting Group (R)	Base	Additive	Product
1	D1	H	LDA	BF <sub>3</sub> OEt <sub>2</sub>	No Reaction
2	D1	H	LDA	-	No Reaction
3	D1	H	LiHMDS	BF <sub>3</sub> OEt <sub>2</sub>	Unknown <sup>a</sup>
4	D1	H	LiHMDS	-	No Reaction
5	D1	H	<i>n</i> BuLi	BF <sub>3</sub> OEt <sub>2</sub>	3.47 (14%)
6	D1	H	<i>n</i> BuLi	-	No Reaction
7	D1	H	LiDMAE	-	No Reaction
8	D2	Boc	LDA	BF <sub>3</sub> OEt <sub>2</sub>	No Reaction
9	D2	Boc	LiHMDS	BF <sub>3</sub> OEt <sub>2</sub>	No Reaction
10	D3	Tos	LiDMAE	-	No Reaction

PG = protecting group.

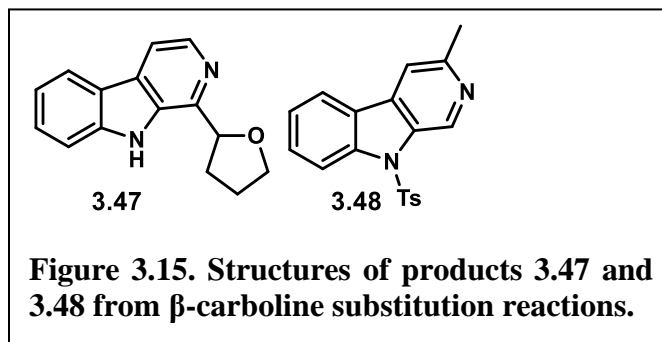
<sup>a</sup> One complex uncharacterizable product was isolated in trace amounts.

Overall, my initial attempts at β-carboline lithiation showed me that the reaction is more complex than a basic deprotonation mechanism. I tried to gain insight into potential issues with this methodology by looking into pKa prediction models by Grzybowski with THF as the solvent.<sup>87</sup> The C4-H and C1-H are the most acidic protons on the β-carboline ring, but they may not be acidic enough to be deprotonated by organolithium bases (**Figure 3.14**). Evidence of lithiation on

pyridine by the superbases LiDMAE,<sup>88</sup> however, may suggest otherwise, because the Grzybowski model predicts the acidity of pyridine C1-H to be approximately 10 pKa units over the  $\beta$ -carboline 1-position (**Figure 3.14**). As such, a general pKa analysis does not explain the outcomes of my lithiation reactions.

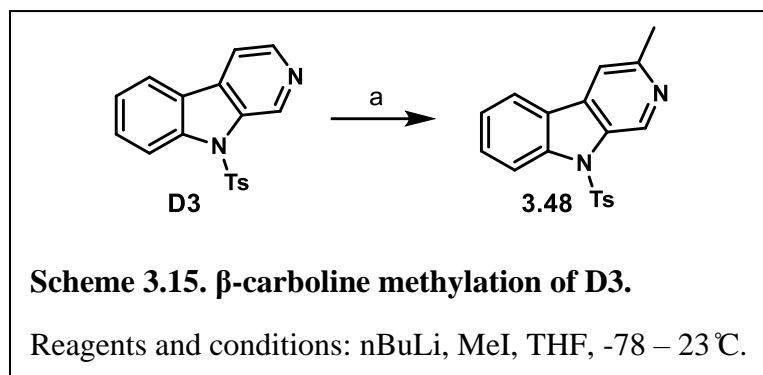


### 3.4.2 Discussion on the products of $\beta$ -carboline substitution reactions.



One  $\beta$ -carboline substitution reaction from **Table 3.10** did provide the new product **3.47**, albeit in a poor 14% yield.  $\beta$ -carboline without a protecting group (**D1**) was dissolved in THF at 0 °C under anhydrous conditions, followed by the addition of  $\text{BF}_3\text{OEt}_2$ . After stirring for about thirty minutes at 0 °C,  $n\text{-BuLi}$  was added and the reaction stirred for another thirty minutes, to allow for deprotonation/lithiation. Electrophile **3.45** was then added dropwise. This reaction seemed promising at first, because a single product appeared by TLC during the reaction. However,

structural characterization by NMR surprisingly found the product to be 1-(tetrahydrofuran-2-yl)-9*H*-pyrido[3,4-*b*]indole (**3.47**). Ethers such as THF have been known to undergo lithiation with *n*-BuLi in a temperature-dependent manner.<sup>89</sup> As such, reducing the temperature to avoid the formation of THF-Li is worth interrogating in future studies. Despite the unwanted side product of this *n*-BuLi reaction, it did provide some useful insight for  $\beta$ -carboline lithiation reactivity. Since THF-Li is expected to be nucleophilic, this suggests that the boron is indeed coordinating with the  $sp^2$  nitrogen, pulling electron density towards the nitrogen atom, and thus forming a relatively electrophilic C1.



After finding that electrophilic trapping by carbonyl substrate **3.45** was largely unsuccessful, I decided to try the stronger electrophile, iodomethane (**Scheme 3.15**) to test if a  $\beta$ -carboline nucleophile was actually being formed, and to generally explore its reactivity. To a solution of *N*-tosyl- $\beta$ -carboline **D3** in THF under anhydrous conditions, *n*-BuLi was added dropwise at -78 °C. Iodomethane was added to the solution before the reaction was allowed to warm to room temperature (23 °C). After workup, purification, and NMR analysis, I found that the tosyl-protected  $\beta$ -carboline was methylated at the C3-position. Despite the undesired regioselectivity, this reaction demonstrated the ability to form a nucleophilic carbon on a  $\beta$ -carboline.



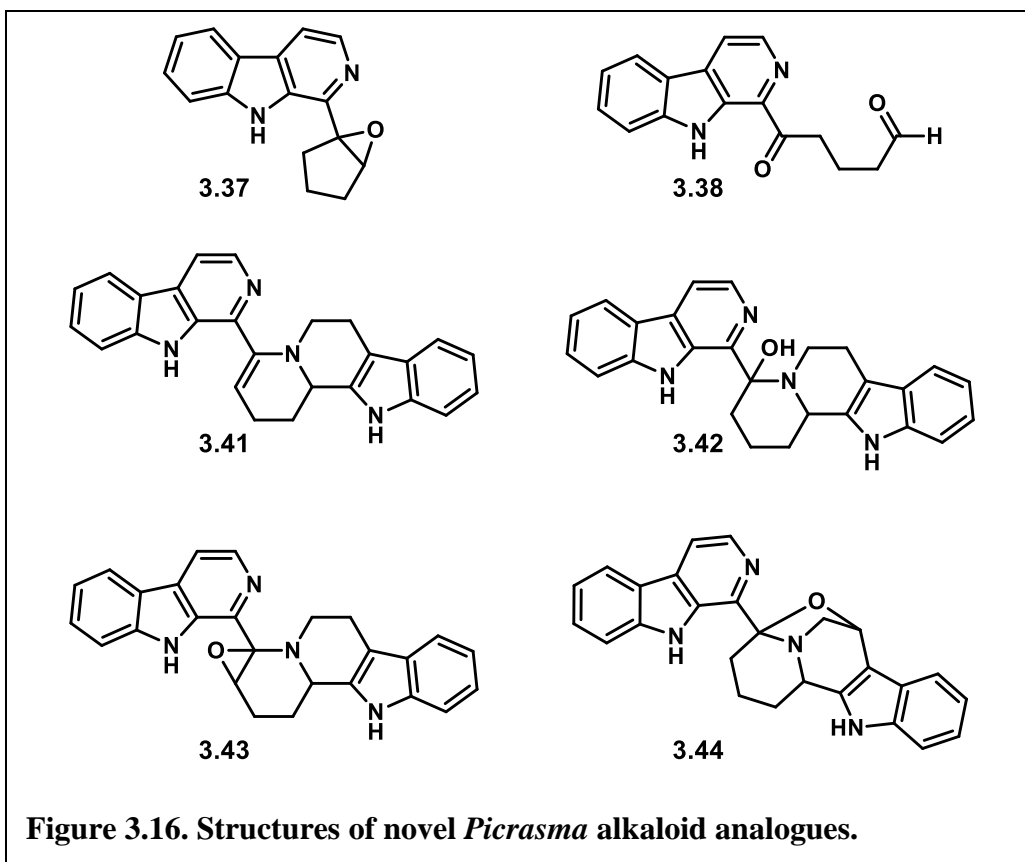
### 3.5 Conclusions and future directions

Towards synthesizing the target molecule, picrasidine C (**3.1**), two distinct approaches were pursued: (1) sequential Pictet-Spengler cyclizations for the construction of each  $\beta$ -carboline heterocycle individually, and (2) direct functionalization of  $\beta$ -carboline via C-H lithiation. Although the initial goal of completing the total synthesis of picrasidine C has yet to be accomplished, interesting synthetic discoveries were made that set the stage for the pursuit of more members of this natural product family.

#### 3.5.1 Six new *Picrasma* alkaloid analogues were synthesized.

The carbon-nitrogen bis- $\beta$ -carboline skeleton of *Picrasma* alkaloids **3.7** – **3.14** was successfully constructed, via the iterative PSR **Approach 1**, laying a foundation for the total synthesis of picrasidine C to be completed in the future. Notably, four new bis- $\beta$ -carbolines (**3.41** – **3.44**) were synthesized along with two new mono- $\beta$ -carbolines (**3.37** – **3.38**), each are novel *Picrasma* alkaloid analogues that await biological activity studies (**Figure 3.16**). These new *Picrasma* analogs also hold synthetic potential, due to the presence of reactive functional groups that provide synthetic handles for structural diversification.

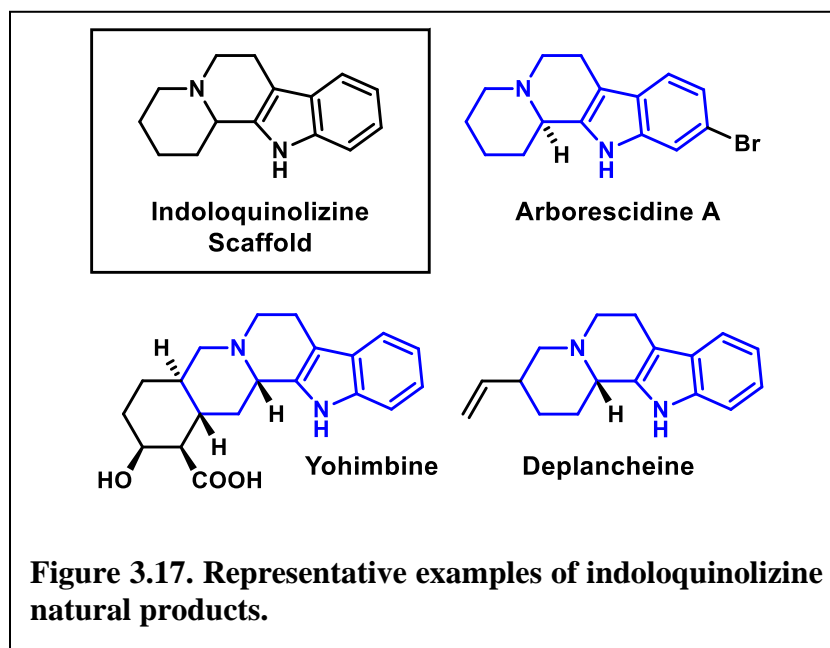
The structural diversity of these newly discovered  $\beta$ -carboline compounds makes them attractive for future biological evaluations. The presence of reactive functional groups such as epoxides **3.37** and **3.43**, aldehyde **3.38**, and enamine **3.41** provides for synthetic handles to either advance this synthetic endeavor or continue to create new *Picrasma* alkaloid analogues. While the oxidation, reduction, and bromination of enamine **3.41** was attempted, complex product mixtures complicated structural characterization. Consequently, studies to advance the total synthesis of *Picrasma* alkaloid family members are still ongoing.



### 3.5.2 A novel cascade reaction for access to indoloquinolizines was discovered.

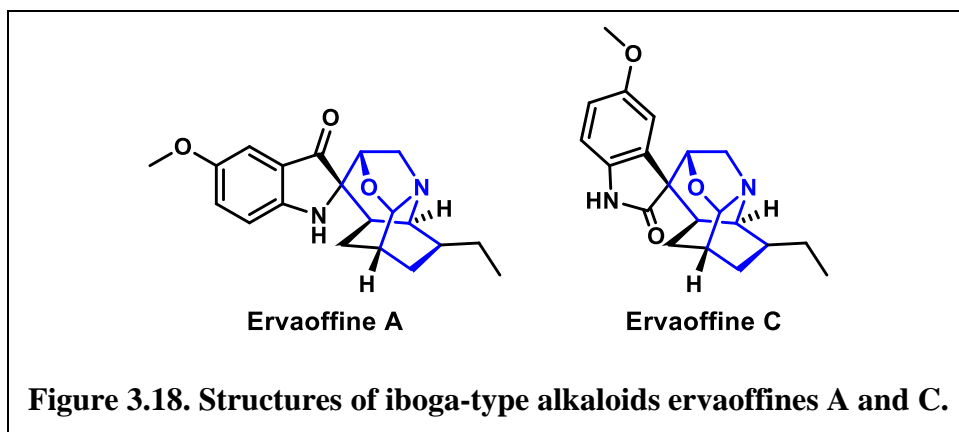
Perhaps serendipitously, the synthesis of **3.41** in **Step 4** of **Approach 1** was achieved from a novel, acid-catalyzed Pictet-Spengler enamine cyclization cascade, providing efficient access to indoloquinolizine heterocycles. Cascade reactions are powerful synthetic strategies, which offer economical and environmentally friendly means for generating molecular complexity.<sup>90</sup> These cascade processes are often associated with cost savings in terms of reagents, catalysts, and solvents, as well as time and effort. The indoloquinolizine scaffold is significant because it is a common building block in several natural products and pharmaceuticals such as arborescidine A,<sup>91</sup> deplancheine,<sup>92</sup> and yohimbine<sup>93</sup> (**Figure 3.17**). Few methods for the synthesis of the indoloquinolizine scaffold have been reported, but they either require multiple steps,<sup>94-96</sup> toxic reagents such as sodium cyanide<sup>97</sup> and phosphorus oxychloride,<sup>98</sup> or heavy metal catalysis.<sup>99</sup> The

cyclization cascade exhibited in **Step 4** is beneficial compared to other methods due to its mild reaction conditions (2 M HCl in methanol, 0 – 23 °C) and its ability to form the tetracyclic indoloquinolizine structure a single step.



### 3.5.3 Complex pentacyclic ring system was synthesized from enamine 3.41 and DDQ.

Compound **3.44** is interesting as it comprises a new oxygen-containing 5-membered ring fused to the  $\beta$ -carboline **B** system. The DDQ controlled benzylic-type oxidation-cyclization cascade reaction used to form this ring system generates two new chiral centers, providing a total of three stereogenic centers in **3.44**. The (6-6-5)-fused heterocyclic octahydro-2*H*-3,6-epoxyquinolizine skeleton (highlighted blue in **Figure 3.18**) is only found in two iboga-type alkaloids, ervaoffines A and C.<sup>80</sup> These intricate oxindole-containing polycyclic compounds have no other structural similarities to the *Picrasma* family of alkaloids but still exhibit a wide variety of biological activities.<sup>100</sup> Overall, compound **3.44** exhibits a novel and complex structure.

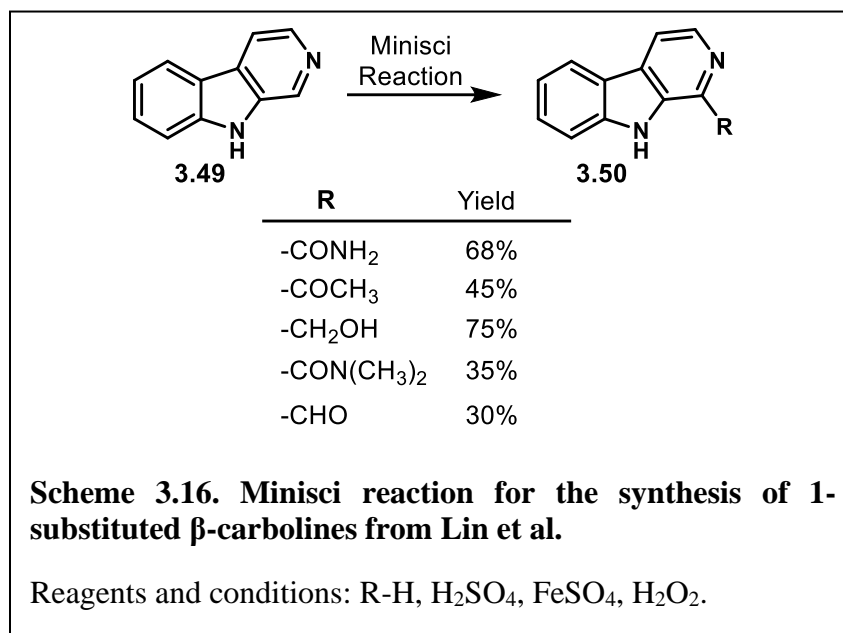


**3.5.4 Approach 2 provides preliminary studies for developing methodology for the direct functionalization of  $\beta$ -carbolines.**

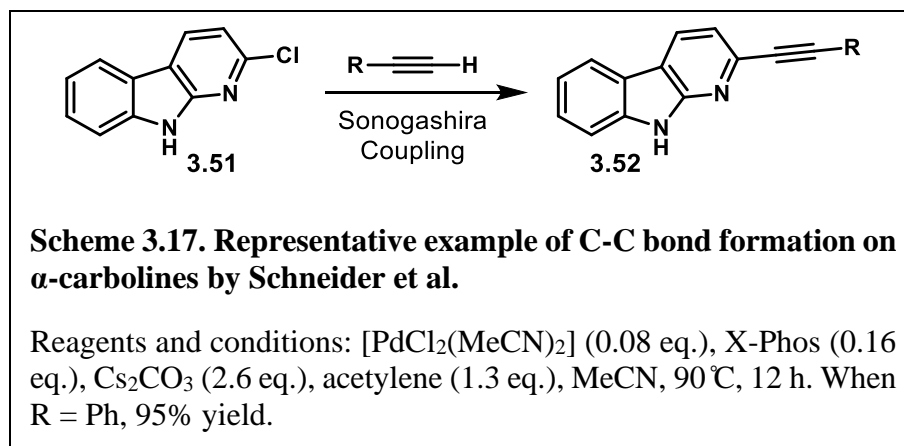
While most of my  $\beta$ -carboline lithiation attempts were unsuccessful, the formation of two substituted  $\beta$ -carbolines (**3.47** and **3.48**) occurred. Compound **3.47** has THF attached at the C1 position, and compound **3.48** has a methyl group attached at the C3 position. Compounds **3.47** and **3.48** might not be new or interesting on their own, but they demonstrate that direct substitution on a  $\beta$ -carboline heterocycle is possible. Future studies on  $\beta$ -carboline functionalization might still be accomplished after some considerations.

First, since the formation of **3.47** may have occurred via nucleophilic aromatic substitution, a new route may be envisioned where the  $\beta$ -carboline acts as an electrophile. For example, the Minisci reaction employs a nucleophilic radical substitution to an electron deficient aromatic system, typically nitrogen heterocycles.<sup>42</sup> Some nucleophilic radicals were successful at functionalizing the  $\beta$ -carboline heterocycle including methanol, formaldehyde, formamide, acetaldehyde, and DMF (**Scheme 3.16**).<sup>101</sup> There are some drawbacks to this reaction, such as the inconsistent yields, the resulting mixture of regioisomers might be difficult to purify, and harsh acidic reagents (concentrated sulfuric acid) might not be a viable option for some substrates. Our

future studies might find utility in this reaction if **Approach 2** was reworked for nucleophilic aromatic substitution.



Secondly, halogenation of the  $\beta$ -carboline was not tried. Substituted  $\alpha$ -carbolines have been synthesized via Sonogashira cross-coupling reactions from the corresponding chloropyrido[2,3-*b*]indoles (**Scheme 3.17**).<sup>102</sup> While  $\alpha$ -carbolines should exhibit different reactivity than  $\beta$ -carbolines and the substrate scope was limited to aromatic and alkyne compounds, C-C bond formation was achieved on an indole-pyridine fused heteroaromatic system. This prompts the possibility that halogenated  $\beta$ -carbolines could undergo coupling reactions, opening new synthetic space for this total synthesis project.



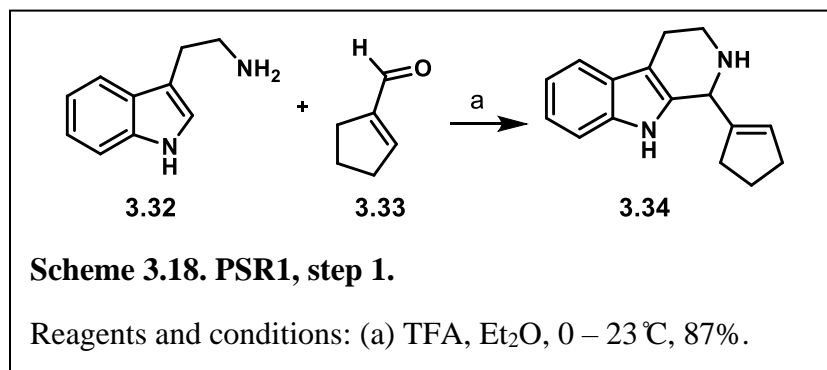
While I was unable to synthesize any picrasidine natural products, great strides were made towards the construction and functionalization of  $\beta$ -carboline heterocycles. The complex heterocycle formation from **Approach 1**, along with the synthesis of 1-THF- $\beta$ -carboline **3.47** during the exploration of **Approach 2** signifies that there are clear paths forward.

## 3.6 Experimental

### 3.6.1 General chemistry methods

All commercial reagents were used without further purification. Distilled water was used for all water necessities in synthetic procedures (e.g., reagent, solvent, work-up). Flash column chromatography was performed with silica gel 60. TLC analyses were completed with EMD Millipore silica gel coated (250  $\mu\text{M}$ ) F254 glass plates and visualized with UV light. NMR samples were prepared in 5 mm tubes with 0.6 mL deuterated solvent. NMR data were all collected on a 300, 400, or 500 MHz (specified below) Varian VNMRs Direct Drive spectrometer equipped with an indirect detection probe. Data was collected at 25 °C unless otherwise indicated. Pulse sequences were used as supplied by Varian VNMRJ 4.2 software. All NMR data was processed in MestreNova v10. Peak positions are reported after reference centering on deuterated solvent of relevance.

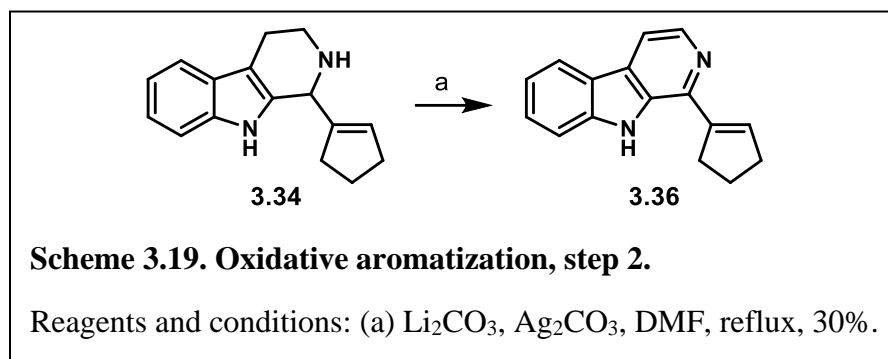
### 3.6.2 Synthetic procedures for Approach 1.



**General procedure for PSR1.** Cyclopentene-1-aldehyde **3.33** was synthesized according to previously existing methods.<sup>103</sup> Tryptamine **3.32** (8.33 mmol) was added to a stirring solution of freshly prepared **3.33** (8.33 mmol) in Et<sub>2</sub>O (50 mL) under nitrogen atmosphere. After the heterogeneous mixture was cooled over an ice water bath to 0 °C, TFA (25 mmol) was added dropwise slowly over 30 minutes affording solution changing in color from green to reddish brown. The mixture stirred as it was allowed to warm to room temperature (23 °C) overnight. Upon reaction completion, solvent was removed via continuous flow of nitrogen gas to afford a sticky, amber-colored oil. The crude oil was dissolved in DCM and poured over dry silica gel (SiO<sub>2</sub>) and then solvent was removed under vacuum. The resulting crude mixture was purified by dry-loaded flash chromatography (50 – 85% ethyl acetate/hexanes plus 1% Et<sub>3</sub>N). Pure fractions were pooled and concentrated in vacuo to yield the THBC **3.34** (7.25 mmol).

**1-(cyclopent-1-en-1-yl)-2,3,4,9-tetrahydro-1H-pyrido[3,4-b]indole (3.34):** Brown oil, 87% yield. <sup>1</sup>H NMR (400 MHz, CDCl<sub>3</sub>) δ 7.74 (s, 1H), 7.50 (d, *J* = 7.6 Hz, 1H), 7.31 (d, *J* = 7.9 Hz, 1H), 7.19 – 7.07 (m, 2H), 5.73 (t, *J* = 2.1 Hz, 1H), 4.86 (s, 1H), 3.43 – 3.29 (m, 1H), 3.14 – 3.02 (m, 1H), 2.88 – 2.69 (m, 2H), 2.43 – 2.34 (m, 3H), 2.33 – 2.21 (m, 4H), 2.04 – 1.79 (m, 2H).

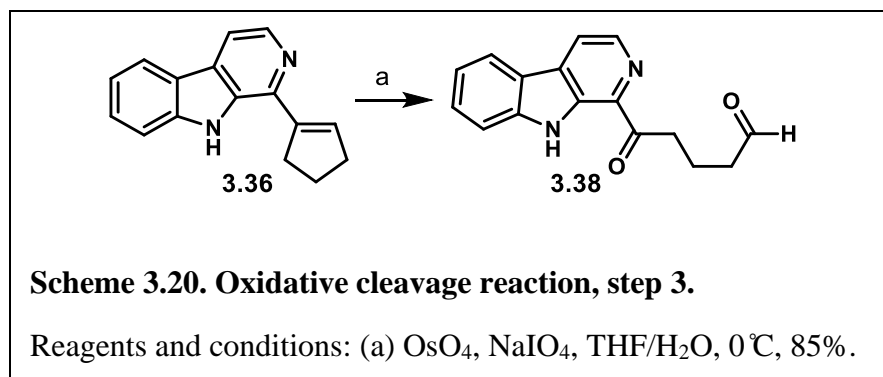
$^{13}\text{C}$  NMR (101 MHz,  $\text{CDCl}_3$ )  $\delta$  143.9, 135.7, 130.0, 127.6, 121.7, 119.5, 118.3, 110.9, 110.8, 109.2, 53.9, 42.6, 32.4, 31.9, 23.6, 22.3.



**General procedure for oxidative aromatization of THBC 3.34.** Dry THBC **3.34** (4.20 mmol) was dissolved in anhydrous, degassed DMF (20 mL).  $\text{Li}_2\text{CO}_3$  (8.40 mmol) and  $\text{Ag}_2\text{CO}_3$  (8.40 mmol) were added under nitrogen atmosphere. The reaction vessel was equipped with a Vigreux condenser, heated at reflux (154 °C), and stirred for 24 hours before cooling to room temperature (23 °C). The resulting heterogenous mixture was filtered over celite and then concentrated in vacuo. The crude product was purified by flash chromatography ( $\text{SiO}_2$ ) using 25% ethyl acetate in hexanes as the eluent. Pure fractions were pooled and concentrated in vacuo to yield  $\beta$ -carboline **3.36** (1.26 mmol).

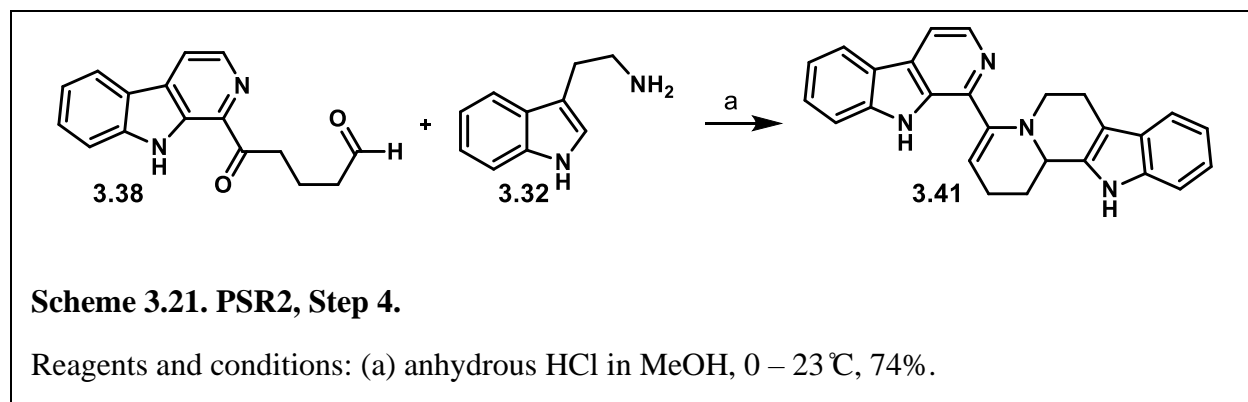
**1-(cyclopent-1-en-1-yl)-9H-pyrido[3,4-b]indole (3.36):** Yellow amorphous solid, 30% yield.  $^1\text{H}$  NMR (500 MHz,  $\text{CD}_3\text{OD}$ )  $\delta$  8.27 (d,  $J = 5.3$  Hz, 0H), 8.18 (d,  $J = 7.9$  Hz, 0H), 8.01 – 7.96 (m, 2H), 7.66 (d,  $J = 8.2$  Hz, 0H), 7.56 (t,  $J = 7.6$  Hz, 0H), 7.28 (t,  $J = 7.5$  Hz, 1H), 6.71 (q,  $J = 2.3$  Hz, 0H), 3.06 (ddt,  $J = 10.0, 4.5, 2.3$  Hz, 1H), 2.79 (tt,  $J = 7.6, 2.5$  Hz, 1H), 2.14 (p,  $J = 7.6$  Hz, 1H).  $^{13}\text{C}$  NMR (151 MHz,  $\text{CD}_3\text{OD}$ )  $\delta$  138.2, 133.7, 129.9, 129.4, 129.3, 122.5, 122.4, 121.0, 120.6, 114.5, 113.8, 113.2, 112.8, 35.1, 33.2, 24.0.





**General procedure of oxidative cleavage reaction.** Aqueous osmium tetroxide (16  $\mu$ mol, 4% in water) was added to a stirring solution of  $\beta$ -carboline **3.36** (0.16 mmol) in THF and water (3:1) at 0 °C. After one hour of stirring, NaIO<sub>4</sub> (0.32 mmol) was added slowly. The reaction was allowed to warm to room temperature overnight and monitored by TLC. Upon consumption of starting material, ethyl acetate was added. The organic layer was washed with water, dried over sodium sulfate, and concentrated in vacuo. The resulting crude oil was purified with flash chromatography (SiO<sub>2</sub>) using 25% ethyl acetate in hexanes as the eluent. Pure fractions were pooled and concentrated in vacuo to yield compound **3.38** as an amorphous yellow solid.

**5-oxo-5-(9H-pyrido[3,4-b]indol-1-yl)pentanal (3.38):** Yellow amorphous solid, 85% yield. <sup>1</sup>H NMR (500 MHz, DMSO)  $\delta$  11.9 (s, 0H), 9.7 (d,  $J$  = 1.5 Hz, 0H), 8.5 (d,  $J$  = 4.9 Hz, 0H), 8.4 (d,  $J$  = 4.9 Hz, 0H), 8.3 (d,  $J$  = 7.9 Hz, 0H), 7.8 (d,  $J$  = 8.2 Hz, 0H), 7.6 (t,  $J$  = 7.7 Hz, 0H), 7.3 (t,  $J$  = 7.5 Hz, 0H), 3.4 (t,  $J$  = 7.3 Hz, 1H), 2.6 (td,  $J$  = 7.2, 1.4 Hz, 1H), 2.0 (p,  $J$  = 7.3 Hz, 1H). <sup>13</sup>C NMR (126 MHz, DMSO)  $\delta$  202.7, 177.4, 141.8, 137.4, 135.6, 134.0, 131.0, 128.9, 121.8, 120.1, 119.4, 113.0, 42.5, 36.4, 16.3.



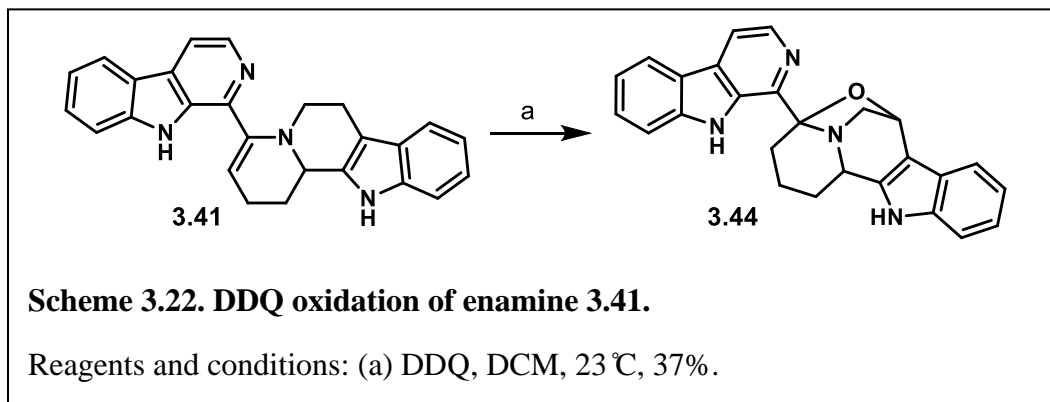
**General procedure for PSR2.** Tryptamine **3.32** (59  $\mu\text{mol}$ ) was added to a solution of aldehyde **3.38** (49  $\mu\text{mol}$ ) dissolved in dry methanol (1 mL) under nitrogen atmosphere at 0 °C followed by dropwise addition of anhydrous HCl solution in methanol (2 M, 24  $\mu\text{L}$ ) over ten minutes. Reaction was warmed to room temperature (23 °C), monitored by TLC, and allowed to stir overnight. Upon consumption of starting material, water and DCM were added. The DCM layer was washed with water, and dried over sodium sulfate, and concentrated under vacuum. The resulting crude oil was purified with flash chromatography ( $\text{SiO}_2$ ) using 70% ethyl acetate/5% triethylamine in hexanes as the eluent. Pure fractions were pooled and concentrated in vacuo to yield compound **3.41** or its hydrate **3.42** as a yellow oil.

**4-(9H-pyrido[3,4-b]indol-1-yl)-1,2,6,7,12,12b-hexahydroindolo[2,3-a]quinolizine**

**(3.41):** Yellow oil, 74% yield.  $^1\text{H}$  NMR (500 MHz, DMSO)  $\delta$  10.99 (s, 1H), 8.32 (d,  $J = 5.2$  Hz, 0H), 8.21 (d,  $J = 7.9$  Hz, 0H), 8.05 (d,  $J = 5.1$  Hz, 0H), 7.67 (d,  $J = 8.2$  Hz, 0H), 7.49 (ddd,  $J = 8.2, 7.0, 1.2$  Hz, 1H), 7.36 (t,  $J = 7.7$  Hz, 1H), 7.22 (t,  $J = 7.5$  Hz, 0H), 7.09 – 7.01 (m, 0H), 6.96 (t,  $J = 7.4$  Hz, 0H), 5.61 (t,  $J = 3.8$  Hz, 0H), 4.58 (d,  $J = 10.0$  Hz, 0H), 2.97 (dt,  $J = 12.2, 4.4$  Hz, 1H), 2.88 (ddd,  $J = 12.5, 9.1, 3.8$  Hz, 1H), 2.71 (ddd,  $J = 14.4, 9.2, 5.0$  Hz, 1H), 2.53 (t,  $J = 3.9$  Hz, 0H), 2.43 (dddd,  $J = 17.7, 10.3, 6.6, 3.1$  Hz, 0H), 2.33 (td,  $J = 5.1, 2.6$  Hz, 0H), 2.28 (ddd,  $J = 12.9, 5.9, 2.8$  Hz, 1H), 2.03 – 1.93 (m, 1H).  $^{13}\text{C}$  NMR (126 MHz, DMSO)  $\delta$  145.4, 141.1, 140.4,

137.7, 136.1, 135.8, 132.8, 128.1, 127.7, 126.6, 121.3, 120.5, 119.2, 118.3, 118.1, 117.4, 113.7, 112.5, 111.0, 110.3, 107.3, 53.5, 45.3, 24.4, 23.0, 21.4. HRMS  $m/z$  391.1923  $[M + H]^+$  (calculated for  $C_{26}H_{22}N_4$ , 390.18).

**4-(9H-pyrido[3,4-b]indol-1-yl)-1,2,3,4,6,7,12,12b-octahydroindolo[2,3-a]quinolizin-4-ol (3.42):** Yellow oil, 20% yield.  $^1H$  NMR (500 MHz, DMSO)  $\delta$  10.8 – 10.5 (m, 1H), 8.3 (d,  $J = 5.4$  Hz, 1H), 8.2 (d,  $J = 7.9$  Hz, 1H), 8.0 (d,  $J = 5.4$  Hz, 1H), 7.7 (d,  $J = 8.3$  Hz, 1H), 7.6 – 7.6 (m, 1H), 7.3 (d,  $J = 7.8$  Hz, 1H), 7.3 – 7.2 (m, 2H), 7.0 (d,  $J = 2.3$  Hz, 1H), 7.0 – 6.9 (m, 1H), 6.8 (t,  $J = 7.4$  Hz, 1H), 6.3 (s, 1H), 6.0 (t,  $J = 2.8$  Hz, 1H), 3.4 (t,  $J = 7.4$  Hz, 0H), 3.3 – 3.2 (m, 1H), 3.0 (ddd,  $J = 15.5, 10.6, 5.2$  Hz, 1H), 2.9 (ddd,  $J = 14.9, 10.1, 6.1$  Hz, 1H), 2.2 – 2.0 (m, 2H), 2.0 (d,  $J = 14.0$  Hz, 1H), 1.9 – 1.8 (m, 2H), 1.6 (d,  $J = 14.6$  Hz, 1H).  $^{13}C$  NMR (126 MHz, DMSO)  $\delta$  144.3, 141.7, 139.3, 137.9, 136.1, 133.6, 128.3, 127.0, 122.5, 122.2, 121.0, 120.7, 119.7, 118.2, 117.7, 114.1, 112.4, 111.2, 110.0, 84.2, 69.8, 46.6, 39.1, 30.5, 25.2, 18.5. HRMS  $m/z$  409.2030  $[M + H]^+$  (calculated for  $C_{26}H_{24}N_4O$ , 408.20).

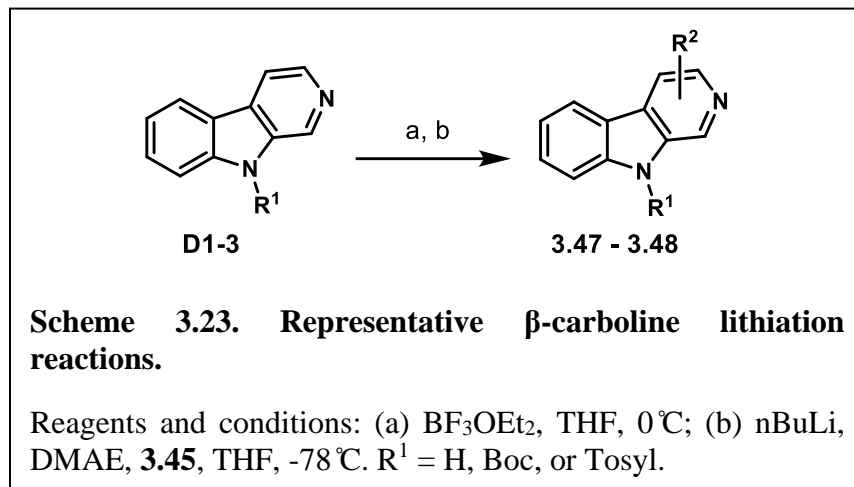


**General procedure for synthesis of 3.44.** 2,3-dichloro-5,6-dicyano-1,4-benzoquinone (DDQ, 31  $\mu$ mol) was added to **3.41** (31  $\mu$ mol) in dry DCM (1 mL) under nitrogen atmosphere at 23 °C. After 12 hours, the reaction was quenched with saturated aqueous sodium carbonate, and the biphasic mixture was extracted with DCM. Organic layers were pooled together and concentrated

under vacuum. The resulting crude oil was purified via flash chromatography (SiO<sub>2</sub>) using 70% ethyl acetate/1% methanol/29% hexanes as the eluent. Pure fractions were pooled together and dried to afford **3.44** as a yellow oil.

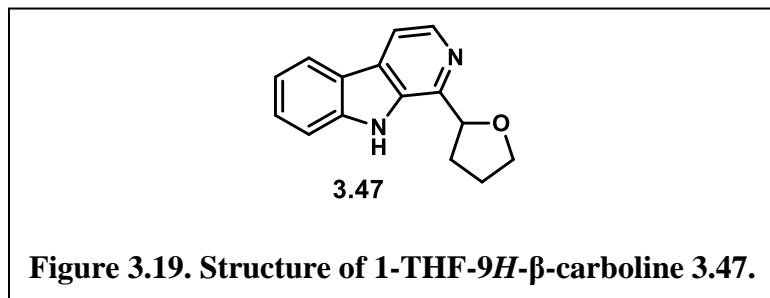
**4-(9H-pyrido[3,4-*b*]indol-1-yl)-1,2,3,4,6,7,12,12b-octahydro-4,7-epoxyindolo[2,3-*a*]quinolizine (3.44):** Yellow oil, 37% yield. <sup>1</sup>H NMR (500 MHz, DMSO) δ 10.97 (d, *J* = 2.6 Hz, 1H), 10.86 – 10.83 (m, 1H), 8.39 (d, *J* = 5.4 Hz, 1H), 8.32 (d, *J* = 5.4 Hz, 1H), 8.27 (dd, *J* = 13.0, 7.9 Hz, 1H), 8.03 (d, *J* = 5.4 Hz, 1H), 8.01 – 7.96 (m, 2H), 7.72 (dd, *J* = 8.3, 2.5 Hz, 2H), 7.64 – 7.56 (m, 2H), 7.38 (d, *J* = 8.1 Hz, 1H), 7.33 (d, *J* = 2.5 Hz, 1H), 7.32 – 7.21 (m, 2H), 7.12 (ddd, *J* = 8.2, 6.9, 1.2 Hz, 1H), 7.08 – 7.02 (m, 1H), 7.02 – 6.93 (m, 2H), 6.82 – 6.74 (m, 1H), 6.19 (q, *J* = 3.1 Hz, 2H), 5.58 (dd, *J* = 9.4, 6.0 Hz, 1H), 5.06 (dd, *J* = 8.8, 3.8 Hz, 1H), 3.63 (dd, *J* = 8.8, 6.1 Hz, 1H), 3.28 (dd, *J* = 8.5, 3.8 Hz, 1H), 2.77 (t, *J* = 8.7 Hz, 1H), 2.58 (t, *J* = 9.1 Hz, 1H), 2.29 – 2.20 (m, 1H), 2.19 – 2.07 (m, 4H), 2.07 – 1.99 (m, 1H), 1.98 – 1.94 (m, 1H), 1.90 (d, *J* = 13.7 Hz, 1H), 1.73 (t, *J* = 16.6 Hz, 2H), 0.77 – 0.64 (m, 2H). <sup>13</sup>C NMR (126 MHz, DMSO) δ 142.3, 139.0, 136.9, 132.4, 128.2, 125.2, 124.3, 123.7, 122.7 (d, *J* = 9.3 Hz), 121.3, 121.2, 121.0, 119.7, 119.4, 118.8, 118.4, 115.3, 114.5, 111.6, 111.3, 110.3, 90.4, 89.7, 73.0, 71.1, 66.7, 52.2, 51.2, 35.0, 34.4, 30.9, 30.5, 18.3, 17.9. HRMS *m/z* 407.187 [M + H]<sup>+</sup> (calculated for C<sub>26</sub>H<sub>22</sub>N<sub>4</sub>O, 406.18).

### 3.6.3 Synthetic procedures for Approach 2.

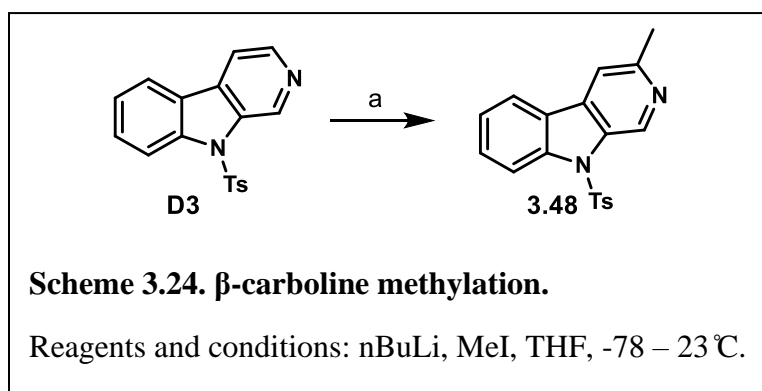


**General procedure for  $\beta$ -carboline lithiation reactions:**  $\beta$ -carbolines **D1 – 3** (0.30 mmol) were dissolved in THF (5 mL) under nitrogen atmosphere and temperature was decreased to  $0^\circ\text{C}$ . Boron trifluoride etherate (0.90 mmol) was added dropwise and the resulting orange- or yellow-colored homogeneous solution was stirred at  $0^\circ\text{C}$  for 30 minutes. In a separate flask flushed with nitrogen gas, lithium 2-dimethylaminoethanolate (LiDMAE) was formed *in situ* from the addition of DMAE (1.20 mmol) dropwise over 15 minutes to a stirring solution of  $n\text{-BuLi}$  (2.38 mmol) in THF (1 mL) at  $0^\circ\text{C}$ . The  $\beta$ -carboline mixture was cooled to  $-78^\circ\text{C}$  before the clear, colorless LiDMAE solution was added via cannula. The resulting mixture was allowed to stir for one hour before electrophilic compound **3.45** was added rapidly. Reaction was monitored by TLC, and after complete consumption of starting material, the reaction was quenched slowly with 1 M aqueous HCl (3 mL) to hydrolyse it. If no reaction occurred after 2 hours, the solution was allowed to warm to room temperature, usually resulting a cloudy and darkened (yellow or orange) heterogeneous mixture which was then quenched with 1 M aqueous HCl (3 mL). In either case, the aqueous layer was then separated and extracted twice with dichloromethane (20 mL). The

combined extracts were dried over sodium sulfate ( $\text{Na}_2\text{SO}_4$ ) and concentrated. The crude product was purified by flash chromatography ( $\text{SiO}_2$ ) using ethyl acetate/hexanes eluents.



**1-(tetrahydrofuran-2-yl)-9H-pyrido[3,4-*b*]indole (3.47):** Synthetic methods as described above for  $\beta$ -carboline lithiation reactions. While quaternary carbons were undetectable by 1D NMR,  $^1\text{H}$  spectra was otherwise identical to literature values,<sup>104</sup> and the structure was further confirmed by HSQC (see **Appendix II**). Yield 14%, amber oil.  $^1\text{H}$  NMR (600 MHz,  $\text{CDCl}_3$ )  $\delta$  9.4 (s, 1H), 8.4 (d,  $J = 5.2$  Hz, 1H), 8.1 (d,  $J = 7.8$  Hz, 1H), 7.9 (d,  $J = 5.2$  Hz, 1H), 7.6 – 7.5 (m, 2H), 7.3 (s, 3H), 5.5 (t,  $J = 7.2$  Hz, 1H), 4.2 (td,  $J = 7.8, 6.1$  Hz, 1H), 4.1 (td,  $J = 8.0, 6.3$  Hz, 1H), 2.6 (td,  $J = 13.0, 7.3$  Hz, 1H), 2.4 – 2.3 (m, 1H), 2.2 – 2.0 (m, 2H).  $^{13}\text{C}$  NMR (151 MHz,  $\text{CDCl}_3$ )  $\delta$  128.5, 121.8, 119.8, 113.6, 111.7, 82.9, 69.2, 32.2, 29.9, 25.7.



**General procedure for  $\beta$ -carboline methylation.** To a yellow solution of N-tosyl- $\beta$ -carboline **D3** (0.09 mmol) in THF (1 mL) under nitrogen atmosphere, n-BuLi (0.18 mmol) was added dropwise at  $-78$   $^\circ\text{C}$ . The resulting mixture appeared darker in color. Methyl iodide (0.09

mmol) was added to the orange solution before the reaction was allowed to warm to room temperature (23 °C). Upon consumption of starting material, monitored by TLC, the reaction was quenched with saturated aqueous ammonium chloride and extracted with DCM. The combined organic layers were concentrated under vacuum, and the crude product was purified by flash chromatography (SiO<sub>2</sub>) using ethyl acetate/hexanes eluents, yielding **3.48** (0.027 mmol).

**3-methyl-9-tosyl-9H-pyrido[3,4-*b*]indole (3.48)**: Amber oil, 30% yield. NMR spectra was compared to literature to confirm structure.<sup>105</sup>

### 3.7 References for Chapter 3

- (1) Rushforth, K. D. *Collins Wildlife Trust Guide Trees: A Photographic Guide to the Trees of Britain and Europe*; Collins Wildlife Trust guides; HarperCollins: London, 1999.
- (2) Wang, N.; Li, Z.-Y.; Zheng, X.-L.; Li, Q.; Yang, X.; Xu, H. Quality Assessment of Kumu Injection, a Traditional Chinese Medicine Preparation, Using HPLC Combined with Chemometric Methods and Qualitative and Quantitative Analysis of Multiple Alkaloids by Single Marker. *Molecules* **2018**, *23* (4), 856. <https://doi.org/10.3390/molecules23040856>.
- (3) de Sousa Falcão, H.; Leite, J. A.; Barbosa-Filho, J. M.; de Athayde-Filho, P. F.; de Oliveira Chaves, M. C.; Moura, M. D.; Ferreira, A. L.; de Almeida, A. B. A.; Souza-Brito, A. R. M.; de Fátima Formiga Melo Diniz, M.; Batista, L. M. Gastric and Duodenal Antiulcer Activity of Alkaloids: A Review. *Molecules* **2008**, *13* (12), 3198–3223. <https://doi.org/10.3390/molecules13123198>.
- (4) Jensen, O.; Nielsen, A. O.; Bjerregaard, P. Pediculosis Capitis Treated with Quassia Tincture. *Acta Derm Venereol* **1978**, *58* (6), 557–559.

- (5) Mohd Jamil, M. D. H.; Taher, M.; Susanti, D.; Rahman, M. A.; Zakaria, Z. A. Phytochemistry, Traditional Use and Pharmacological Activity of *Picrasma Quassioides*: A Critical Reviews. *Nutrients* **2020**, *12* (9), 2584. <https://doi.org/10.3390/nu12092584>.
- (6) Zhao, S.; Kanno, Y.; Li, W.; Sasaki, T.; Zhang, X.; Wang, J.; Cheng, M.; Koike, K.; Nemoto, K.; Li, H. Identification of Picrasidine C as a Subtype-Selective PPAR $\alpha$  Agonist. *J. Nat. Prod.* **2016**, *79* (12), 3127–3133. <https://doi.org/10.1021/acs.jnatprod.6b00883>.
- (7) Koike, K.; Ohmoto, T. Studies on the Alkaloids from *Picrasma Quassioides* BENNET.VII. : Structures of  $\beta$ -Carboline Dimer Alkaloids, Picrasidines-H and -R. *Chemical & Pharmaceutical Bulletin* **1986**, *34* (5), 2090–2093. <https://doi.org/10.1248/cpb.34.2090>.
- (8) Jiao, W.-H.; Gao, H.; Li, C.-Y.; Zhao, F.; Jiang, R.-W.; Wang, Y.; Zhou, G.-X.; Yao, X.-S. Quassidines A–D, Bis- $\beta$ -Carboline Alkaloids from the Stems of *Picrasma Quassioides*. *J. Nat. Prod.* **2010**, *73* (2), 167–171. <https://doi.org/10.1021/np900538r>.
- (9) Guo-hua, S.; Wei-hua, J.; Fan, Y.; Hou-wen, L. Three Bis- $\beta$ -Carboline Alkaloids from *Picrasma Quassioides* and Their Bioactivities. *Chinese Traditional and Herbal Drugs* **2015**, *46* (6), 803–807. <https://doi.org/10.7501/j.issn.0253-2670.2015.06.004>.
- (10) Yamashita, N.; Kondo, M.; Zhao, S.; Li, W.; Koike, K.; Nemoto, K.; Kanno, Y. Picrasidine G Decreases Viability of MDA-MB 468 EGFR-Overexpressing Triple-Negative Breast Cancer Cells through Inhibition of EGFR/STAT3 Signaling Pathway. *Bioorganic & Medicinal Chemistry Letters* **2017**, *27* (11), 2608–2612. <https://doi.org/10.1016/j.bmcl.2017.03.061>.
- (11) Higuchi, T.; Ohmoto, T.; Koike, K. Picrasidine-T, a Dimeric  $\beta$ -Carboline Alkaloid from *Picrasma Quassioides*. *Phytochemistry* **1987**, *26*, 3375–3377.



- (12) Jiao, W.-H.; Chen, G.-D.; Gao, H.; Li, J.; Gu, B.-B.; Xu, T.-T.; Yu, H.-B.; Shi, G.-H.; Yang, F.; Yao, X.-S.; Lin, H.-W. ( $\pm$ )-Quassidines I and J, Two Pairs of Cytotoxic Bis- $\beta$ -Carboline Alkaloid Enantiomers from *Picrasma Quassioides*. *J. Nat. Prod.* **2015**, *78* (1), 125–130. <https://doi.org/10.1021/np500801s>.
- (13) Zhang, J.; Zhao, S.-S.; Xie, J.; Yang, J.; Chen, G.-D.; Hu, D.; Zhang, W.-G.; Wang, C.-X.; Yao, X.-S.; Gao, H. N-Methoxy- $\beta$ -Carboline Alkaloids with Inhibitory Activities against A $\beta$ 42 Aggregation and Acetylcholinesterase from the Stems of *Picrasma Quassioides*. *Bioorganic Chemistry* **2020**, *101*, 104043. <https://doi.org/10.1016/j.bioorg.2020.104043>.
- (14) Ohmoto, T.; Koike, K. Studies on the Alkaloids from *Picrasma Quassioides* BENNET. V. Structures of Picrasidines L, M, and P. *Chem. Pharm. Bull.* **1985**, *33* (9), 3847–3851. <https://doi.org/10.1248/cpb.33.3847>.
- (15) Zhao, S.; Kanno, Y.; Li, W.; Wakatabi, H.; Sasaki, T.; Koike, K.; Nemoto, K.; Li, H. Picrasidine N Is a Subtype-Selective PPAR $\beta/\delta$  Agonist. *J. Nat. Prod.* **2016**, *79* (4), 879–885. <https://doi.org/10.1021/acs.jnatprod.5b00909>.
- (16) Zhao, W.-Y.; Song, X.-Y.; Zhao, L.; Zou, C.-X.; Zhou, W.-Y.; Lin, B.; Yao, G.-D.; Huang, X.-X.; Song, S.-J. Quassinoids from *Picrasma Quassioides* and Their Neuroprotective Effects. *J. Nat. Prod.* **2019**, *82* (4), 714–723. <https://doi.org/10.1021/acs.jnatprod.8b00470>.
- (17) Ohmoto, T.; Koike, K. Studies on the Constituents of *Picrasma Quassioides* BENNET. I. On the Alkaloidal Constituents. *Chemical & Pharmaceutical Bulletin* **1982**, *30* (4), 1204–1209. <https://doi.org/10.1248/cpb.30.1204>.
- (18) Jiang, M.-X.; Zhou, Y.-J. Canthin-6-One Alkaloids from *Picrasma Quassioides* and Their Cytotoxic Activity. *J Asian Nat Prod Res* **2008**, *10* (11–12), 1009–1012. <https://doi.org/10.1080/10286020802277956>.

- (19) Sung, Y.; Koike, K.; Nikaido, T.; Ohmoto, T.; Sankawa, U. Inhibitors of Cyclic AMP Phosphodiesterase in *Picrasma Quassioides* Bennet, and Inhibitory Activities of Related Beta-Carboline Alkaloids. *Chem Pharm Bull (Tokyo)* **1984**, *32* (5), 1872–1877. <https://doi.org/10.1248/cpb.32.1872>.
- (20) Villarroel-Vicente, C.; Gutiérrez-Palomo, S.; Ferri, J.; Cortes, D.; Cabedo, N. Natural Products and Analogs as Preventive Agents for Metabolic Syndrome via Peroxisome Proliferator-Activated Receptors: An Overview. *European Journal of Medicinal Chemistry* **2021**, *221*, 113535. <https://doi.org/10.1016/j.ejmech.2021.113535>.
- (21) Biscetti, F.; Gaetani, E.; Flex, A.; Aprahamian, T.; Hopkins, T.; Straface, G.; Pecorini, G.; Stigliano, E.; Smith, R. C.; Angelini, F.; Castellot, J. J.; Pola, R. Selective Activation of Peroxisome Proliferator–Activated Receptor (PPAR) $\alpha$  and PPAR $\gamma$  Induces Neoangiogenesis Through a Vascular Endothelial Growth Factor–Dependent Mechanism. *Diabetes* **2008**, *57* (5), 1394–1404. <https://doi.org/10.2337/db07-0765>.
- (22) Batista, F. A. H.; Trivella, D. B. B.; Bernardes, A.; Gratieri, J.; Oliveira, P. S. L.; Figueira, A. C. M.; Webb, P.; Polikarpov, I. Structural Insights into Human Peroxisome Proliferator Activated Receptor Delta (PPAR-Delta) Selective Ligand Binding. *PLOS ONE* **2012**, *7* (5), e33643. <https://doi.org/10.1371/journal.pone.0033643>.
- (23) Dou, X.; Duerfeldt, A. S. Small-Molecule Modulation of PPARs for the Treatment of Prevalent Vascular Retinal Diseases. *International Journal of Molecular Sciences* **2020**, *21* (23), 9251. <https://doi.org/10.3390/ijms21239251>.
- (24) Jiao, W.-H.; Gao, H.; Zhao, F.; Lin, H.-W.; Pan, Y.-M.; Zhou, G.-X.; Yao, X.-S. Anti-Inflammatory Alkaloids from the Stems of *Picrasma Quassioides* BENNET. *Chem. Pharm. Bull.* **2011**, *59* (3), 359–364. <https://doi.org/10.1248/cpb.59.359>.

- (25) Liu, J.; Davidson, R. S.; Howarth, O. W. Full Assignments of Proton and Carbon Signals of Picrasidine-G by 1D and 2D NMR Methods. *Magn. Reson. Chem.* **1993**, *31* (12), 1091–1092. <https://doi.org/10.1002/mrc.1260311212>.
- (26) Li, F.; Wang, H.; Wang, Y.; Feng, S.; Hu, B.; Zhang, X.; Wang, J.; Li, W.; Cheng, M. Computational Investigation Reveals Picrasidine C as Selective PPAR $\alpha$  Lead: Binding Pattern, Selectivity Mechanism and ADME/Tox Profile. *Journal of Biomolecular Structure and Dynamics* **2020**, *38* (18), 5401–5418. <https://doi.org/10.1080/07391102.2019.1699861>.
- (27) Pictet, A.; Spengler, Theod. Über Die Bildung von Isochinolin-Derivaten Durch Einwirkung von Methylal Auf Phenyl-Äthylamin, Phenyl-Alanin Und Tyrosin. *Berichte der deutschen chemischen Gesellschaft* **1911**, *44* (3), 2030–2036. <https://doi.org/10.1002/cber.19110440309>.
- (28) Yokoyama, A.; Ohwada, T.; Shudo, K. Prototype Pictet–Spengler Reactions Catalyzed by Superacids. Involvement of Dicationic Superelectrophiles. *J. Org. Chem.* **1999**, *64* (2), 611–617. <https://doi.org/10.1021/jo982019e>.
- (29) Bischler, Aug.; Napieralski, B. Zur Kenntniss Einer Neuen Isochinolinsynthese. *Berichte der deutschen chemischen Gesellschaft* **1893**, *26* (2), 1903–1908. <https://doi.org/10.1002/cber.189302602143>.
- (30) Murakami, Y.; Yokoyama, Y.; Aoki, C.; Suzuki, H.; Sakurai, K.; Shinohara, T.; Miyagi, C.; Kimura, Y.; Takahashi, T.; Watanabe, T.; Ohmoto, T. Synthetic Studies of Indoles and Related Compounds. A New Synthesis of Crenatine from Ethyl Indole-2-Carboxylate. *Chem. Pharm. Bull.* **1991**, *39* (9), 2189–2195.
- (31) Hagen, T. J.; Narayanan, K.; Names, J.; Cook, J. M. DDQ Oxidations in the Indole Area. Synthesis of 4-Alkoxy-.Beta.-Carbolines Including the Natural Products Crenatine and 1-

- Methoxycanthin-6-One. *J. Org. Chem.* **1989**, *54* (9), 2170–2178.  
<https://doi.org/10.1021/jo00270a029>.
- (32) Showalter, H. D. H. Progress in the Synthesis of Canthine Alkaloids and Ring-Truncated Congeners. *J. Nat. Prod.* **2013**, *76* (3), 455–467. <https://doi.org/10.1021/np300753z>.
- (33) Li, J.; Wang, T.; Yu, P.; Peterson, A.; Weber, R.; Soerens, D.; Grubisha, D.; Bennett, D.; Cook, J. M. General Approach for the Synthesis of Ajmaline/Sarpagine Indole Alkaloids: Enantiospecific Total Synthesis of (+)-Ajmaline, Alkaloid G, and Norsuaveoline via the Asymmetric Pictet–Spengler Reaction. *J. Am. Chem. Soc.* **1999**, *121* (30), 6998–7010. <https://doi.org/10.1021/ja990184l>.
- (34) Suzuki, H.; Iwata(nee Miyaga), C.; Sakurai, K.; Tokumoto, K.; Takahashi, H.; Hanada, M.; Yokoyama, Y.; Murakami, Y. A General Synthetic Route for 1-Substituted 4-Oxygenated  $\beta$ -Carbolines (Synthetic Studies on Indoles and Related Compounds 41). *Tetrahedron* **1997**, *53* (5), 1593–1606. [https://doi.org/10.1016/S0040-4020\(96\)01112-X](https://doi.org/10.1016/S0040-4020(96)01112-X).
- (35) Cain, M.; Mantei, R.; Cook, J. M. Dichlorodicyanoquinone Oxidations in the Indole Area. Synthesis of Crenatine. *J. Org. Chem.* **1982**, *47* (25), 4933–4936. <https://doi.org/10.1021/jo00146a021>.
- (36) Koike, K.; Yoshino, H.; Li, H.; Sasaki, T.; Li, W. Determination of the Absolute Configuration of Picrasidine Y, a Naturally Occurring  $\beta$ -Carboline Alkaloid. *Tetrahedron Letters* **2015**, *56* (38), 5306–5308. <https://doi.org/10.1016/j.tetlet.2015.07.079>.
- (37) Shelar, S. V.; Argade, N. P. Total Synthesis of Bioactive Canthine Alkaloid Cordatanine Comprising in Situ Double Oxidative Aromatization of Tetrahydrocarbazole. *ACS Omega* **2017**, *2* (7), 3945–3950. <https://doi.org/10.1021/acsomega.7b00609>.

- (38) Suzuki, H.; Ebihara, Y.; Yokoyama, Y.; Murakami, Y. Total Synthesis of the Structure Proposed for Picrasidine-H (Dimeric 4-Methoxy-P-Carboline Alkaloid). *Heterocycles* **1997**, *16*, 57–60.
- (39) Omura, K.; Swern, D. Oxidation of Alcohols by “Activated” Dimethyl Sulfoxide. a Preparative, Steric and Mechanistic Study. *Tetrahedron* **1978**, *34* (11), 1651–1660. [https://doi.org/10.1016/0040-4020\(78\)80197-5](https://doi.org/10.1016/0040-4020(78)80197-5).
- (40) Gros, P.; Fort, Y.; Caubère, P. Aggregative Activation in Heterocyclic Chemistry. Part 5.† Lithiation of Pyridine and Quinoline with the Complex Base BuLi·Me<sub>2</sub>N(CH<sub>2</sub>)<sub>2</sub>OLi (BuLi·LiDMAE). *J. Chem. Soc., Perkin Trans. 1* **1997**, No. 24, 3597–3600. <https://doi.org/10.1039/A705027E>.
- (41) Li, B.; Wu, Z.-H.; Gu, Y.-F.; Sun, C.-L.; Wang, B.-Q.; Shi, Z.-J. Direct Cross-Coupling of C-H Bonds with Grignard Reagents through Cobalt Catalysis. *Angewandte Chemie International Edition* **2011**, *50* (5), 1109–1113. <https://doi.org/10.1002/anie.201005394>.
- (42) Minisci, F.; Bernardi, R.; Bertini, F.; Galli, R.; Perchinummo, M. Nucleophilic Character of Alkyl Radicals—VI: A New Convenient Selective Alkylation of Heteroaromatic Bases. *Tetrahedron* **1971**, *27* (15), 3575–3579. [https://doi.org/10.1016/S0040-4020\(01\)97768-3](https://doi.org/10.1016/S0040-4020(01)97768-3).
- (43) Andreeva, I. V.; Artemyeva, V. N.; Nesterov, V. V.; Kukarkina, N. V. Methods of Acrolein Polymerization and Investigation of Structures of the Polymers Obtained | EndNote Click. *Journal of Polymer Science* **1979**, *17*, 3415–3424.
- (44) Li, S. Chapter 12 - Fundamentals of Polymerization Reaction Engineering. In *Reaction Engineering*; Li, S., Ed.; Butterworth-Heinemann: Boston, 2017; pp 541–598. <https://doi.org/10.1016/B978-0-12-410416-7.00012-4>.

- (45) Kamal, A.; Srinivasulu, V.; Nayak, V. L.; Sathish, M.; Shankaraiah, N.; Bagul, C.; Reddy, N. V. S.; Rangaraj, N.; Nagesh, N. Design and Synthesis of C3-Pyrazole/Chalcone-Linked Beta-Carboline Hybrids: Antitopoisomerase I, DNA-Interactive, and Apoptosis-Inducing Anticancer Agents. *Chem. Med. Chem.* **2014**, *9* (9), 2084–2098. <https://doi.org/10.1002/cmdc.201300406>.
- (46) Cain, M.; Campos, O.; Guzman, F.; Cook, J. M. Selenium Dioxide Oxidations in the Indole Area. Synthesis of  $\beta$ -Carboline Alkaloids. *7*.
- (47) Gaikwad, S.; Kamble, D.; Lokhande, P. Iodine-Catalyzed Chemoselective Dehydrogenation and Aromatization of Tetrahydro- $\beta$ -Carbolines: A Short Synthesis of Kumujian-C, Eudistomin-U, Norharmane, Harmane Harmalan and Isoeudistomine-M. *Tetrahedron Letters* **2018**, *59* (25), 2387–2392. <https://doi.org/10.1016/j.tetlet.2018.04.043>.
- (48) Kamal, A.; Tangella, Y.; Manasa, K. L.; Sathish, M.; Srinivasulu, V.; Chetna, J.; Alarifi, A.  $\text{PhI}(\text{OAc})_2$ -Mediated One-Pot Oxidative Decarboxylation and Aromatization of Tetrahydro- $\beta$ -Carbolines: Synthesis of Norharmane, Harmane, Eudistomin U and Eudistomin I. *Org. Biomol. Chem.* **2015**, *13* (32), 8652–8662. <https://doi.org/10.1039/C5OB00871A>.
- (49) Hati, S.; Sen, S. N-Bromo-Succinimide Promoted Synthesis of  $\beta$ -Carbolines and 3,4-Dihydro- $\beta$ -Carbolines from Tetrahydro- $\beta$ -Carbolines. *Tetrahedron Letters* **2016**, *57* (9), 1040–1043. <https://doi.org/10.1016/j.tetlet.2016.01.081>.
- (50) Rinehart, K. L.; Kobayashi, J.; Harbour, G. C.; Gilmore, J.; Mascal, M.; Holt, T. G.; Shield, L. S.; Lafargue, F. Eudistomins A-Q, Beta-Carbolines from the Antiviral Caribbean Tunicate Eudistoma Olivaceum. *J. Am. Chem. Soc.* **1987**, *109* (11), 3378–3387. <https://doi.org/10.1021/ja00245a031>.

- (51) D'Agostino, I.; Giacchello, I.; Nannetti, G.; Fallacara, A. L.; Deodato, D.; Musumeci, F.; Grossi, G.; Palù, G.; Cau, Y.; Trist, I. M.; Loregian, A.; Schenone, S.; Botta, M. Synthesis and Biological Evaluation of a Library of Hybrid Derivatives as Inhibitors of Influenza Virus PA-PB1 Interaction. *European Journal of Medicinal Chemistry* **2018**, *157*, 743–758. <https://doi.org/10.1016/j.ejmech.2018.08.032>.
- (52) Su, D. S.; Zhang, J.; Frank, B.; Thomas, A.; Wang, X.; Paraknowitsch, J.; Schlögl, R. Metal-Free Heterogeneous Catalysis for Sustainable Chemistry. *ChemSusChem* **2010**, *3* (2), 169–180. <https://doi.org/10.1002/cssc.200900180>.
- (53) Hati, S.; Holzgrabe, U.; Sen, S. Oxidative Dehydrogenation of C–C and C–N Bonds: A Convenient Approach to Access Diverse (Dihydro)Heteroaromatic Compounds. *Beilstein J Org Chem* **2017**, *13*, 1670–1692. <https://doi.org/10.3762/bjoc.13.162>.
- (54) Schlitzer, S. C.; Arunprasath, D.; Stevens, K. G.; Sharma, I. A Metal-Free Aromatic Cascade for the Synthesis of Diverse Heterocycles. *Org Chem Front* **2020**, *7* (7), 913–918. <https://doi.org/10.1039/c9qo01336a>.
- (55) Kamal, A.; Sathish, M.; Prasanthi, A. V. G.; Chetna, J.; Tangella, Y.; Srinivasulu, V.; Shankaraiah, N.; Alarifi, A. An Efficient One-Pot Decarboxylative Aromatization of Tetrahydro- $\beta$ -Carbolines by Using N-Chlorosuccinimide: Total Synthesis of Norharmane, Harmane and Eudistomins. *RSC Adv.* **2015**, *5* (109), 90121–90126. <https://doi.org/10.1039/C5RA16221A>.
- (56) Zhao, Z.; Sun, Y.; Wang, L.; Chen, X.; Sun, Y.; Lin, L.; Tang, Y.; Li, F.; Chen, D. Organic Base-Promoted Efficient Dehydrogenative/Decarboxylative Aromatization of Tetrahydro- $\beta$ -Carbolines into  $\beta$ -Carbolines under Air. *Tetrahedron Letters* **2019**, *60* (11), 800–804. <https://doi.org/10.1016/j.tetlet.2019.02.020>.

- (57) Zheng, B.; Trieu, T. H.; Li, F.-L.; Zhu, X.-L.; He, Y.-G.; Fan, Q.-Q.; Shi, X.-X. Copper-Catalyzed Benign and Efficient Oxidation of Tetrahydroisoquinolines and Dihydroisoquinolines Using Air as a Clean Oxidant. *ACS Omega* **2018**, *3* (7), 8243–8252. <https://doi.org/10.1021/acsomega.8b00855>.
- (58) Aronica, L. A.; Albano, G. Supported Metal Catalysts for the Synthesis of N-Heterocycles. *Catalysts* **2022**, *12* (1), 68. <https://doi.org/10.3390/catal12010068>.
- (59) Durham, S. D.; Sierra, B.; Gomez, M. J.; Tran, J. K.; Anderson, M. O.; Whittington-Davis, N. A.; Eagon, S. Synthesis of  $\beta$ -Carbolines via a Silver-Mediated Oxidation of Tetrahydro- $\beta$ -Carbolines. *Tetrahedron Letters* **2017**, *58* (28), 2747–2750. <https://doi.org/10.1016/j.tetlet.2017.05.098>.
- (60) Gawande, M. B.; Shelke, S. N.; Zboril, R.; Varma, R. S. Microwave-Assisted Chemistry: Synthetic Applications for Rapid Assembly of Nanomaterials and Organics. *Acc. Chem. Res.* **2014**, *47* (4), 1338–1348. <https://doi.org/10.1021/ar400309b>.
- (61) Eagon, S.; Anderson, M. O. Microwave-Assisted Synthesis of Tetrahydro- $\beta$ -Carbolines and  $\beta$ -Carbolines: Microwave-Assisted Synthesis of  $\beta$ -Carbolines and Congeners. *Eur. J. Org. Chem.* **2014**, *2014* (8), 1653–1665. <https://doi.org/10.1002/ejoc.201301580>.
- (62) Van Ornum, S. G.; Champeau, R. M.; Pariza, R. Ozonolysis Applications in Drug Synthesis. *Chem. Rev.* **2006**, *106* (7), 2990–3001. <https://doi.org/10.1021/cr040682z>.
- (63) Mecozzi, F.; Dong, J. J.; Angelone, D.; Browne, W. R.; Eisink, N. N. H. M. Oxidative Cleavage of Alkene C=C Bonds Using a Manganese Catalyzed Oxidation with H<sub>2</sub>O<sub>2</sub> Combined with Periodate Oxidation. *European Journal of Organic Chemistry* **2019**, *2019* (42), 7151–7158. <https://doi.org/10.1002/ejoc.201901380>.



- (64) Criegee, R. Mechanism of Ozonolysis. *Angewandte Chemie International Edition in English* **1975**, *14* (11), 745–752. <https://doi.org/10.1002/anie.197507451>.
- (65) Kuczkowski, R. L. Formation and Structure of Ozonides. *Acc. Chem. Res.* **1983**, *16* (2), 42–47. <https://doi.org/10.1021/ar00086a002>.
- (66) Burnett, R. T.; Brook, J. R.; Yung, W. T.; Dales, R. E.; Krewski, D. Association between Ozone and Hospitalization for Respiratory Diseases in 16 Canadian Cities. *Environmental Research* **1997**, *72* (1), 24–31. <https://doi.org/10.1006/enrs.1996.3685>.
- (67) Miyamoto, K.; Tada, N.; Ochiai, M. Activated Iodosylbenzene Monomer as an Ozone Equivalent: Oxidative Cleavage of Carbon–Carbon Double Bonds in the Presence of Water. *J. Am. Chem. Soc.* **2007**, *129* (10), 2772–2773. <https://doi.org/10.1021/ja070179e>.
- (68) Rajagopalan, A.; Lara, M.; Kroutil, W. Oxidative Alkene Cleavage by Chemical and Enzymatic Methods. *Adv. Synth. Catal.* **2013**, *355* (17), 3321–3335. <https://doi.org/10.1002/adsc.201300882>.
- (69) Travis, B. R.; Narayan, R. S.; Borhan, B. Osmium Tetroxide-Promoted Catalytic Oxidative Cleavage of Olefins: An Organometallic Ozonolysis. *J. Am. Chem. Soc.* **2002**, *124* (15), 3824–3825. <https://doi.org/10.1021/ja017295g>.
- (70) Kurti, L.; Czako, B. *Strategic Applications of Named Reactions in Organic Synthesis: Background and Detailed Mechanisms.*; Elsevier Science: Burlington, 2005.
- (71) Pappo, R.; Allen, Jr., D.; Lemieux, R.; Johnson, W. Notes - Osmium Tetroxide-Catalyzed Periodate Oxidation of Olefinic Bonds. *J. Org. Chem.* **1956**, *21* (4), 478–479. <https://doi.org/10.1021/jo01110a606>.

- (72) Kim, C.; Traylor, T. G.; Perrin, C. L. MCPBA Epoxidation of Alkenes: Reinvestigation of Correlation between Rate and Ionization Potential. *J. Am. Chem. Soc.* **1998**, *120* (37), 9513–9516. <https://doi.org/10.1021/ja981531e>.
- (73) Scott Obach, R.; Kalgutkar, A. S. Reactive Electrophiles and Metabolic Activation. In *Comprehensive Toxicology (Second Edition)*; McQueen, C. A., Ed.; Elsevier: Oxford, 2010; pp 309–347. <https://doi.org/10.1016/B978-0-08-046884-6.00115-9>.
- (74) Sharma, S. D.; Bhaduri, S.; Kaur, G. Diastereoselective Synthesis of 1,3-Disubstituted 1,2,3,4-Tetrahydro- $\beta$ -Carbolines Using Pictet-Spengler Reaction in Non-Acidic Aprotic Media. *Indian. J. Org. Chem.* **2007**, *38* (14), 2710–2715. <https://doi.org/10.1002/chin.200714162>.
- (75) Whaley, W. M.; Govindachari, T. R. The Pictet-Spengler Synthesis of Tetrahydroisoquinolines and Related Compounds. In *Organic Reactions*; John Wiley & Sons, Ltd, 2011; pp 151–190. <https://doi.org/10.1002/0471264180.or006.03>.
- (76) Micovic, V.; Mihailovic, M. The Reduction of Acid Amides with Lithium Aluminum Hydride. *J. Org. Chem.* **1953**, *18* (9), 1190–1200. <https://doi.org/10.1021/jo50015a017>.
- (77) R. Juárez, J.; Castro, A.; Romero, O.; L. Terán, J.; Gnecco, D.; Orea, L.; Mendoza, A. Oxidation and Aromatization of the Enantiopure Piperidine Derived from (R)-(-)-2-Phenylglycinol to (1'R)-(-)-1-(2'-Hydroxy-1'-Phenylethyl)-1H-Pyridin-2-One. *HETEROCYCLES* **2014**, *89* (3), 725. <https://doi.org/10.3987/COM-13-12911>.
- (78) Alsharif, M. A.; Raja, Q. A.; Majeed, N. A.; Jassas, R. S.; Alsimaree, A. A.; Sadiq, A.; Naeem, N.; Mughal, E. U.; Alsantali, R. I.; Moussa, Z.; Ahmed, S. A. DDQ as a Versatile and Easily Recyclable Oxidant: A Systematic Review. *RSC Adv.* **2021**, *11* (47), 29826–29858. <https://doi.org/10.1039/D1RA04575J>.

- (79) Batista, V. S.; Crabtree, R. H.; Konezny, S. J.; Luca, O. R.; Praetorius, J. M. Oxidative Functionalization of Benzylic C–H Bonds by DDQ. *New J. Chem.* **2012**, *36* (5), 1141–1144. <https://doi.org/10.1039/C2NJ40021A>.
- (80) Tang, B.-Q.; Wang, W.-J.; Huang, X.-J.; Li, G.-Q.; Wang, L.; Jiang, R.-W.; Yang, T.-T.; Shi, L.; Zhang, X.-Q.; Ye, W.-C. Iboga-Type Alkaloids from *Ervatamia Officinalis*. *J. Nat. Prod.* **2014**, *77* (8), 1839–1846. <https://doi.org/10.1021/np500240b>.
- (81) Watanabe, M.; Snieckus, V. Tandem Directed Metalation Reactions. Short Syntheses of Polycyclic Aromatic Hydrocarbons and Ellipticine Alkaloids. 4.
- (82) Manolikakes, S. M.; Barl, N. M.; Sämman, C.; Knochel, P. Regioselective Functionalization of Pyridines Using a Directed Metalation or a Halogen/Metal Exchange. *Zeitschrift für Naturforschung B* **2013**, *68* (5–6), 411–422. <https://doi.org/10.5560/znb.2013-3061>.
- (83) Lazaar, J.; Rebstock, A.-S.; Mongin, F.; Godard, A.; Trécourt, F.; Marsais, F.; Quéguiner, G. Directed Lithiation of Unprotected Pyridinecarboxylic Acids: Syntheses of Halo Derivatives. *Tetrahedron* **2002**, *58* (33), 6723–6728. [https://doi.org/10.1016/S0040-4020\(02\)00673-7](https://doi.org/10.1016/S0040-4020(02)00673-7).
- (84) Comins, D. L.; Jianhua, G. N- vs. O-Alkylation in the Mitsunobu Reaction of 2-Pyridone. *Tetrahedron Letters* **1994**, *35* (18), 2819–2822. [https://doi.org/10.1016/S0040-4039\(00\)76633-0](https://doi.org/10.1016/S0040-4039(00)76633-0).
- (85) Jaric, M.; Haag, B. A.; Manolikakes, S. M.; Knochel, P. Selective and Multiple Functionalization of Pyridines and Alkaloids *via* Mg- and Zn-Organometallic Intermediates. *Org. Lett.* **2011**, *13* (9), 2306–2309. <https://doi.org/10.1021/ol200563j>.
- (86) Ren, H.; Knochel, P. Regioselective Functionalization of Trisubstituted Pyridines Using a Bromine–Magnesium Exchange. *Chem. Commun.* **2006**, No. 7, 726–728. <https://doi.org/10.1039/B515168F>.

- (87) Roszak, R.; Beker, W.; Molga, K.; Grzybowski, B. A. Rapid and Accurate Prediction of PKa Values of C–H Acids Using Graph Convolutional Neural Networks. *J. Am. Chem. Soc.* **2019**, *141* (43), 17142–17149. <https://doi.org/10.1021/jacs.9b05895>.
- (88) Gros, P.; Choppin, S.; Mathieu, J.; Fort, Y. Lithiation of 2-Heterosubstituted Pyridines with BuLi–LiDMAE: Evidence for Regiospecificity at C-6. *J. Org. Chem.* **2002**, *67* (1), 234–237. <https://doi.org/10.1021/jo015855o>.
- (89) Schlosser, M. *Organometallics in Organic Synthesis*; Wiley, 1994; Vol. 172.
- (90) Nicolaou, K. C.; Chen, J. S. The Art of Total Synthesis Through Cascade Reactions. *Chem Soc Rev* **2009**, *38* (11), 2993–3009. <https://doi.org/10.1039/b903290h>.
- (91) Chbani, M.; Païs, M.; Delauneux, J.-M.; Debitus, C. Brominated Indole Alkaloids from the Marine Tunicate Pseudodistoma Arborescens. *J. Nat. Prod.* **1993**, *56* (1), 99–104. <https://doi.org/10.1021/np50091a014>.
- (92) Guillaume, D.; Morfaux, A. M.; Richard, B.; Massiot, G.; Le Men-Olivier, L.; Pusset, J.; Sévenet, T. Some Alkaloids of Alstonia Undulata. *Phytochemistry* **1984**, *23* (10), 2407–2408. [https://doi.org/10.1016/S0031-9422\(00\)80574-9](https://doi.org/10.1016/S0031-9422(00)80574-9).
- (93) Kao, H.-K.; Lin, X.-J.; Hong, B.-C.; Yang, V.-W.; Lee, G.-H. Enantioselective Synthesis of Yohimbine Analogues by an Organocatalytic and Pot-Economic Strategy. *J. Org. Chem.* **2019**, *84* (18), 12138–12147. <https://doi.org/10.1021/acs.joc.9b01193>.
- (94) Wenkert, E.; Dave, K. G.; Haglid, F. General Methods of Synthesis of Indole Alkaloids. V. Syntheses of d,l-Corynantheidol and d,l-Epialloyohimbane<sup>1,2</sup>. *J. Am. Chem. Soc.* **1965**, *87* (23), 5461–5467. <https://doi.org/10.1021/ja00951a037>.

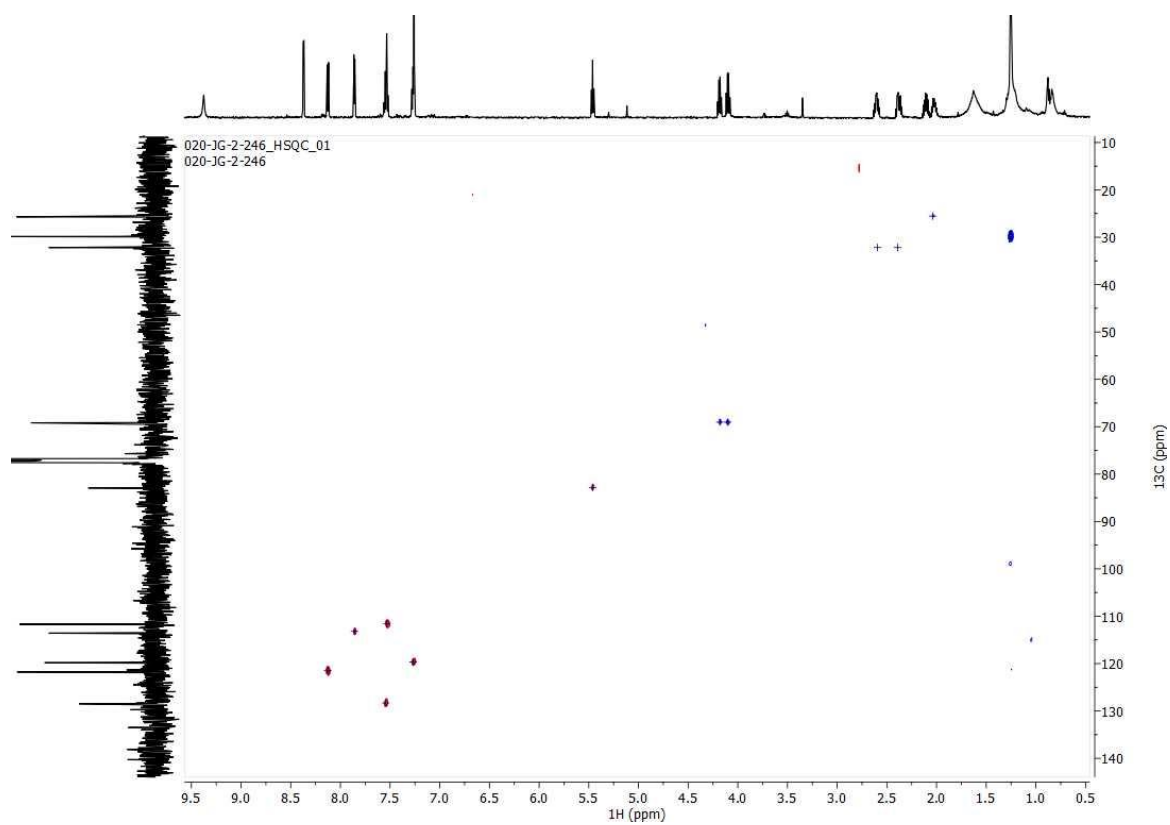
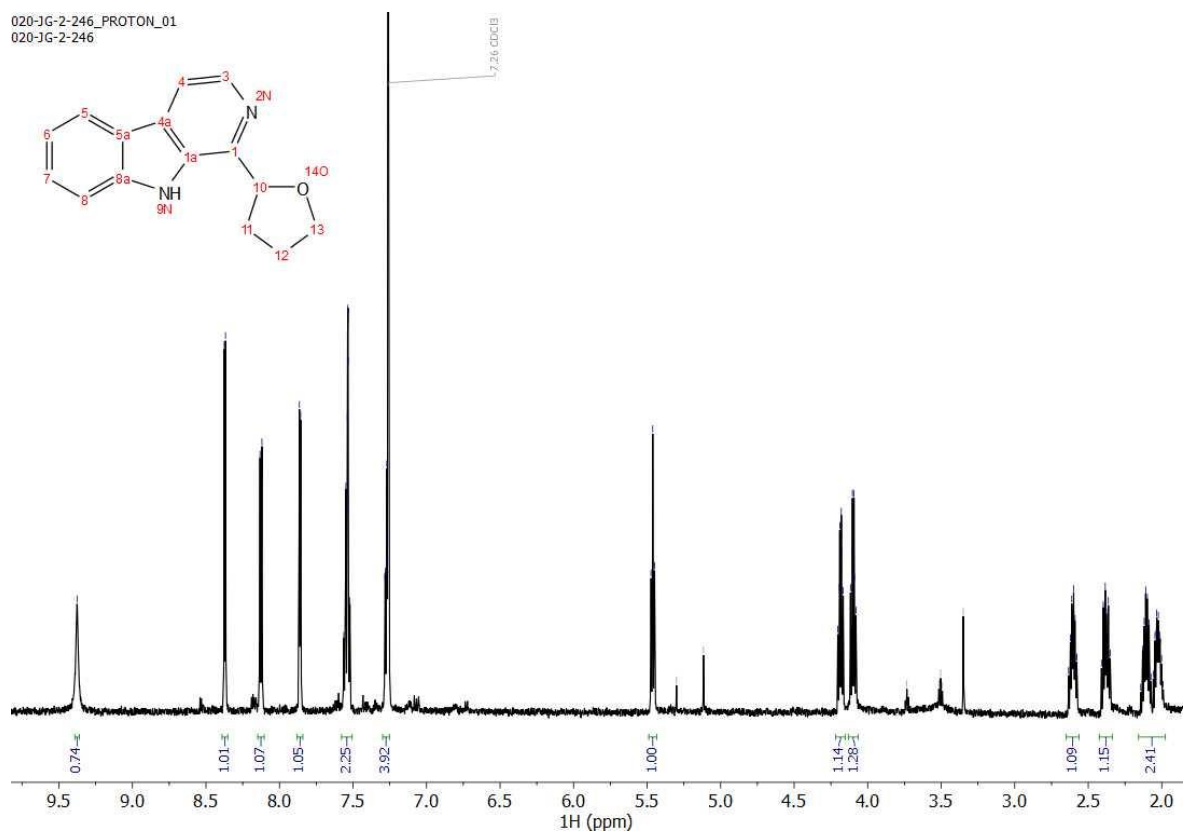
- (95) Liu, X.; Wang, T.; Xu, Q.; Ma, C.; Cook, J. M. Enantiospecific Total Synthesis of the Enantiomer of the Indole Alkaloid Affinisine. *Tetrahedron Letters* **2000**, *41* (33), 6299–6303. [https://doi.org/10.1016/S0040-4039\(00\)01061-3](https://doi.org/10.1016/S0040-4039(00)01061-3).
- (96) Sydorenko, N.; Zificsak, C. A.; Gerasyuto, A. I.; Hsung, R. P. Total Syntheses of Enantiomerically Enriched R-(+)- and S-(–)-Deplancheine. *Org. Biomol. Chem.* **2005**, *3* (11), 2140–2144. <https://doi.org/10.1039/B503862F>.
- (97) Park, E.; Cheon, C.-H. A General Strategy for the Synthesis of Indoloquinolizine Alkaloids via a Cyanide-Catalyzed Imino-Stetter Reaction. *Organic & Biomolecular Chemistry* **2017**, *15* (48), 10265–10275. <https://doi.org/10.1039/C7OB02691A>.
- (98) Fujii, T.; Yoshifuji, S.; Ito, H. Quinolizidines. XXV. An Extension of the “Lactim Ether Route” to the Racemic Syntheses of Several Indolo[2,3-a]Quinolizidine Alkaloids. *Chem. Pharm. Bull.* **1988**, *36* (9), 3348–3353. <https://doi.org/10.1248/cpb.36.3348>.
- (99) Wang, Y.; Zhang, P.; Di, X.; Dai, Q.; Zhang, Z.-M.; Zhang, J. Gold-Catalyzed Asymmetric Intramolecular Cyclization of N-Allenamides for the Synthesis of Chiral Tetrahydrocarbolines. *Angewandte Chemie International Edition* **2017**, *56* (50), 15905–15909. <https://doi.org/10.1002/anie.201709595>.
- (100) Lavaud, C.; Massiot, G. The Iboga Alkaloids. *Prog Chem Org Nat Prod* **2017**, *105*, 89–136. [https://doi.org/10.1007/978-3-319-49712-9\\_2](https://doi.org/10.1007/978-3-319-49712-9_2).
- (101) Lin, G.; Wang, Y.; Zhou, Q.; Tang, W.; Wang, J.; Lu, T. A Facile Synthesis of 1-Substituted  $\beta$ -Carboline Derivatives via Minisci-Reaction. *Synthetic Communications* **2011**, *41* (23), 3541–3550. <https://doi.org/10.1080/00397911.2010.519092>.
- (102) Schneider, C.; Goyard, D.; Gueyrard, D.; Joseph, B.; Goekjian, P. G. Synthesis of 2-, 3-, and 4-Substituted Pyrido[2,3-b]Indoles by C–N, C–O, and C–C(Sp) Bond Formation.

*European Journal of Organic Chemistry* **2010**, 2010 (34), 6665–6677.  
<https://doi.org/10.1002/ejoc.201000795>.

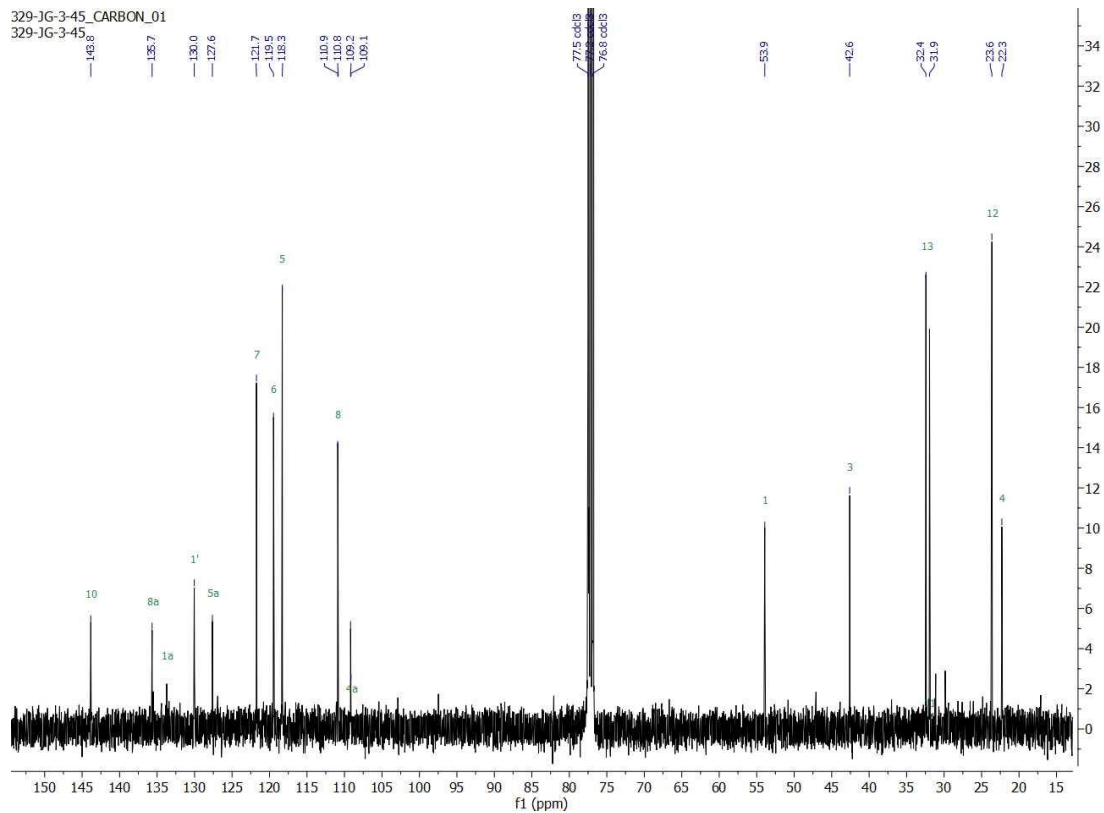
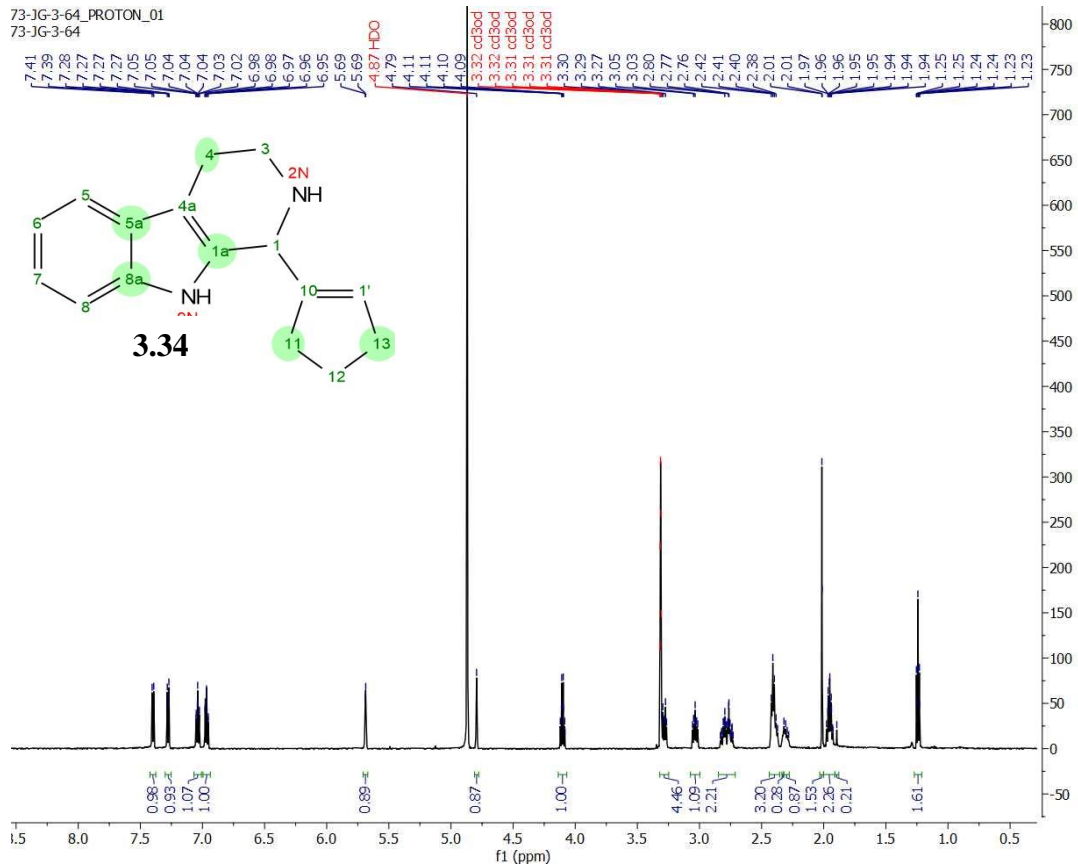
- (103) Meyers, M. J.; Arhancet, G. B.; Hockerman, S. L.; Chen, X.; Long, S. A.; Mahoney, M. W.; Rico, J. R.; Garland, D. J.; Blinn, James. R.; Collins, J. T.; Yang, S.; Huang, H.-C.; McGee, K. F.; Wendling, J. M.; Dietz, J. D.; Payne, M. A.; Homer, B. L.; Heron, M. I.; Reitz, D. B.; Hu, X. Discovery of (3S,3aR)-2-(3-Chloro-4-Cyanophenyl)-3-Cyclopentyl-3,3a,4,5-Tetrahydro-2H-Benzo[g]Indazole-7-Carboxylic Acid (PF-3882845), an Orally Efficacious Mineralocorticoid Receptor (MR) Antagonist for Hypertension and Nephropathy. *J. Med. Chem.* **2010**, 53 (16), 5979–6002. <https://doi.org/10.1021/jm100505n>.
- (104) Li, X.; Liu, C.; Guo, S.; Wang, W.; Zhang, Y. PIFA-Mediated Cross-Dehydrogenative Coupling of N-Heteroarenes with Cyclic Ethers: Ethanol as an Efficient Promoter. *European Journal of Organic Chemistry* **2021**, 2021 (3), 411–421. <https://doi.org/10.1002/ejoc.202001354>.
- (105) Dhiman, S.; Mishra, U. K.; Ramasastry, S. S. V. One-Pot Trimetallic Relay Catalysis: A Unified Approach for the Synthesis of  $\beta$ -Carbolines and Other [c]-Fused Pyridines. *Angewandte Chemie International Edition* **2016**, 55 (27), 7737–7741. <https://doi.org/10.1002/anie.201600840>.

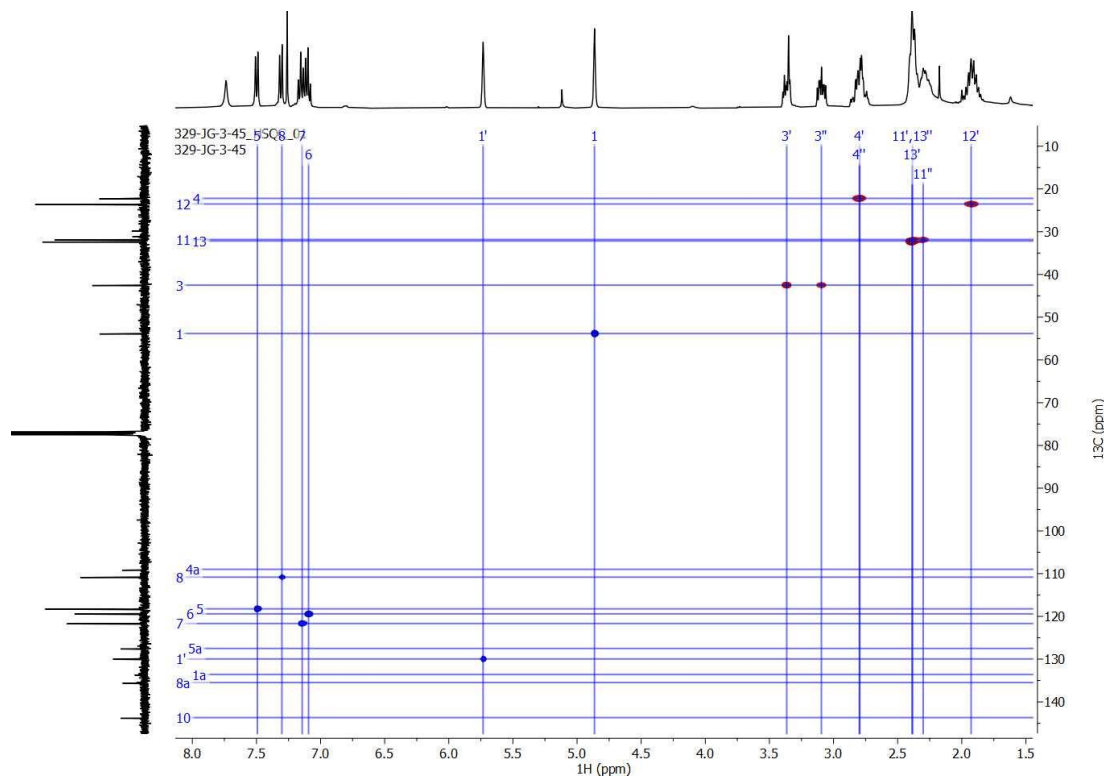
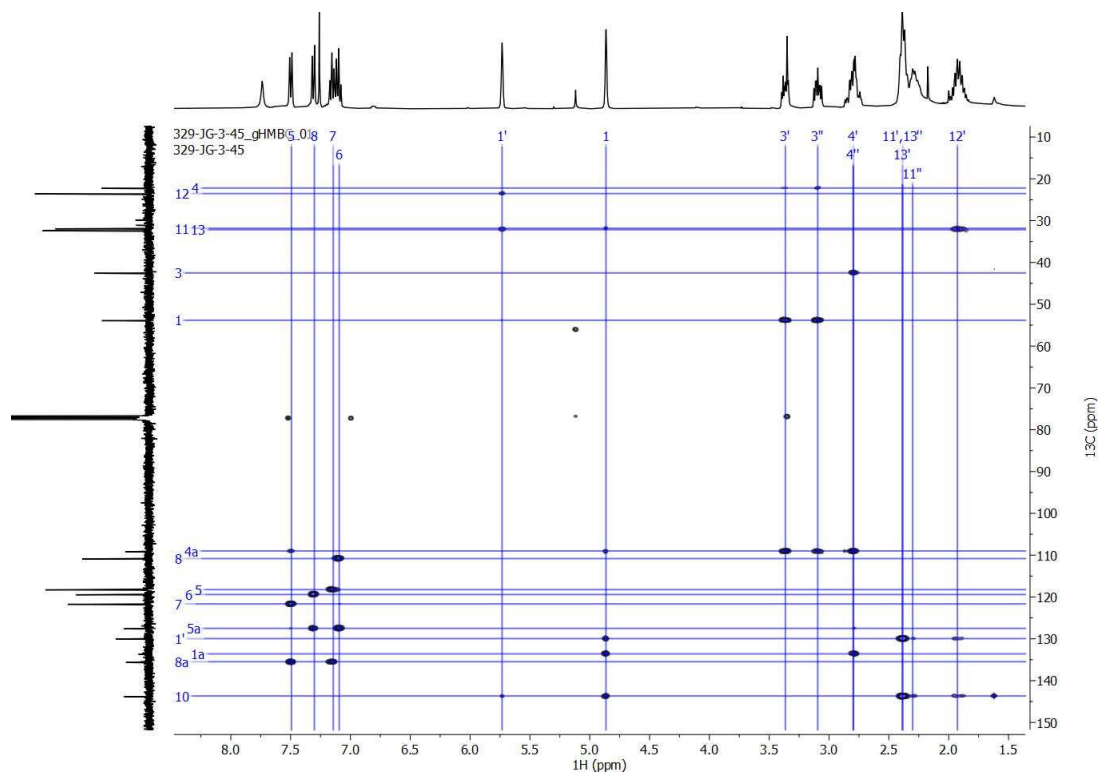
## **Appendix II. Spectra Relevant to Chapter 3**

020-JG-2-246\_PROTON\_01  
020-JG-2-246

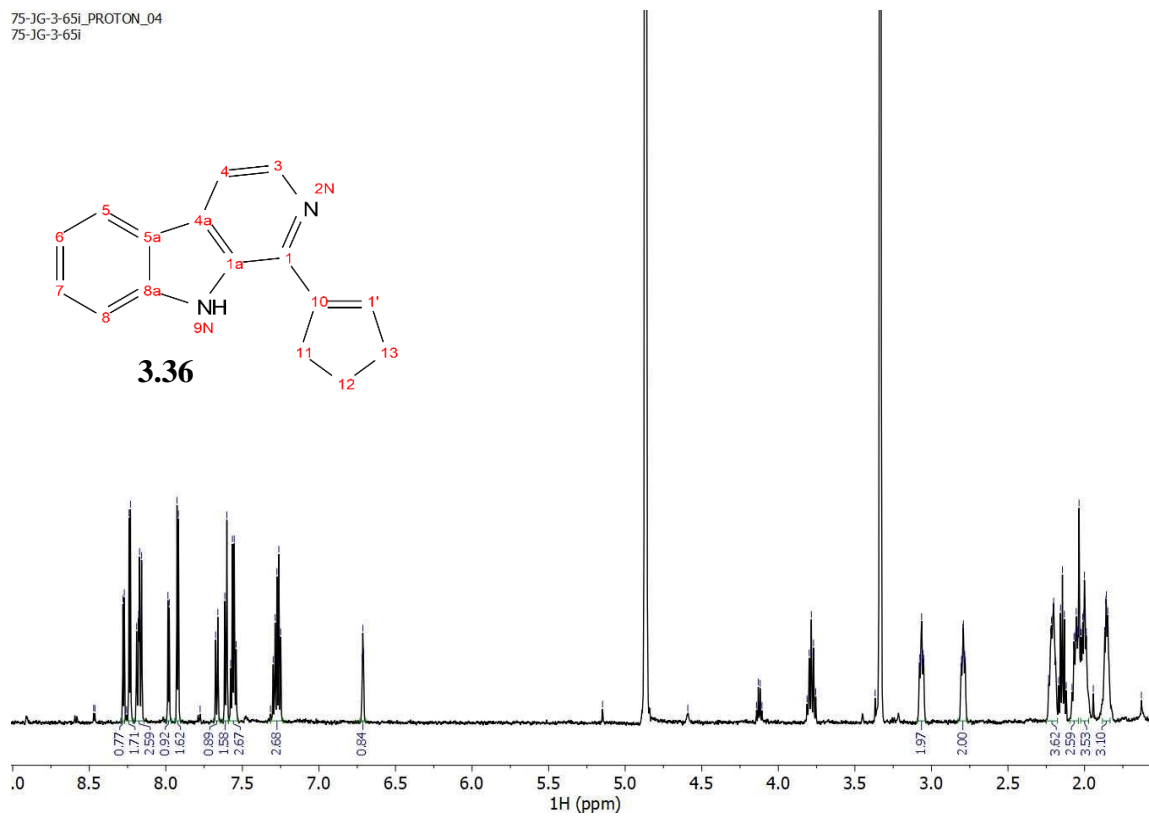
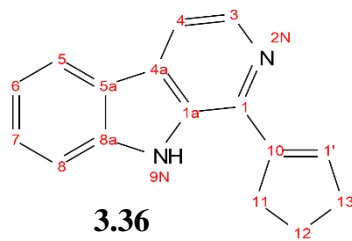




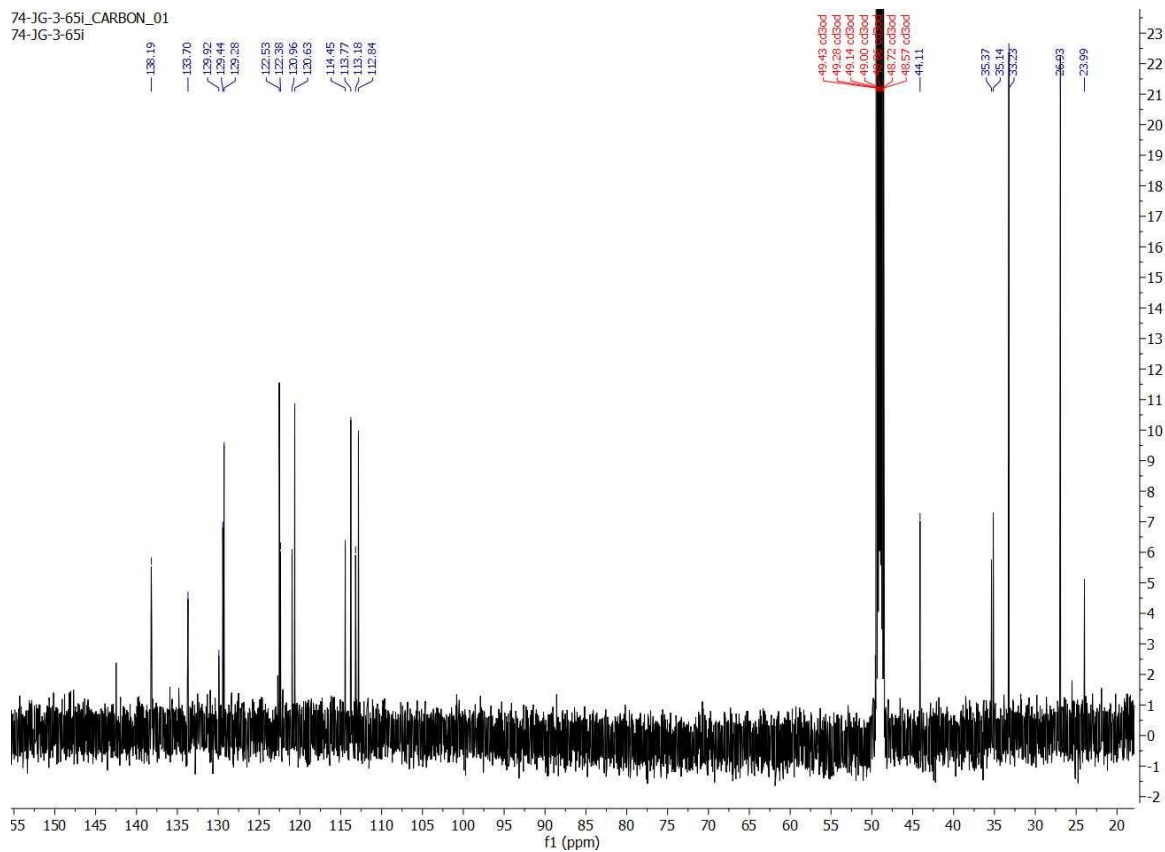




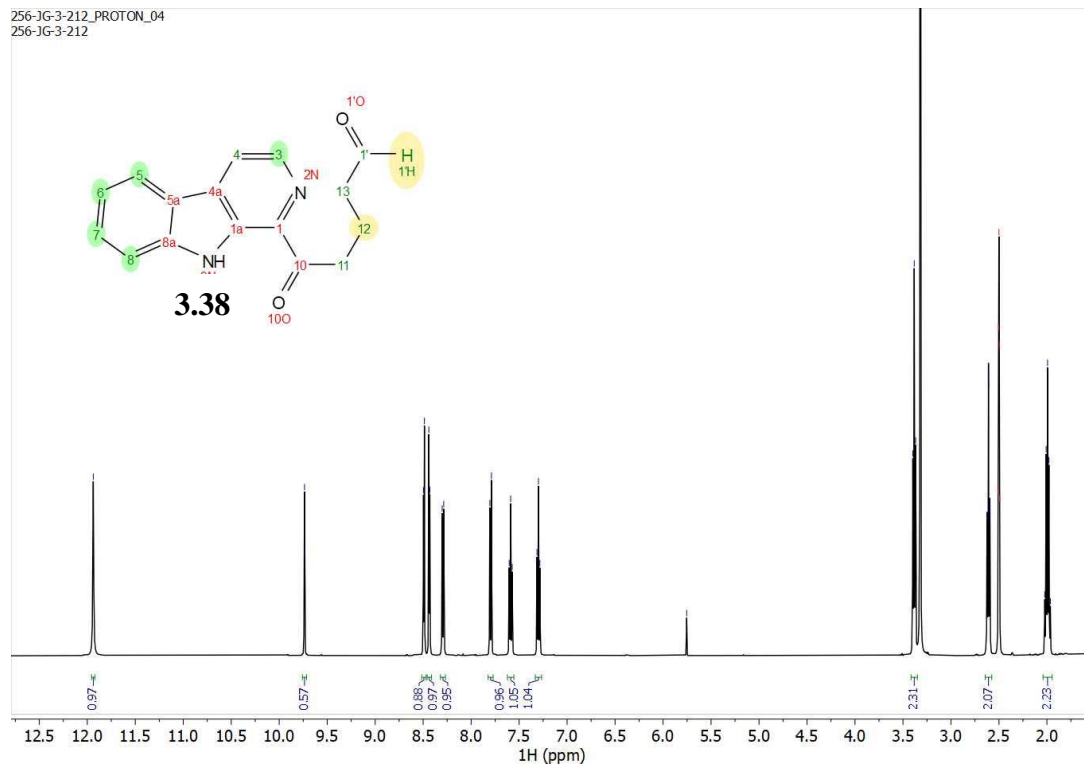
75-JG-3-65I\_PROTON\_04  
75-JG-3-65I



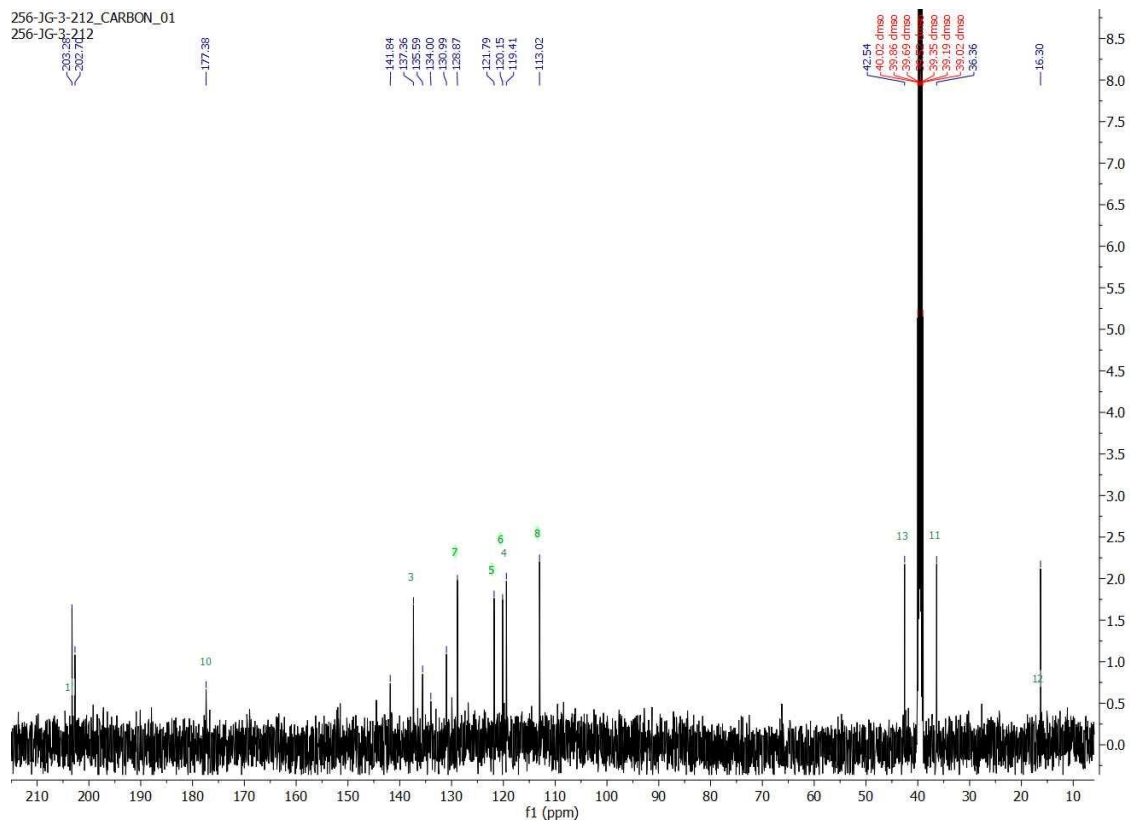
74-JG-3-65I\_CARBON\_01  
74-JG-3-65I

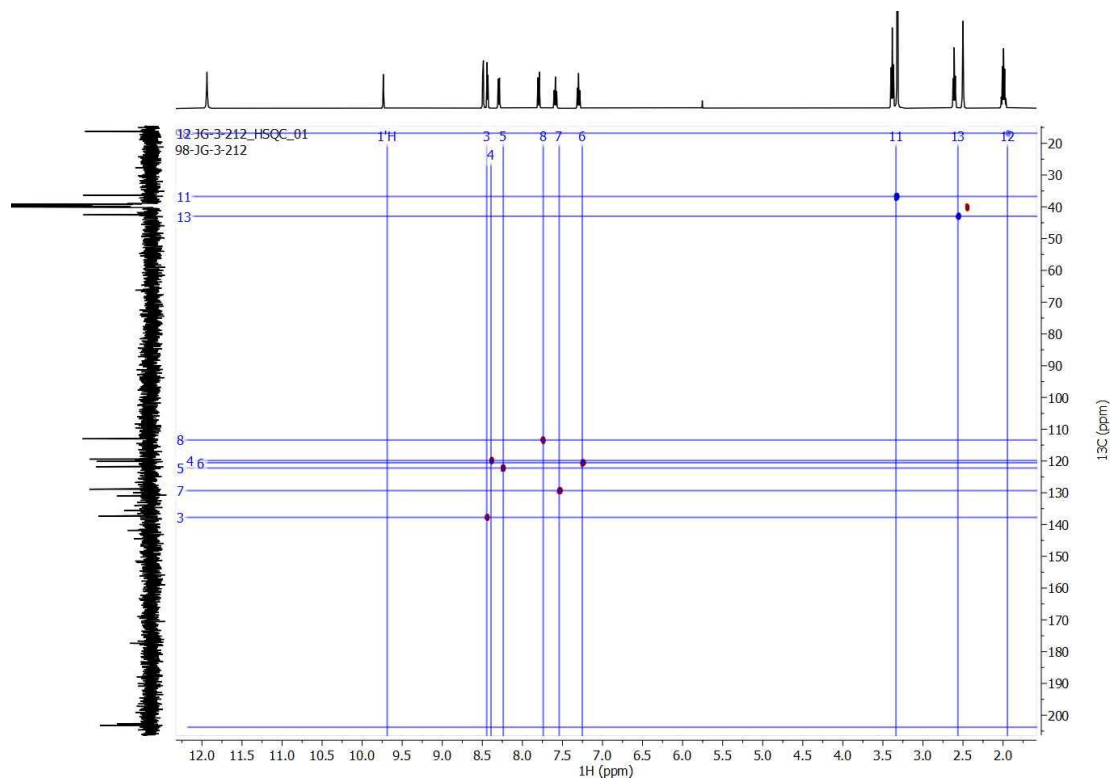
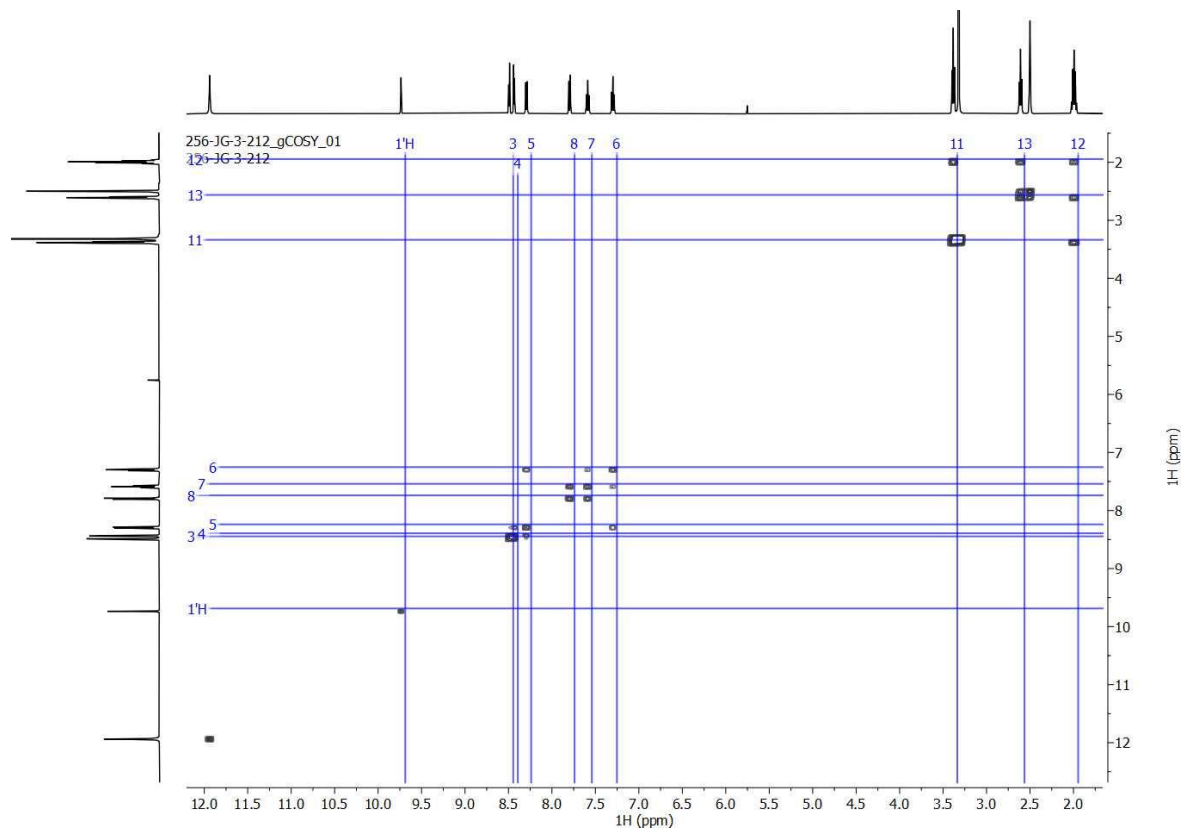


256-JG-3-212\_PROTON\_04  
256-JG-3-212

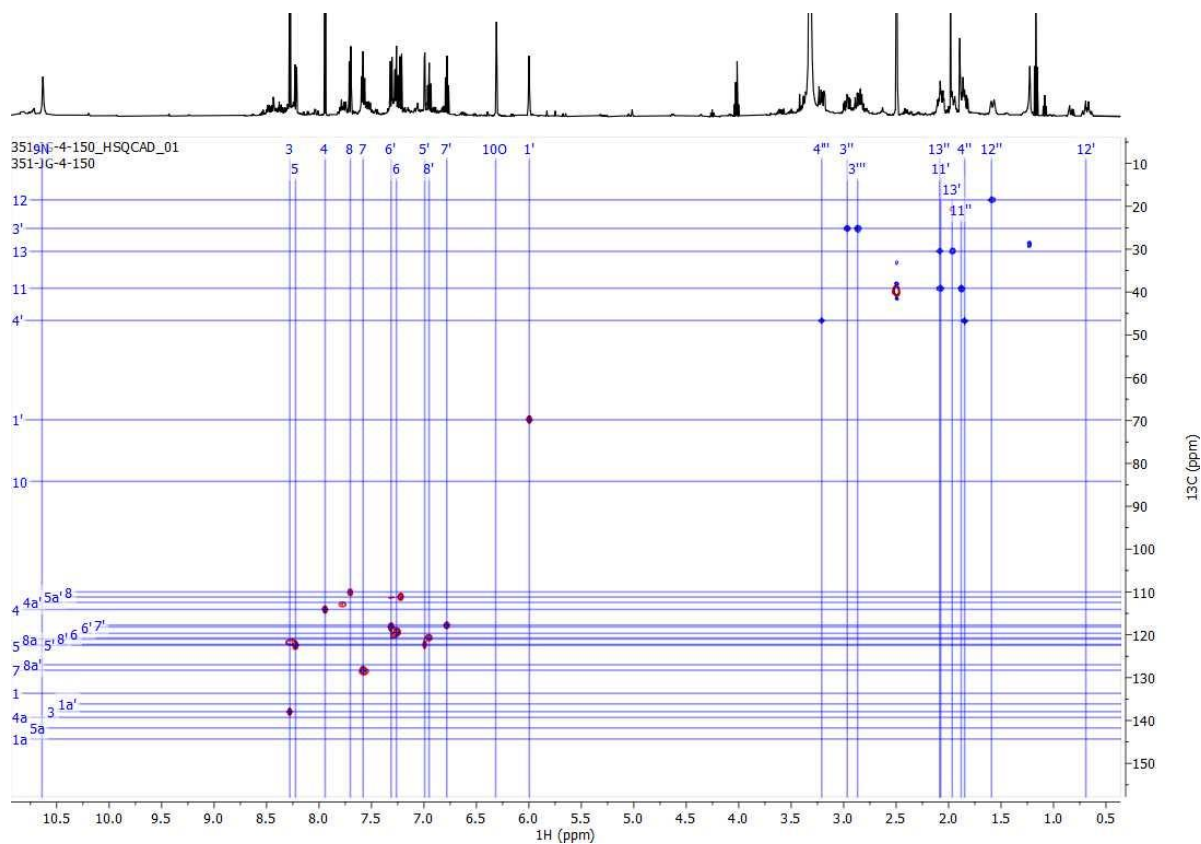
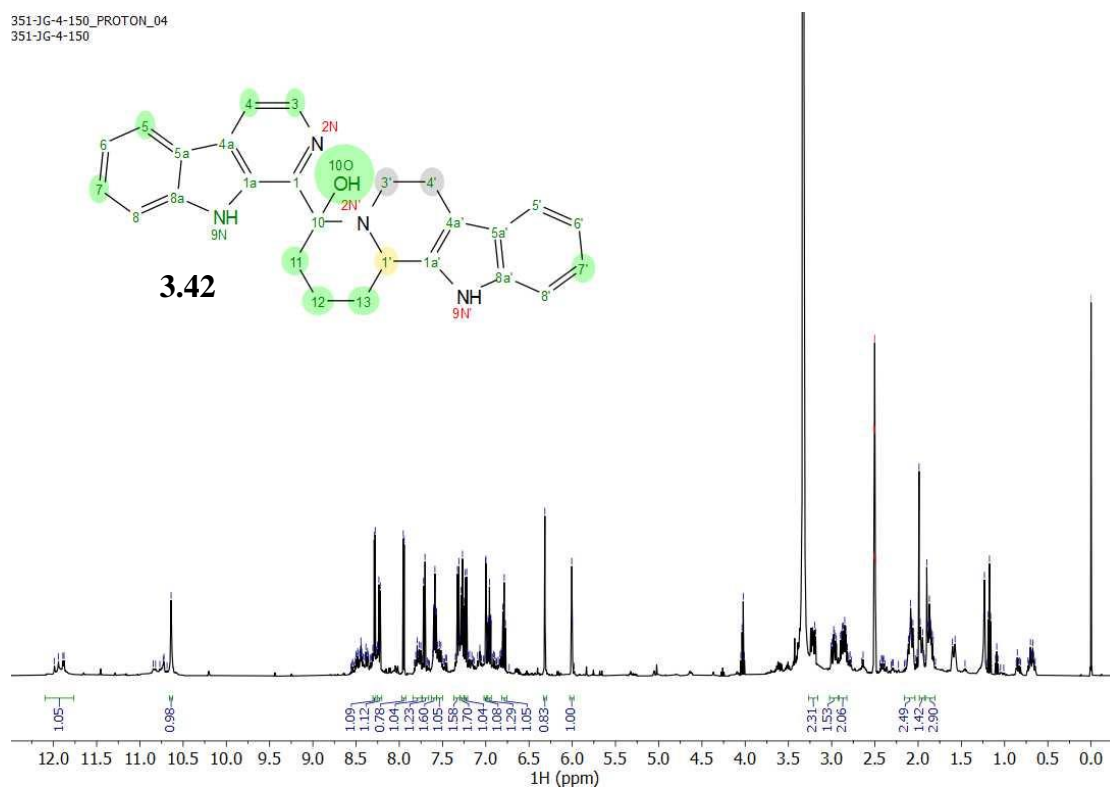


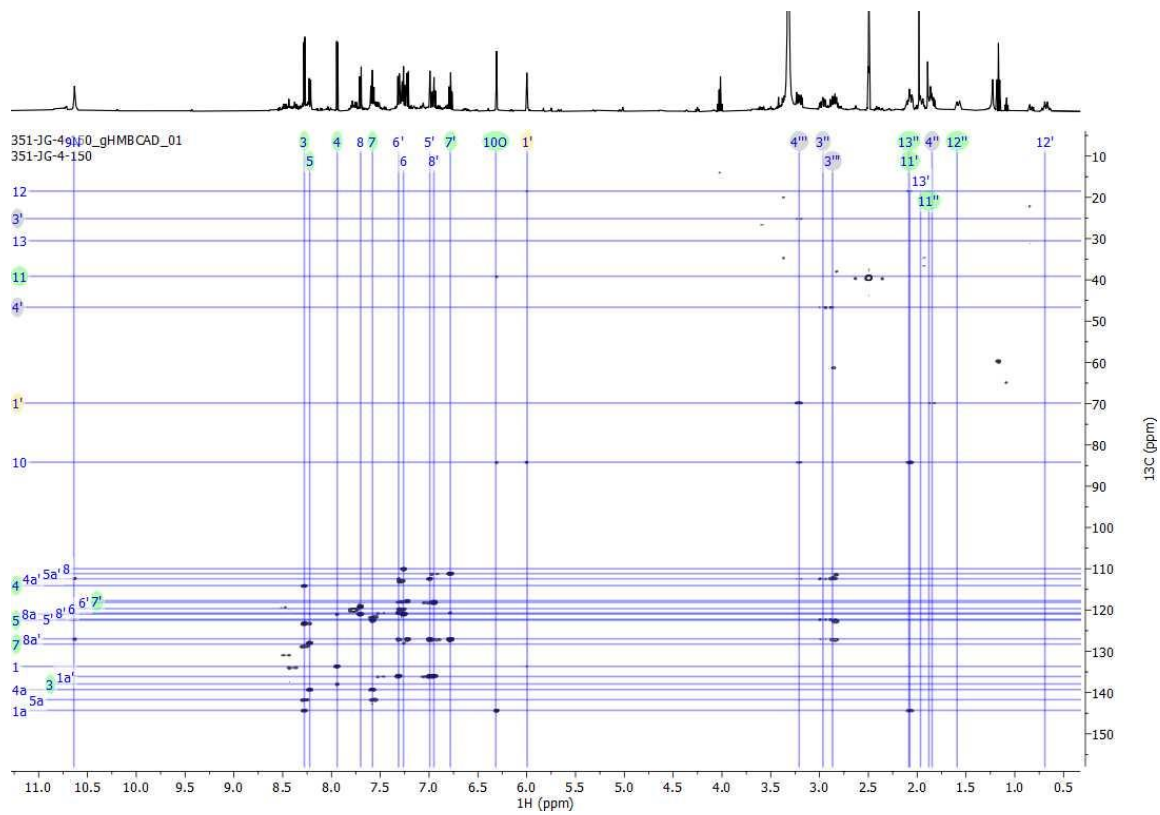
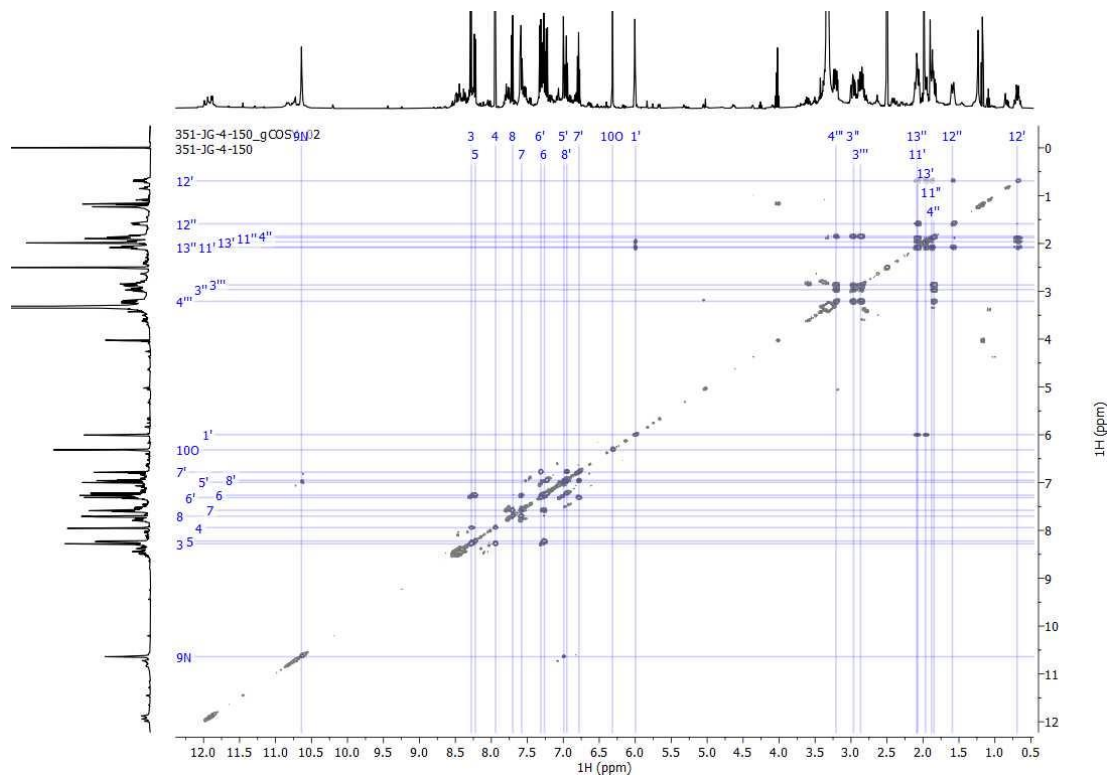
256-JG-3-212\_CARBON\_01  
256-JG-3-212



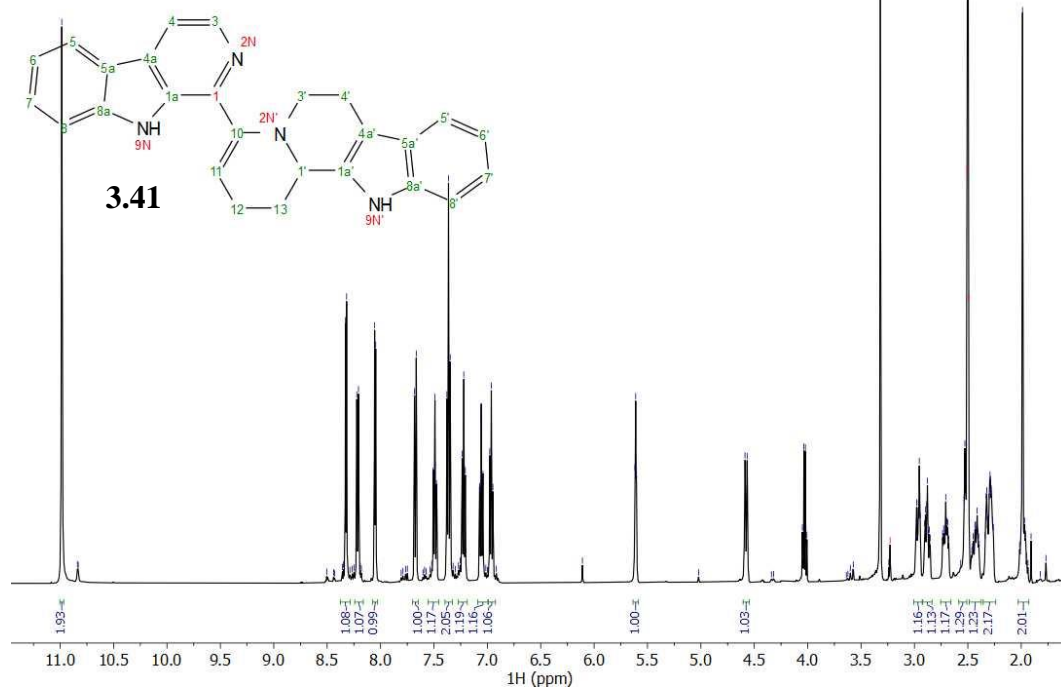


351-JG-4-150\_PROTON\_04  
351-JG-4-150

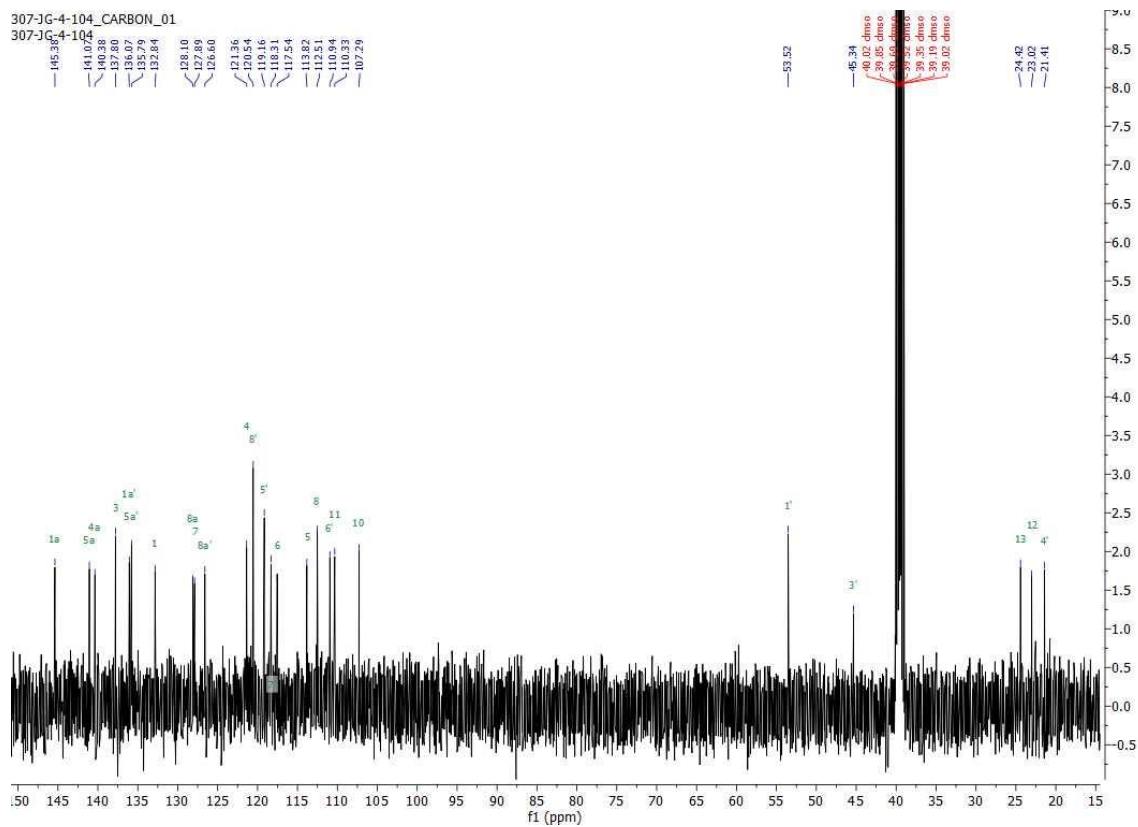




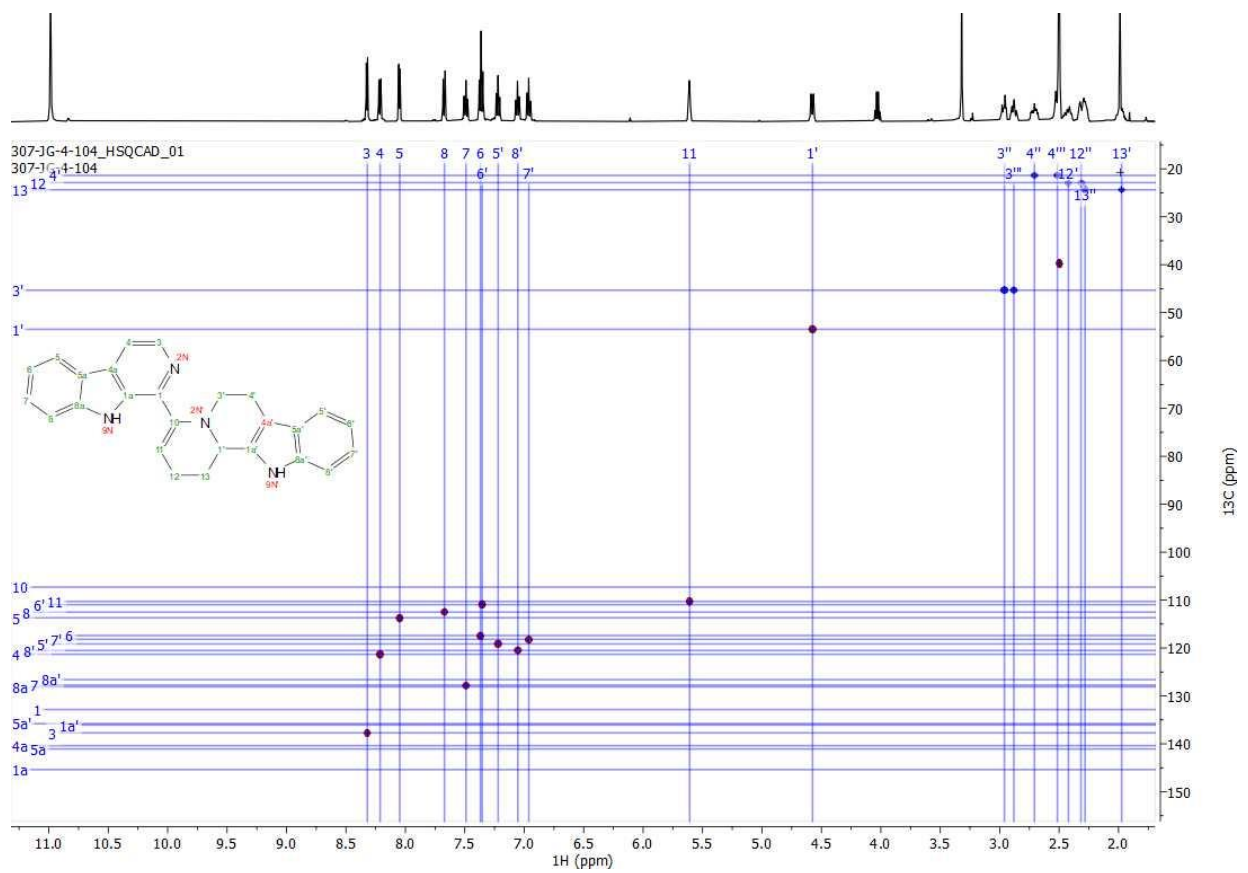
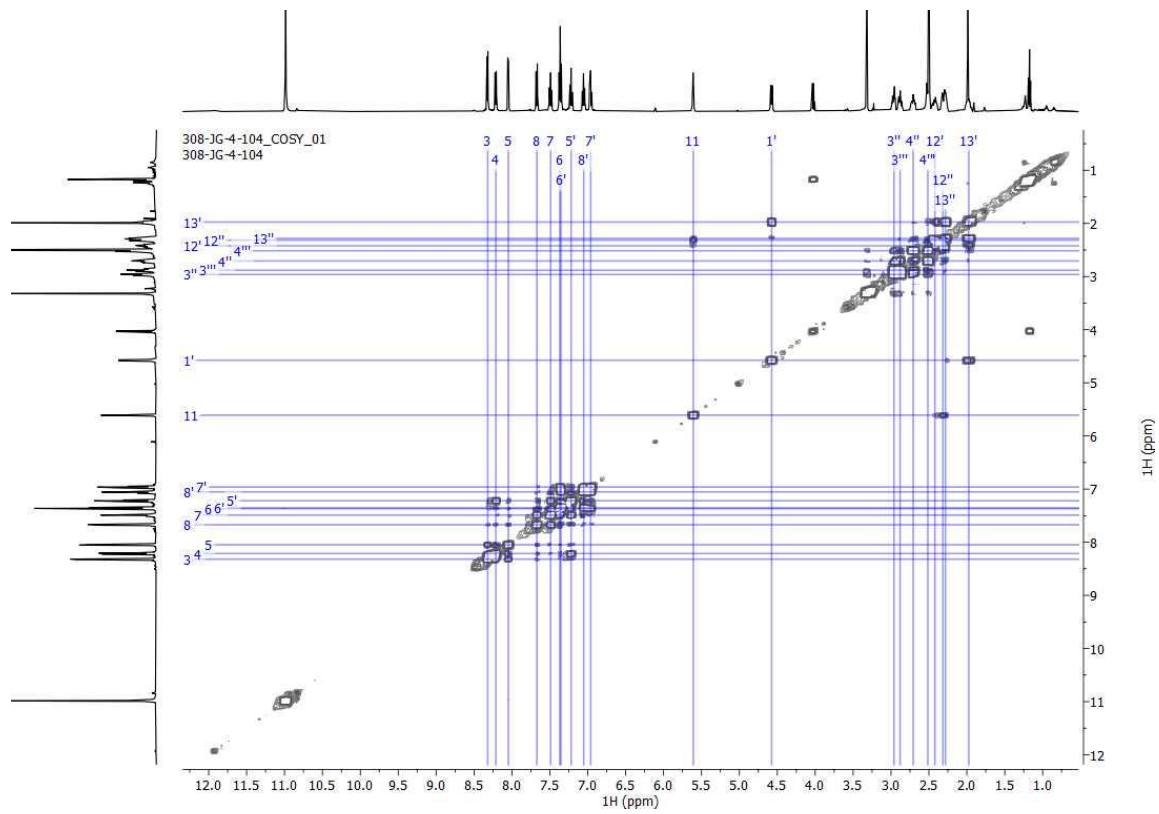
307-JG-4-104\_PROTON\_02  
307-JG-4-104



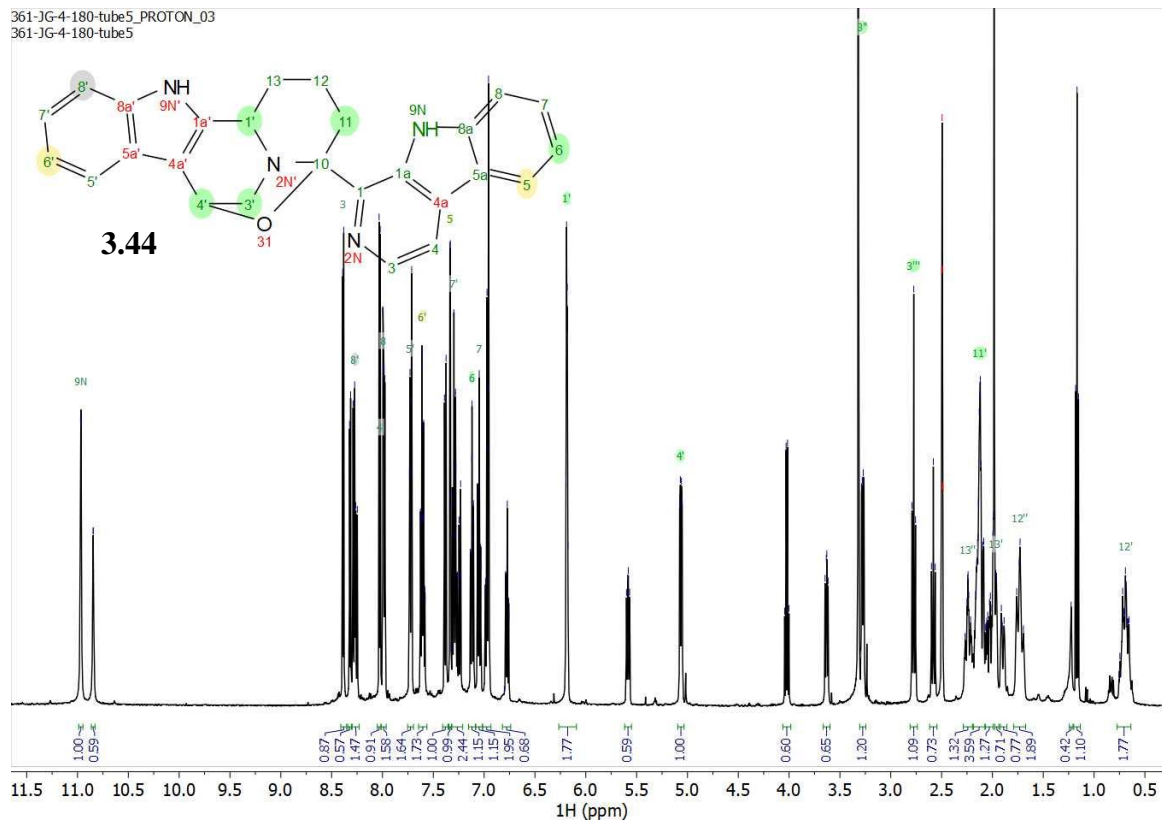
307-JG-4-104\_CARBON\_01  
307-JG-4-104



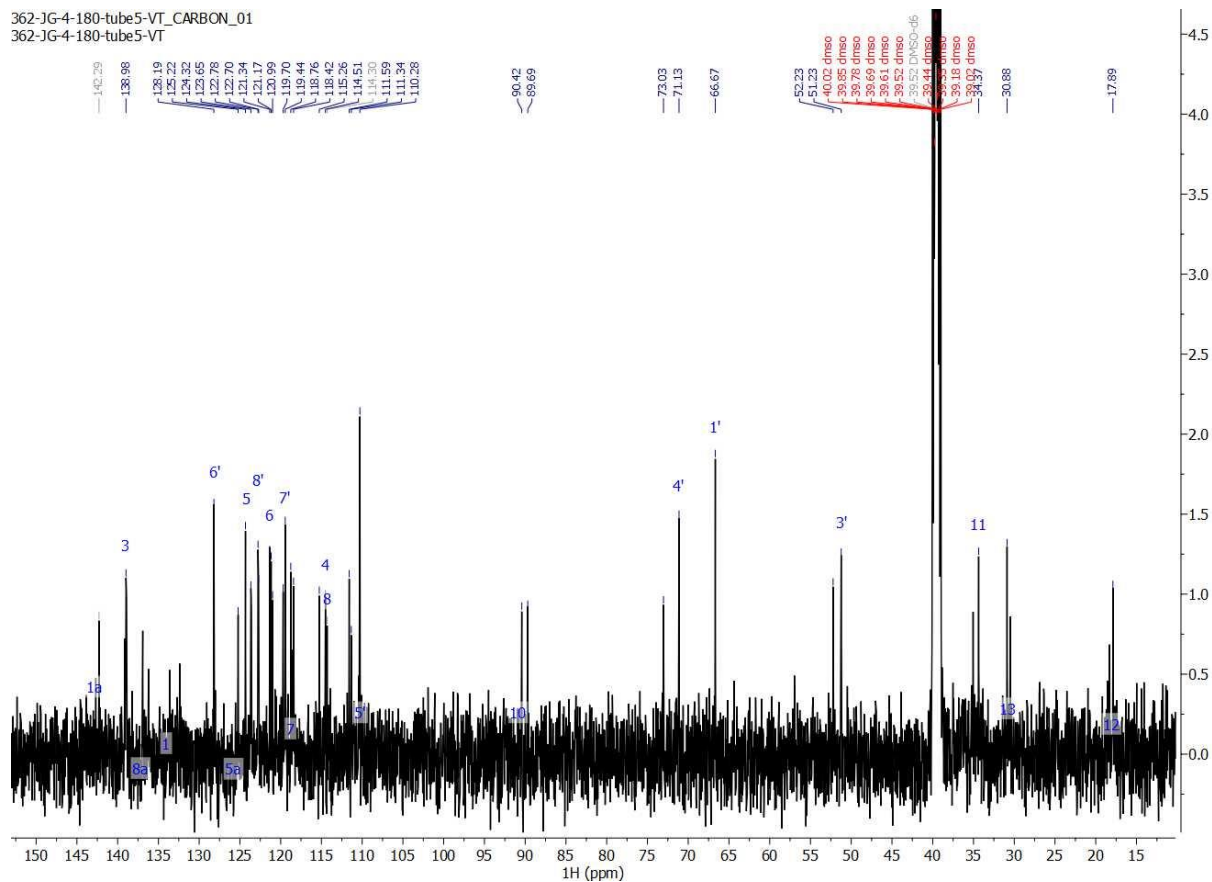


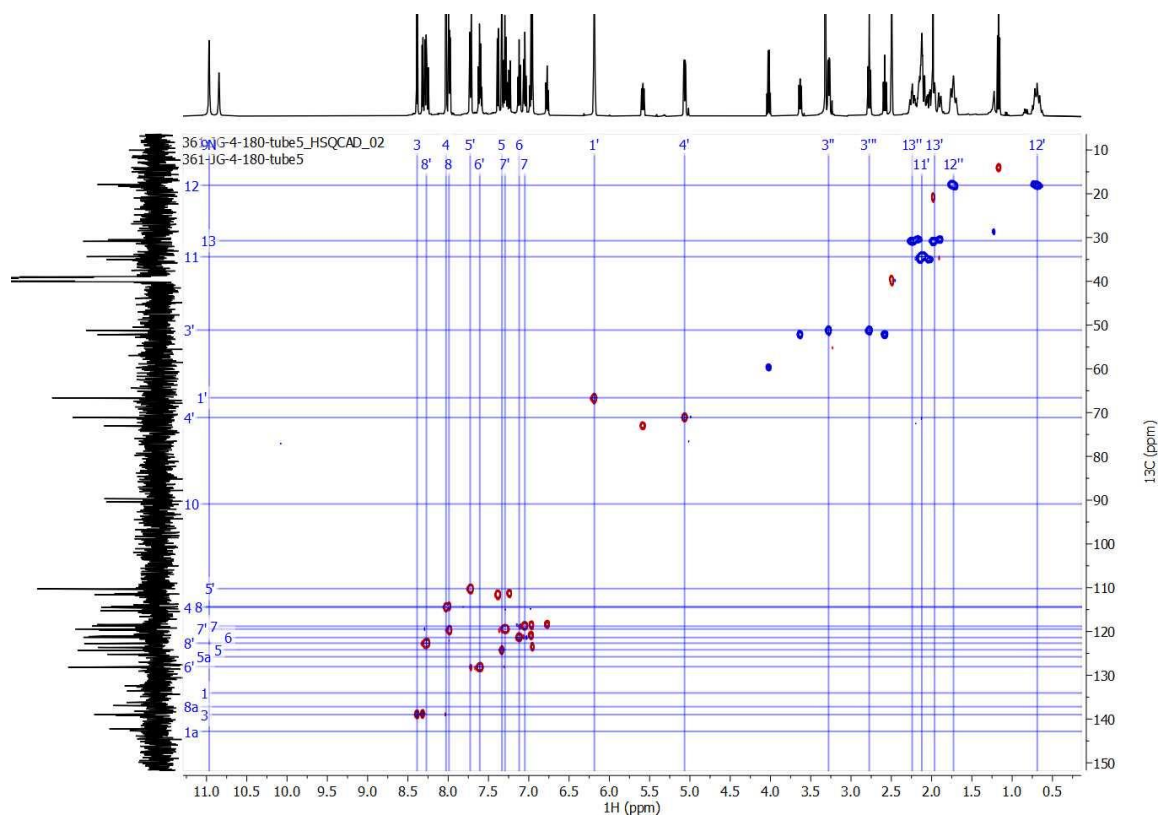
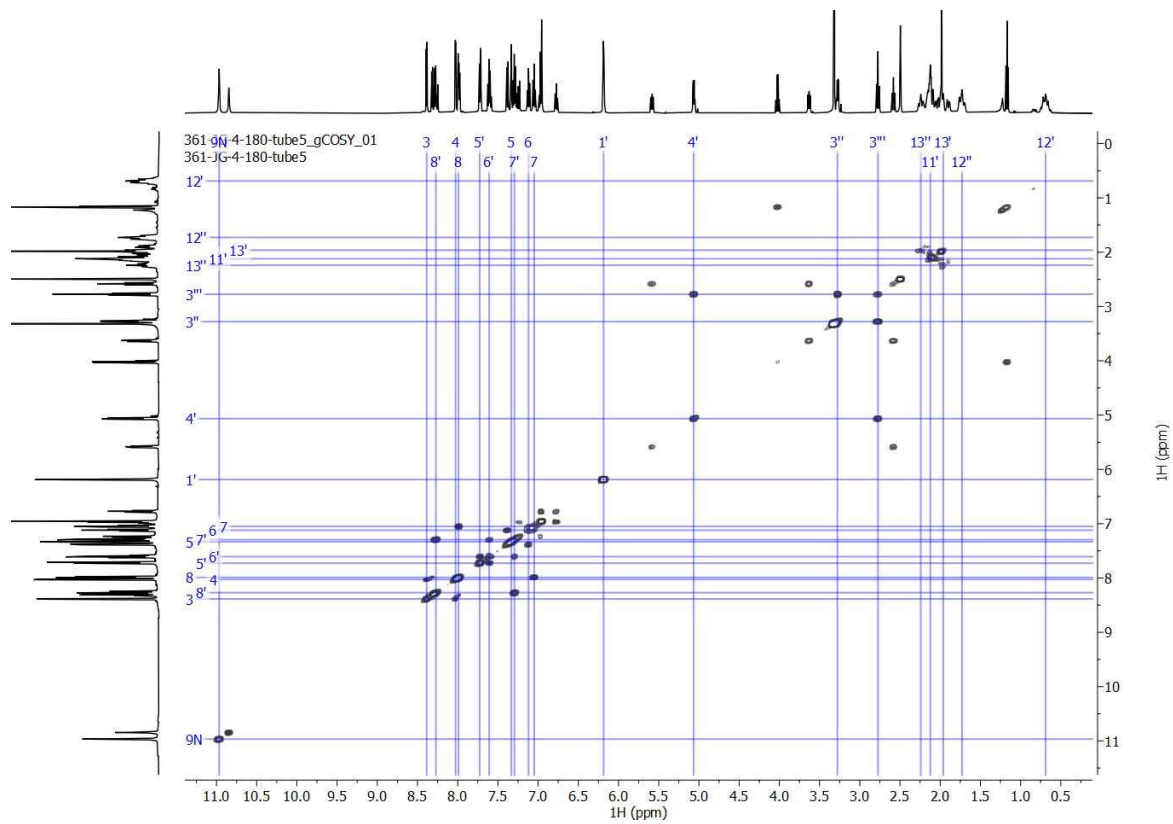


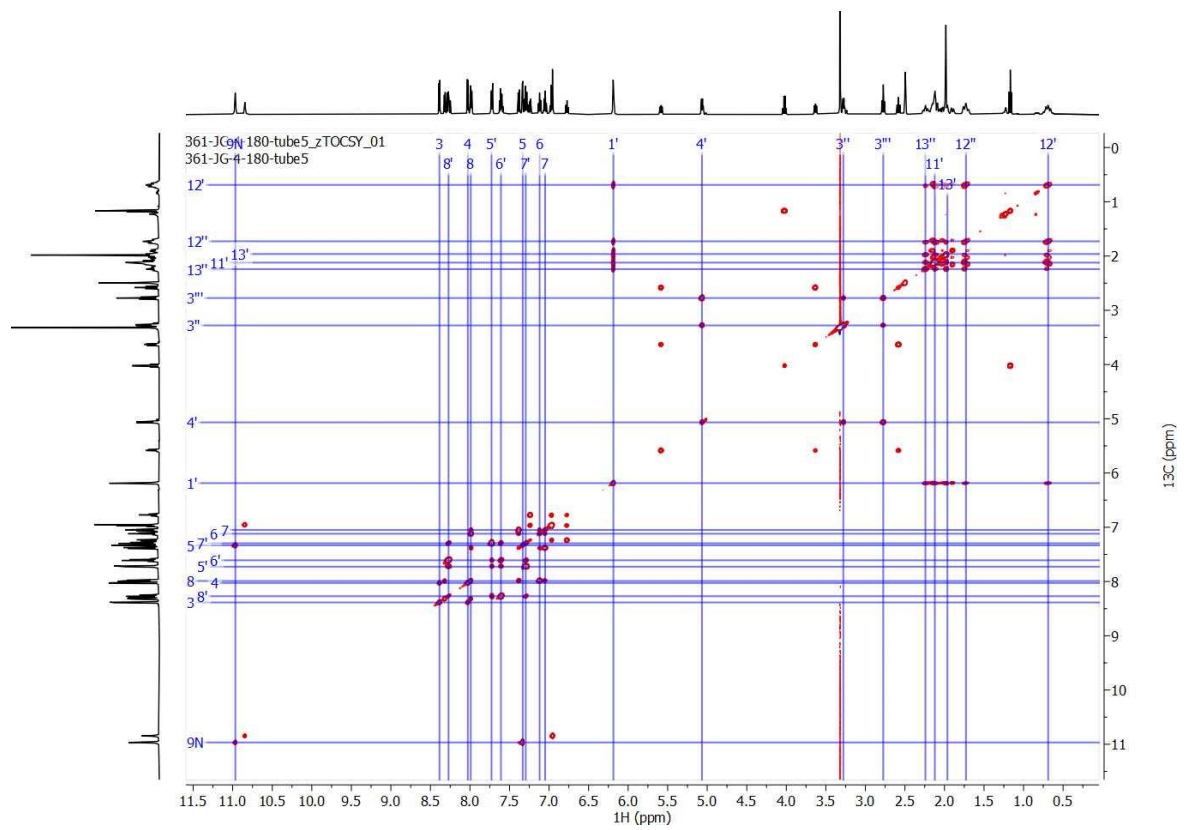
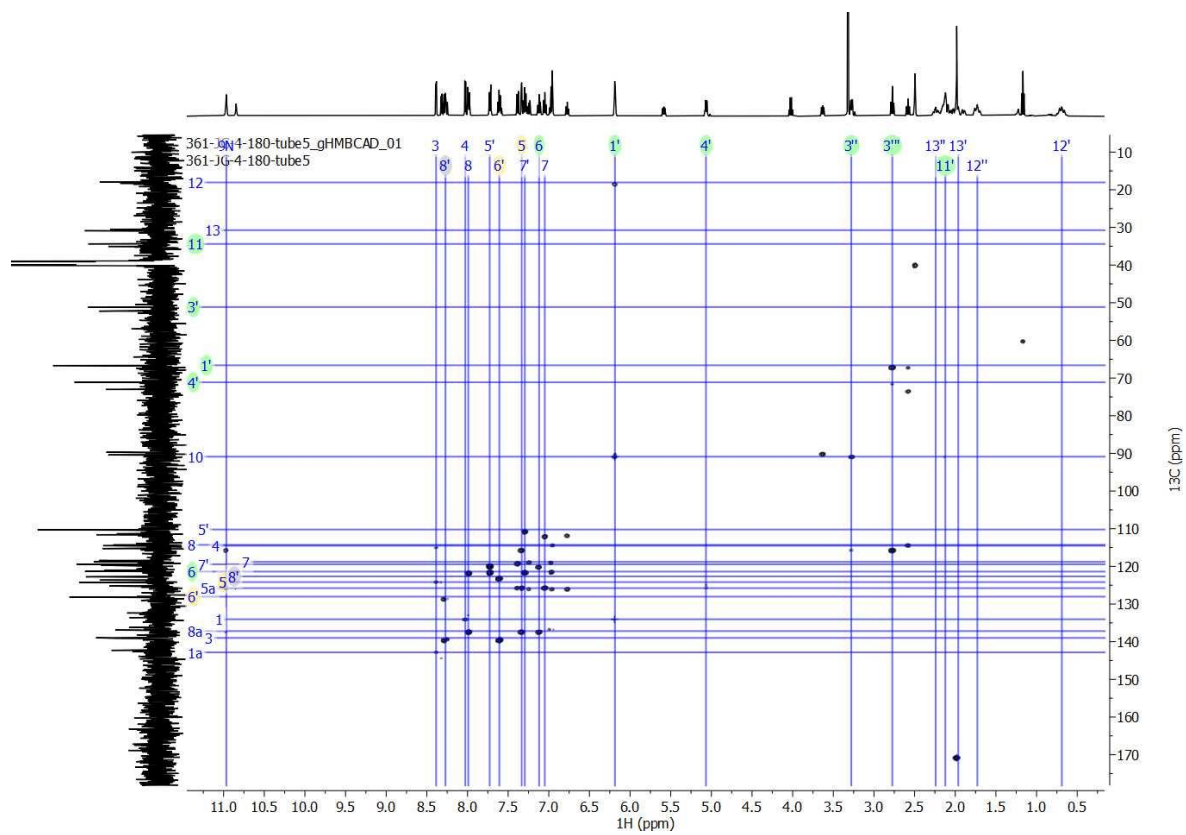
361-JG-4-180-tube5\_PROTON\_03  
361-JG-4-180-tube5

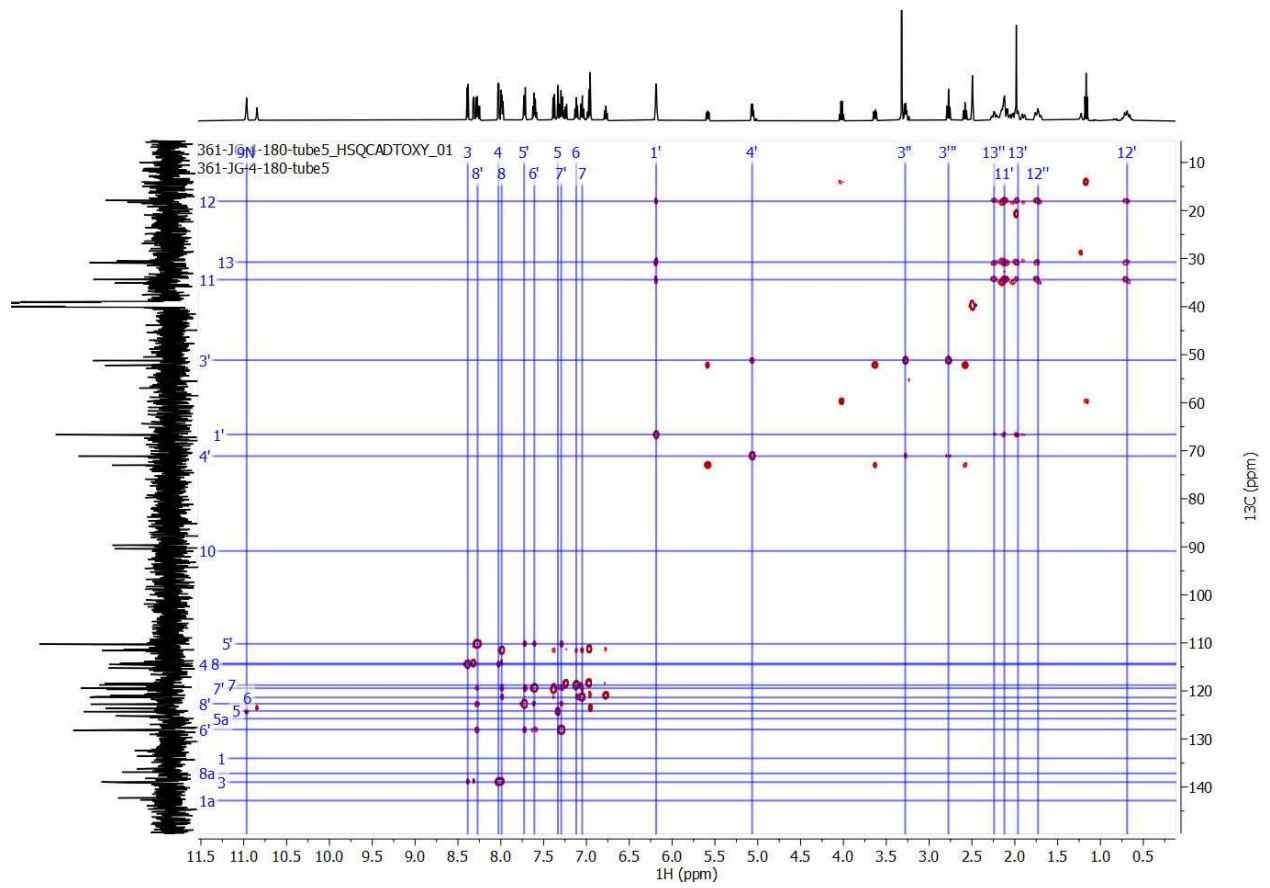


362-JG-4-180-tube5-VT\_CARBON\_01  
362-JG-4-180-tube5-VT









## Chapter 4: SARS-CoV-2 protease inhibitors

**Abstract.** The novel severe acute respiratory syndrome coronavirus 2 (SARS-CoV-2), initially detected in Wuhan City, Hubei province, China on December 31, 2019, quickly took the world by storm. The global death toll from COVID-19 surpassed 200,000 by April 2020, estimating an approximately 5.9% case fatality rate. With the world in turmoil, scientists everywhere fully focused their research efforts to fight this global pandemic, because the need for effective treatment was obvious and immediate. Since our lab had already built a ~300 compound small molecule library with an emphasis on putative protease modulators, and there were significant structural similarities between the compounds in our library and compounds with reported antiviral activity against coronaviruses, we were curious to see if any of our existing compounds were active against SARS-CoV-2. This, along with *in silico* modelling of SARS-CoV M<sup>pro</sup> homologues, inspired our two objectives for this exploratory project aiming to expand the chemical space of anti-coronavirus compounds: (1) screen our existing small molecule library via a phenotypic viral replication inhibition assay, and (2) design and synthesize new SARS-CoV-2 protease inhibitors based on recently published results from fragment-based screens.

**Allocation of Contribution.** I produced the results presented in this chapter with the following exceptions. Existing compounds **4.20 – 4.33, 4.36, and 4.42 – 4.44** from the Duerfeldt lab small molecule library were synthesized by Dr. Ziwei Hu, Mr. Quentin Gibaut, and Mr. Quentin Avila. Compounds **4.20 – 4.44** were sent to Dr. John Tejjaro at the Scripps Research Institute (TSRI) for evaluation in their cellular SARS-CoV-2 infection inhibition assay. Mr. Avila and Ms. Katelyn Stevens participated in writing the grant proposal that funded this project and investigated the piperazine and urea scaffolds, respectively. Docking studies in section 4.2.2 were completed by Mr. Avila.

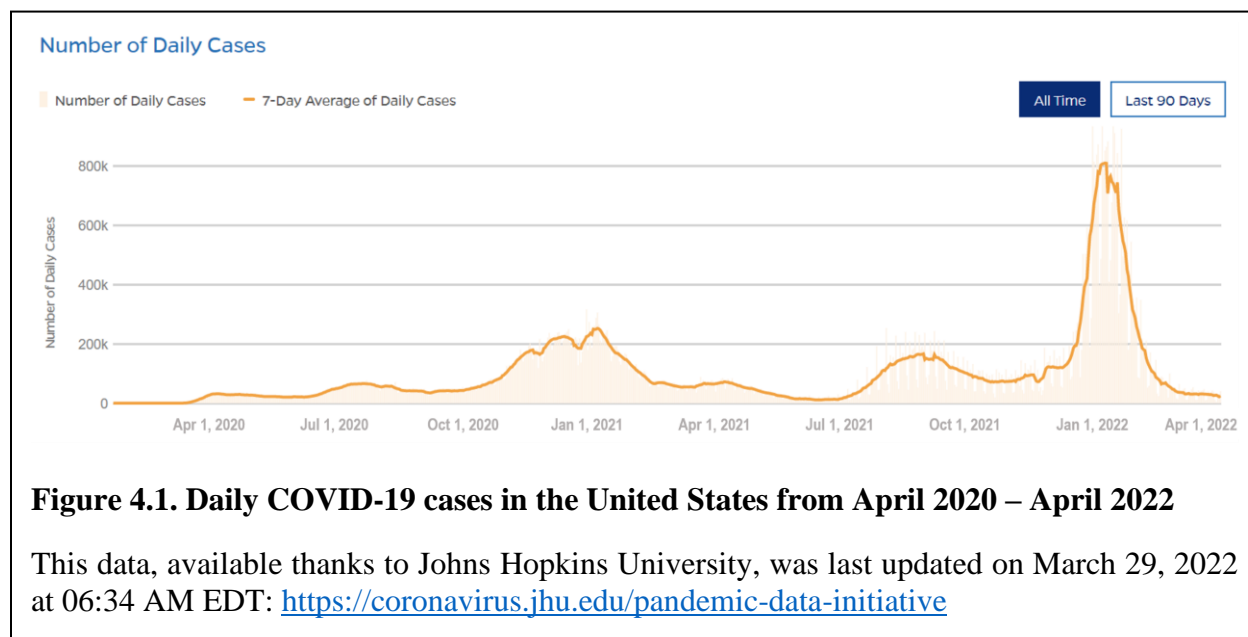
## **4.1 Introduction**

### **4.1.1 SARS-CoV-2 and the COVID-19 global pandemic.**

On March 11, 2020, the World Health Organization (WHO) released a monumental announcement declaring a global pandemic due to the outbreak of the novel severe acute respiratory syndrome coronavirus 2 (SARS-CoV-2). Widespread panic and general unrest immediately ensued as the coronavirus disease 2019 (COVID-19) rapidly spread at alarming rates and reached over 100 countries in less than three months.<sup>1,2</sup> The global death toll from coronavirus disease 2019 (COVID-19) surpassed 200,000 by April 2020, estimating a ~5.9% case fatality rate at the time.<sup>3</sup> As of March 2022, we have been living through this pandemic for over two years, and ~490 million infections have been reported, resulting in over six million deaths.<sup>4</sup> In addition to pervasive infections, economies have been devastated,<sup>5</sup> healthcare systems are vastly overwhelmed,<sup>6</sup> and political dissension is on the rise.<sup>7</sup> Virtually no home has been untouched by the consequences of this pandemic. Emergency department visits for suspected suicide attempts among adolescent girls (12 – 17 years old) increased by 26.2% and 50.6% during the summer and winter months of 2020, respectively, when compared with the corresponding periods in 2019.<sup>8</sup>

With the world in turmoil, scientists everywhere fully focused their research efforts to fight this pandemic, because the need for an effective treatment was obvious and immediate. As several research labs including my own were forced to shut down to eliminate possible exposure and transmission of the airborne virus, scientists everywhere were implored to rally together to fight off the novel coronavirus SARS-CoV-2. For example, the Center for Systems Science and Engineering (CSSE) at Johns Hopkins University in Baltimore, Maryland developed an online interactive dashboard in response to this ongoing public health emergency. The database allows researchers, public health authorities, and the general public to visualize and track reported

COVID-19 cases in real time.<sup>4</sup> The number of cases reported daily in the United States is visualized in Figure 4.1, thanks to their database. You can see in **Figure 4.1** that even after two years into the fight against COVID-19, the United States set their record for highest number of daily cases in January 2022 where 800k – 1.3 million new cases were reported almost every day. This pandemic is not over, and therefore, development of appropriate prevention and treatment techniques is still an ongoing and very worthy endeavor.



On a personal note, when the University of Oklahoma (OU) forced the closure of research labs starting on March 24, 2020, with no plans of reopening, it was the first time in my scientific career where I was incapable and unallowed to continue research. Working from home as a synthetic chemist proved to be rather difficult and, ultimately, unproductive, so when my university generously requested for research proposals to join in the fight against COVID-19, I jumped at the chance of returning to the lab. The Office of the Vice President for Research and Partnerships (OVPRP) at the University of Oklahoma created the COVID-19 Rapid Response Research Seed Grant, offering an opportunity for research groups to contribute to the growing

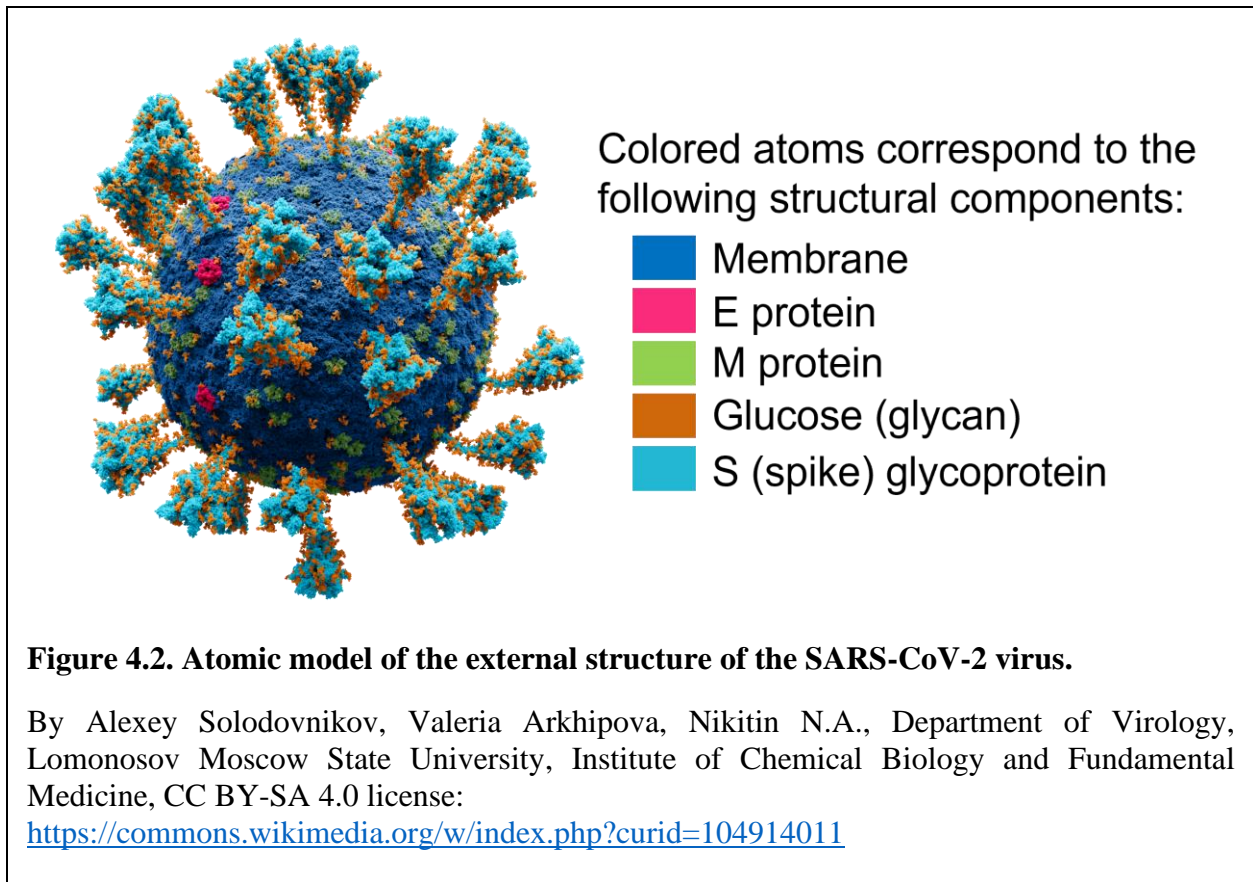


global efforts. My colleagues, Mr. Quentin Avila and Ms. Katelyn Stevens, and I worked together to submit a proposal where we aimed to leverage our lab's expertise in developing small molecule protease modulators to design SARS-CoV-2 main protease (M<sup>Pro</sup>) inhibitors.

Since our lab had already built a ~300 compound small molecule library while developing protease<sup>9</sup> and phosphatase<sup>10</sup> modulators for bacterial targets, we were curious to see if any of our existing compounds were active against SARS-CoV-2. Although bacterial and viral targets exhibit obvious differences and each organism should be studied individually,<sup>11</sup> there were significant structural similarities between the compounds in our library and compounds with reported antiviral activity against coronaviruses (discussed more in-depth in **Section 4.2.1**). This, along with *in silico* modelling of SARS-CoV M<sup>Pro</sup> homologues (discussed more in-depth in **Section 4.2.2**), inspired us to expand the chemical space of the current arsenal of coronavirus-active drugs. Our strategy consisted of two objectives: (1) screen our existing small molecule library via phenotypic viral replication inhibition assays, and (2) design and synthesize new SARS-CoV-2 protease inhibitors through a fragment-based approach.

#### **4.1.2 Learning from older coronaviruses: potential antiviral targets.**

Coronaviruses have been a major public health concern since the beginning of the 21<sup>st</sup> century because of the highly contagious and lethal respiratory diseases they cause. Named after their crown-like appearance, coronaviruses are positive sense, single stranded RNA viruses that cause disease in mammals and birds.<sup>12</sup> There are seven reported human coronaviruses, and each are predominantly transmitted through respiratory droplets, allowing for easy human-to-human transmission.<sup>13</sup> Structurally, the coronavirus nucleocapsid (N) protein, involved in packaging the RNA genome, is enveloped by a lipid bilayer that anchors the membrane (M), envelope (E), and spike (S) proteins (**Figure 4.2**).<sup>14</sup>



The first serious coronavirus outbreak appeared in 2003 in southern China.<sup>15</sup> It was identified as severe acute respiratory syndrome coronavirus (SARS-CoV) and soon infected ~8,000 people in >30 countries over 5 continents with a crude fatality rate of ~10%.<sup>16</sup> Afterwards, in 2012, another outbreak caused by Middle East respiratory syndrome coronavirus (MERS-CoV) was first isolated from a patient with severe pneumonia and acute renal failure in Saudi Arabia.<sup>17</sup> MERS-CoV eventually spread to 27 countries, where 2,279 cases were reported to WHO with a ~35% fatality rate by 2015.<sup>18,19</sup> The newest coronavirus, SARS-CoV-2, shares ~85% sequence homology with the 2003 SARS-CoV genome<sup>20</sup> and ~50% sequence homology with MERS-CoV genome.<sup>21</sup> Clinical presentation of COVID-19 also seem to resemble SARS-CoV infections.<sup>22</sup>

Since SARS-CoV-2 exhibits significant homology to previous variants, along with the availability of its genome sequence,<sup>23</sup> *in silico* modeling and computational drug screening proved

to be a useful technique to accelerate drug discovery programs. To advance our efforts even more quickly, drugs either already approved by the Food and Drug Administration (FDA) or currently in the pipeline provided a suitable starting point. A number of both viral proteins and host receptors have been explored as anti-coronavirus drug targets. The role that each target candidate plays in viral infection and the structures of their drug candidates are shown in **Table 4.1** and **Figure 4.3**, respectively. To avoid off-target interactions, we decided to focus our efforts on viral protein target candidates over host proteins.

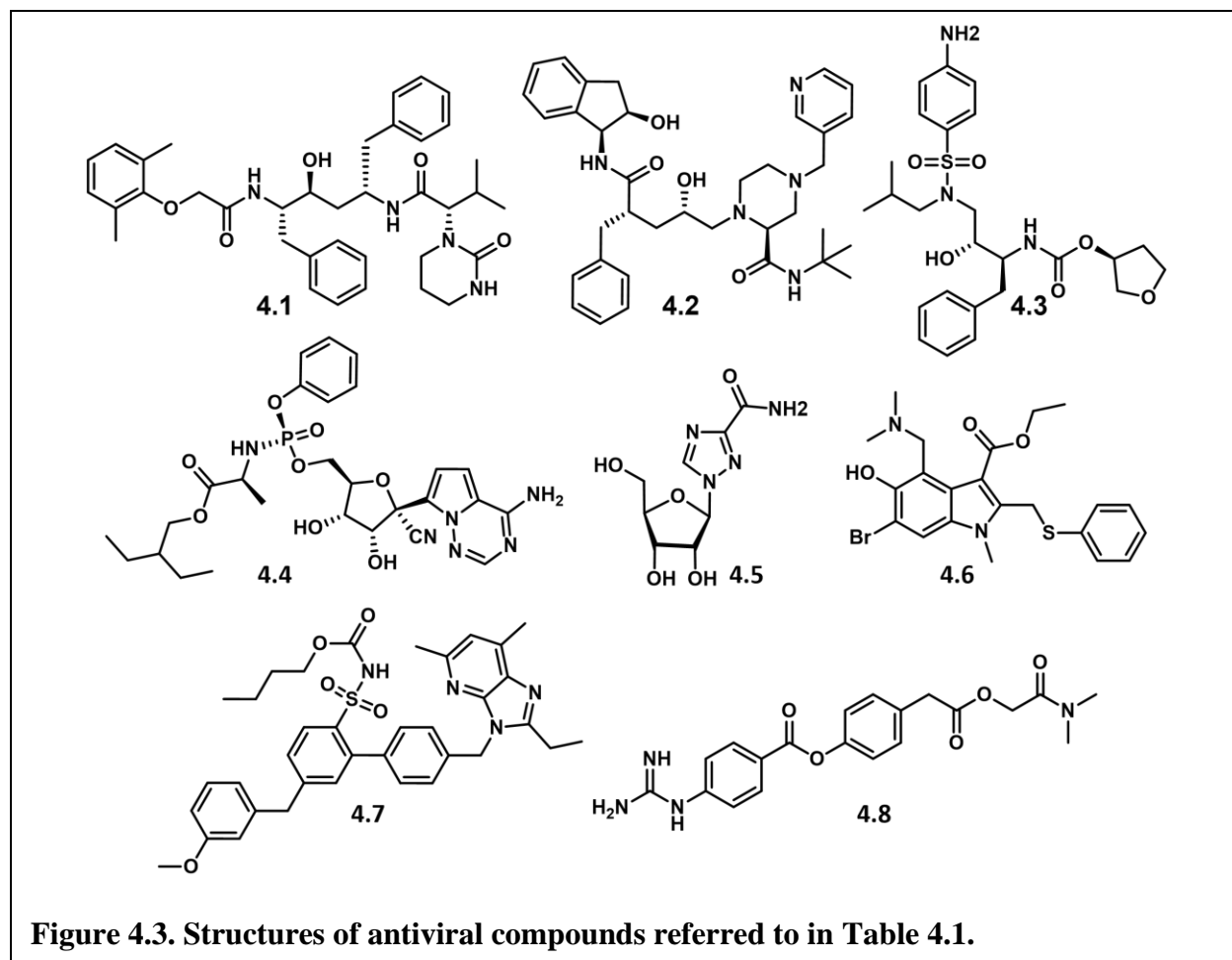
**Table 4.1. Potential targets for SARS-CoV-2 chemotherapeutics.**

Target Candidate	Full Name	Role in Viral Infection	Drug Candidate
<i>viral targets</i>			
3CL <sup>pro</sup> / M <sup>pro</sup>	3-chemotrypsin-like or main protease	proteolysis of viral polyproteins, assists in cellular entry	lopinavir ( <b>4.1</b> ) <sup>24</sup>
PL <sup>pro</sup>	papain-like protease	proteolysis of viral polyproteins, assists in cellular entry	indinavir ( <b>4.2</b> ), <sup>25</sup> amprenavir ( <b>4.3</b> ) <sup>26</sup>
RdRp	RNA-dependent RNA polymerase	involved in replicating viral genome	remdesivir ( <b>4.4</b> ), <sup>27</sup> ribavirin ( <b>4.5</b> ) <sup>28</sup>
S protein	spike glycoprotein	mediates cellular entry and has high affinity to the ACE2 receptor	umifenovir ( <b>4.6</b> ) <sup>29</sup>
<i>host (human) targets</i>			
ACE2	angiotensin-converting enzyme 2	Receptor with high affinity for the S protein	umifenovir ( <b>4.6</b> ) <sup>30</sup>
AT <sub>2</sub> R	angiotensin II receptor	effector involved in body fluid balance and electrolyte homeostasis	L-163491 ( <b>4.7</b> ) <sup>31</sup>
TMPRSS2	transmembrane protease, serine 2	activates viral glycoproteins to facilitate S protein and ACE2 binding	Camostat ( <b>4.8</b> ) <sup>32</sup>

The spike (S) protein, for example, is integral to cellular entry and host infection and is one of the targets under investigation for antiviral drug discovery, especially for antibody

neutralization approaches. The S protein binds to the receptor on the target cell and is the sole viral membrane protein responsible for cell entry.<sup>33</sup> A defined receptor-binding domain (RBD) of the SARS-CoV spike specifically recognizes the angiotensin-converting enzyme 2 (ACE2) receptor in its host. There are 14 residues in the RBD that participate in ACE2 binding, of which 9 are fully conserved and 4 are partially conserved among SARS-CoV and SARS-CoV-2.<sup>34</sup> This minor genetic variance enabled SARS-CoV-2 to efficiently bind to the receptor with enhanced affinity and specificity to human ACE2, improving the virulence compared to SARS-CoV.<sup>21</sup> Overall, the sequence similarity between the SARS-CoV and SARS-CoV-2 spike proteins is ~73 – 76% for the RBD and ~76 – 78% for the whole S protein.<sup>34</sup>

Notably, umifenovir (**4.6**), sold under the brand name Arbidol, exhibits activity for both viral and host targets: the S protein and ACE2, respectively (**Table 4.1**). **4.6** is a broad-spectrum antiviral medication used in Russia and China to treat influenza, coronavirus, and adenovirus, among others.<sup>35</sup> Molecular dynamics simulations by Tripathi et al. helped to elucidate the mechanism of S protein and ACE2 complex (S-ACE2) binding interface disruption by umifenovir.<sup>30</sup> Their results suggested that **4.6** has higher binding affinity to the S-ACE2 interface over the separated S protein and ACE2 receptor. Since the S protein plays an integral role in host infection, and S protein-targeting drugs such as **4.6** also induce the production of interferon and lymphocytes,<sup>36</sup> there is a high safety risk when developing S protein-active compounds. Thus, we decided against pursuing the S protein as a target of interest in this project.



Two proteases within the SARS-CoV-2 genome were more attractive targets for our compounds, especially since several compounds in our small molecule library engage bacterial protease targets. The SARS-CoV-2 genome encodes two polyproteins, pp1a and pp1ab, and four structural proteins.<sup>37</sup> The polyproteins are cleaved by proteases for the generation of non-structural proteins essential for viral replication.<sup>38</sup> These two proteases involved in viral replication are the main protease ( $M^{pro}$ ), which is frequently also called 3-chymotrypsin-like protease ( $3CL^{pro}$ ),<sup>3</sup> and the papain-like protease ( $PL^{pro}$ ).<sup>39</sup> A comparison of the MERS-CoV, SARS-CoV, and SARS-CoV-2  $M^{pro}$  sequence revealed that the SARS-CoV-2  $M^{pro}$  is 96% and 51% similar to SARS-CoV and MERS-CoV, respectively.<sup>40</sup> Our preliminary work towards expanding the chemical space of coronavirus protease inhibitors of  $M^{pro}$  will be discussed in this chapter.

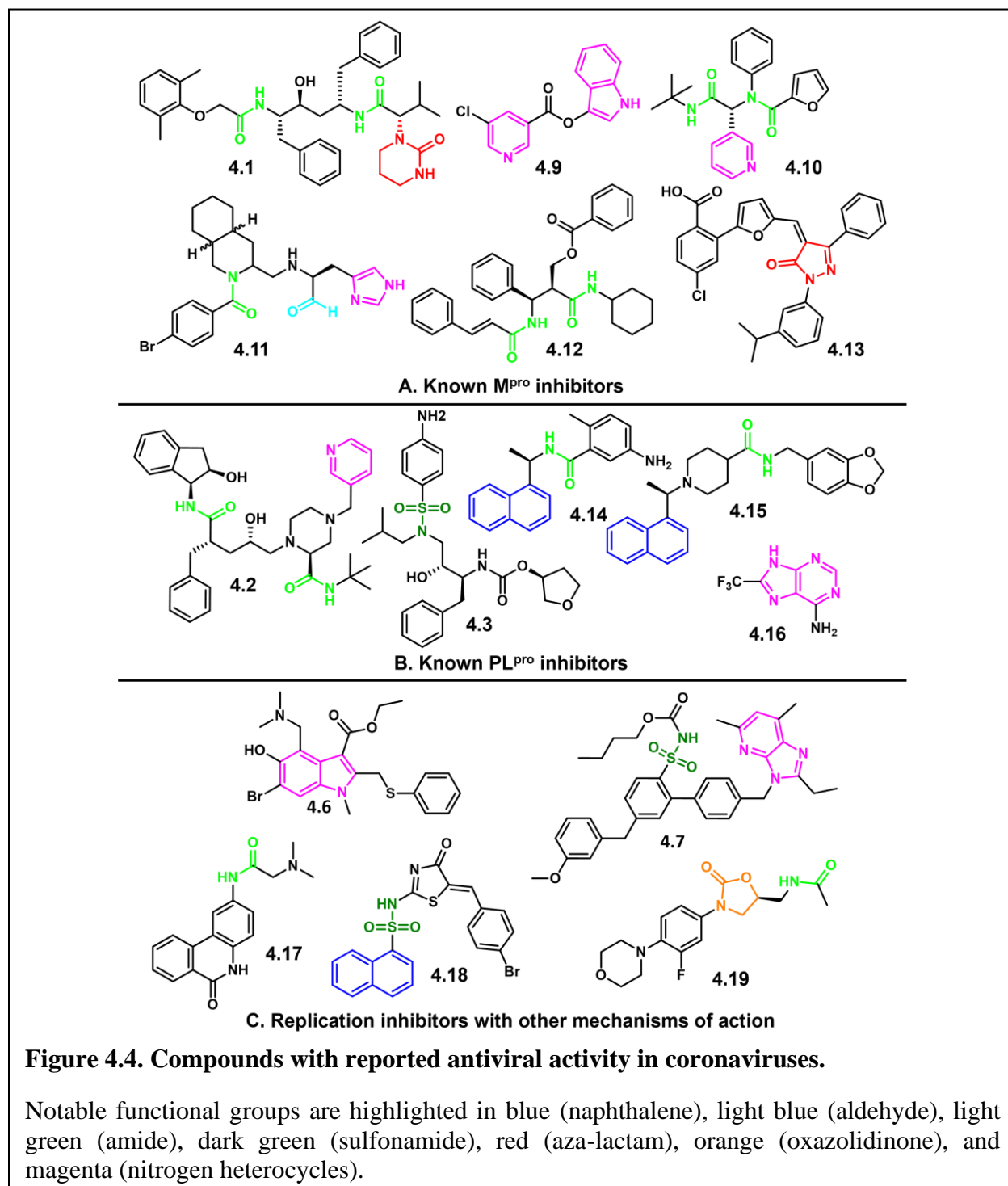
## 4.2 Results and discussion

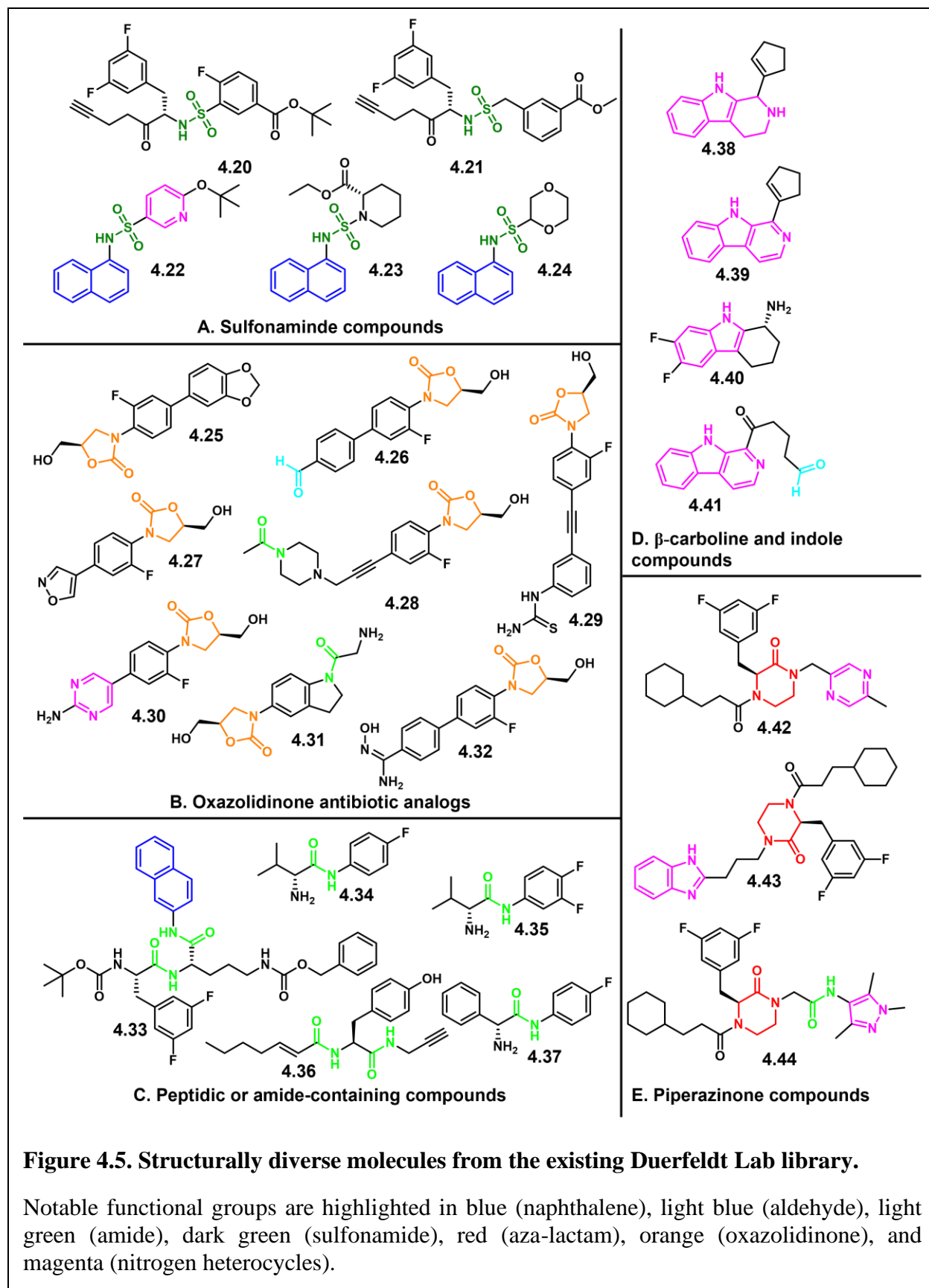
### 4.2.1 Structural comparisons inspire viral replication inhibition screen of existing compounds in the Duerfeldt lab library.

Several known coronavirus M<sup>pro</sup> and PL<sup>pro</sup> inhibitors contain structural similarities to existing compounds in the Duerfeldt lab small molecule library. We hypothesized that screening a representative subset of our compound library, which features structurally diverse scaffolds, some of which include chemotypes identified in reported screens,<sup>41,42</sup> could potentially expand the chemical space being explored in the search of SARS-CoV-2 replication inhibitors. Some representative examples of anti-coronavirus compounds are shown in **Figure 4.4**. The rationale behind our motivation for submitting compounds from our library to evaluate for viral replication inhibition is described herein.

The M<sup>pro</sup> inhibitors include antiretrovirals typically prescribed for human immunodeficiency virus (HIV) such as lopinavir (**4.1**) in combination with ritonavir (structure not shown), which inhibits M<sup>pro</sup> activity of both SARS-CoV and MERS-CoV.<sup>43</sup> However, in a systematic review of randomized controlled trials employing lopinavir-ritonavir in COVID-19 patients found that this combination did not improve mortality rate and exhibited a significantly high risk of adverse events when compared to supportive care or placebo.<sup>44</sup> Additionally, chloropyridyl ester **4.9** exhibits SARS-CoV M<sup>pro</sup> enzymatic inhibitory activity (IC<sub>50</sub> = 30 nM),<sup>45</sup> but was found to have inconsistent cellular stability in cell-based assays.<sup>46</sup> **4.13** is also a neuraminidase inhibitor for influenza and has been explored as a broad-spectrum antiviral.<sup>38</sup> Notably, **4.1** is a peptide-based structure that includes a key pyrimidinone moiety, and **4.13** contains a pyrazolone core, both of which fall under the aza-lactam structural umbrella (red,

**Figure 4.4A).** Similarly, the aza-lactam scaffold within the piperazinone compounds in our library motivated us to submit compounds **4.42 – 4.44** (**Figure 4.5E**) for biological evaluation.







Amide-containing compounds **4.10**, **4.11**, and **4.12** are representative examples of peptidomimetic M<sup>pro</sup> inhibitors.<sup>47,48</sup> Other peptide-like anti-coronavirus compounds include PL<sup>pro</sup> inhibitors **4.2** and **4.14 – 4.15**. Naphthalene amides **4.14** and **4.15** exhibit potent SARS-CoV PL<sup>pro</sup> activity where IC<sub>50</sub> = 0.60 and 0.67 μM, respectively.<sup>49</sup> Interestingly, they did not show any inhibitory activity against MERS-CoV PL<sup>pro</sup>, suggesting that inhibitor recognition specificity of MERS-CoV and SARS-CoV PL<sup>pro</sup> may differ significantly.<sup>50</sup> The peptide-like nature of these coronavirus protease inhibitors motivated us to submit amide-containing compounds **4.33 – 4.37** from our library for biological evaluation (**Figure 4.5C**).

Markedly, several nitrogen-containing heterocycles (magenta, **Figure 4.4**) can be found in a number of anti-coronavirus compounds. For example, **4.16** is a trifluoromethyl derivative of purine that was first synthesized in 1958 as a potent anti-cancer drug,<sup>51</sup> but was also found to be a non-selective PL<sup>pro</sup> inhibitor during a high-throughput screen of 25,000 compounds with similar inhibitory strength for both SARS- and MERS-CoV.<sup>50</sup> This, in addition to the diverse nitrogen heterocycles within compounds **4.6**, **4.7**, and **4.9**, led to our submission of indole and β-carboline compounds (**Figure 4.5D**) for biological evaluation.

Other notable functional groups include naphthalenes (blue, **Figure 4.4**), which can be found in a number of compounds in our library, and sulfonamide (dark green, **Figure 4.4**) derivatives which are structurally similar to compounds **4.20 – 4.24** from our library (**Figure 4.5A**). Specifically, compound **4.18** exhibits an under-characterized anti-coronavirus mechanism,<sup>52,53</sup> but it is remarkably similar in structure to our naphthyl-sulfonamide compounds **4.22 – 4.24**. Finally, linezolid (**4.19**), an oxazolidinone antimicrobial<sup>54</sup> that generally inhibits protein synthesis,<sup>55</sup> was recently found to effectively treat pneumonia symptoms in COVID-19

patients.<sup>56</sup> Our lab has recently developed a number of oxazolidinone analogs, thus motivating us to include compounds **4.25** – **4.32** in our viral replication inhibition evaluation (**Figure 4.5B**).

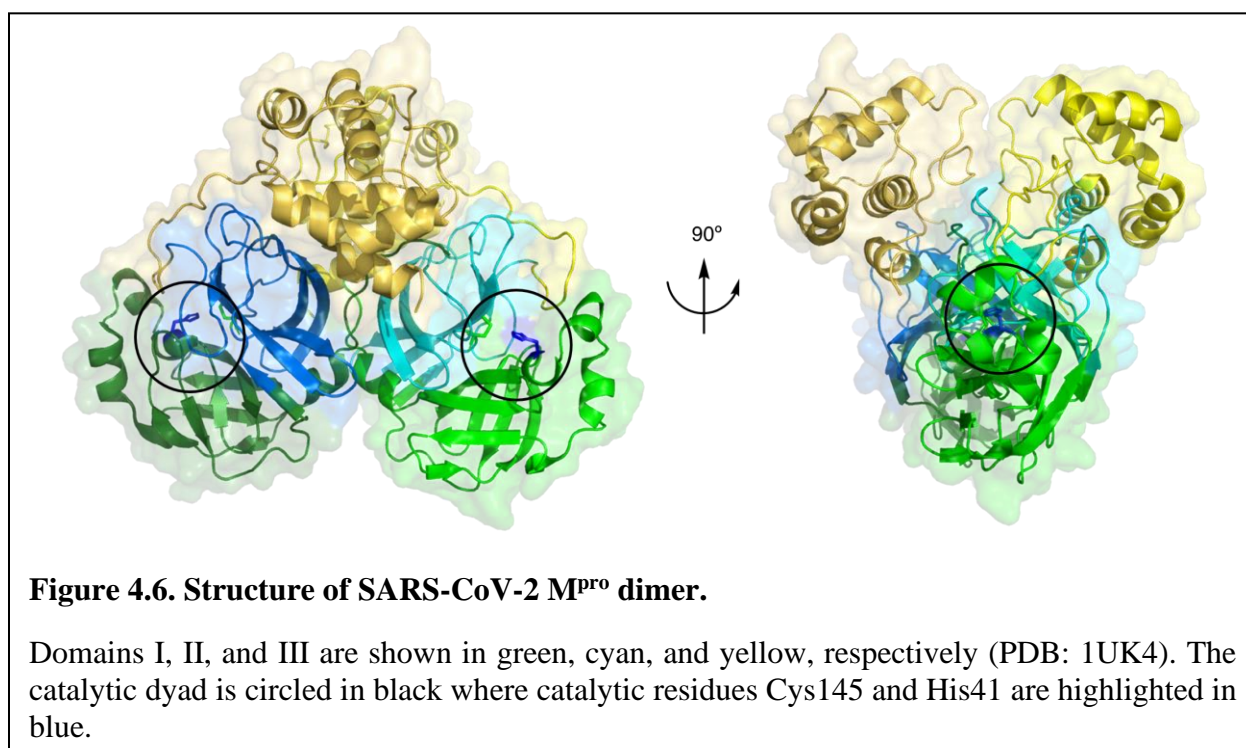
Overall, we planned to screen our ~300 compound library for replication inhibition activity of SARS-CoV-2. To start, 25 compounds (**4.20** – **4.44**) were sent to Dr. John Teijaro at the Scripps Research Institute (TSRI) for evaluation in an established phenotypic cellular assay.<sup>57</sup> In this assay, VeroE6 cells were plated in 384-well plates at a concentration of 5000 cells per well. Compounds (initial concentration of 1  $\mu$ M) were added to the wells concomitantly with SARS-CoV-2. The virus, isolated from a patient's sputum in San Diego, California, was added to the wells at a multiplicity of infection (MOI) of 0.1. Over the course of 3 days, morphological changes in cells were monitored daily to determine viral cytopathic effect (CPE). On day 3, CPE was quantified by microscopy and cell titer glo viability staining. Remdesivir and hydroxychloroquine were used as controls because of their reported anti-coronavirus activity.<sup>58,59</sup> We intended to follow up compounds which were identified to prevent CPE with plaque-forming assays to quantify viral loads, perform pharmacokinetic analyses, and more sophisticated *in vitro* and *in vivo* animal models.<sup>60</sup> Unfortunately, all of our submitted compounds were found to be inactive. This, along with the deprioritizing of our project by Scripps due to the overwhelming demand on their facilities, prevented further screening of our library.

#### **4.2.2 Structure and function of M<sup>Pro</sup> provides insights for the rational design of M<sup>Pro</sup> inhibitors.**

Since the coronavirus PL<sup>Pro</sup> is involved in regulation of host interferon and nuclear factor  $\kappa$ B (NF- $\kappa$ B) pathways,<sup>61</sup> and dysregulation of NF- $\kappa$ B can lead to inflammatory diseases and tumorigenesis,<sup>62</sup> it is possible that PL<sup>Pro</sup> inhibitors might lead to more off-target downstream (and potentially detrimental) effects. With recent reports on the positive safety profiles of M<sup>Pro</sup>

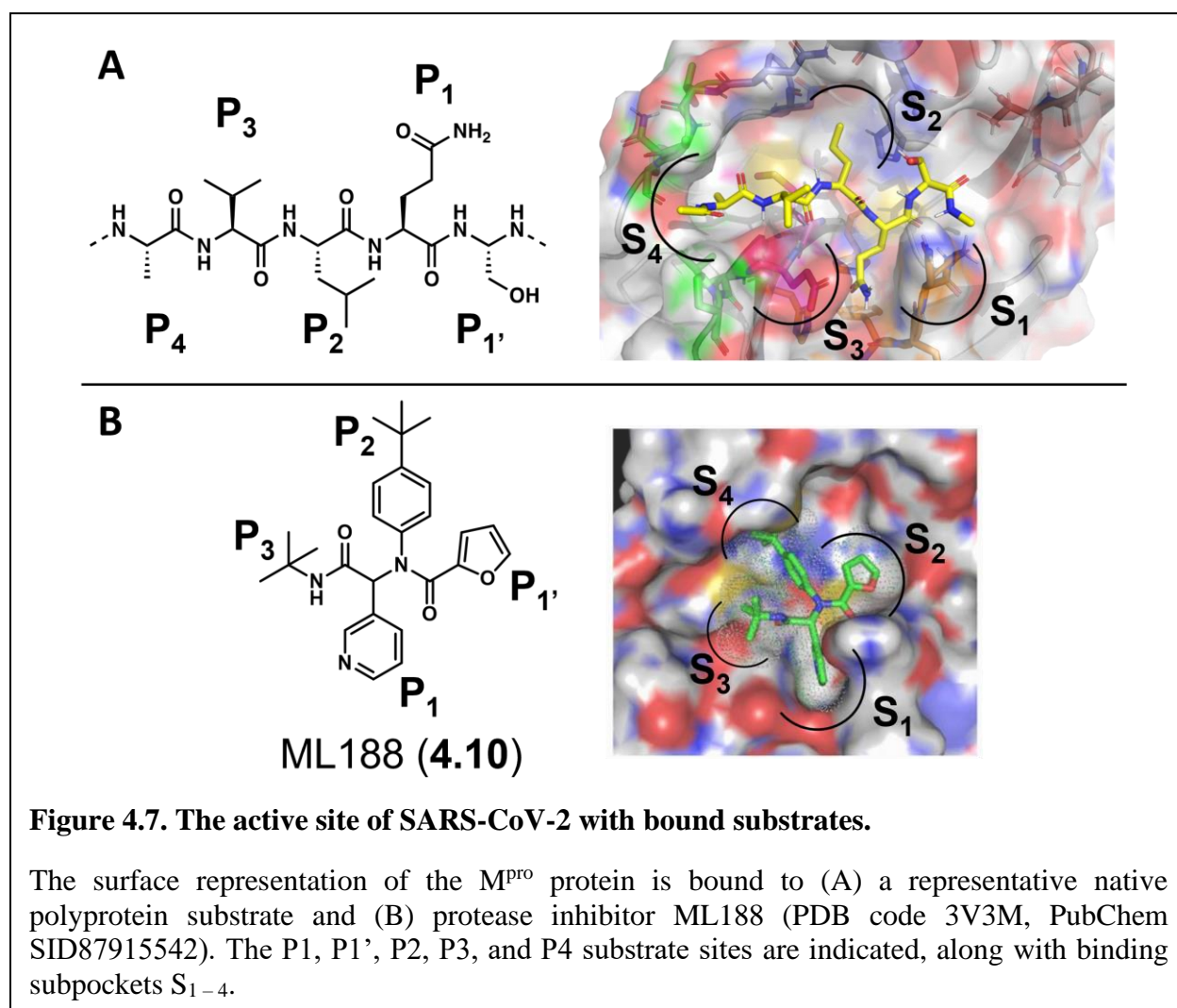
inhibitors,<sup>63,64</sup> we decided to focus our efforts on exploring the chemical space and structure-activity relationships (SAR) of M<sup>Pro</sup> inhibitors.

The M<sup>Pro</sup> protein from SARS-CoV-2 is formed by three domains: domain I, residues 10 – 99 (green, **Figure 4.6**); domain II, residues 100 – 182 (cyan, **Figure 4.6**); and domain III, residues 198 – 303 (yellow, **Figure 4.6**). Domains I and II are six-stranded antiparallel  $\beta$ -barrel structures, and domain III, a globular cluster of five  $\alpha$ -helices, is connected to domain II by a long linker loop.<sup>65</sup> The SARS-CoV-2 M<sup>Pro</sup> forms an A-A' dimer, primarily between domain II of molecule A and the NH<sub>2</sub>-terminal residues (N-finger) of molecule A' oriented perpendicularly (**Figure 4.6**).<sup>3</sup> Enzyme dimerization is necessary for catalytic activity.<sup>66</sup>



The M<sup>Pro</sup> active site is located at a shallow crevice in the I/II interdomain region.<sup>65</sup> M<sup>Pro</sup> is a cysteine protease, where His41 and Cys145 comprise the catalytic dyad. In contrast to serine proteases and other cysteine proteases, which have a catalytic triad,<sup>67</sup> there is no third catalytic residue present. During proteolytic cleavage of the polyprotein, His41 acts as a base to catalyze

the Cys145 nucleophilic reaction.<sup>68</sup> The proteolytic activity of M<sup>PRO</sup> occurs at  $\geq 11$  sites and involves Leu-Gln↓(Ser,Ala,Gly) sequences (cleavage site indicated by ↓), a cleavage pattern that is conserved in the M<sup>PRO</sup> from SARS-CoV.<sup>69</sup> The presence of a glutamine (Gln) residue at P<sub>1</sub> (**Figure 4.7A**) is a common feature shared among M<sup>PRO</sup> substrates, while no known human cysteine protease cleaves after Gln.<sup>64</sup> This, in addition to the protease being essential to viral replication, suggests that SARS-CoV-2 M<sup>PRO</sup> inhibition is an attractive approach for antiviral therapy to treat COVID-19.<sup>70</sup>



A comparative molecular field analysis (CoMFA) model was constructed to optimize octapeptide-based inhibitors,<sup>71</sup> and a substrate specificity profile was determined from a systematic

saturation mutagenesis study that was conducted at the P3, P4, and P5 positions of the substrate,<sup>72</sup> providing a basis for peptidomimetic inhibitor design. First-generation protease inhibitors often maintain a peptidic nature, achieve sub-micromolar activity, and demonstrate a strong SAR between M<sup>pro</sup> and its substrates.<sup>68,73–77</sup>

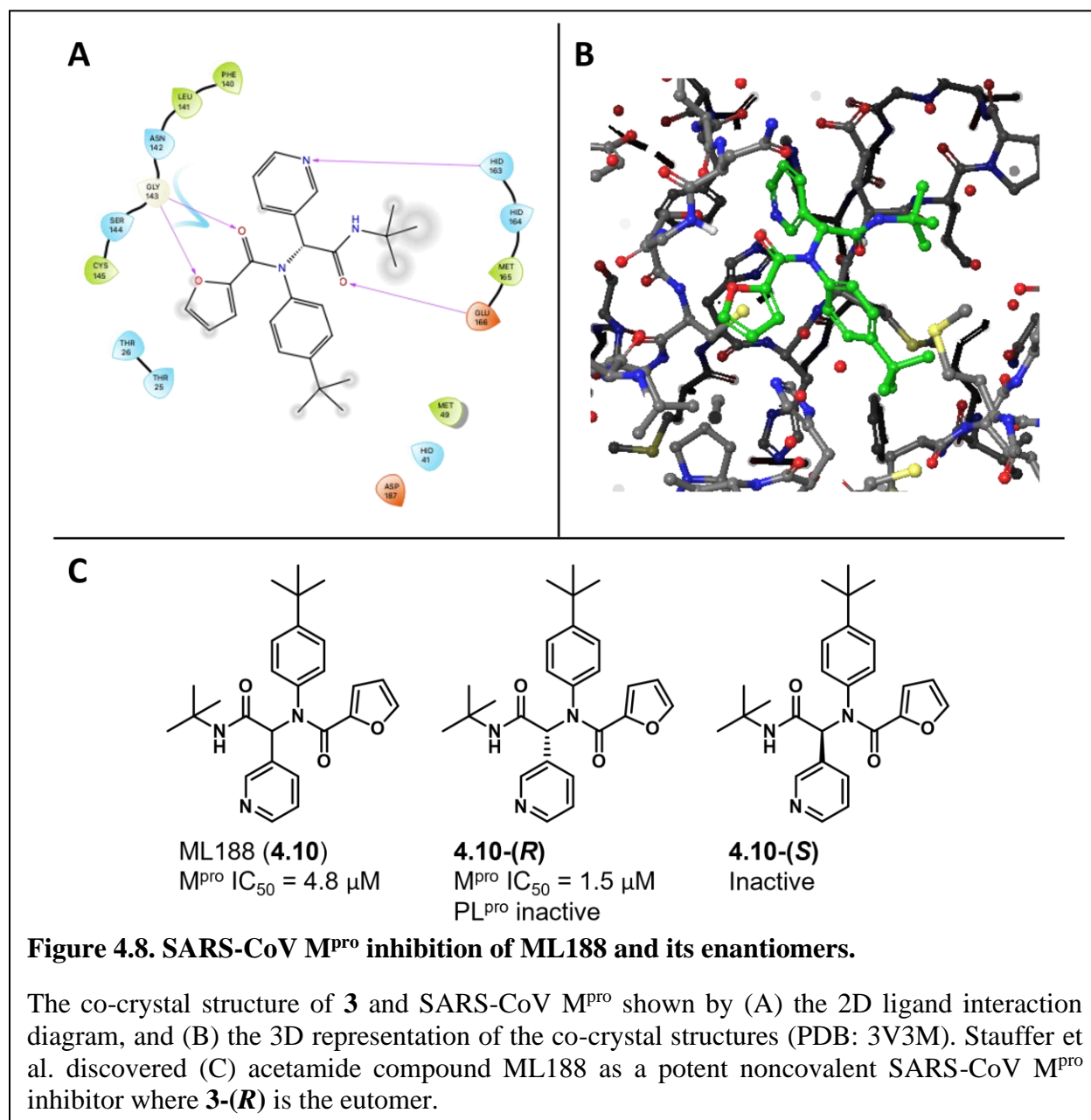
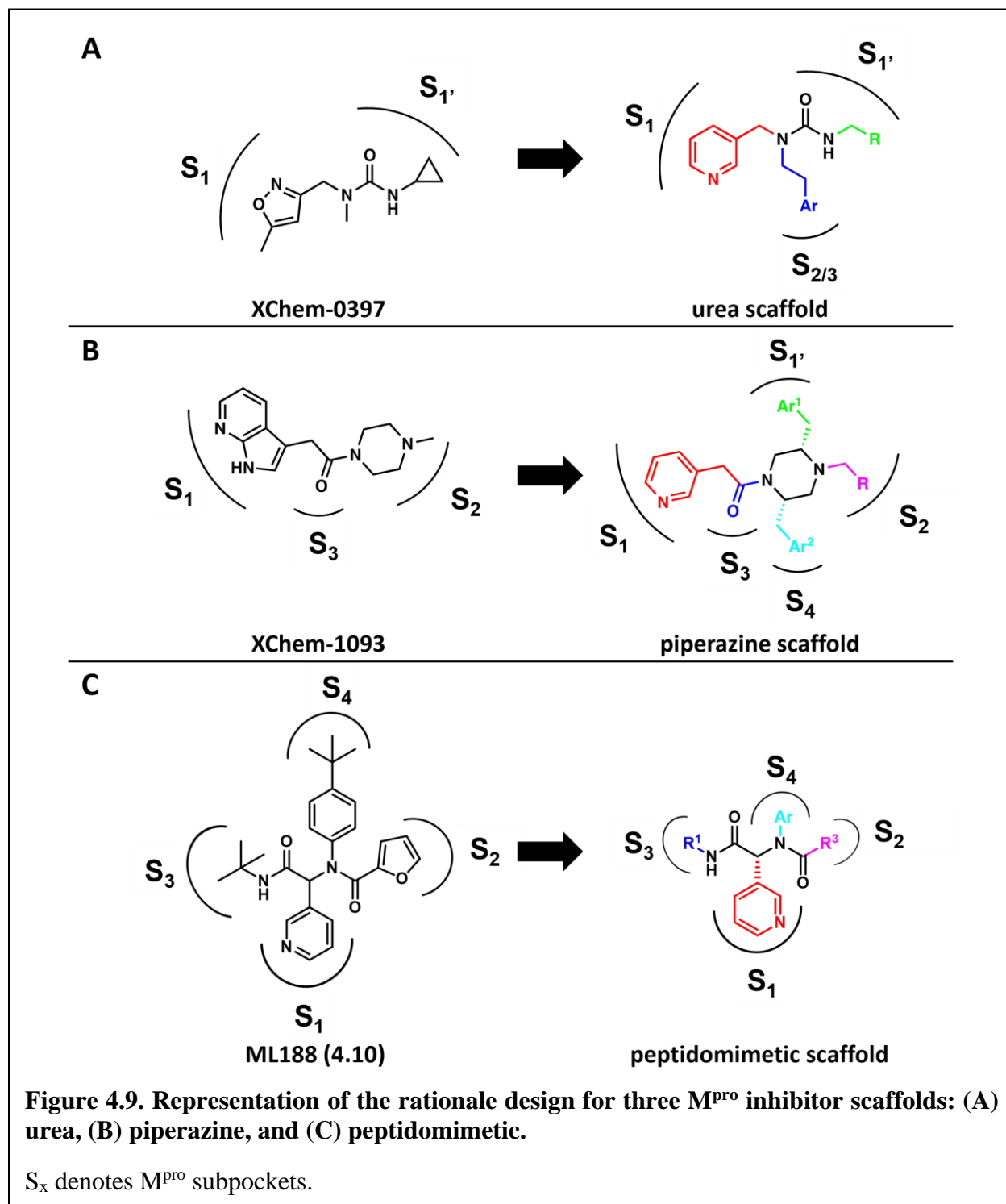


**Figure 4.8** summarizes the findings from an optimization of a series of N-(tert-butyl)-2-(N-arylamido)-2-(pyridine-3-yl) acetamides by Stauffer et al., which exemplifies the utility of

SAR studies to discover potent small molecule inhibitors of SARS-CoV M<sup>pro</sup>.<sup>48</sup> X-ray analysis of the M<sup>pro</sup> – **4.10-(R)** complex revealed key interactions crucial for activity: (1) a hydrogen bonding interaction between the pyridine nitrogen and the His163 sidechain within the S<sub>1</sub> subpocket, (2) the furan oxygen and the amide carbonyl oxygen provide a bifurcated interaction with the Gly143 backbone NH (**Figure 4.8A**), and (3) the *R*-enantiomer preferentially occupies the S<sub>3</sub> – S<sub>1</sub> subpockets (**Figure 4.8C**).<sup>48</sup> Notably, this study also demonstrated that while the pyridine ring (P<sub>2</sub>) engages in a key binding interaction, P<sub>1</sub> and P<sub>2</sub> on the substrate are tolerable to structural changes, but structural diversity in P<sub>3</sub> was not explored. Further, analogs can be accessed by multicomponent Ugi-coupling reaction, providing robust chemistry for analog generation. This peptidomimetic scaffold has been subject of structural optimization to improve potency against SARS-CoV M<sup>pro</sup> and recently SARS-CoV-2 M<sup>pro</sup>.

In continuation of our goal to expand the chemical space and structural diversity of M<sup>pro</sup> inhibitors, we gained inspiration from a remarkable database provided by the United Kingdom's national synchrotron. Diamond Light Source produced an apo-structure of SARS-CoV-2 M<sup>pro</sup> (PDB: 6YB7) and conducted a large-scale crystallographic fragment screen against the coronavirus protein. This crystallographic experiment resulted in the screening of 1500 crystals where 74 hits were identified, which included 22 noncovalent and 48 covalent hits bound to the active site of M<sup>pro</sup>, and 3 hits identified as binding to the dimer interface.<sup>78</sup> From these hits, novel inhibitor chemotypes were identified (**Figure 4.9**) from the molecular fragments that Diamond Light Source found to bind to the active site of M<sup>pro</sup>. It should be noted that no enzymatic assays were used to confirm their results, and fragment hits were determined by the strength of intermolecular interactions with the binding site only.<sup>78</sup> Notable interactions include (1)  $\pi$ - $\pi$  stacking or hydrophobic contact with His41 in the S<sub>2</sub> subpocket, and (2) hydrogen bonding with

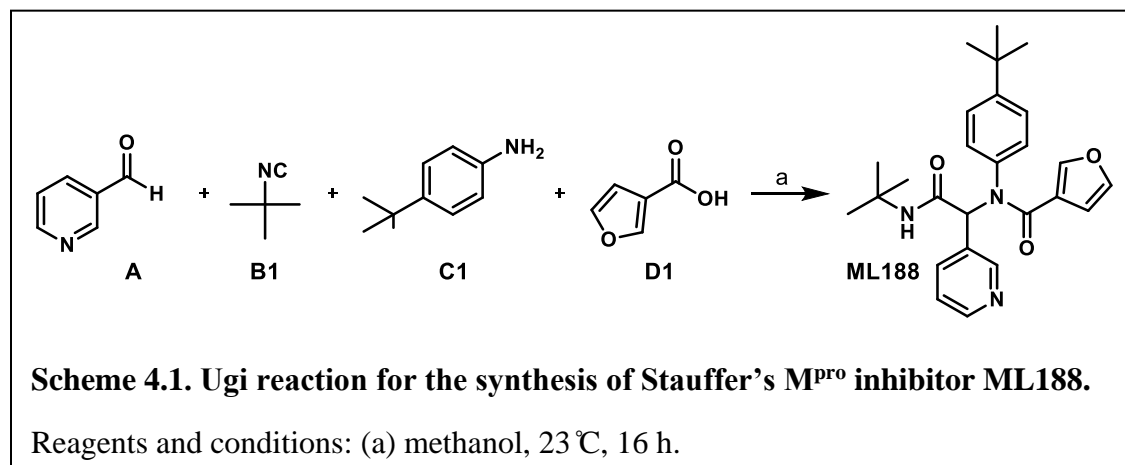
His163 (predominantly with a pyridyl group) in the  $S_1$  subpocket. Secondary to these, hydrogen bonding with the Gly143 ( $S_{1'}$ ) and Glu166 ( $S_3$ ) backbone NHs also provide notable interactions.



The results from the Diamond Light Source crystallographic screen inspired the design of three M<sup>Pro</sup> inhibitor scaffolds: urea, piperazine, and peptidomimetic (**Figure 4.9**). Considering the urgency of the COVID-19 pandemic and immediate need for chemotherapeutics, these scaffolds were chosen not only for their ability to span multiple subsites of the binding pocket, but also based on the following criteria: relatively straightforward synthetic methods, affordable building blocks, and multiple substitution sites for diversity-oriented synthesis. These criteria we expected to provide a rapid synthesis of a library of analogs within each scaffold. Efforts towards generating a library of the peptidomimetic scaffold are reported herein.

#### 4.2.3 Synthesis of peptidomimetic analogs.

The urea and piperazine scaffolds were pursued by Ms. Katelyn Stevens and Mr. Quentin Avila, respectively. Thus, I was charged with synthesizing peptidomimetic analogs. First, racemic ML188 (**3**) was synthesized via the four-component Ugi coupling reaction (**Scheme 4.1**). ML188 is a noncovalent M<sup>Pro</sup> inhibitor and was generated to be used as a control for protease activity assays.<sup>16</sup> Afterwards, I synthesized 18 other peptidomimetic compounds (**Figure 4.10**).

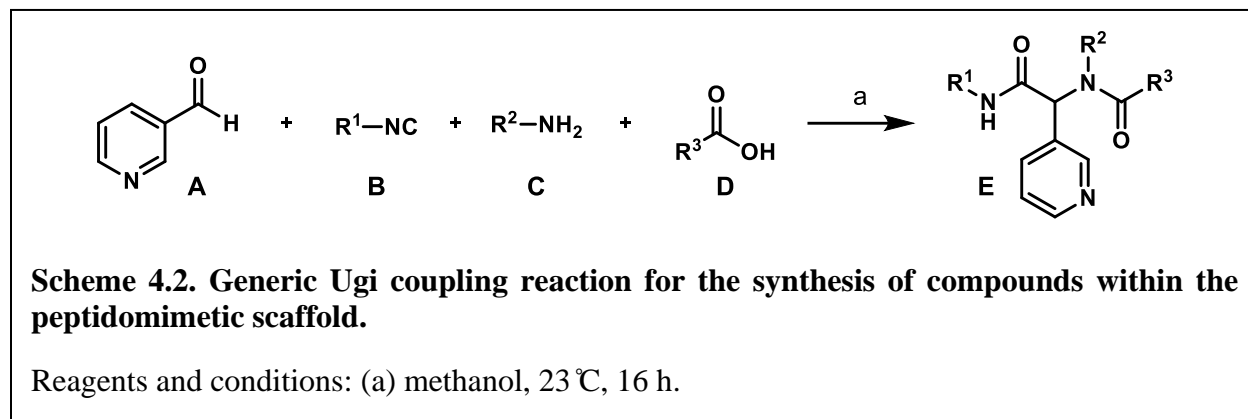


It should be noted that while the *R*-enantiomer of **4.10** was identified as the eutomer, my approach involved starting with synthesizing the racemic mixtures of each compound so that



several analogs could be generated rapidly. If any of the racemic compounds were to show significant protease inhibition activity, then either purification of the enantiomers or a stereoselective synthetic method can be employed to provide the pure enantiomers. This would allow us to then determine the eutomer and distomer of active racemic compounds.

The Ugi coupling is a multi-component reaction where a carbonyl compound, an amine, an isocyanide, and a carboxylic acid react to form a bis-amide product in one pot (**Scheme 4.2**).<sup>79</sup> Nicotinic aldehyde (**A**) was employed in every reaction, as it provided the pyridine moiety that is integral to the peptidomimetic scaffold. Cyclohexyl or *tert*-butyl isocyanides were used for component **B**, several aromatic amines were used for component **C**, and a wide assortment of carboxylic acids were used for component **D**.



For this reaction, the aldehyde, amine, and carboxylic acid were dissolved in reagent-grade methanol at room temperature, followed by addition of the isocyanide. The reaction was then allowed to stir overnight, and the product was purified the following morning. The Ugi reaction does not typically require anhydrous conditions,<sup>80</sup> but each reaction was conducted under nitrogen atmosphere.<sup>81</sup>

Fortunately, the Ugi reaction has a straightforward procedure and was widely successful for generating compounds. In fact, 5 compounds were synthesized with yields >90% (**JG55**, **JG56**,

**JG59, JG5.09, JG5.16**). Interestingly, compounds **JG52** and **JG53** were produced when I attempted to increase the rate of the reaction by adding acetic acid. I thought acetic acid would act as a mildly acidic catalyst, but, unsurprisingly, the acetate ion competed with the desired carboxylic acid nucleophile, resulting in a terminal methyl group on the bis-amide products. The competition between the carboxylic acid anions resulted in poor yields of 8% and 26% for compounds **JG52** and **JG53**, respectively. I found that low concentrations of hydrochloric acid are suitable for increasing the acidity of the reaction mixture when necessary.

In addition to the 18 compounds I synthesized, noopept was also tested for M<sup>pro</sup> proteolytic activity (**Figure 4.10**). Noopept, or N-phenylacetyl-L-prolylglycine ethyl ester, is an approved drug in Russia and is available without a prescription. As a research nootropic in the United States, it has been evaluated for neuroprotective effects to prevent and treat Alzheimer's disease.<sup>82</sup> While it has been found to slightly stimulate brain-derived neurotrophic factor (BDNF) expression in rat hippocampus, its mechanism of action is unknown.<sup>83</sup> As a proline-containing dipeptide that was readily available, I included it in the biological assessment because of its bis-amide structure.

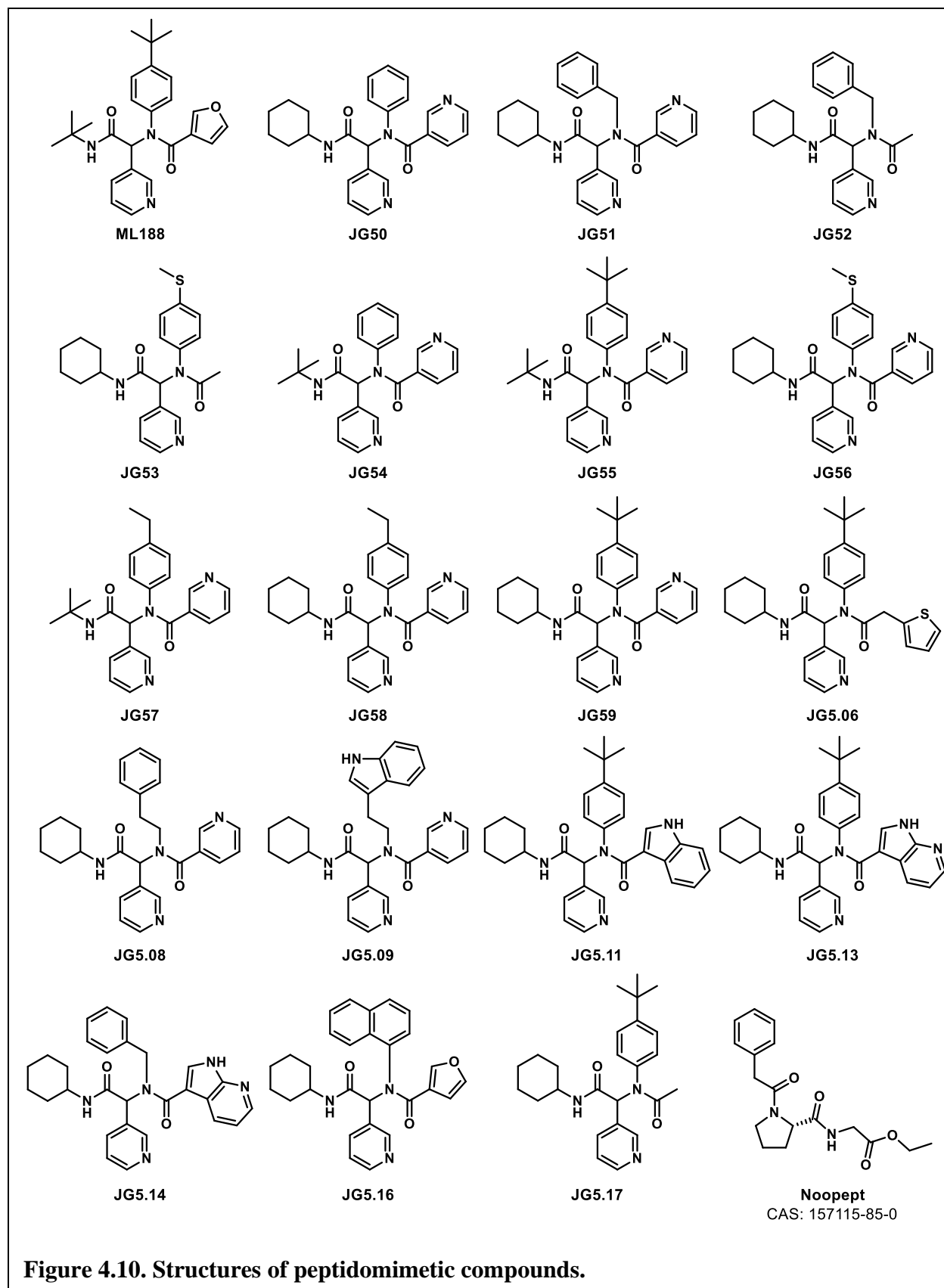
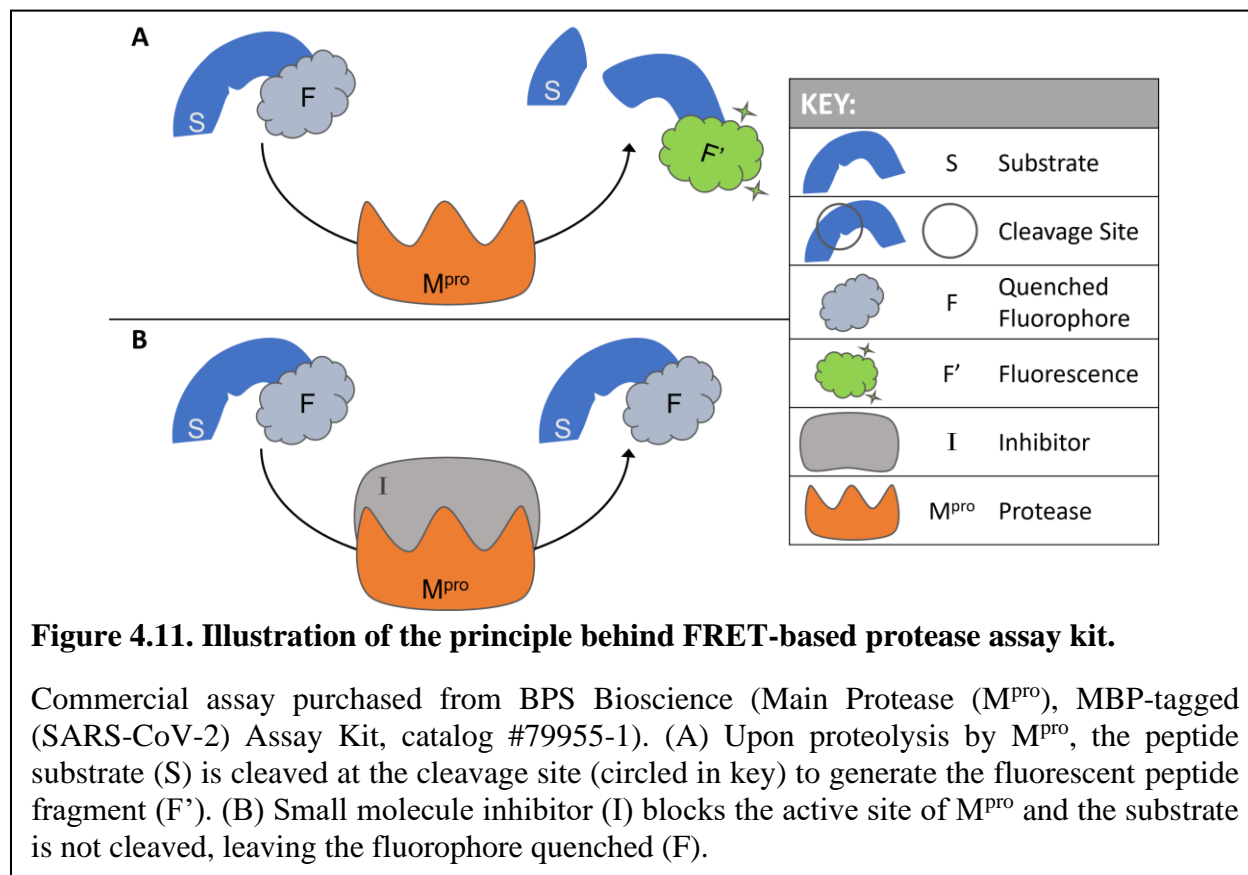


**Figure 4.10. Structures of peptidomimetic compounds.**

#### 4.2.4 Preliminary biological evaluation for M<sup>pro</sup> inhibition.



A commercial kit from BPS Bioscience was used to evaluate M<sup>pro</sup> inhibitory activity of each compound. The principle behind the protease assay kit is illustrated in **Figure 4.11**. Briefly, the M<sup>pro</sup> substrate is an internally quenched 14-residue fluorogenic (FRET) peptide dabcyL-KTSAVLQ↓SGFRKME-edans (cleavage site indicated by ↓).<sup>84</sup> The intact substrate holds the donor (edans) and acceptor (dabcyL) fluorophores in close proximity, thus the energy emitted from edans is quenched by dabcyL (S-F complex in **Figure 4.11**).<sup>85</sup> Upon proteolysis by M<sup>pro</sup>, the peptide substrate is cleaved, creating distance between the fluorophores, generating the highly fluorescent peptide fragment SGFRKME-edans (F' in **Figure 4.11**). The fluorescence intensity increases proportionally to the activity of M<sup>pro</sup>.<sup>86</sup> Thus, blank-corrected fluorescence values were used to calculate percent inhibition with the following equation:<sup>87</sup>

**Equation 1.** Percent Inhibition = 100 \* [1-(sample/control)]

19 compounds (18 synthesized and 1 commercially available) within the peptidomimetic scaffold were evaluated for M<sup>pro</sup> inhibitory activity using a commercial enzymatic activity assay kit. The protease (3 – 5 ng/μL) in assay buffer, stabilized with 1 mM dithiothreitol (DTT), was incubated with the test inhibitor (200 μM) for 30 min at 25 °C before the reaction was started by substrate addition. Fluorescence readings were taken every hour until a maximum value of the negative control (M<sup>pro</sup> incubated in absence of inhibitor) was achieved. ML188 (**4.10**) was used as the positive control because it is a known non-covalent M<sup>pro</sup> inhibitor.<sup>48,88</sup> Each reaction was conducted in technical duplicate with four biological replicates to provide four percent inhibition values for each compound. The average percent inhibition for each compound is listed in **Table 4.2**.

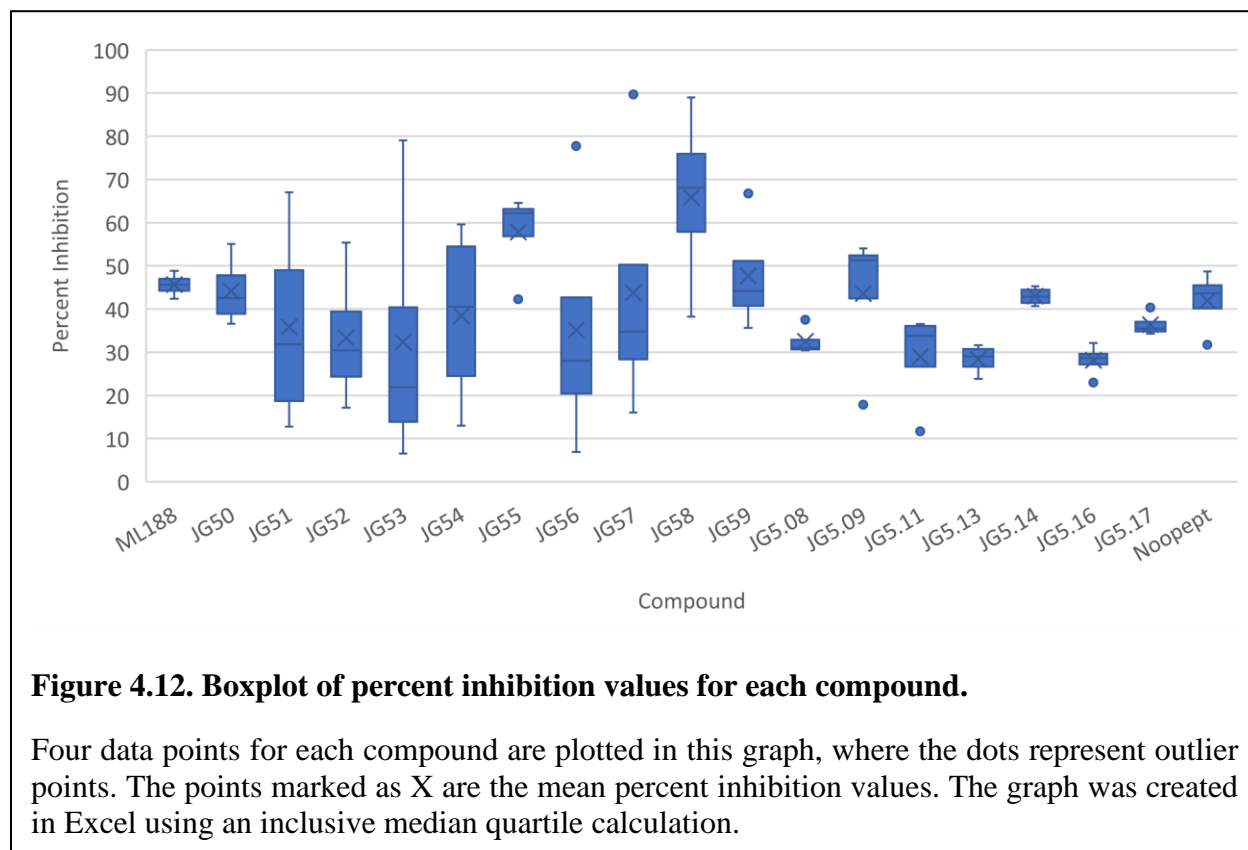
**Table 4.2. Average percent inhibition for each compound at 200 μM.**

Compound	Mean Inhibition (%)	Compound	Mean Inhibition (%)
ML188	46	JG59	48
JG50	44	JG5.06	ND <sup>a</sup>
JG51	36	JG5.08	33
JG52	33	JG5.09	44
JG53	32	JG5.11	29
JG54	38	JG5.13	28
JG55	58	JG5.14	43
JG56	35	JG5.16	28
JG57	44	JG5.17	36
JG58	66	Noopept	42

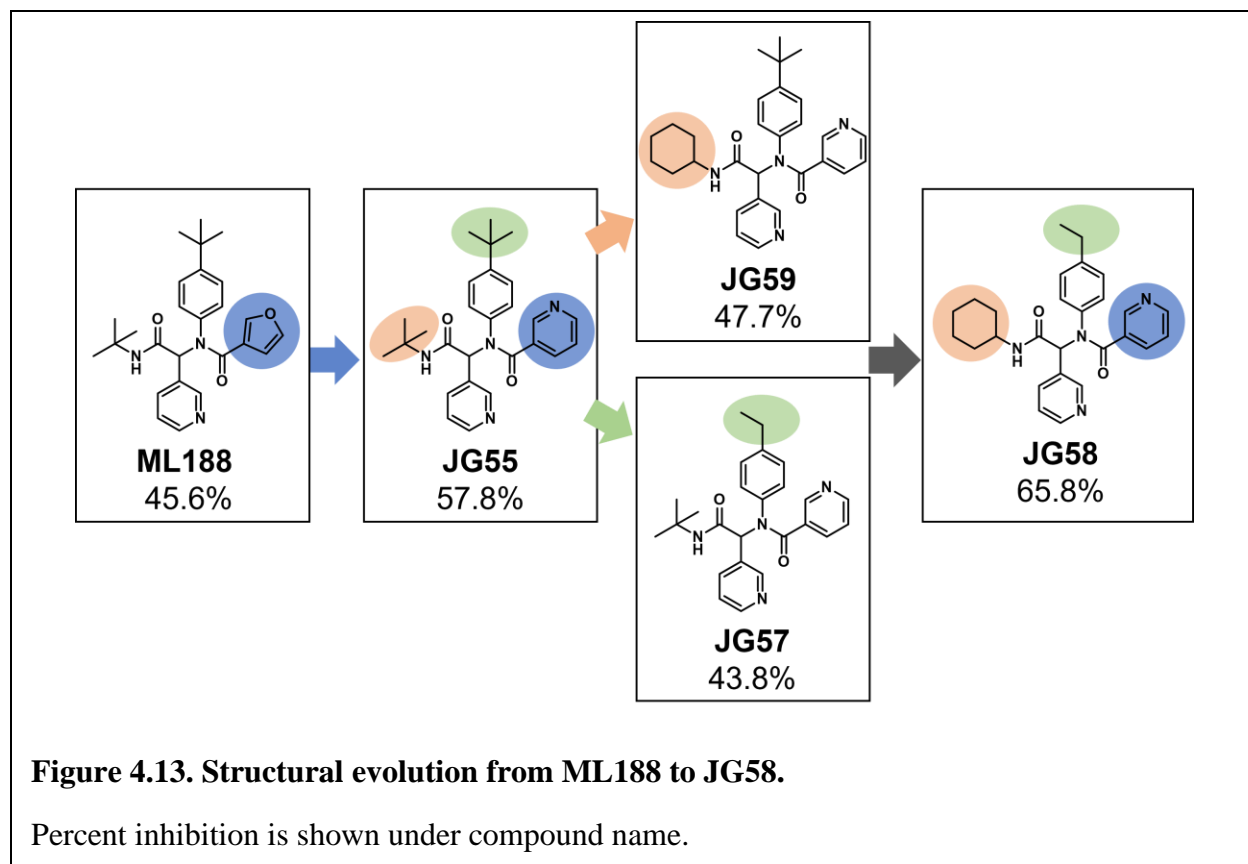
<sup>a</sup> JG5.06 was omitted from enzymatic assays because it is insoluble assay buffer. ND = no data.

As shown in **Figure 4.12**, percent inhibition data is presented as a box and whisker plot with outliers and mean values visually represented. In this graph, the significant outliers are marked as single points (dots), and the mean values are denoted by the X. The control compound,

ML188, gave relatively consistent results with an average inhibition of 46%. Compounds with mean inhibition at or above ML188 include **JG59** (48%), **JG55** (58%), and **JG58** (66%).



Utilizing bio-isosteric replacement strategies, replacing the furan heterocycle with a pyridine resulted in ~10% increase in inhibitory activity (blue, **Figure 4.13**), which led me to pursue pyridine and nitrogen heterocycles at this position. Interestingly, replacing the t-butyl groups with cyclohexyl and ethyl groups (highlighted in orange and green, respectively in **Figure 4.13**) resulted in decreased activity, with compounds **JG59** and **JG57** showing similar percent inhibition as ML188. However, when incorporation of the cyclohexyl (orange), ethyl (green), and pyridine (blue) groups simultaneously, led to **JG58** which exhibits a ~20% increase in inhibitory activity compared to ML188 (**Figure 4.13**).



### 4.3 Conclusions

Overall, during our exploratory investigation into SARS-CoV-2 protease inhibitors, we found that our previous research on bacterial protease inhibitors does not translate to coronavirus targets, and the 25 compounds we had evaluated for viral replication inhibition were all inactive. We also designed three scaffolds (urea, piperazine, and peptidomimetic) based on computational modeling of the M<sup>Pro</sup> active site, and I synthesized and tested 18 peptidomimetic compounds where preliminary data suggested that 3 of my compounds exhibit modest to improved inhibitory activity when compared to the ML188 control.

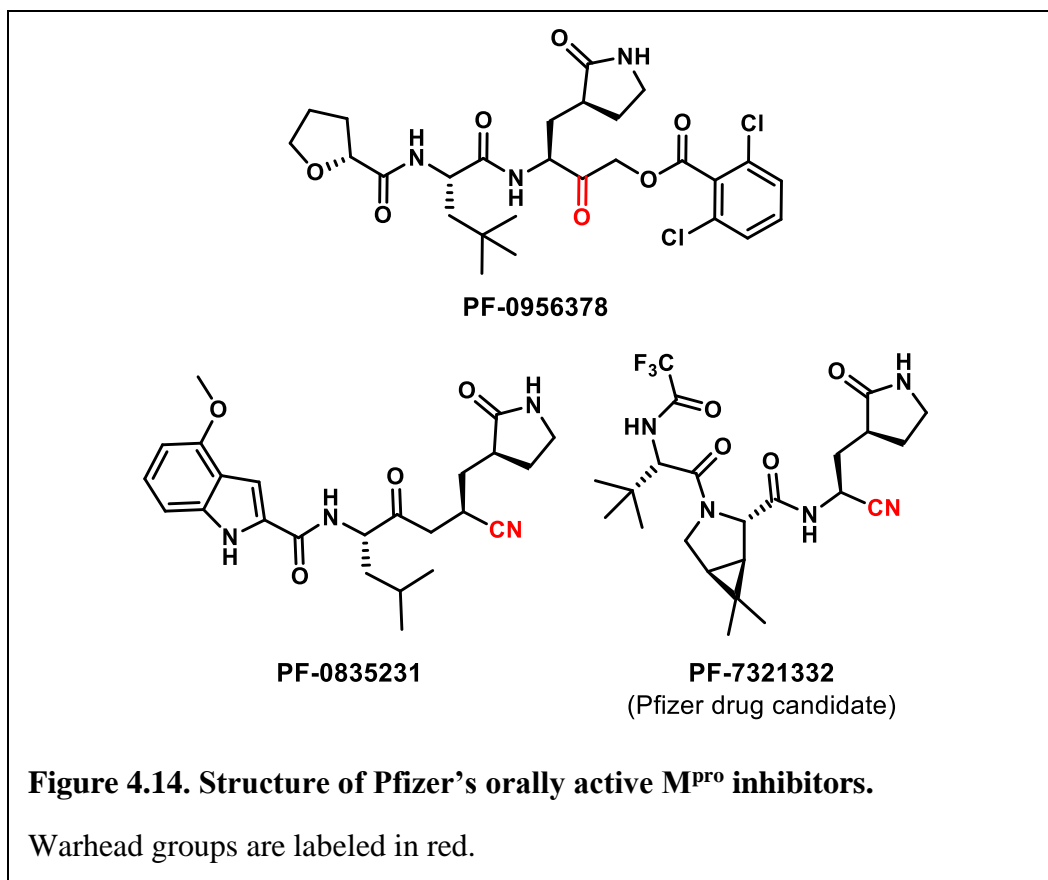


**Figure 4.14. Structure of Pfizer’s orally active M<sup>pro</sup> inhibitors.**

Warhead groups are labeled in red.

While we investigated noncovalent M<sup>pro</sup> inhibitors, other laboratories pursued inhibitors that covalently bind to the M<sup>pro</sup> catalytic dyad.<sup>40,64,89</sup> Covalent inhibitors sometimes pose the risk of unpredictable toxicity because of the reactive electrophilic moieties that make up the “warhead” functional group. Reactive warheads include Michael acceptors,<sup>90</sup> α-ketoamides (boceprevir,<sup>68</sup> or broad-spectrum inhibitors<sup>74</sup>), thioacetals,<sup>41</sup> or nitriles.<sup>64</sup> Covalent inhibitors can be reversible, such as PF-0835231 and PF-7321332, or irreversible such as PF-0956378 (**Figure 4.14**). For compound PF-7321332, the nitrile forms a reversible covalent thioimidate adduct with the nucleophilic Cys145. These structures were recently unveiled at the American Chemical Society (ACS) Spring 2021 meeting<sup>91</sup> by Pfizer, an American multinational pharmaceutical and biotechnology corporation,<sup>92</sup> The compound PF-7321332, also known as Nirmatrelvir,<sup>93</sup> can be orally administered, has good selectivity and safety profile, and protects against infection in a mouse



model.<sup>94</sup> The covalent M<sup>pro</sup> inhibitor is currently in Phase 1 clinical trials, and it is the first orally administered compound in the clinic that targets M<sup>pro</sup>. This has also been approved for emergency use by the FDA.

When the opportunity was presented to contribute to the effort towards discovering new antivirals effective against SARS-CoV-2, we felt compelled to contribute. We chose to pursue the design and development of SARS-CoV-2 main protease inhibitors. After exploring the M<sup>pro</sup> active site computationally, investigating new chemotypes, and evaluating some peptidomimetic compounds for protease activity, we have experimentally validated a peptidomimetic M<sup>pro</sup> inhibitory chemotype and have set the stage for the continued evolution of this scaffold.

#### **4.4 Perspective**

The idea for this project arose when my roommate, Mr. Quentin Avila, and I were sitting at home contemplating the COVID-19 pandemic and corresponding country-wide lockdown that started in March 2020. At first, we were genuinely curious to learn more about the SARS-CoV-2 virus, especially its transmission and what kind of procedures we should follow to stay safe. Eventually, after weeks of lockdown amounted to an unfortunate lack of research productivity, we were hyper aware of the delay that the pandemic was causing to our graduation studies and research productivity. Consequently, when the OU OVPRP provided an opportunity for researchers to join the fight against COVID-19, Mr. Avila and I worked together to not only teach ourselves basic virology but also to identify an approach to translate our lab's expertise into an anti-coronavirus medicinal chemistry project, all in a single week. We were happily surprised when we found that our efforts resulted in being awarded the COVID-19 Rapid Response Seed Grant. We were proud

to say we were contributing to the global effort in finding SARS-CoV-2 treatments, and we were also excited to be allowed back into the laboratory.

The grant provided funding and was written for a six-month project. Thankfully, our lab mate, Ms. Katelyn Stevens, volunteered to help us. It was surreal to be the only three graduate students present in our research building, especially in addition to the extreme precautions we were taking in order to limit exposure and possible spread of the virus. The entire situation was surreal, as the COVID-19 pandemic surmounted to the monumental and most pivotal event of our generation. Family members started getting sick, lives were being lost all around us, and for a moment, we were unsure if the pandemic was ever going to end. On the other hand, research labs all over the world were working towards a common goal. We were all united against a common enemy, but that did not negate the competition. It usually takes 10 – 15 years for a new molecular entity to go from research and development to clinical trials, but Pfizer discovered a SARS-CoV-2 M<sup>pro</sup> inhibitor that gained emergency use authorization from the FDA in less than two years, a truly astonishing feat.

Thus, while I might have found a few compounds that were active against M<sup>pro</sup>, even with improved activity compared to the controls, our control (ML188) is leagues behind the compounds that bigger pharmaceutical companies have found since the start of this project. I am still proud, however, to say that while Quentin and I sifted through the vast amount of coronavirus literature that existed in early 2020, we came to the same conclusion as a leading pharmaceutical company as to which coronavirus protein made the best drug target. This project also served to be an exercise in implementing all that we have learned while in graduate school. We fabricated an idea to solve a very pertinent global problem, were awarded funding to pursue such an idea, executed

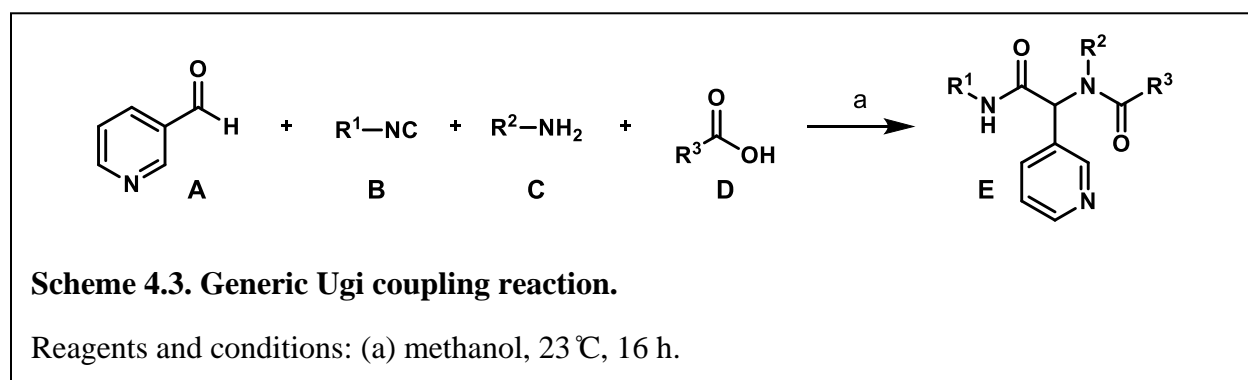
experiments to test our hypotheses, and came to a conclusion that coincides with the current state of the art.

## 4.5 Experimental

### 4.5.1 General chemistry methods.

All commercial reagents were used without further purification. Distilled water was used for all water necessities in synthetic procedures (e.g., reagent, solvent, work-up). Flash column chromatography was performed with silica gel 60. Thin layer chromatography (TLC) analyses were completed with EMD Millipore silica gel coated (250  $\mu$ M) F254 glass plates and visualized with UV light. NMR samples were prepared in 5 mm tubes with 0.6 mL deuterated solvent. NMR data were all collected on a 300, 400, or 500 MHz (specified below) Varian VNMRs Direct Drive spectrometer equipped with an indirect detection probe. Data was collected at 25 °C unless otherwise indicated. Pulse sequences were used as supplied by Varian VNMRJ 4.2 software. All NMR data was processed in MestreNova v10. Peak positions are reported after reference centering on deuterated solvent of relevance.

### 4.5.2 Synthetic procedures.



**General procedure for Ugi coupling reaction.** Nicotinaldehyde **A** (0.32 mmol), acid **D** (0.32 mmol), and amine **C** (0.32 mmol) were dissolved in dry methanol (1.5 mL) at room temperature (23 °C) under nitrogen atmosphere. Then isocyanide **B** (0.32 mmol) was added. The reaction stirred at room temperature overnight and reaction progress was monitored by TLC. When consumption of the aldehyde was seen by TLC, solvent was removed under vacuum to afford product mixture as an amorphous solid or crude oil, depending on compound. The crude product was dissolved in dichloromethane and purified by flash chromatography (SiO<sub>2</sub>) using ethyl acetate/hexanes eluents basified with 1% triethylamine. Pure fractions were pooled and concentrated in vacuo to afford Ugi compounds listed below.

**N-(2-(cyclohexylamino)-2-oxo-1-(pyridin-3-yl)ethyl)-N-phenylnicotinamide (JG50):**

White amorphous solid, 20% yield. <sup>1</sup>H NMR (500 MHz, CDCl<sub>3</sub>) δ 8.55 (dd, *J* = 4.7, 1.6 Hz, 1H), 8.25 (s, 1H), 7.44 (d, *J* = 8.1 Hz, 1H), 7.32 – 7.17 (m, 2H), 7.08 (t, *J* = 7.6 Hz, 2H), 6.89 (t, *J* = 7.4 Hz, 2H), 6.72 (d, *J* = 7.9 Hz, 2H), 6.50 (d, *J* = 7.6 Hz, 2H), 5.04 (s, 1H), 2.20 – 2.09 (m, 1H), 2.10 – 1.99 (m, 1H), 1.78 – 1.68 (m, 1H), 1.68 – 1.57 (m, 2H), 1.50 – 1.32 (m, 2H), 1.31 – 1.20 (m, 2H), 1.22 – 1.04 (m, 2H).

**N-benzyl-N-(2-(cyclohexylamino)-2-oxo-1-(pyridin-3-yl)ethyl)nicotinamide (JG51):**

White amorphous solid, 60% yield. <sup>1</sup>H NMR (600 MHz, CDCl<sub>3</sub>) δ 8.81 (d, *J* = 5.2 Hz, 1H), 8.71 (d, *J* = 5.2 Hz, 1H), 8.64 – 8.51 (m, 2H), 8.01 – 7.91 (m, 1H), 7.85 (d, *J* = 7.7 Hz, 1H), 7.44 (dq, *J* = 11.3, 6.2 Hz, 1H), 7.37 (q, *J* = 6.7 Hz, 2H), 7.32 (d, *J* = 6.4 Hz, 1H), 7.27 (d, *J* = 6.6 Hz, 4H), 7.07 (d, *J* = 6.7 Hz, 3H), 6.36 (d, *J* = 8.0 Hz, 1H), 5.80 (s, 1H), 4.89 (d, *J* = 16.9 Hz, 1H), 4.66 (d, *J* = 16.5 Hz, 1H), 2.18 – 2.11 (m, 1H), 2.07 – 1.93 (m, 1H), 1.83 – 1.73 (m, 3H), 1.74 – 1.66 (m, 2H), 1.52 – 1.41 (m, 2H), 1.27 – 1.18 (m, 2H).

**2-(N-benzylacetamido)-N-cyclohexyl-2-(pyridin-3-yl)acetamide (JG52):** White amorphous solid, 8% yield. <sup>1</sup>H NMR (600 MHz, CDCl<sub>3</sub>) δ 8.50 (d, *J* = 2.3 Hz, 1H), 8.44 (d, *J* = 4.8 Hz, 1H), 7.75 (d, *J* = 8.0 Hz, 1H), 7.19 (t, *J* = 7.3 Hz, 2H), 7.17 – 7.11 (m, 2H), 6.98 (d, *J* = 7.4 Hz, 2H), 5.94 (s, 1H), 4.75 (d, *J* = 17.6 Hz, 1H), 4.60 (d, *J* = 17.6 Hz, 1H), 2.13 (s, 3H), 1.94 – 1.82 (m, 2H), 1.71 – 1.61 (m, 3H), 1.62 – 1.53 (m, 1H), 1.41 – 1.27 (m, 2H), 1.20 – 1.02 (m, 3H).

**N-cyclohexyl-2-(N-(4-(methylthio)phenyl)acetamido)-2-(pyridin-3-yl)acetamide (JG53):** White amorphous solid, 26% yield. <sup>1</sup>H NMR (600 MHz, CDCl<sub>3</sub>) δ 8.44 (dd, *J* = 4.8, 1.6 Hz, 1H), 8.40 (d, *J* = 2.2 Hz, 1H), 7.40 (dt, *J* = 8.1, 2.0 Hz, 1H), 7.09 – 7.03 (m, 3H), 6.09 (s, 1H), 5.98 (d, *J* = 8.1 Hz, 1H), 3.84 – 3.75 (m, 1H), 2.42 (s, 3H), 2.01 – 1.93 (m, 1H), 1.85 (s, 5H), 1.76 – 1.55 (m, 3H), 1.42 – 1.27 (m, 2H), 1.27 – 1.01 (m, 3H).

**N-(2-(tert-butylamino)-2-oxo-1-(pyridin-3-yl)ethyl)-N-phenylnicotinamide (JG54):** White amorphous solid, 24% yield. <sup>1</sup>H NMR (600 MHz, CDCl<sub>3</sub>) δ 8.51 (dd, *J* = 4.8, 2.2 Hz, 2H), 8.46 (dd, *J* = 5.0, 1.7 Hz, 1H), 8.40 (dd, *J* = 4.9, 1.7 Hz, 1H), 7.57 (dt, *J* = 8.1, 2.1 Hz, 1H), 7.53 (dt, *J* = 8.0, 2.0 Hz, 1H), 7.15 – 7.08 (m, 1H), 7.08 – 7.01 (m, 3H), 7.02 – 6.95 (m, 2H), 6.17 (d, *J* = 2.7 Hz, 1H), 5.96 (s, 1H), 1.37 (s, 9H).

**N-(4-(tert-butyl)phenyl)-N-(2-(tert-butylamino)-2-oxo-1-(pyridin-3-yl)ethyl)nicotinamide (JG55):** White amorphous solid, 93% yield. <sup>1</sup>H NMR (500 MHz, CDCl<sub>3</sub>) δ 8.54 – 8.48 (m, 2H), 8.46 (d, *J* = 5.8 Hz, 1H), 8.42 – 8.37 (m, 1H), 7.60 – 7.55 (m, 1H), 7.51 (d, *J* = 7.5 Hz, 1H), 7.12 – 7.02 (m, 4H), 6.87 (s, 1H), 6.10 (s, 1H), 6.03 (d, *J* = 8.3 Hz, 1H), 1.37 (s, 9H), 1.17 – 1.11 (s, 9H).

**N-(2-(cyclohexylamino)-2-oxo-1-(pyridin-3-yl)ethyl)-N-(4-(methylthio)phenyl)**

**nicotinamide (JG56):** White amorphous solid, 91% yield. <sup>1</sup>H NMR (500 MHz, CDCl<sub>3</sub>) δ 8.78 (s, 1H), 8.61 – 8.52 (m, 2H), 8.47 (dt, *J* = 4.8, 2.4 Hz, 1H), 7.84 (d, *J* = 8.0 Hz, 1H), 7.71 – 7.59 (m, 1H), 7.37 (dd, *J* = 8.0, 5.6 Hz, 1H), 7.18 (dd, *J* = 8.0, 5.0 Hz, 1H), 6.92 (d, *J* = 6.6 Hz, 3H), 6.41 (s, 1H), 3.90 – 3.79 (m, 1H), 2.36 (s, 3H), 2.00 – 1.95 (m, 2H), 1.92 – 1.83 (m, 1H), 1.76 – 1.65 (m, 1H), 1.64 – 1.57 (m, 1H), 1.44 – 1.09 (m, 6H).

**N-(2-(tert-butylamino)-2-oxo-1-(pyridin-3-yl)ethyl)-N-(4-ethylphenyl)nicotinamide**

**(JG57):** White amorphous solid, 76% yield. <sup>1</sup>H NMR (500 MHz, CDCl<sub>3</sub>) δ 8.56 (d, *J* = 11.8 Hz, 1H), 8.52 (d, *J* = 2.2 Hz, 1H), 8.49 (d, *J* = 5.1 Hz, 1H), 8.43 (dt, *J* = 4.6, 2.3 Hz, 1H), 7.65 – 7.54 (m, 2H), 7.23 – 7.13 (m, 1H), 7.13 – 7.04 (m, 1H), 6.95 – 6.78 (m, 2H), 6.22 – 6.11 (m, 1H), 5.98 – 5.94 (m, 1H), 3.43 – 3.22 (m, 1H), 2.48 (q, *J* = 3.3 Hz, 2H), 1.39 (s, 9H), 1.09 (t, *J* = 2.7 Hz, 3H).

**N-(2-(cyclohexylamino)-2-oxo-1-(pyridin-3-yl)ethyl)-N-(4-ethylphenyl)nicotinamide**

**(JG58):** White amorphous solid, 70% yield. <sup>1</sup>H NMR (600 MHz, CDCl<sub>3</sub>) δ 8.57 – 8.43 (m, 3H), 8.39 (d, *J* = 4.9 Hz, 1H), 7.58 (d, *J* = 8.1 Hz, 1H), 7.51 (d, *J* = 8.0 Hz, 1H), 7.10 (dd, *J* = 8.0, 4.7 Hz, 1H), 7.06 (dd, *J* = 8.0, 4.8 Hz, 1H), 6.86 (d, *J* = 6.0 Hz, 4H), 6.20 (s, 1H), 3.93 – 3.76 (m, 1H), 2.44 (q, *J* = 7.6 Hz, 2H), 2.01 – 1.89 (m, 1H), 1.90 – 1.82 (m, 1H), 1.76 – 1.60 (m, 3H), 1.60 – 1.53 (m, 1H), 1.41 – 1.27 (m, 2H), 1.25 – 1.07 (m, 3H), 1.05 (t, *J* = 7.6 Hz, 3H).

**N-(4-(tert-butyl)phenyl)-N-(2-(cyclohexylamino)-2-oxo-1-(pyridin-3-**

**yl)ethyl)nicotinamide (JG59):** White amorphous solid, 93% yield. <sup>1</sup>H NMR (500 MHz, CDCl<sub>3</sub>) δ 8.65 (s, 1H), 8.54 (dq, *J* = 3.3, 1.2 Hz, 2H), 8.45 (dt, *J* = 5.1, 1.2 Hz, 1H), 7.79 (s, 1H), 7.64 (dd, *J* = 8.1, 2.1 Hz, 1H), 7.29 (s, 1H), 7.16 – 7.09 (m, 2H), 6.89 (d, *J* = 8.0 Hz, 1H), 6.25 (d, *J* = 2.6 Hz, 1H), 6.20 (s, 1H), 3.86 (m, 1H), 1.98 (d, *J* = 12.2 Hz, 1H), 1.90 (d, *J* = 12.0 Hz, 1H), 1.75 –

1.66 (m, 3H), 1.61 (dd,  $J = 13.0, 4.0$  Hz, 1H), 1.45 – 1.30 (m, 3H), 1.24 – 1.20 (m, 1H), 1.18 (m, 1H).

**N-(4-(tert-butyl)phenyl)-N-(2-(cyclohexylamino)-2-oxo-1-(pyridin-3-yl)ethyl)-2-(thiophen-2-yl)acetamide (JG5.06):** Yellow amorphous solid, 62% yield.  $^1\text{H}$  NMR (400 MHz,  $\text{CD}_3\text{OD}$ )  $\delta$  8.30 (d,  $J = 3.1$  Hz, 2H), 7.52 (d,  $J = 8.0$  Hz, 1H), 7.37 – 7.08 (m, 5H), 6.88 (dd,  $J = 5.2, 3.5$  Hz, 1H), 6.70 (d,  $J = 3.4$  Hz, 1H), 6.08 (s, 1H), 3.65 (s, 2H), 1.92 (m, 2H), 1.74 (m, 2H), 1.62 (m, 2H), 1.44 – 1.27 (m, 3H), 1.24 (s, 9H), 1.22 – 1.01 (m, 2H).

**N-(2-(cyclohexylamino)-2-oxo-1-(pyridin-3-yl)ethyl)-N-phenethylnicotinamide (JG5.08):** White amorphous solid, 77% yield.  $^1\text{H}$  NMR (400 MHz,  $\text{CD}_3\text{OD}$ )  $\delta$  8.69 – 8.60 (m, 3H), 8.60 – 8.56 (m, 2H), 8.10 – 7.96 (m, 1H), 7.87 (d,  $J = 7.9$  Hz, 1H), 7.55 (dt,  $J = 13.0, 6.1$  Hz, 2H), 7.15 – 7.09 (m, 2H), 6.61 (s, 1H), 6.06 (s, 1H), 3.73 (tt,  $J = 10.8, 3.9$  Hz, 2H), 3.50 – 3.45 (m, 2H), 2.22 – 2.10 (m, 1H), 1.95 – 1.86 (m, 2H), 1.86 – 1.63 (m, 4H), 1.63 – 1.58 (m, 1H), 1.46 – 1.28 (m, 3H).

**N-(2-(1H-indol-3-yl)ethyl)-N-(2-(cyclohexylamino)-2-oxo-1-(pyridin-3-yl)ethyl)nicotinamide (JG5.09):** Amorphous yellow solid, 97% yield.  $^1\text{H}$  NMR (400 MHz,  $\text{CD}_3\text{OD}$ )  $\delta$  8.76 (s, 1H), 8.62 – 8.58 (m, 1H), 8.55 – 8.49 (m, 1H), 8.09 – 8.05 (m, 1H), 7.65 – 7.60 (m, 1H), 7.55 – 7.50 (m, 1H), 7.36 – 7.21 (m, 2H), 7.02 (t,  $J = 7.5$  Hz, 2H), 6.80 (s, 1H), 6.69 (s, 1H), 6.02 (s, 1H), 3.80 – 3.68 (m, 2H), 3.61 – 3.56 (m, 1H), 2.87 – 2.76 (m, 1H), 2.50 – 2.38 (m, 1H), 1.95 – 1.87 (m, 1H), 1.86 – 1.57 (m, 6H), 1.44 – 1.29 (m, 4H).

**N-(4-(tert-butyl)phenyl)-N-(2-(cyclohexylamino)-2-oxo-1-(pyridin-3-yl)ethyl)-1H-indole-3-carboxamide (JG5.11):** Yellow oil, 30% yield.  $^1\text{H}$  NMR (400 MHz,  $\text{CD}_3\text{OD}$ )  $\delta$  8.42 (d,  $J = 2.2$  Hz, 1H), 8.35 (dd,  $J = 5.0, 1.6$  Hz, 1H), 8.31 – 8.15 (m, 1H), 7.67 (dt,  $J = 8.0, 1.9$  Hz, 1H),

7.26 (td,  $J = 8.2, 5.6$  Hz, 3H), 7.23 – 7.09 (m, 4H), 6.39 (s, 1H), 6.09 (s, 1H), 3.75 (m, 1H), 2.02 – 1.90 (m, 1H), 1.79 (q,  $J = 6.0$  Hz, 2H), 1.67 (m, 3H), 1.44 – 1.30 (m, 5H), 1.27 (s, 9H).

**N-(4-(tert-butyl)phenyl)-N-(2-(cyclohexylamino)-2-oxo-1-(pyridin-3-yl)ethyl)-1H-pyrrolo[2,3-b]pyridine-3-carboxamide (JG5.13):** Amber oil, 10% yield.  $^1\text{H}$  NMR (500 MHz, dmso)  $\delta$  11.84 (d,  $J = 2.9$  Hz, 1H), 8.53 (dd,  $J = 8.0, 1.7$  Hz, 1H), 8.39 – 8.31 (m, 2H), 8.23 (dd,  $J = 4.7, 1.7$  Hz, 1H), 8.13 (d,  $J = 7.7$  Hz, 1H), 7.43 (dt,  $J = 7.9, 1.9$  Hz, 1H), 7.26 (d,  $J = 7.8$  Hz, 2H), 7.16 (ddd,  $J = 7.9, 6.5, 4.6$  Hz, 3H), 6.30 (s, 1H), 5.73 (d,  $J = 3.1$  Hz, 1H), 4.07 (s, 1H), 3.58 (dd,  $J = 7.5, 3.8$  Hz, 1H), 3.33 (s, 2H), 1.72 (d,  $J = 10.8$  Hz, 1H), 1.69 – 1.64 (m, 2H), 1.59 (d,  $J = 12.8$  Hz, 1H), 1.52 (d,  $J = 12.7$  Hz, 1H), 1.13 – 0.95 (m, 3H).

**N-benzyl-N-(2-(cyclohexylamino)-2-oxo-1-(pyridin-3-yl)ethyl)-1H-pyrrolo[2,3-b]pyridine-3-carboxamide (JG5.14):** Amber oil, 10% yield.  $^1\text{H}$  NMR (500 MHz, DMSO)  $\delta$  12.08 (s, 1H), 8.39 (s, 1H), 8.34 (dd,  $J = 4.9, 1.8$  Hz, 1H), 8.31 – 8.25 (m, 2H), 8.08 (d,  $J = 7.7$  Hz, 1H), 7.64 (d,  $J = 8.0$  Hz, 1H), 7.57 (s, 1H), 7.25 – 7.17 (m, 2H), 7.16 – 7.00 (m, 5H), 6.08 (s, 1H), 5.04 (d,  $J = 17.3$  Hz, 1H), 4.66 (d,  $J = 17.4$  Hz, 1H), 3.54 (d,  $J = 7.4$  Hz, 0H), 1.65 (s, 3H), 1.51 (d,  $J = 12.3$  Hz, 1H), 1.23 (s, 3H), 1.06 (dq,  $J = 37.6, 11.3$  Hz, 3H).

**N-(2-(cyclohexylamino)-2-oxo-1-(pyridin-3-yl)ethyl)-N-(naphthalen-1-yl)furan-3-carboxamide (JG5.16):** White amorphous solid, 94% yield.  $^1\text{H}$  NMR (500 MHz, DMSO)  $\delta$  8.32 (d,  $J = 2.2$  Hz, 1H), 8.13 (dd,  $J = 17.2, 7.4$  Hz, 3H), 8.00 (d,  $J = 4.7$  Hz, 1H), 7.86 – 7.79 (m, 2H), 7.75 (dt,  $J = 13.4, 10.5$  Hz, 2H), 7.57 – 7.42 (m, 4H), 7.36 (td,  $J = 5.9, 2.8$  Hz, 4H), 7.32 – 7.25 (m, 1H), 6.81 (dd,  $J = 7.9, 4.8$  Hz, 1H), 6.35 (s, 1H), 6.13 (s, 1H), 5.10 (s, 1H), 4.03 (q,  $J = 7.2$  Hz, 1H), 3.62 (d,  $J = 9.1$  Hz, 1H), 1.99 (d,  $J = 1.1$  Hz, 2H), 1.82 (d,  $J = 11.2$  Hz, 1H), 1.71 (d,  $J = 13.4$  Hz, 2H), 1.61 (d,  $J = 15.4$  Hz, 2H), 1.53 (d,  $J = 13.8$  Hz, 3H), 1.26 – 1.14 (m, 6H), 1.09 (s, 1H), 0.95 (q,  $J = 10.8$  Hz, 2H).



## **2-(N-(4-(tert-butyl)phenyl)acetamido)-N-cyclohexyl-2-(pyridin-3-yl)acetamide**

**(JG5.17):** White amorphous solid, 25% yield. <sup>1</sup>H NMR (500 MHz, DMSO)  $\delta$  8.31 – 8.21 (m, 2H), 8.02 (d,  $J = 7.7$  Hz, 1H), 7.29 (dt,  $J = 8.1, 2.0$  Hz, 1H), 7.19 (d,  $J = 7.9$  Hz, 2H), 7.10 (dd,  $J = 7.9, 4.8$  Hz, 2H), 6.04 (s, 1H), 3.59 – 3.50 (m, 1H), 1.73 (s, 1H), 1.70 (s, 3H), 1.68 – 1.49 (m, 5H), 1.17 (m, 5H).

### **4.5.3 Computational methods.**

The Schrödinger's software suite was used to prepare and optimize the protein and ligands, and to conduct the docking studies with the co-crystal structure of ML188 and SARS-CoV M<sup>PRO</sup> (PDB: 3V3M). The protein structure was refined with the Protein Preparation Wizard to add hydrogens, assign hydrogen bonds, fill missing side chains, and minimize the protein structure. The ligands were minimized using the OPLS\_2005 force field and the protonation state of the molecules were generated at pH = 7.4. The minimized ligands were docked in the binding pocket with Glide at the extra precision (XP) level and the state penalties were added to the docking score.

### **4.5.4 Viral replication cellular assay.**

A small molecule screening assay to assess inhibition of SARS-CoV-2 infection *in vitro*, developed and performed by Tejjaro, et al.,<sup>57</sup> was used to screen compounds **4.20** – **4.44**. Screening took place in 384-well plates using VeroE6 cells. Cells were plated in 384-well plates at a concentration of 5000 cells per well. SARS-CoV-2, isolated from a patients' sputum in San Diego, was added to the wells at a multiplicity of infection (MOI) of 0.1 and compounds were added to wells concomitantly with virus. Each compound was tested in triplicate and initially at 1 $\mu$ M. Over the course of 3 days, we monitored viral cytopathic effect (CPE) in the wells daily, and on day 3 CPE will be quantified by microscopy and cell titer glo viability staining. We used remdesivir and hydroxychloroquine as controls, as they have been reported to inhibit Coronavirus infection in

cells.<sup>58,59</sup> Identification of compounds which prevent CPE would be followed up by assessing a dose curve and analysis of viral titers in the supernatant by plaque forming assay to quantify viral loads in the cultures of both control and compound treated cells. Compounds with optimal biophysical properties would be followed up in more sophisticated *in vitro* assays and *in vivo* animal models following pharmacokinetic analysis. For animals studies we will use the human ACE2 knock-in mouse model which allows for production infection and pathology following SARS-CoV infection in the lungs.

#### **4.5.5 Enzymatic inhibition assays.**

Compounds were screened by a commercial enzymatic inhibition assay purchased from BPS Bioscience (3CL Protease, MBP-tagged (SARS-CoV-2) Assay Kit, catalog #79955-1). The kit was designed to measure 3CL protease activity for screening and profiling applications, in a homogeneous assay with no time-consuming washing steps. Provided by the kit were recombinant 3CL protease (MBP-tag), 3CL protease substrate (10 mM), fluorogenic 3CL protease assay buffer, and compound GC376 as a positive control. All assays were performed in black, low binding microtiter 96-well plates in the provided activity buffer with 1 mM dithiothreitol (DTT). Reactions contained 3 – 5 ng/μL 3CL protease. 3CL protease was incubated for 30 minutes at 25 °C with or without inhibitors. Reactions were started with the addition of the protease substrate and fluorescence was read at 0, 0.5, 1, 2, 3, 4 and 12 hours by an iTECAN Infinite M200 plate reader (excitation, 360 nm; emission, 460 nm) at room temperature.

## 4.6 References for Chapter 4

- (1) Coronavirus Disease (COVID-19) Situation Reports  
<https://www.who.int/emergencies/diseases/novel-coronavirus-2019/situation-reports>.
- (2) Ravelo, J. L.; Jerving, S. COVID-19 in 2020 — a timeline of the coronavirus outbreak  
<https://www.devex.com/news/sponsored/covid-19-in-2020-a-timeline-of-the-coronavirus-outbreak-99634>.
- (3) Zhang, L.; Lin, D.; Sun, X.; Curth, U.; Drosten, C.; Sauerhering, L.; Becker, S.; Rox, K.; Hilgenfeld, R. Crystal Structure of SARS-CoV-2 Main Protease Provides a Basis for Design of Improved  $\alpha$ -Ketoamide Inhibitors. *Science* **2020**, eabb3405.  
<https://doi.org/10.1126/science.abb3405>.
- (4) Dong, E.; Du, H.; Gardner, L. An Interactive Web-Based Dashboard to Track COVID-19 in Real Time. *The Lancet Infectious Diseases* **2020**, 20 (5), 533–534.  
[https://doi.org/10.1016/S1473-3099\(20\)30120-1](https://doi.org/10.1016/S1473-3099(20)30120-1).
- (5) Oum, S.; Kates, J.; Wexler, A. Economic Impact of COVID-19 on PEPFAR Countries. *KFF*, 2022.
- (6) How Covid is Straining the Healthcare System <https://health.clevelandclinic.org/how-the-pandemic-is-straining-the-healthcare-system-and-what-you-can-do-to-help/>.
- (7) The Pandemic Has Exacerbated Existing Political Discontent. *The Economist*. July 31, 2021.
- (8) Yard, E.; Radhakrishnan, L.; Ballesteros, M. F.; Sheppard, M.; Gates, A.; Stein, Z.; Hartnett, K.; Kite-Powell, A.; Rodgers, L.; Adjemian, J.; Ehlman, D. C.; Holland, K.; Idaikkadar, N.; Ivey-Stephenson, A.; Martinez, P.; Law, R.; Stone, D. M. Emergency Department Visits for Suspected Suicide Attempts Among Persons Aged 12–25 Years Before and During the

- COVID-19 Pandemic — United States, January 2019–May 2021. *MMWR Morb Mortal Wkly Rep* **2021**, *70* (24), 888–894. <https://doi.org/10.15585/mmwr.mm7024e1>.
- (9) Lavey, N. P.; Shadid, T.; Ballard, J. D.; Duerfeldt, A. S. Clostridium Difficile ClpP Homologues Are Capable of Uncoupled Activity and Exhibit Different Levels of Susceptibility to Acyldepsipeptide Modulation. *ACS Infect. Dis.* **2019**, *5* (1), 79–89. <https://doi.org/10.1021/acsinfecdis.8b00199>.
- (10) Li, Y.; Gardner, J. J.; Fortney, K. R.; Leus, I. V.; Bonifay, V.; Zgurskaya, H. I.; Pletnev, A. A.; Zhang, S.; Zhang, Z.-Y.; Gribble, G. W.; Spinola, S. M.; Duerfeldt, A. S. First-Generation Structure-Activity Relationship Studies of 2,3,4,9-Tetrahydro-1H-Carbazol-1-Amines as CpxA Phosphatase Inhibitors. *Bioorganic & Medicinal Chemistry Letters* **2019**, *29* (14), 1836–1841. <https://doi.org/10.1016/j.bmcl.2019.05.003>.
- (11) Hughes, D.; Andersson, D. I. Evolutionary Consequences of Drug Resistance: Shared Principles across Diverse Targets and Organisms. *Nat Rev Genet* **2015**, *16* (8), 459–471. <https://doi.org/10.1038/nrg3922>.
- (12) Woo, P. C. Y.; Huang, Y.; Lau, S. K. P.; Yuen, K.-Y. Coronavirus Genomics and Bioinformatics Analysis. *Viruses* **2010**, *2* (8), 1804–1820. <https://doi.org/10.3390/v2081803>.
- (13) Rahman, Md. T.; Sobur, Md. A.; Islam, Md. S.; Ievy, S.; Hossain, Md. J.; El Zowalaty, M. E.; Rahman, A. T.; Ashour, H. M. Zoonotic Diseases: Etiology, Impact, and Control. *Microorganisms* **2020**, *8* (9), 1405. <https://doi.org/10.3390/microorganisms8091405>.
- (14) Lai, M. M. C.; Cavanagh, D. The Molecular Biology of Coronaviruses. In *Advances in Virus Research*; Maramorosch, K., Murphy, F. A., Shatkin, A. J., Eds.; Academic Press, 1997; Vol. 48, pp 1–100. [https://doi.org/10.1016/S0065-3527\(08\)60286-9](https://doi.org/10.1016/S0065-3527(08)60286-9).

- (15) Peiris, J.; Chu, C.; Cheng, V.; Chan, K.; Hung, I.; Poon, L.; Law, K.; Tang, B.; Hon, T.; Chan, C.; Chan, K.; Ng, J.; Zheng, B.; Ng, W.; Lai, R.; Guan, Y.; Yuen, K. Clinical Progression and Viral Load in a Community Outbreak of Coronavirus-Associated SARS Pneumonia: A Prospective Study. *The Lancet* **2003**, *361* (9371), 1767–1772. [https://doi.org/10.1016/S0140-6736\(03\)13412-5](https://doi.org/10.1016/S0140-6736(03)13412-5).
- (16) Cheng, V. C. C.; Lau, S. K. P.; Woo, P. C. Y.; Yuen, K. Y. Severe Acute Respiratory Syndrome Coronavirus as an Agent of Emerging and Reemerging Infection. *Clinical Microbiology Reviews* **2007**, *20* (4), 660–694. <https://doi.org/10.1128/CMR.00023-07>.
- (17) Zaki, A. M.; van Boheemen, S.; Bestebroer, T. M.; Osterhaus, A. D. M. E.; Fouchier, R. A. M. Isolation of a Novel Coronavirus from a Man with Pneumonia in Saudi Arabia. *New England Journal of Medicine* **2012**, *367* (19), 1814–1820. <https://doi.org/10.1056/NEJMoa1211721>.
- (18) Killerby, M. E.; Biggs, H. M.; Midgley, C. M.; Gerber, S. I.; Watson, J. T. Middle East Respiratory Syndrome Coronavirus Transmission. *Emerg Infect Dis* **2020**, *26* (2), 191–198. <https://doi.org/10.3201/eid2602.190697>.
- (19) Al-Tawfiq, J. A. Middle East Respiratory Syndrome-Coronavirus Infection: An Overview. *Journal of Infection and Public Health* **2013**, *6* (5), 319–322. <https://doi.org/10.1016/j.jiph.2013.06.001>.
- (20) Morse, J. S.; Lalonde, T.; Xu, S.; Liu, W. R. Learning from the Past: Possible Urgent Prevention and Treatment Options for Severe Acute Respiratory Infections Caused by 2019-nCoV. *Chembiochem* **2020**, *21* (5), 730–738. <https://doi.org/10.1002/cbic.202000047>.

- (21) Krishnamoorthy, S.; Swain, B.; Verma, R. S.; Gunthe, S. S. SARS-CoV, MERS-CoV, and 2019-NCoV Viruses: An Overview of Origin, Evolution, and Genetic Variations. *Virusdisease* **2020**, *31* (4), 411–423. <https://doi.org/10.1007/s13337-020-00632-9>.
- (22) Huang, C.; Wang, Y.; Li, X.; Ren, L.; Zhao, J.; Hu, Y.; Zhang, L.; Fan, G.; Xu, J.; Gu, X.; Cheng, Z.; Yu, T.; Xia, J.; Wei, Y.; Wu, W.; Xie, X.; Yin, W.; Li, H.; Liu, M.; Xiao, Y.; Gao, H.; Guo, L.; Xie, J.; Wang, G.; Jiang, R.; Gao, Z.; Jin, Q.; Wang, J.; Cao, B. Clinical Features of Patients Infected with 2019 Novel Coronavirus in Wuhan, China. *Lancet* **2020**, *395* (10223), 497–506. [https://doi.org/10.1016/S0140-6736\(20\)30183-5](https://doi.org/10.1016/S0140-6736(20)30183-5).
- (23) Wu, F.; Zhao, S.; Yu, B.; Chen, Y.-M.; Wang, W.; Song, Z.-G.; Hu, Y.; Tao, Z.-W.; Tian, J.-H.; Pei, Y.-Y.; Yuan, M.-L.; Zhang, Y.-L.; Dai, F.-H.; Liu, Y.; Wang, Q.-M.; Zheng, J.-J.; Xu, L.; Holmes, E. C.; Zhang, Y.-Z. A New Coronavirus Associated with Human Respiratory Disease in China. *Nature* **2020**, *579* (7798), 265–269. <https://doi.org/10.1038/s41586-020-2008-3>.
- (24) Wu, C.-Y.; Jan, J.-T.; Ma, S.-H.; Kuo, C.-J.; Juan, H.-F.; Cheng, Y.-S. E.; Hsu, H.-H.; Huang, H.-C.; Wu, D.; Brik, A.; Liang, F.-S.; Liu, R.-S.; Fang, J.-M.; Chen, S.-T.; Liang, P.-H.; Wong, C.-H. Small Molecules Targeting Severe Acute Respiratory Syndrome Human Coronavirus. *Proceedings of the National Academy of Sciences* **2004**, *101* (27), 10012–10017. <https://doi.org/10.1073/pnas.0403596101>.
- (25) Delre, P.; Caporuscio, F.; Saviano, M.; Mangiatordi, G. F. Repurposing Known Drugs as Covalent and Non-Covalent Inhibitors of the SARS-CoV-2 Papain-Like Protease. *Frontiers in Chemistry* **2020**, *8*.
- (26) Alamri, M. A.; Tahir ul Qamar, M.; Mirza, M. U.; Alqahtani, S. M.; Froeyen, M.; Chen, L.-L. Discovery of Human Coronaviruses Pan-Papain-like Protease Inhibitors Using

- Computational Approaches. *Journal of Pharmaceutical Analysis* **2020**, *10* (6), 546–559. <https://doi.org/10.1016/j.jpha.2020.08.012>.
- (27) Tchesnokov, E. P.; Feng, J. Y.; Porter, D. P.; Götte, M. Mechanism of Inhibition of Ebola Virus RNA-Dependent RNA Polymerase by Remdesivir. *Viruses* **2019**, *11* (4), 326. <https://doi.org/10.3390/v11040326>.
- (28) Crotty, S.; Cameron, C.; Andino, R. Ribavirin's Antiviral Mechanism of Action: Lethal Mutagenesis? *J Mol Med* **2002**, *80* (2), 86–95. <https://doi.org/10.1007/s00109-001-0308-0>.
- (29) Shuster, A.; Pechalrieu, D.; Jackson, C. B.; Abegg, D.; Choe, H.; Adibekian, A. Clinical Antiviral Drug Arbidol Inhibits Infection by SARS-CoV-2 and Variants through Direct Binding to the Spike Protein. *ACS Chem Biol* **2021**, [acscchembio.1c00756](https://doi.org/10.1021/acscchembio.1c00756). <https://doi.org/10.1021/acscchembio.1c00756>.
- (30) Padhi, A. K.; Seal, A.; Khan, J. M.; Ahamed, M.; Tripathi, T. Unraveling the Mechanism of Arbidol Binding and Inhibition of SARS-CoV-2: Insights from Atomistic Simulations. *Eur J Pharmacol* **2021**, *894*, 173836. <https://doi.org/10.1016/j.ejphar.2020.173836>.
- (31) De Witt, B. J.; Garrison, E. A.; Champion, H. C.; Kadowitz, P. J. L-163,491 Is a Partial Angiotensin AT1 Receptor Agonist in the Hindquarters Vascular Bed of the Cat. *European Journal of Pharmacology* **2000**, *404* (1), 213–219. [https://doi.org/10.1016/S0014-2999\(00\)00612-9](https://doi.org/10.1016/S0014-2999(00)00612-9).
- (32) Kawase, M.; Shirato, K.; van der Hoek, L.; Taguchi, F.; Matsuyama, S. Simultaneous Treatment of Human Bronchial Epithelial Cells with Serine and Cysteine Protease Inhibitors Prevents Severe Acute Respiratory Syndrome Coronavirus Entry. *Journal of Virology* **2012**, *86* (12), 6537–6545. <https://doi.org/10.1128/JVI.00094-12>.

- (33) Bosch, B. J.; van der Zee, R.; de Haan, C. A. M.; Rottier, P. J. M. The Coronavirus Spike Protein Is a Class I Virus Fusion Protein: Structural and Functional Characterization of the Fusion Core Complex. *Journal of Virology* **2003**, *77* (16), 8801–8811. <https://doi.org/10.1128/JVI.77.16.8801-8811.2003>.
- (34) Wan, Y.; Shang, J.; Graham, R.; Baric, R. S.; Li, F. Receptor Recognition by the Novel Coronavirus from Wuhan: An Analysis Based on Decade-Long Structural Studies of SARS Coronavirus. *J Virol* **2020**, *94* (7), e00127-20. <https://doi.org/10.1128/JVI.00127-20>.
- (35) Leneva, I. A.; Russell, R. J.; Boriskin, Y. S.; Hay, A. J. Characteristics of Arbidol-Resistant Mutants of Influenza Virus: Implications for the Mechanism of Anti-Influenza Action of Arbidol. *Antiviral Research* **2009**, *81* (2), 132–140. <https://doi.org/10.1016/j.antiviral.2008.10.009>.
- (36) Xu, P.; Huang, J.; Fan, Z.; Huang, W.; Qi, M.; Lin, X.; Song, W.; Yi, L. Arbidol/IFN-A2b Therapy for Patients with Corona Virus Disease 2019: A Retrospective Multicenter Cohort Study. *Microbes and Infection* **2020**, *22* (4), 200–205. <https://doi.org/10.1016/j.micinf.2020.05.012>.
- (37) Brant, A. C.; Tian, W.; Majerciak, V.; Yang, W.; Zheng, Z.-M. SARS-CoV-2: From Its Discovery to Genome Structure, Transcription, and Replication. *Cell & Bioscience* **2021**, *11* (1), 136. <https://doi.org/10.1186/s13578-021-00643-z>.
- (38) Kumar, V.; Tan, K.-P.; Wang, Y.-M.; Lin, S.-W.; Liang, P.-H. Identification, Synthesis and Evaluation of SARS-CoV and MERS-CoV 3C-like Protease Inhibitors. *Bioorganic & Medicinal Chemistry* **2016**, *24* (13), 3035–3042. <https://doi.org/10.1016/j.bmc.2016.05.013>.
- (39) Arya, R.; Das, A.; Prashar, V.; Kumar, M. Potential Inhibitors against Papain-like Protease of Novel Coronavirus (SARS-CoV-2) from FDA Approved Drugs. **8**.



- (40) Cho, E.; Rosa, M.; Anjum, R.; Mehmood, S.; Soban, M.; Mujtaba, M.; Bux, K.; Moin, S. T.; Tanweer, M.; Dantu, S.; Pandini, A.; Yin, J.; Ma, H.; Ramanathan, A.; Islam, B.; Mey, A. S. J. S.; Bhowmik, D.; Haider, S. Dynamic Profiling of  $\beta$ -Coronavirus 3CL Mpro Protease Ligand-Binding Sites. *J. Chem. Inf. Model.* **2021**, *61* (6), 3058–3073. <https://doi.org/10.1021/acs.jcim.1c00449>.
- (41) Pillaiyar, T.; Meenakshisundaram, S.; Manickam, M. Recent Discovery and Development of Inhibitors Targeting Coronaviruses. *Drug Discovery Today* **2020**, S1359644620300416. <https://doi.org/10.1016/j.drudis.2020.01.015>.
- (42) Wu, C.; Liu, Y.; Yang, Y.; Zhang, P.; Zhong, W.; Wang, Y.; Wang, Q.; Xu, Y.; Li, M.; Li, X.; Zheng, M.; Chen, L.; Li, H. Analysis of Therapeutic Targets for SARS-CoV-2 and Discovery of Potential Drugs by Computational Methods. *Acta Pharmaceutica Sinica B* **2020**, *10* (5), 766–788. <https://doi.org/10.1016/j.apsb.2020.02.008>.
- (43) Yao, T.-T.; Qian, J.-D.; Zhu, W.-Y.; Wang, Y.; Wang, G.-Q. A Systematic Review of Lopinavir Therapy for SARS Coronavirus and MERS Coronavirus-A Possible Reference for Coronavirus Disease-19 Treatment Option. *J Med Virol* **2020**, *92* (6), 556–563. <https://doi.org/10.1002/jmv.25729>.
- (44) Patel, T. K.; Patel, P. B.; Barvaliya, M.; Saurabh, M. K.; Bhalla, H. L.; Khosla, P. P. Efficacy and Safety of Lopinavir-Ritonavir in COVID-19: A Systematic Review of Randomized Controlled Trials. *J Infect Public Health* **2021**, *14* (6), 740–748. <https://doi.org/10.1016/j.jiph.2021.03.015>.
- (45) Ghosh, A. K.; Gong, G.; Grum-Tokars, V.; Mulhearn, D. C.; Baker, S. C.; Coughlin, M.; Prabhakar, B. S.; Sleeman, K.; Johnson, M. E.; Mesecar, A. D. Design, Synthesis and Antiviral Efficacy of a Series of Potent Chloropyridyl Ester-Derived SARS-CoV 3CLpro

- Inhibitors. *Bioorganic & Medicinal Chemistry Letters* **2008**, *18* (20), 5684–5688.  
<https://doi.org/10.1016/j.bmcl.2008.08.082>.
- (46) Cao, W.; Cho, C.-C. D.; Geng, Z. Z.; Shaabani, N.; Ma, X. R.; Vatansever, E. C.; Alugubelli, Y. R.; Ma, Y.; Chaki, S. P.; Ellenburg, W. H.; Yang, K. S.; Qiao, Y.; Allen, R.; Neuman, B. W.; Ji, H.; Xu, S.; Liu, W. R. Evaluation of SARS-CoV-2 Main Protease Inhibitors Using a Novel Cell-Based Assay. *ACS Cent. Sci.* **2022**, *8* (2), 192–204.  
<https://doi.org/10.1021/acscentsci.1c00910>.
- (47) Galasiti Kankanamalage, A. C.; Kim, Y.; Damalanka, V. C.; Rathnayake, A. D.; Fehr, A. R.; Mehzabeen, N.; Battaile, K. P.; Lovell, S.; Lushington, G. H.; Perlman, S.; Chang, K.-O.; Groutas, W. C. Structure-Guided Design of Potent and Permeable Inhibitors of MERS Coronavirus 3CL Protease That Utilize a Piperidine Moiety as a Novel Design Element. *European Journal of Medicinal Chemistry* **2018**, *150*, 334–346.  
<https://doi.org/10.1016/j.ejmech.2018.03.004>.
- (48) Jacobs, J.; Grum-Tokars, V.; Zhou, Y.; Turlington, M.; Saldanha, S. A.; Chase, P.; Eggler, A.; Dawson, E. S.; Baez-Santos, Y. M.; Tomar, S.; Mielech, A. M.; Baker, S. C.; Lindsley, C. W.; Hodder, P.; Mesecar, A.; Stauffer, S. R. Discovery, Synthesis, And Structure-Based Optimization of a Series of *N*-(*Tert*-Butyl)-2-(*N*-Arylamido)-2-(Pyridin-3-Yl) Acetamides (ML188) as Potent Noncovalent Small Molecule Inhibitors of the Severe Acute Respiratory Syndrome Coronavirus (SARS-CoV) 3CL Protease. *J. Med. Chem.* **2013**, *56* (2), 534–546.  
<https://doi.org/10.1021/jm301580n>.
- (49) Báez-Santos, Y. M.; Barraza, S. J.; Wilson, M. W.; Agius, M. P.; Mielech, A. M.; Davis, N. M.; Baker, S. C.; Larsen, S. D.; Mesecar, A. D. X-Ray Structural and Biological Evaluation

- of a Series of Potent and Highly Selective Inhibitors of Human Coronavirus Papain-like Proteases. *J. Med. Chem.* **2014**, *57* (6), 2393–2412. <https://doi.org/10.1021/jm401712t>.
- (50) Lee, H.; Lei, H.; Santarsiero, B. D.; Gatuz, J. L.; Cao, S.; Rice, A. J.; Patel, K.; Szypulinski, M. Z.; Ojeda, I.; Ghosh, A. K.; Johnson, M. E. Inhibitor Recognition Specificity of MERS-CoV Papain-like Protease May Differ from That of SARS-CoV. *ACS Chem. Biol.* **2015**, *10* (6), 1456–1465. <https://doi.org/10.1021/cb500917m>.
- (51) Giner-Sorolla, A.; Bendich, A. Fluorine-Containing Pyrimidines and Purines: Synthesis and Properties of Trifluoromethyl Pyrimidines and Purines<sup>1</sup>. *J. Am. Chem. Soc.* **1958**, *80* (21), 5744–5752. <https://doi.org/10.1021/ja01554a041>.
- (52) Pervushin, K.; Tan, E.; Parthasarathy, K.; Lin, X.; Jiang, F. L.; Yu, D.; Vararattanavech, A.; Soong, T. W.; Liu, D. X.; Torres, J. Structure and Inhibition of the SARS Coronavirus Envelope Protein Ion Channel. *PLOS Pathogens* **2009**, *5* (7), e1000511. <https://doi.org/10.1371/journal.ppat.1000511>.
- (53) Milewska, A.; Nowak, P.; Owczarek, K.; Szczepanski, A.; Zarebski, M.; Hoang, A.; Berniak, K.; Wojarski, J.; Zeglen, S.; Baster, Z.; Rajfur, Z.; Pyrc, K. Entry of Human Coronavirus NL63 into the Cell. *Journal of Virology* **2018**, *92* (3). <https://doi.org/10.1128/JVI.01933-17>.
- (54) Roger, C.; Roberts, J. A.; Muller, L. Clinical Pharmacokinetics and Pharmacodynamics of Oxazolidinones. *Clin Pharmacokinet* **2018**, *57* (5), 559–575. <https://doi.org/10.1007/s40262-017-0601-x>.
- (55) Swaney, S. M.; Aoki, H.; Ganoza, M. C.; Shinabarger, D. L. The Oxazolidinone Linezolid Inhibits Initiation of Protein Synthesis in Bacteria. *Antimicrob Agents Chemother* **1998**, *42* (12), 3251–3255. <https://doi.org/10.1128/AAC.42.12.3251>.

- (56) Moghadam, V. D.; Momenimovahed, Z.; Ghorbani, M.; Khodadadi, J. Linezolid a Potential Treatment for COVID-19 Coinfections. *Braz J Anesthesiol* **2021**, *71* (2), 198. <https://doi.org/10.1016/j.bjane.2020.12.019>.
- (57) Bakowski, M. A.; Beutler, N.; Wolff, K. C.; Kirkpatrick, M. G.; Chen, E.; Nguyen, T.-T. H.; Riva, L.; Shaabani, N.; Parren, M.; Ricketts, J.; Gupta, A. K.; Pan, K.; Kuo, P.; Fuller, M.; Garcia, E.; Teijaro, J. R.; Yang, L.; Sahoo, D.; Chi, V.; Huang, E.; Vargas, N.; Roberts, A. J.; Das, S.; Ghosh, P.; Woods, A. K.; Joseph, S. B.; Hull, M. V.; Schultz, P. G.; Burton, D. R.; Chatterjee, A. K.; McNamara, C. W.; Rogers, T. F. Drug Repurposing Screens Identify Chemical Entities for the Development of COVID-19 Interventions. *Nat Commun* **2021**, *12* (1), 1–14. <https://doi.org/10.1038/s41467-021-23328-0>.
- (58) Beigel, J. H.; Tomashek, K. M.; Dodd, L. E.; Mehta, A. K.; Zingman, B. S.; Kalil, A. C.; Hohmann, E.; Chu, H. Y.; Luetkemeyer, A.; Kline, S.; Lopez de Castilla, D.; Finberg, R. W.; Dierberg, K.; Tapson, V.; Hsieh, L.; Patterson, T. F.; Paredes, R.; Sweeney, D. A.; Short, W. R.; Touloumi, G.; Lye, D. C.; Ohmagari, N.; Oh, M.; Ruiz-Palacios, G. M.; Benfield, T.; Fätkenheuer, G.; Kortepeter, M. G.; Atmar, R. L.; Creech, C. B.; Lundgren, J.; Babiker, A. G.; Pett, S.; Neaton, J. D.; Burgess, T. H.; Bonnett, T.; Green, M.; Makowski, M.; Osinusi, A.; Nayak, S.; Lane, H. C. Remdesivir for the Treatment of Covid-19 — Final Report. *New England Journal of Medicine* **2020**, *383* (19), 1813–1826. <https://doi.org/10.1056/NEJMoa2007764>.
- (59) Sinha, N.; Balayla, G. Hydroxychloroquine and COVID-19. *Postgraduate Medical Journal* **2020**, *96* (1139), 550–555. <https://doi.org/10.1136/postgradmedj-2020-137785>.
- (60) Isolation of Potent SARS-CoV-2 Neutralizing Antibodies and Protection from Disease in a Small Animal Model. *Science*.

- (61) Shin, D.; Mukherjee, R.; Grewe, D.; Bojkova, D.; Baek, K.; Bhattacharya, A.; Schulz, L.; Widera, M.; Mehdipour, A. R.; Tascher, G.; Geurink, P. P.; Wilhelm, A.; van der Heden van Noort, G. J.; Ovaa, H.; Müller, S.; Knobloch, K.-P.; Rajalingam, K.; Schulman, B. A.; Cinatl, J.; Hummer, G.; Ciesek, S.; Dikic, I. Papain-like Protease Regulates SARS-CoV-2 Viral Spread and Innate Immunity. *Nature* **2020**, *587* (7835), 657–662. <https://doi.org/10.1038/s41586-020-2601-5>.
- (62) Pfeffer, L. M. The Role of Nuclear Factor KB in the Interferon Response. *J Interferon Cytokine Res* **2011**, *31* (7), 553–559. <https://doi.org/10.1089/jir.2011.0028>.
- (63) Lin, Y.; Zang, R.; Ma, Y.; Wang, Z.; Li, L.; Ding, S.; Zhang, R.; Wei, Z.; Yang, J.; Wang, X. Xanthohumol Is a Potent Pan-Inhibitor of Coronaviruses Targeting Main Protease. *International Journal of Molecular Sciences* **2021**, *22* (22), 12134. <https://doi.org/10.3390/ijms222212134>.
- (64) Owen, D. R.; Allerton, C. M. N.; Anderson, A. S.; Aschenbrenner, L.; Avery, M.; Berritt, S.; Boras, B.; Cardin, R. D.; Carlo, A.; Coffman, K. J.; Dantonio, A.; Di, L.; Eng, H.; Ferre, R.; Gajiwala, K. S.; Gibson, S. A.; Greasley, S. E.; Hurst, B. L.; Kadar, E. P.; Kalgutkar, A. S.; Lee, J. C.; Lee, J.; Liu, W.; Mason, S. W.; Noell, S.; Novak, J. J.; Obach, R. S.; Ogilvie, K.; Patel, N. C.; Pettersson, M.; Rai, D. K.; Reese, M. R.; Sammons, M. F.; Sathish, J. G.; Singh, R. S. P.; Stepan, C. M.; Stewart, A. E.; Tuttle, J. B.; Updyke, L.; Verhoest, P. R.; Wei, L.; Yang, Q.; Zhu, Y. An Oral SARS-CoV-2 Mpro Inhibitor Clinical Candidate for the Treatment of COVID-19. *Science* **2021**, *374* (6575), 1586–1593. <https://doi.org/10.1126/science.abl4784>.
- (65) Suárez, D.; Díaz, N. SARS-CoV-2 Main Protease: A Molecular Dynamics Study. *J. Chem. Inf. Model.* **2020**, *60* (12), 5815–5831. <https://doi.org/10.1021/acs.jcim.0c00575>.

- (66) Anand, K.; Palm, G. J.; Mesters, J. R.; Siddell, S. G.; Ziebuhr, J.; Hilgenfeld, R. Structure of Coronavirus Main Proteinase Reveals Combination of a Chymotrypsin Fold with an Extra  $\alpha$ -Helical Domain. *EMBO J* **2002**, *21* (13), 3213–3224. <https://doi.org/10.1093/emboj/cdf327>.
- (67) Dodson, G.; Wlodawer, A. Catalytic Triads and Their Relatives. *Trends in Biochemical Sciences* **1998**, *23* (9), 347–352. [https://doi.org/10.1016/S0968-0004\(98\)01254-7](https://doi.org/10.1016/S0968-0004(98)01254-7).
- (68) Ma, C.; Sacco, M. D.; Hurst, B.; Townsend, J. A.; Hu, Y.; Szeto, T.; Zhang, X.; Tarbet, B.; Marty, M. T.; Chen, Y.; Wang, J. Boceprevir, GC-376, and Calpain Inhibitors II, XII Inhibit SARS-CoV-2 Viral Replication by Targeting the Viral Main Protease. *Cell Res* **2020**, *30* (8), 678–692. <https://doi.org/10.1038/s41422-020-0356-z>.
- (69) Anand, K.; Ziebuhr, J.; Wadhwani, P.; Mesters, J. R.; Hilgenfeld, R. Coronavirus Main Proteinase (3CLpro) Structure: Basis for Design of Anti-SARS Drugs. *Science* **2003**, *300* (5626), 1763–1767. <https://doi.org/10.1126/science.1085658>.
- (70) Yang, H.; Bartlam, M.; Rao, Z. Drug Design Targeting the Main Protease, the Achilles' Heel of Coronaviruses. *Curr Pharm Des* **2006**, *12* (35), 4573–4590. <https://doi.org/10.2174/138161206779010369>.
- (71) Fan, K.; Ma, L.; Han, X.; Liang, H.; Wei, P.; Liu, Y.; Lai, L. The Substrate Specificity of SARS Coronavirus 3C-like Proteinase. *Biochem Biophys Res Commun* **2005**, *329* (3), 934–940. <https://doi.org/10.1016/j.bbrc.2005.02.061>.
- (72) Chuck, C.-P.; Chow, H.-F.; Wan, D. C.-C.; Wong, K.-B. Profiling of Substrate Specificities of 3C-Like Proteases from Group 1, 2a, 2b, and 3 Coronaviruses. *PLOS ONE* **2011**, *6* (11), e27228. <https://doi.org/10.1371/journal.pone.0027228>.
- (73) Jin, Z.; Du, X.; Xu, Y.; Deng, Y.; Liu, M.; Zhao, Y.; Zhang, B.; Li, X.; Zhang, L.; Peng, C.; Duan, Y.; Yu, J.; Wang, L.; Yang, K.; Liu, F.; Jiang, R.; Yang, X.; You, T.; Liu, X.; Yang,

- X.; Bai, F.; Liu, H.; Liu, X.; Guddat, L. W.; Xu, W.; Xiao, G.; Qin, C.; Shi, Z.; Jiang, H.; Rao, Z.; Yang, H. Structure of Mpro from SARS-CoV-2 and Discovery of Its Inhibitors. *Nature* **2020**, 582 (7811), 289–293. <https://doi.org/10.1038/s41586-020-2223-y>.
- (74) Zhang, L.; Lin, D.; Sun, X.; Curth, U.; Drosten, C.; Sauerhering, L.; Becker, S.; Rox, K.; Hilgenfeld, R. Crystal Structure of SARS-CoV-2 Main Protease Provides a Basis for Design of Improved  $\alpha$ -Ketoamide Inhibitors. *Science* **2020**, 368 (6489), 409–412. <https://doi.org/10.1126/science.abb3405>.
- (75) Yang, H.; Yang, M.; Ding, Y.; Liu, Y.; Lou, Z.; Zhou, Z.; Sun, L.; Mo, L.; Ye, S.; Pang, H.; Gao, G. F.; Anand, K.; Bartlam, M.; Hilgenfeld, R.; Rao, Z. The Crystal Structures of Severe Acute Respiratory Syndrome Virus Main Protease and Its Complex with an Inhibitor. *Proceedings of the National Academy of Sciences* **2003**, 100 (23), 13190–13195. <https://doi.org/10.1073/pnas.1835675100>.
- (76) Ghosh, A. K.; Xi, K.; Johnson, M. E.; Baker, S. C.; Mesecar, A. D. Progress in Anti-SARS Coronavirus Chemistry, Biology and Chemotherapy. *Annu Rep Med Chem* **2007**, 41, 183–196. [https://doi.org/10.1016/S0065-7743\(06\)41011-3](https://doi.org/10.1016/S0065-7743(06)41011-3).
- (77) Jain, R. P.; Pettersson, H. I.; Zhang, J.; Aull, K. D.; Fortin, P. D.; Huitema, C.; Eltis, L. D.; Parrish, J. C.; James, M. N. G.; Wishart, D. S.; Vederas, J. C. Synthesis and Evaluation of Keto-Glutamine Analogues as Potent Inhibitors of Severe Acute Respiratory Syndrome 3CLpro. *J. Med. Chem.* **2004**, 47 (25), 6113–6116. <https://doi.org/10.1021/jm0494873>.
- (78) O'Reilly, M.; Cleasby, A.; Davies, T. G.; Hall, R. J.; Ludlow, R. F.; Murray, C. W.; Tisi, D.; Jhoti, H. Crystallographic Screening Using Ultra-Low-Molecular-Weight Ligands to Guide Drug Design. *Drug Discovery Today* **2019**, 24 (5), 1081–1086. <https://doi.org/10.1016/j.drudis.2019.03.009>.

- (79) Ugi, I. The  $\alpha$ -Addition of Immonium Ions and Anions to Isonitriles Accompanied by Secondary Reactions. *Angewandte Chemie International Edition in English* **1962**, *1* (1), 8–21. <https://doi.org/10.1002/anie.196200081>.
- (80) Bienaymé, H.; Hulme, C.; Odon, G.; Schmitt, P. Maximizing Synthetic Efficiency: Multi-Component Transformations Lead the Way. *Chemistry – A European Journal* **2000**, *6* (18), 3321–3329. [https://doi.org/10.1002/1521-3765\(20000915\)6:18<3321::AID-CHEM3321>3.0.CO;2-A](https://doi.org/10.1002/1521-3765(20000915)6:18<3321::AID-CHEM3321>3.0.CO;2-A).
- (81) Ugi, I.; Werner, B.; Dömling, A. The Chemistry of Isocyanides, Their MultiComponent Reactions and Their Libraries. *Molecules* **2003**, *8* (1), 53–66. <https://doi.org/10.3390/80100053>.
- (82) Ostrovskaya, R. U.; Gruden, M. A.; Bobkova, N. A.; Sewell, R. D. E.; Gudasheva, T. A.; Samokhin, A. N.; Seredinin, S. B.; Noppe, W.; Sherstnev, V. V.; Morozova-Roche, L. A. The Nootropic and Neuroprotective Proline-Containing Dipeptide Noopept Restores Spatial Memory and Increases Immunoreactivity to Amyloid in an Alzheimer's Disease Model. *J Psychopharmacol* **2007**, *21* (6), 611–619. <https://doi.org/10.1177/0269881106071335>.
- (83) Ostrovskaya, R. U.; Gudasheva, T. A.; Zaplina, A. P.; Vahitova, Ju. V.; Salimgareeva, M. H.; Jamidanov, R. S.; Seredenin, S. B. Noopept Stimulates the Expression of NGF and BDNF in Rat Hippocampus. *Bull Exp Biol Med* **2008**, *146* (3), 334–337. <https://doi.org/10.1007/s10517-008-0297-x>.
- (84) PubChem Bioassay Record for AID 756284, Source: ChEMBL <https://pubchem.ncbi.nlm.nih.gov/bioassay/756284>.
- (85) 3CL Protease, MBP-tagged (SARS-CoV-2) Assay Kit <https://bpsbioscience.com/3cl-protease-sars-cov-2-assay-kit-79955>.

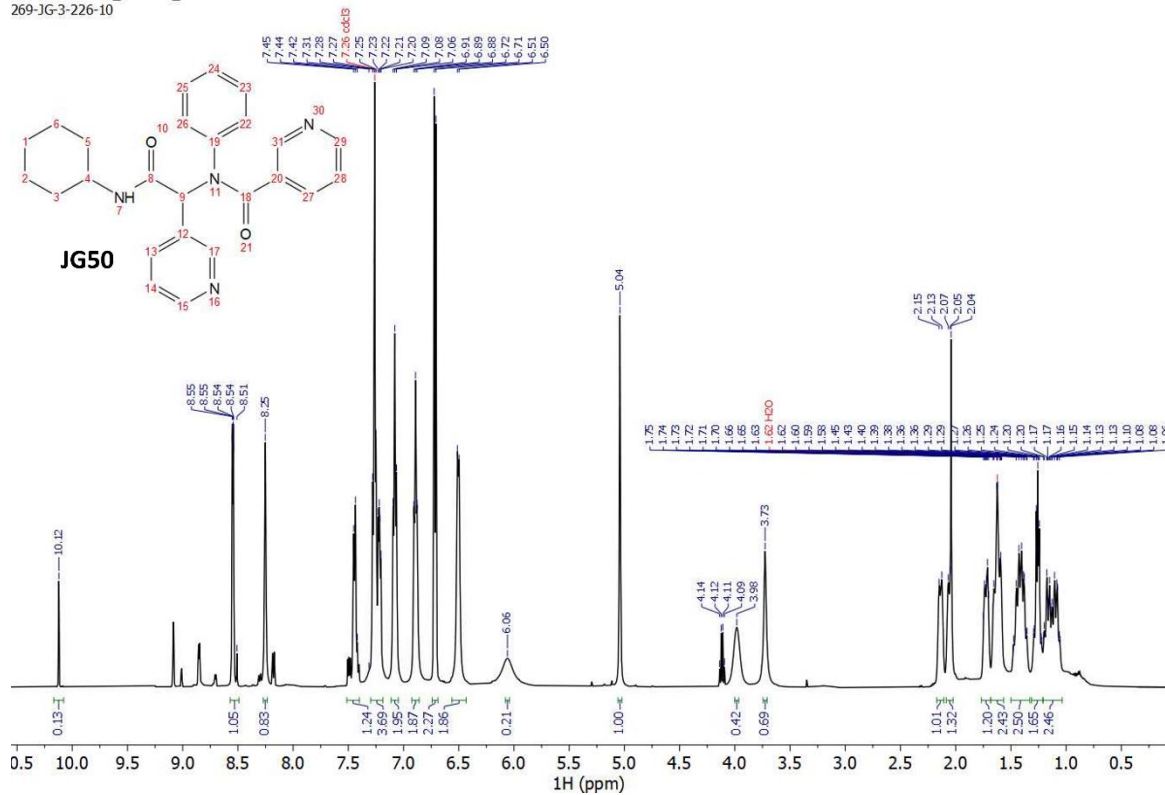


- (86) Kim, Y.; Liu, H.; Kankanamalage, A. C. G.; Weerasekara, S.; Hua, D. H.; Groutas, W. C.; Chang, K.-O.; Pedersen, N. C. Reversal of the Progression of Fatal Coronavirus Infection in Cats by a Broad-Spectrum Coronavirus Protease Inhibitor. *PLoS Pathogens* **2016**, *12* (3), e1005531. <https://doi.org/10.1371/journal.ppat.1005531>.
- (87) Larsen, R. S.; Zylka, M. J.; Scott, J. E. A High Throughput Assay to Identify Small Molecule Modulators of Prostatic Acid Phosphatase. *Curr Chem Genomics* **2009**, *3*, 42–49. <https://doi.org/10.2174/1875397300903010042>.
- (88) Turlington, M.; Chun, A.; Tomar, S.; Eggler, A.; Grum-Tokars, V.; Jacobs, J.; Daniels, J. S.; Dawson, E.; Saldanha, A.; Chase, P.; Baez-Santos, Y. M.; Lindsley, C. W.; Hodder, P.; Mesecar, A. D.; Stauffer, S. R. Discovery of N-(Benzo[1,2,3]Triazol-1-Yl)-N-(Benzyl)Acetamido)Phenyl) Carboxamides as Severe Acute Respiratory Syndrome Coronavirus (SARS-CoV) 3CLpro Inhibitors: Identification of ML300 and Noncovalent Nanomolar Inhibitors with an Induced-Fit Binding. *Bioorganic & Medicinal Chemistry Letters* **2013**, *23* (22), 6172–6177. <https://doi.org/10.1016/j.bmcl.2013.08.112>.
- (89) Hoffman, R. L.; Kania, R. S.; Brothers, M. A.; Davies, J. F.; Ferre, R. A.; Gajiwala, K. S.; He, M.; Hogan, R. J.; Kozminski, K.; Li, L. Y.; Lockner, J. W.; Lou, J.; Marra, M. T.; Mitchell, L. J.; Murray, B. W.; Nieman, J. A.; Noell, S.; Planken, S. P.; Rowe, T.; Ryan, K.; Smith, G. J.; Solowiej, J. E.; Stepan, C. M.; Taggart, B. Discovery of Ketone-Based Covalent Inhibitors of Coronavirus 3CL Proteases for the Potential Therapeutic Treatment of COVID-19. *J. Med. Chem.* **2020**, *63* (21), 12725–12747. <https://doi.org/10.1021/acs.jmedchem.0c01063>.
- (90) Xue, X.; Yang, H.; Shen, W.; Zhao, Q.; Li, J.; Yang, K.; Chen, C.; Jin, Y.; Bartlam, M.; Rao, Z. Production of Authentic SARS-CoV Mpro with Enhanced Activity: Application as a

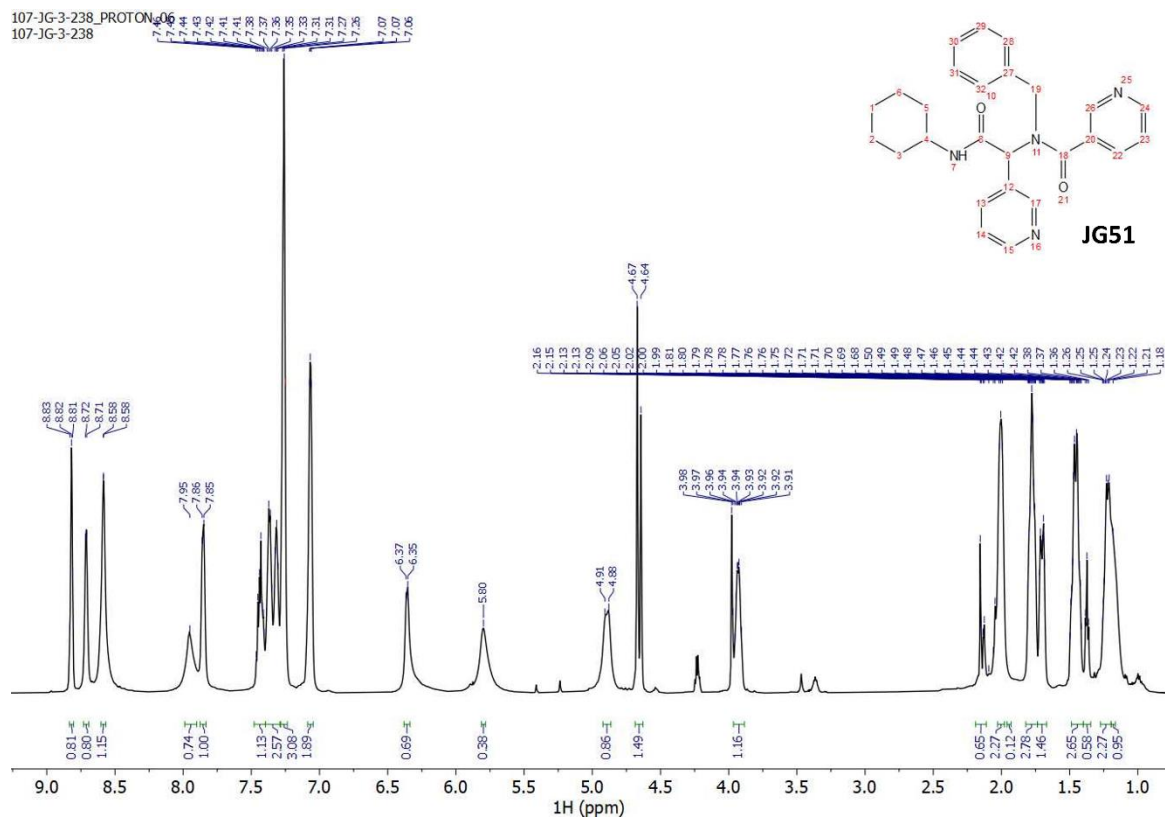
- Novel Tag-Cleavage Endopeptidase for Protein Overproduction. *J Mol Biol* **2007**, *366* (3), 965–975. <https://doi.org/10.1016/j.jmb.2006.11.073>.
- (91) Pfizer unveils its oral SARS-CoV-2 inhibitor <http://cen.acs.org/acs-news/acs-meeting-news/Pfizer-unveils-oral-SARS-CoV/99/i13> (accessed 2022 -02 -28).
- (92) *The Encyclopedia of New York City*; Jackson, K. T., New-York Historical Society, Eds.; Yale University Press ; New-York Historical Society: New Haven, Conn. : New York, 1995.
- (93) Ahmad, B.; Batool, M.; Ain, Q. ul; Kim, M. S.; Choi, S. Exploring the Binding Mechanism of PF-07321332 SARS-CoV-2 Protease Inhibitor through Molecular Dynamics and Binding Free Energy Simulations. *International Journal of Molecular Sciences* **2021**, *22* (17), 9124. <https://doi.org/10.3390/ijms22179124>.
- (94) Leist, S. R.; Dinno, K. H.; Schäfer, A.; Tse, L. V.; Okuda, K.; Hou, Y. J.; West, A.; Edwards, C. E.; Sanders, W.; Fritch, E. J.; Gully, K. L.; Scobey, T.; Brown, A. J.; Sheahan, T. P.; Moorman, N. J.; Boucher, R. C.; Gralinski, L. E.; Montgomery, S. A.; Baric, R. S. A Mouse-Adapted SARS-CoV-2 Induces Acute Lung Injury and Mortality in Standard Laboratory Mice. *Cell* **2020**, *183* (4), 1070-1085.e12. <https://doi.org/10.1016/j.cell.2020.09.050>.

## **Appendix II. Spectra Relevant to Chapter 4**

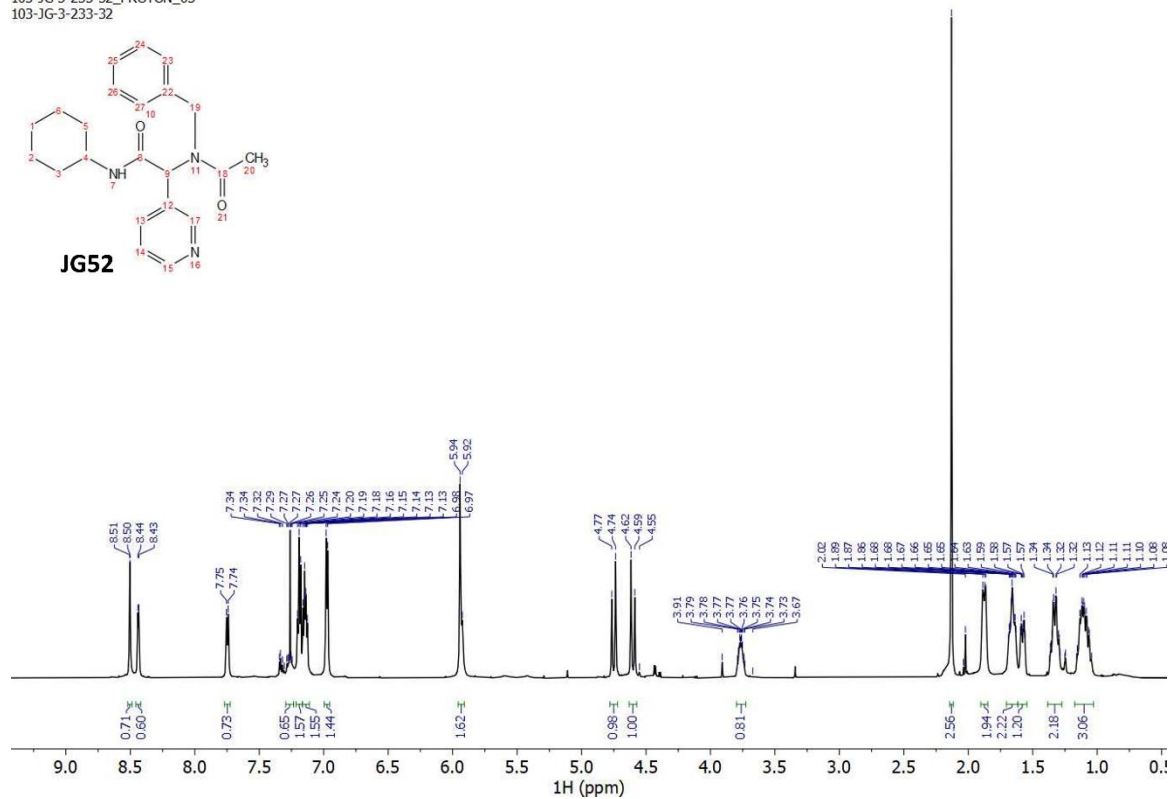
269-JG-3-226-10\_PROTON\_03  
269-JG-3-226-10



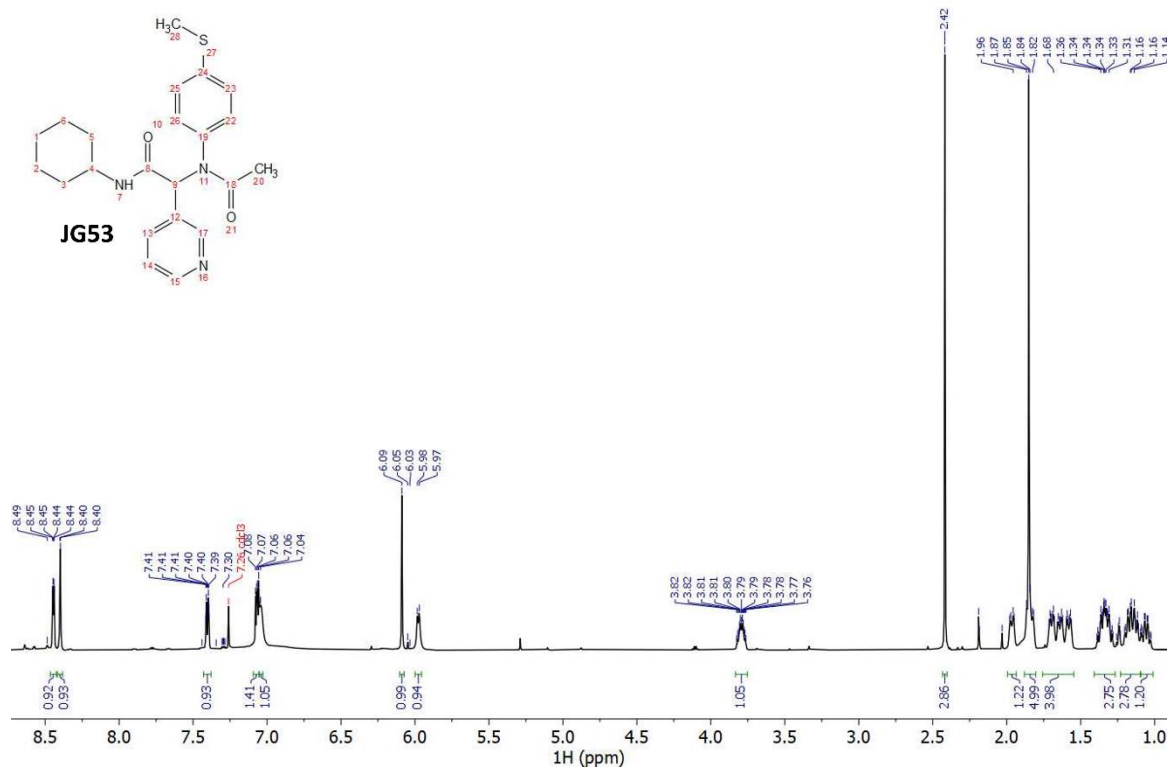
107-JG-3-238\_PROTON\_04  
107-JG-3-238



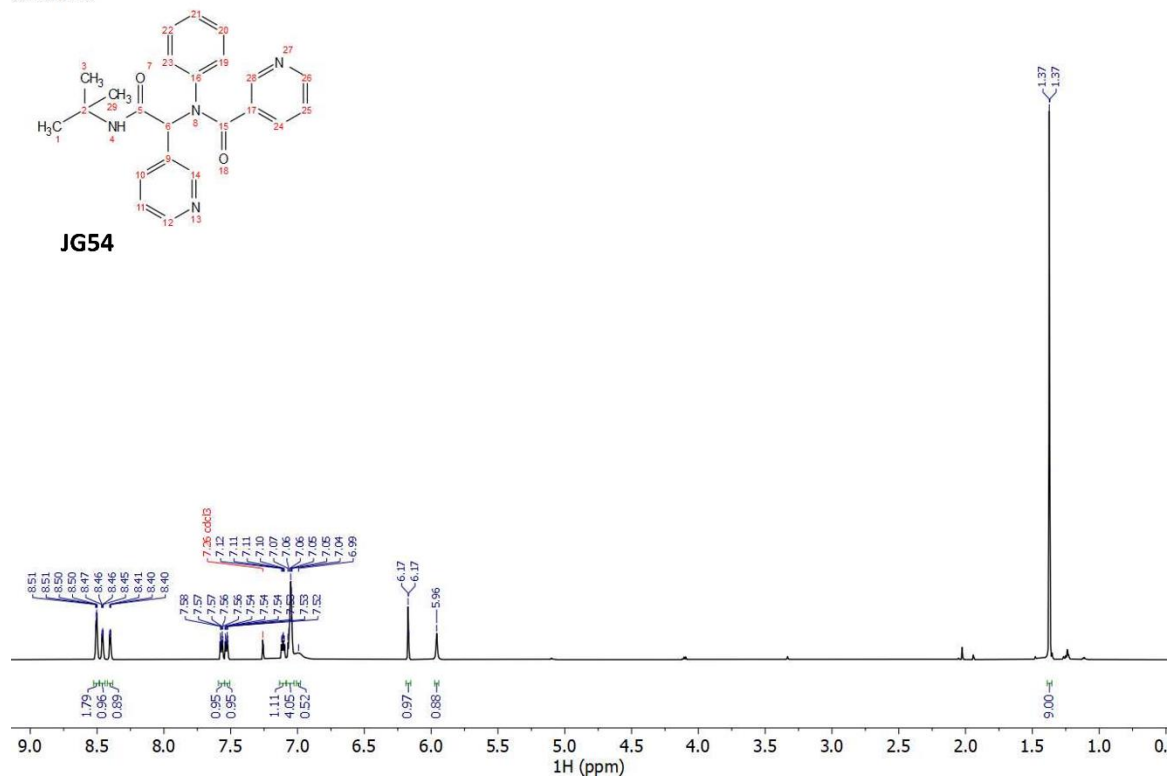
103-JG-3-233-32\_PROTON\_03  
103-JG-3-233-32



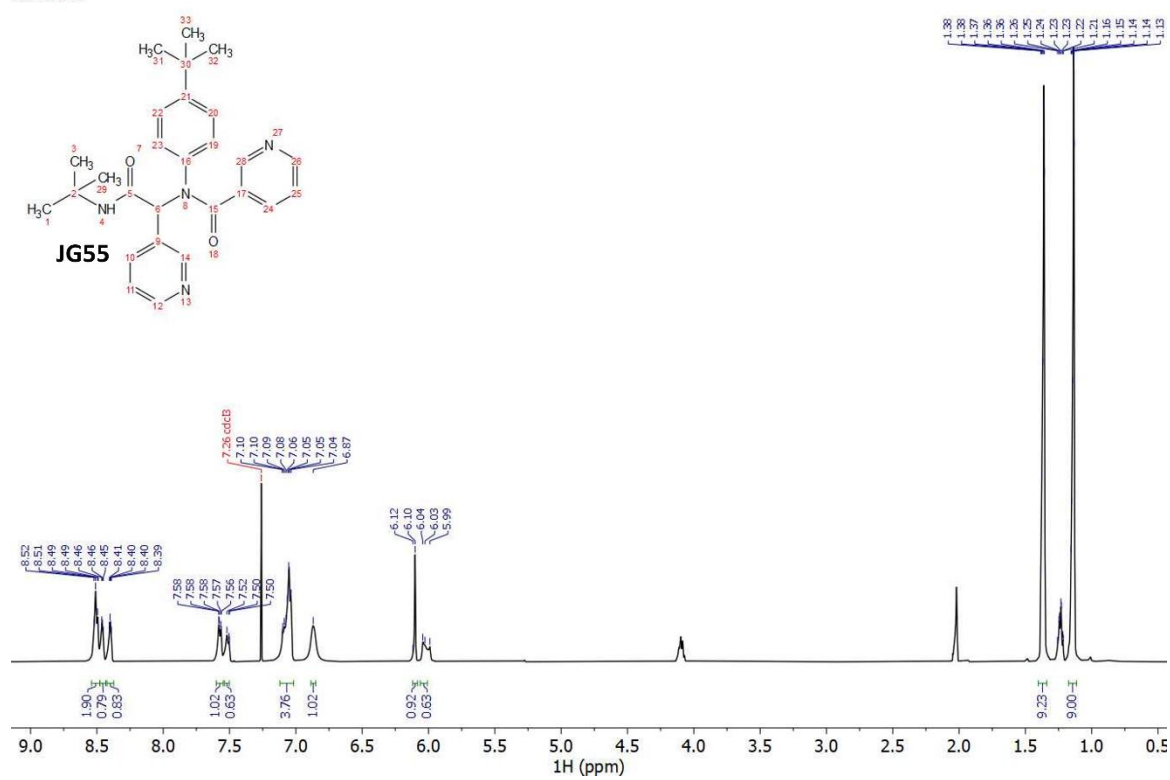
106-JG-3-235-again\_PROTON\_03  
106-JG-3-235-again



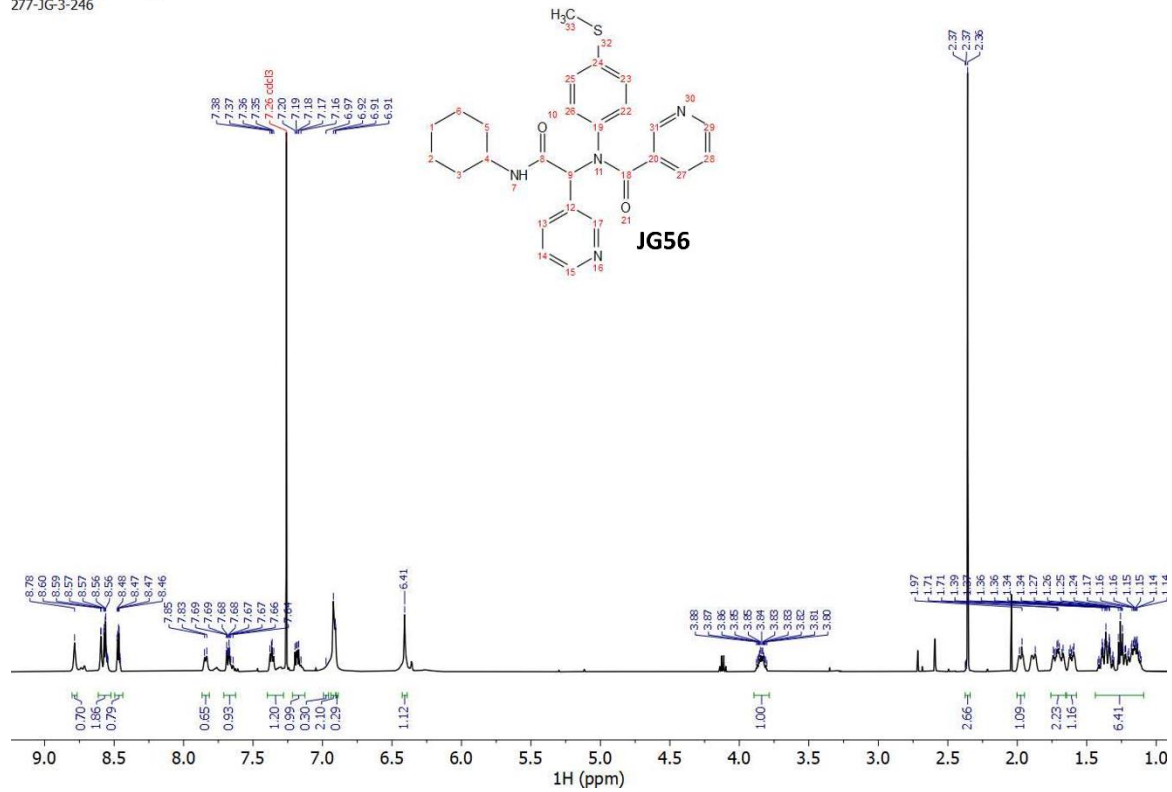
109-JG-3-243\_PROTON\_05  
109-JG-3-243



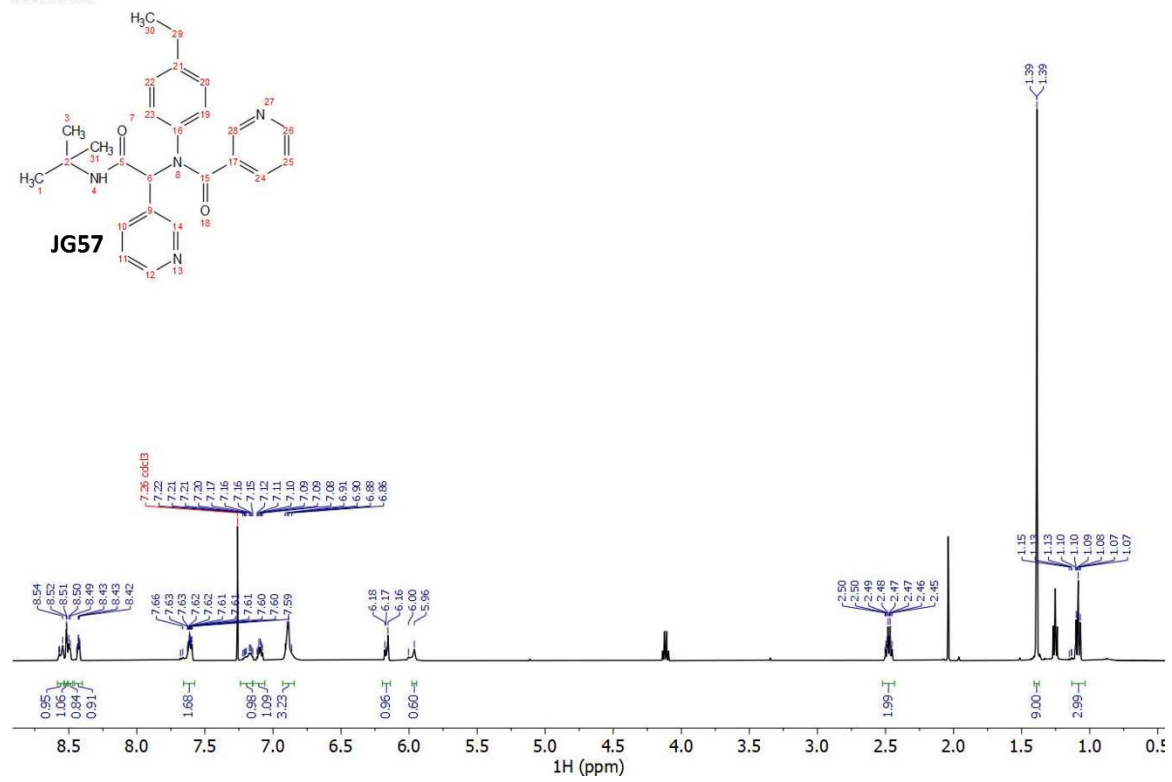
281-JG-5-02\_PROTON\_03  
281-JG-5-02



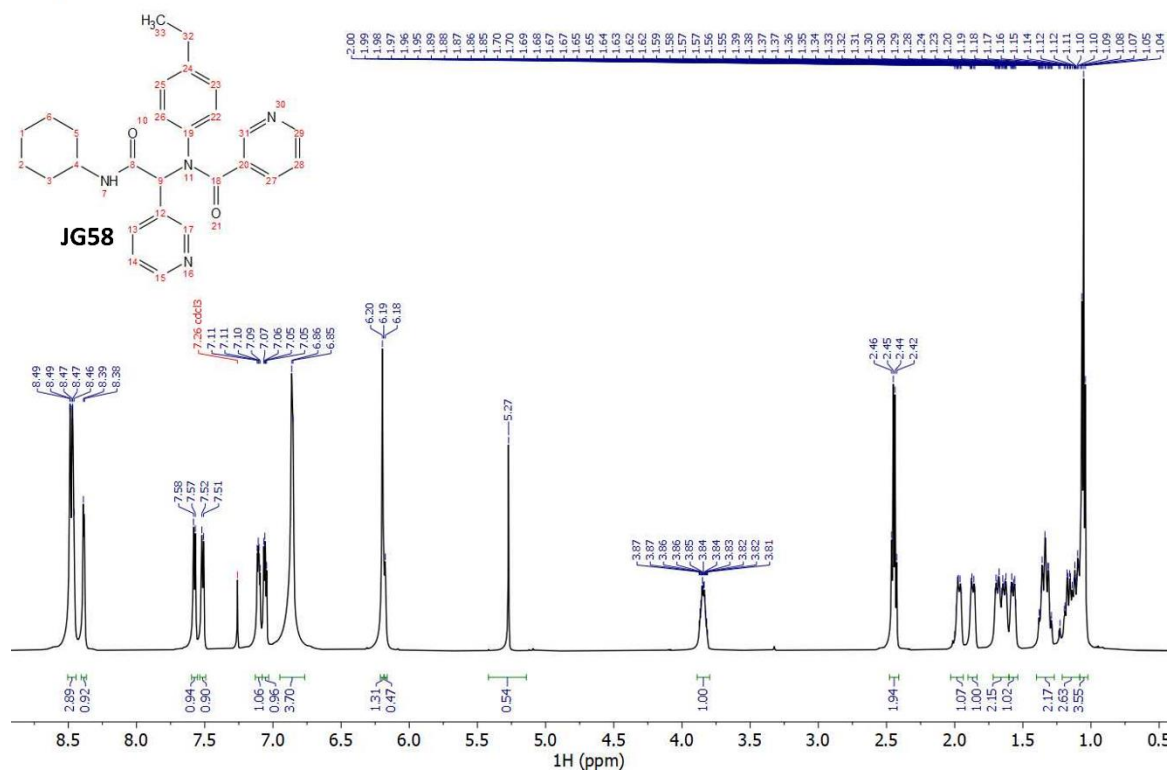
277-JG-3-246\_PROTON\_04  
 277-JG-3-246



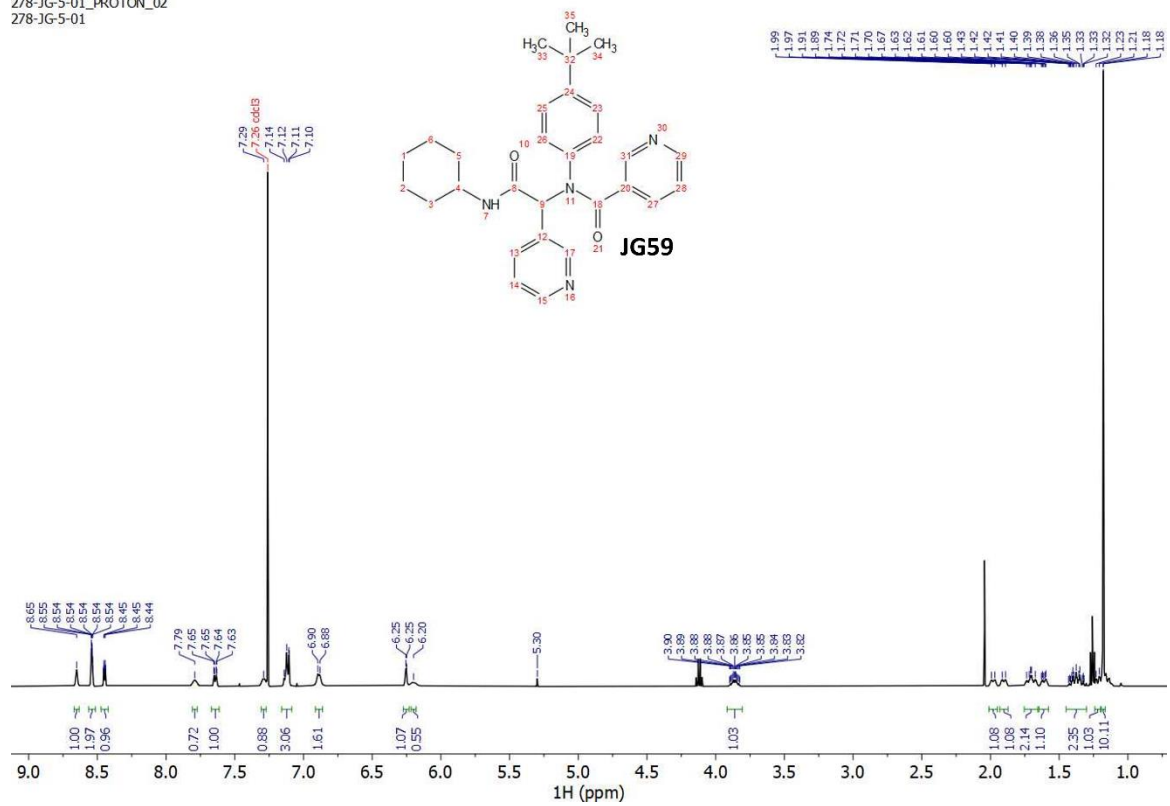
276-JG-3-245\_PROTON\_05  
 276-JG-3-245



110-JG-3-244\_PROTON\_04  
110-JG-3-244

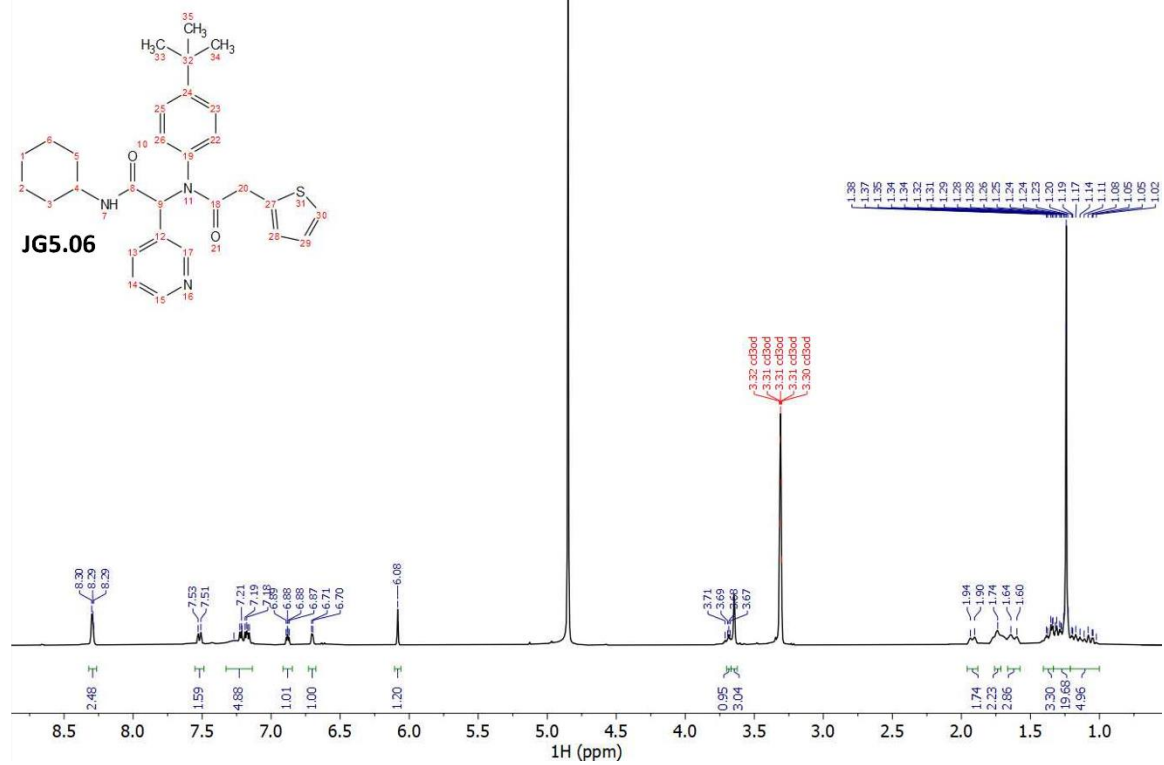


278-JG-5-01\_PROTON\_02  
278-JG-5-01

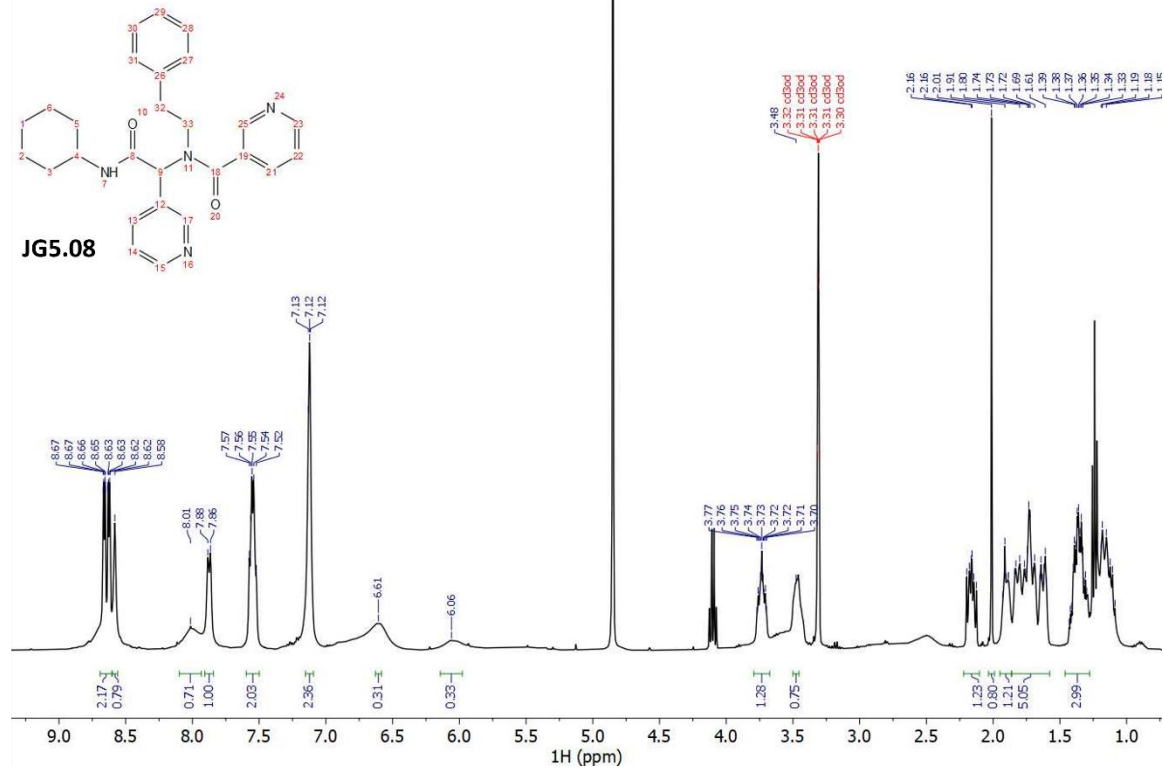




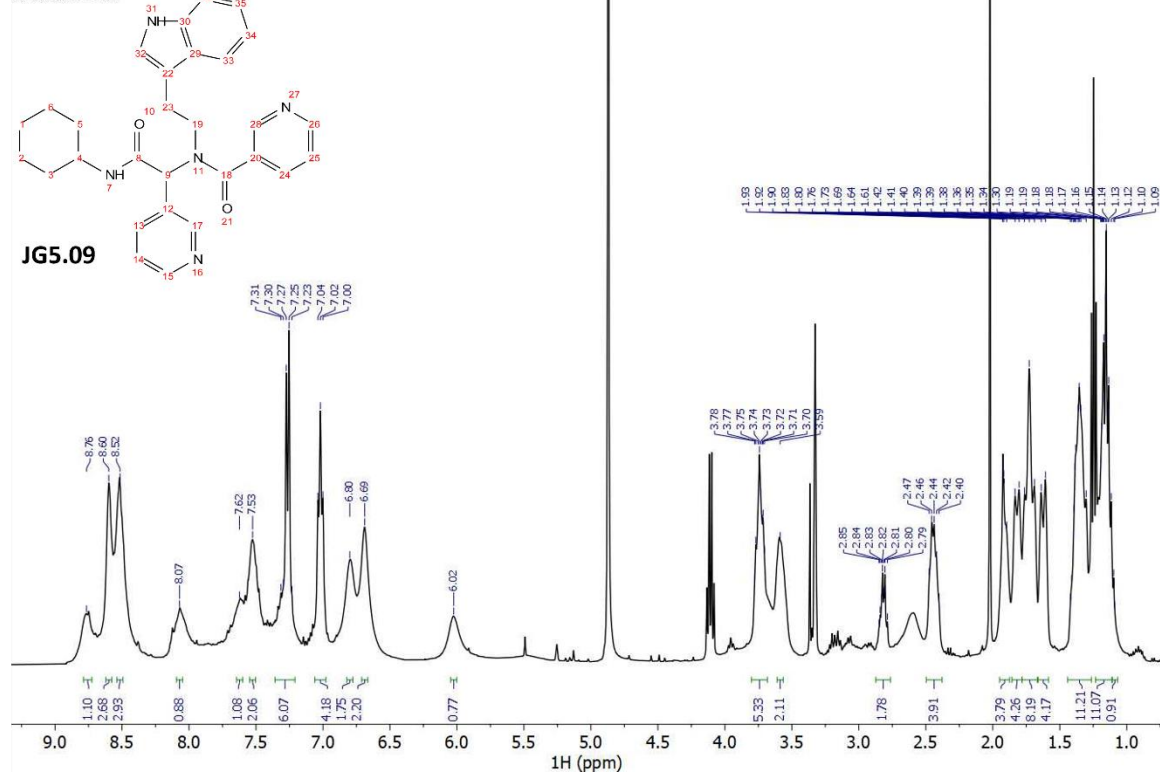
20-28-JG-5-06\_PROTON\_03  
20-28-JG-5-06



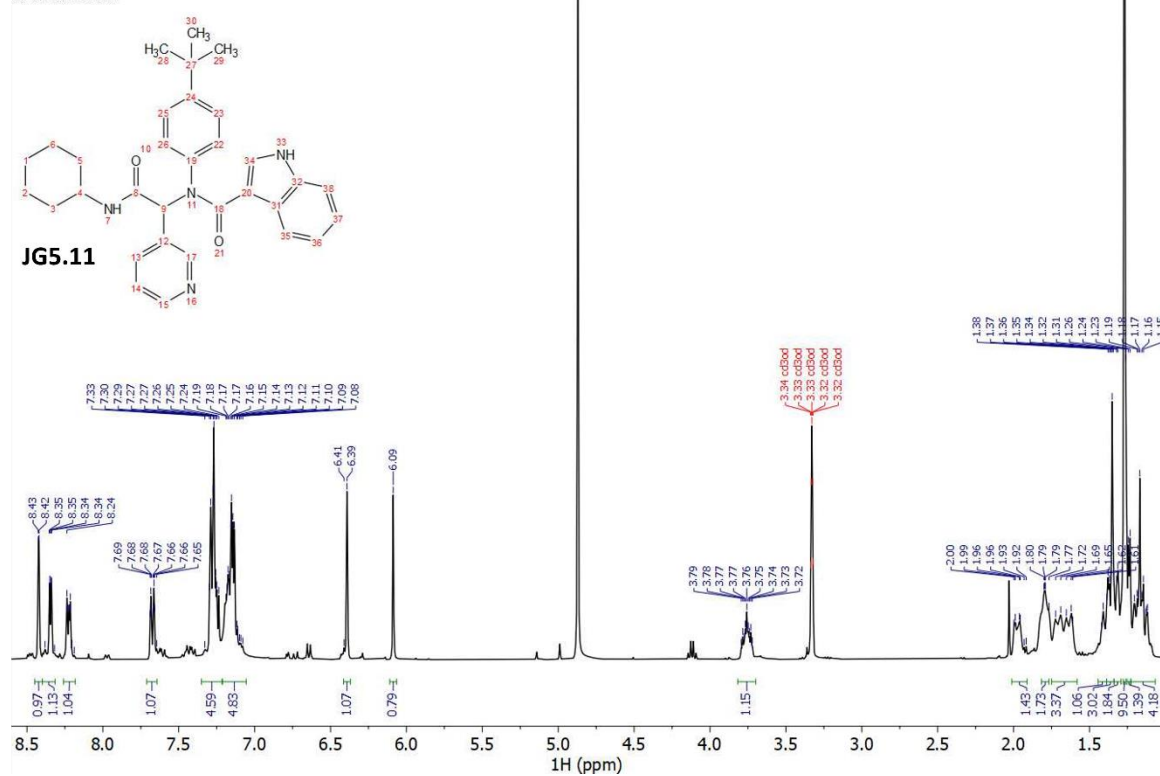
20-25-JG-5-08\_PROTON\_03  
20-25-JG-5-08



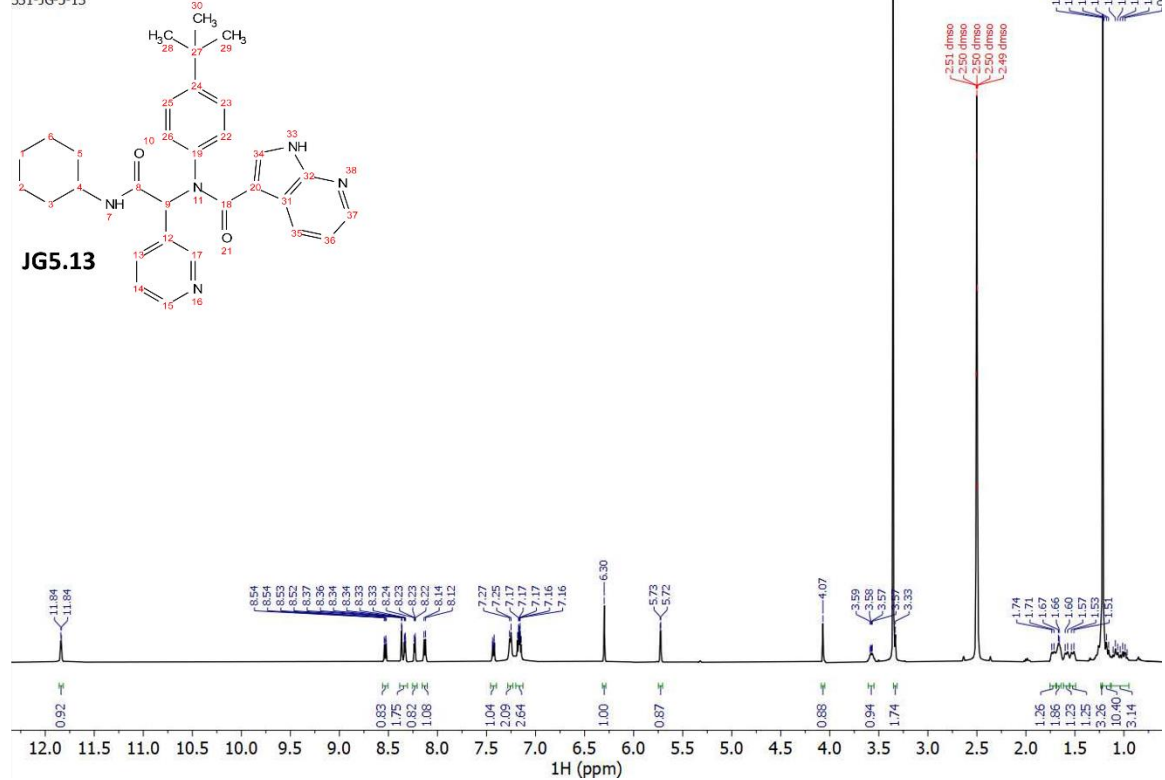
20-26-JG-5-09-23\_PROTON\_03  
20-26-JG-5-09-23



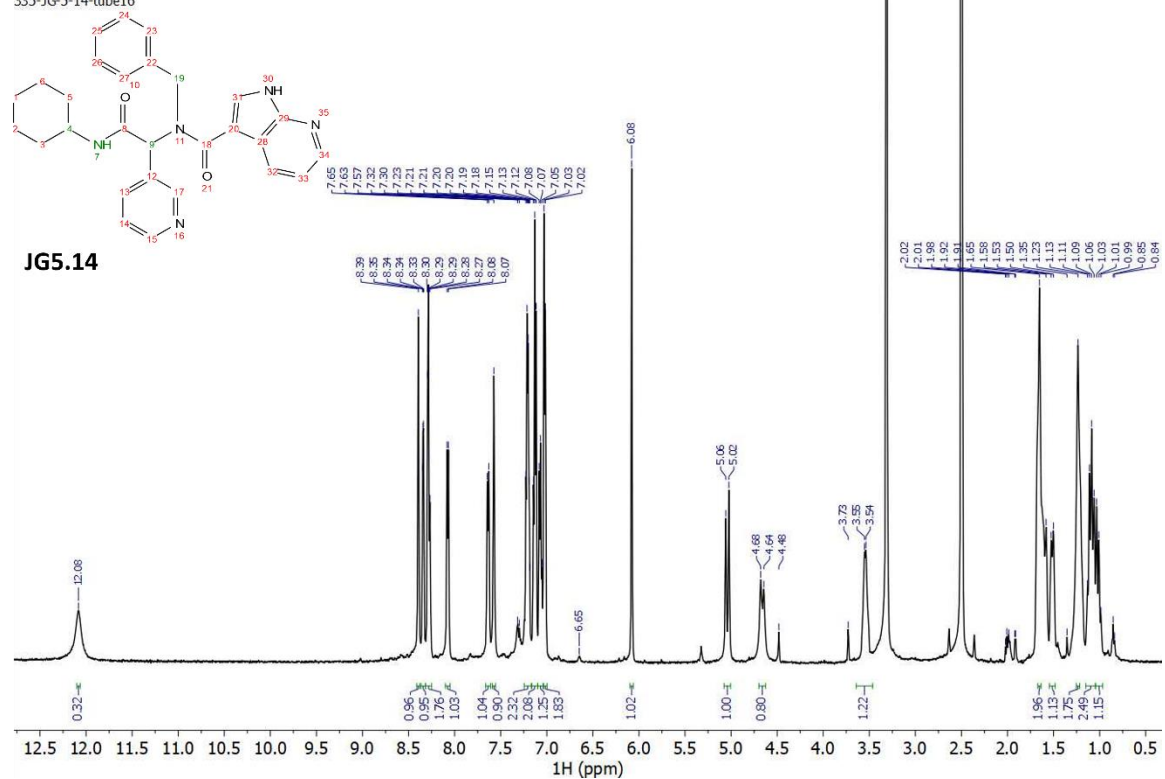
20-27-JG-5-11-35\_PROTON\_03  
20-27-JG-5-11-35



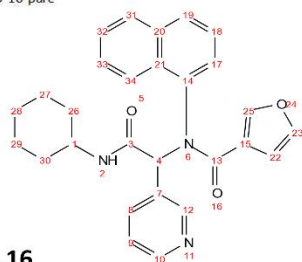
331-JG-5-13\_PROTON\_03  
331-JG-5-13



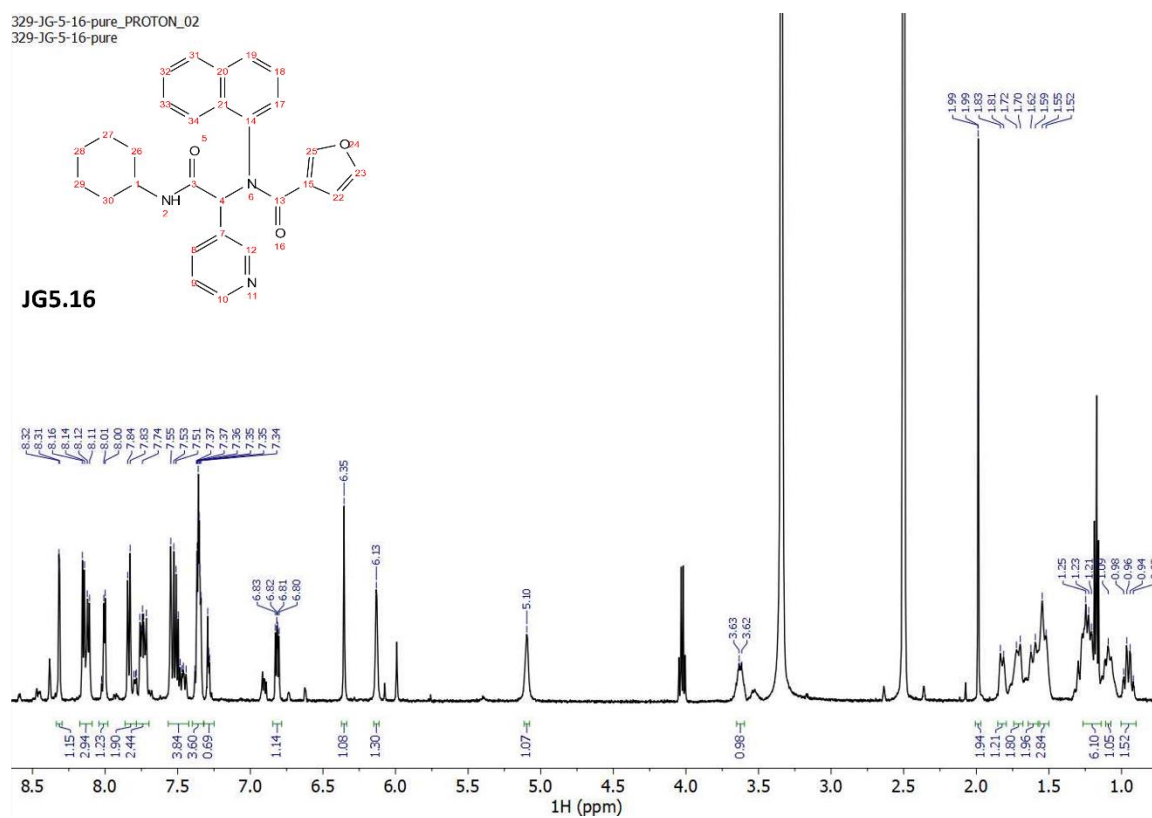
335-JG-5-14-tube16\_PROTON\_03  
335-JG-5-14-tube16



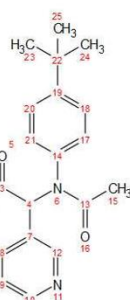
329-JG-5-16-pure\_PROTON\_02  
329-JG-5-16-pure



JG5.16



330-JG-5-17\_PROTON\_02  
330-JG-5-17



JG5.17

